The dynamic behaviour of multi-story reinforced concrete building in a seismic and windy environment

Örvar Jónsson

Thesis of 30 ECTS credits
Master of Science in Civil Engineering with specialization in Structural Design.

January 2014

The dynamic behaviour of multi-story reinforced concrete building in a seismic and windy environment

Örvar Jónsson

Thesis of 30 ECTS credits submitted to the School of Science and Engineering
at Reykjavík University in partial fulfillment
of the requirements for the degree of
Master of Science in Civil Engineering with specialization in Structural Design

January 2014

Supervisor:

Jónas Þór Snæbjörnsson
Professor, Reykjavík University, Iceland

Examiner:

Sigurður Unnar Sigurðsson, M.Sc.
Earthquake Engineering Research Centre, University of Iceland, Iceland

Abstract

The focus of this study, in the field of wind and earthquake engineering, is on the dynamic behaviour of a multi-story reinforced concrete building and how it responds to wind and earthquake induced excitations. Tall buildings are often of complex geometry while the building design codes, used to evaluate the dynamic properties of structures in the design phase, are based on simplified generic assumptions, which are primarily appropriate for relatively simple structures. Therefore a full-scale validation of dynamic behaviour of buildings undergoing wind and earthquake excitations is important. The building examined is a 14 storey tall, reinforced concrete, office building. With a quite complex geometry of the structure, the dynamic behaviour of the structure may not be completely predictable at first sight. The building is equipped with a monitoring system, which has been used to record the acceleration response of the structure in about 24 years. The dynamic properties of the structure are evaluated using a system identification process based on the recorded acceleration response. A finite element model is constructed to further interpret the recorded data to gain understanding of the dynamic behaviour of the building. The dynamic response of the structure is compared to estimated response using design code guidelines to investigate if simple design code methods can predict the building behaviour with reasonable accuracy and at last assessment is made on whether the building fulfils criteria's for comfort of the building inhabitants during wind induced excitations. From the system identification, the natural frequencies of the building were seen to gradually decrease over time. The wind induced response, estimated by the use of three international design code guidelines showed a wide variety in results and did not represent the true behaviour of the building adequately when compared to the recorded response. The human comfort criteria's, presented by two international design codes, were seen to be breached on numerous occasions, leading to the question whether the building inhabitants are experiencing discomfort under wind induced excitations.

Keywords: Building, wind excitation, earthquake excitation, dynamics, acceleration response, reinforced concrete, finite element modelling, system identification, design guidelines, human comfort criteria.

Ágrip

Titill á íslensku: Sveiflufræðileg hegðun margra hæða steinsteyptrar byggingar í jarðskjálfta- og vindasömu umhverfi.

Þetta verkefni er á sviði vind- og jarðskjálftaverkfræði og fjallar um sveiflufræðilega hegðun margra hæða bygginga úr steinsteypu og hvernig slíkar byggingar svara vind- og jarðskjálftaáraun. Háar byggingar eru oft flóknar í lögun og hegðun þeirra margslungin á sama tíma og hönnunarstaðlar eru byggðir á einföldum lýsingum á álagsferlum og almennum hönnunar forsendum, sem eiga fyrst og fremst við tiltölulega einföld mannvirki. Þess vegna er mikilvægt að rannsaka sérstaklega sveiflufræðilega hegðun stærri mannvirkja og flókinna bygginga sem undirgangast mikla vind- og jarðskjálftaáraun. Meðal annars til að staðfesta að hegðun þeirra uppfylli hönnunarviðmið og kröfur.

Byggingin sem sérstaklega er fjallað um í þessu verkefni, er 14 hæða hátt steinsteypt skrifstofuhúsnæði. Þar sem form byggingarinnar er nokkuð óreglulegt þá er erfitt að sjá fyrir sveiflufræðilega hegðun hússins nema með nánari greiningu. Byggingin er útbúin hröðunarmælum sem hafa vaktað svörun hússins í u.þ.b. 24 ár. Með kerfisgreiningu eru sveiflufræðilegir eiginleikar byggingarnir metnir. Gert er tölvulíkan af byggingunni sem túlkar enn frekar gögnin sem mæld hafa verið með hröðunarmælunum á nokkrum stöðum í húsinu til að öðlast frekari skilning á hegðun byggingarinnar. Svörun byggingarinnar við vindáraun er borin saman við áætlaða svörun, metna með einfölduðum reikniaðferðum hönnunarstaðla, til að kanna hvort aðferðir einfaldra hönnunarstaðla geti áætlað hegðun byggingarinnar með ásættanlegum hætti. Að lokum er lagt mat á hvort byggingin uppfylli kröfur um þægindi manna sem starfa eða dvelja í byggingunni á meðan byggingin verður fyrir örvun af völdum sterkra vinda. Af kerfisgreiningunni sést að á þeim árum sem liðin eru frá því að hröðunarmælingarnar hófust, þá hafa eigintíðnir byggingarinnar lækkað smám saman. Niðurstöður mats á áætlaðri svörun byggingarinnar vegna vindáraun, metin með þremur alþjóðlegum hönnunarstöðlum bar ekki vel saman þar sem talsvert mikill munur er á niðurstöðunum og gáfu hönnunarstaðlarnir almennt ekki fullnægjandi mynd af hegðun bygginarinnar þegar áætluð svörun var borin saman við mælda svörun byggingarinnar. Hröðunarsvörun byggingarinnar hefur í fjölda skipta farið yfir þau mörk sem sett eru fram sem viðmiðunarkröfur um þægindi fólks í byggingunni af tveimur alþjóðlegum stöðlum. Talsverður munur er á þessum kröfum þessara tveggja staðla, sem gefur vísbendingu um þá óvissu sem ávallt mun tengjast slíku mati. Þessar niðurstöður vekja engu að síður upp þá

spurningu hvort fólk í byggingunni finni fyrir raunverulegri vanlíðan þegar hún titrar vegna vindáraunar í stærri stormum.

Lykilorð: Byggingar, vindáraun, jarðskjálftaáraun, hröðunarsvörun, steinsteypa, einingarlíkön, sveiflugreining, kerfisgreining, hönnunarstaðlar.

The dynamic behaviour of multi-story reinforced concrete building in a seismic and windy environment

Örvar Jónsson

30 ECTS thesis submitted to the School of Science and Engineering
at Reykjavík University in partial fulfillment
of the requirements for the degree of
Master of Science in Civil Engineering with specialization in Structural Design

January 2014

Student: Örvar Jónsson

Örvar Jónsson

Supervisor: Jónas Þór Snæbjörnsson

Jónas Þór Snæbjörnsson

Examiner: Sigurður U. Sigurðsson

Sigurður Unnar Sigurðsson

Acknowledgements

My sincere gratitude is expressed to my supervisor, Jónas Þór Snæbjörnsson, for his great amount of time and valuable work, knowledge and guidance in order to improve this work.

I thank the Earthquake Engineering Research Center of the University of Iceland and the Icelandic Meteorological Office for the access to their data.

Finally, I would like to thank my family for their support and patience during the past years of study at the Reykjavik University.

Contents

List of figures

List of tables

List of symbols

Roman letters

a_j	Auto regressive poles
c	Damping
$[C]$	Damping matrix
E	Modulus of elasticity
H	Height of building
k	Stiffness
$[K]$	Stiffness matrix
m	Mass
$[M]$	Mass matrix
p	Auto regressive model order
P	External force
p_0	Maximum amplitude of external force
R_a	Acceleration response factor
R_d	Deformation response factor
R_v	Velocity response factor
t	Time
T_n	Natural period of the n-th mode of vibration
u	Displacement
u'	Fluctuating component of wind velocity
$(u_{st})_0$	Static deformation
$\bar{U}$	Mean wind velocity
$\{u\}$	Displacement vector
$\dot{u}$	Velocity
$\{\dot{u}\}$	Velocity vector

$\ddot{u}$	Acceleration
$\ddot{u}_g$	Ground acceleration
$\{\ddot{u}\}$	Acceleration vector
V_L	Longitudinal pulse velocity
x_n	Input time series of an auto regressive analysis
y_n	Output time series of an auto regressive analysis
Z	Height above ground

Greek letters

β	Mode shape exponent
ζ	Critical damping ratio
ρ	Density
υ	Poisson's ratio
ϕ_n	Mode shape of the n-th mode of vibration
ω_n	Natural frequency of the n-th mode of vibration

In addition to the symbols listed in this section, are symbols used in the design code procedures of acceleration response estimation, listed along with the procedures in Appendix B.

List of abbreviation

AIJ	Architectural Institute of Japan
ASCE	American Society of Civil Engineers
EERC-UI	Earthquake Engineering Research Centre of the University of Iceland
IMO	Icelandic Meteorological Office
MDOF	Multi degree of freedom
PGA	Peak ground acceleration
PRA	Peak response acceleration
PSD	Power spectral density
SDOF	Single degree of freedom

1. Introduction

1.1. Background

This study, which is within the field of wind and earthquake engineering, focuses on the dynamic behaviour of a multi-story reinforced concrete building and how it responds to wind and earthquake induced excitation.

The geometrical and structural complexity of buildings, especially taller buildings, is constantly increasing. Building design codes are on the other hand based on simplified and generic assumptions, which are first and foremost appropriate for relatively simple structures. This is why full-scale validation of structural response through recorded wind- and earthquake excitation is important.

1.2. Problem statement

The main focus of this project will be to analyse the recorded dynamic properties and response characteristics of a 14 story office building during wind and earthquake induced excitations and to compare those to simple codified methods for response estimation in order to evaluate their general applicability in design practice. The geometry of the building is rather complex as the floor plans are changing along the height of the building, resulting in a more complex structure than the design codes normally assume and therefore the guidelines they provid may not give correct estimates of dynamic properties and response characteristics for the building. With a monitoring system installed in the building supplying full scale records of the building response on regular basis since 1990, a considerable amount of data is available for investigation.

1.3. Aim and objectives

The aim of this study is to gain knowledge and better understanding of dynamic properties and behaviour of structures in a seismic and windy environment and to evaluate the applicability of design code estimation of acceleration response for a structure with somewhat complex geometry.

The main objectives of the study are:

1. To analyse the response and dynamic properties of the structure.
2. To make comparison of the response of the structure to the simple codified methods in order to evaluate their applicability in design practice.
3. To verify whether the acceleration response exceeds the acceptable human comfort levels.

1.4. Research methodology

This research is a case study which is based on full scale experimental data, dynamic analysis and finite element modelling. The full scale experimental data is provided by the Earthquake Engineering Research Centre of the University of Iceland (EERC-UI) which manages the monitoring system of the building. The building has been instrumented since January 1989 with eight acceleration sensors located at three different levels of the building. Measurements for the basic wind and weather data is also available from a meteorological site located about 500 m S-W of the building. Over the past 24 years the acceleration response of the building has been recorded during numerous earthquakes and storm events.

The dynamic response of the structure is analysed and compared to estimated response using simplified buffeting theory presented in design guidelines to provide structural designers with simple design methods to predict the building behaviour with reasonable accuracy during the design phase. The analysis of the dynamic behaviour of the structure will involve structural modelling using finite element modelling and system identification based on the recorded data. Long term variability of the natural frequencies and critical damping ratios which are key parameters in earthquake and wind resistance structural design are also to be examined as radical changes in those parameters can be vital for the building behaviour and even a predictor for potential structural damage.

The finite element modelling is carried out using the computer software SAP2000 (*SAP 2000*, 2010) and all other calculations are done using the computer software MATLAB (*MATLAB*, 2011).

1.5. Scope of work

This thesis is divided into seven main chapters with the addition of references and appendices.

The first chapter introduces the project of the thesis and clarifies the aim, objectives and outlines of the work.

Chapter two gives a brief overview of literature topics that are important in relation to the content of the thesis including the basics of dynamics of structures, wind and earthquake induced excitation on buildings, human comfort during a wind induced excitation, a system identification process and structural modelling.

The third chapter gives a concise description of the building and the monitoring system installed in it and gives an overview of the recorded response and the meteorological data.

Chapter four deals with the analysis of the recorded response during wind and earthquake induced excitations and includes the system identification process

The fifth chapter presents the finite element modelling of the building used for further interpretation of the recorded response and better understanding of the building behaviour.

Chapter six deals with the response prediction, evaluated by the simplified procedures presented in design codes. It also presents human comfort criteria's and gives a comparison of these criteria's to the recorded response.

The seventh chapter discusses the conclusion of the main topics and the results of the thesis. It also gives recommendations for further research from questions that arose during the work of the thesis.

2. A brief review of structural dynamics

This chapter gives a brief overview of topics that are important in relation to the content of the thesis. Firstly, the basics of dynamics of structures are presented. Then there is a brief discussion of the wind and earthquake induced excitation on buildings as well as human comfort and perception of motion during a wind induced excitation. Finally, there is a discussion about the dynamic properties of structures, evaluated with a system identification process based on recorded response and through structural modelling thas is used to gain a better understanding of the overall behaviour of the building, as its response has only been monitored at a two levels, the 8^{th} and 14^{th} (top) floor.

2.1. Dynamics of structures

Most buildings undergo dynamic excitation from earthquake or wind storms over their lifetime, causing them to vibrate in response to the dynamic excitation. The simplest structures can be described as a single degree of freedom system (SDOF).

From a structural engineering perspective, a SDOF system can be thought of as a lumped mass, *m*, supported by a massless column with certain stiffness, *k*, see Figure 2.1. The mass is considered to be able to move or vibrate in one direction, perpendicular to the column. As the vibration of the structure diminishes in amplitude as the excitation ceases, rather than continuing to oscillate, it is considered to have certain amount of damping, *c*.

The simplest model of a SDOF system is often expressed as a mass-spring-damper system as shown in Figure 2.1. The mass is assumed to be rigid, the spring and the damper assumed to have no mass and the mass is only considered to be able to move in one direction, along the length of the spring, and is thus a system of a single degree of freedom (Chopra, 2006).

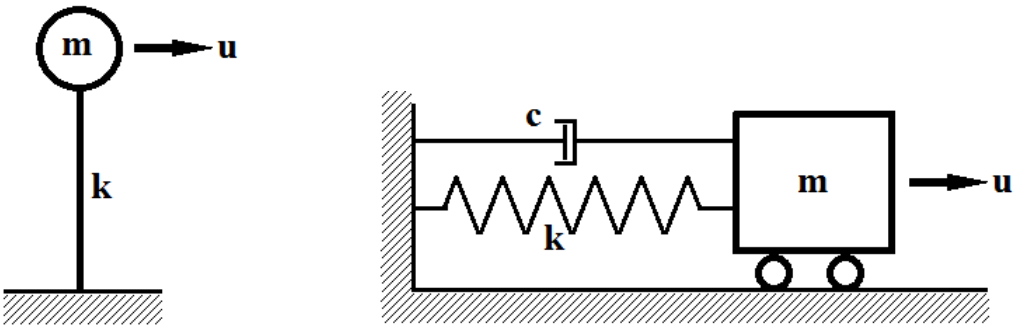

(a) **(b)**

Figure 2.1: SDOF systems. (a) Lumped mass and a column system and (b) A mass spring damper system.

When a structure has been disrupted from its static state and is vibrating freely without external load, such as seismic or wind load, it is referred to as free vibration of the structure.

The equation of motion for a free vibration of this system can be expressed as:

$$\boldsymbol{m\ddot{u} + c\dot{u} + ku = 0} \qquad \textbf{(2.1)}$$

where $\ddot{u}$ is the acceleration, $\dot{u}$ is the velocity and u is the displacement of the system (Chopra, 2006).

When a structure undergoes a free vibration, it is bound to vibrate at its natural frequency, which can be explained as the number of vibration cycles over a time unit, measured in radians per second. The natural frequency of a SDOF system can be evaluated by:

$$\boldsymbol{\omega_n = \sqrt{k/m}} \qquad \textbf{(2.2)}$$

The natural frequency of a SDOF system is dependent on the stiffness and the mass. The natural frequency increases with increased stiffness and decreases with increased mass and vice versa(Chopra, 2006)

The natural period of the structure is the time the structure takes to complete one cycle of vibration and can be derived from the natural frequency as:

$$\boldsymbol{T_n = \frac{2\pi}{\omega_n}} \qquad \textbf{(2.3)}$$

The damping, c, is a measure of the kinetic energy reduction in each cycle of vibration of a SDOF system. The critical damping ratio is a function of the damping, the mass and the natural frequency of the system and is expressed by (Chopra, 2006):

$$\zeta = \frac{c}{2m\omega_n} \quad (2.4)$$

A system can be critically damped if the critical damping ratio is equal to 1, overdamped if the critical damping ratio is over 1 or underdamped if the critical damping ratio is less than one. All buildings, bridges, dams and such structures are underdamped, usually with a critical damping ratio less than 0,10 (Chopra, 2006). Figure 2.2 shows a free vibration response of a underdamped SDOF system. It shows the decay in amplitude for each cycle as a results of the damping of the structure. If a system had no damping it would keep vibrating with the same amplitude indefinitely, but that is not the case for real structures.

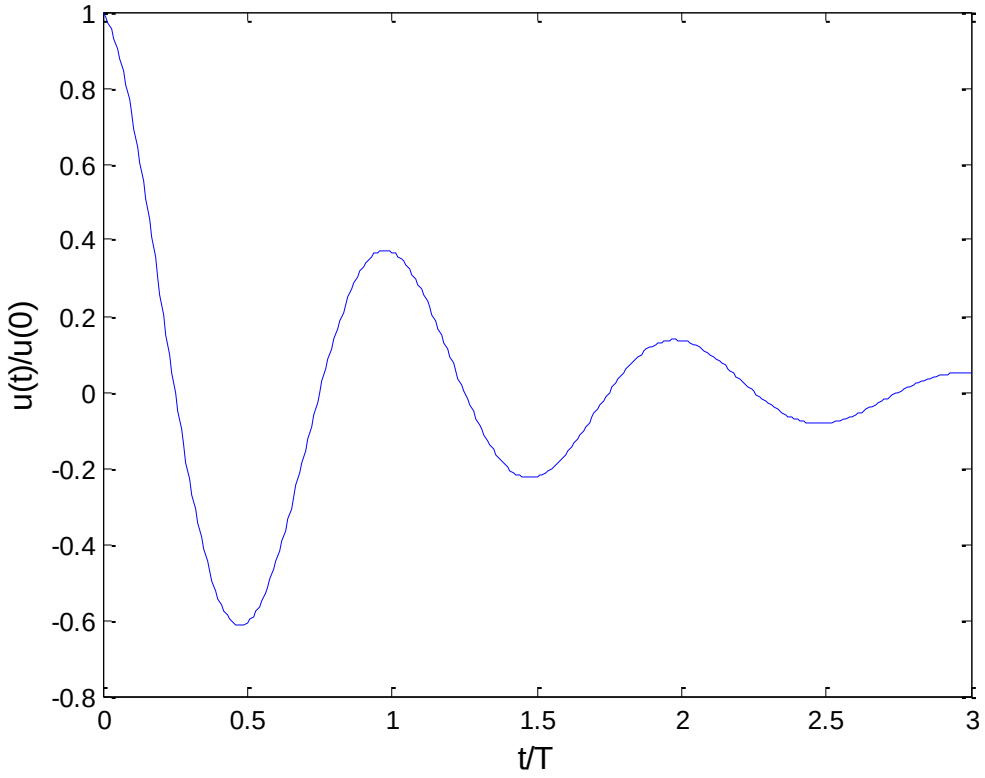

Figure 2.2: Free vibration of a underdamped systems.

In order to disrupt a system from its static state, an external force is required to force the system to vibrate. The equation of motion for a forced vibration of this system can be expressed as:

$$m\ddot{u} + c\dot{u} + ku = P \quad (2.5)$$

where *P* is the external force acting on the system, such as seismic action or wind loading (Chopra, 2006). An example can be taken using a harmonic sinusoidal excitation where the equation of motion becomes:

$$m\ddot{u} + c\dot{u} + ku = p_0 \cdot \sin(\omega \cdot t) \quad (2.6)$$

where the external force is acting on the system with a certain frequency, ω, and the maximum amplitude of the force is p_0. If the external force is exciting the system with a frequency different to the natural frequency of the structure the response of the system has two states, a transient state at first but after a while the response of the system reaches a steady state (Chopra, 2006) (Gil-Martín, Carbonell-Márquez, Hernández-Montes, Aschheim, & Pasadas-Fernández, 2012). At first the system vibrates with its natural frequency along the excitation path, but due to the damping of the system the response reaches the steady state as the free vibration of the system decays and the system vibrates with the frequency of the external force. The response of a system undergoing such excitation is shown in Figure 2.3 for a system with a natural frequency 5 times higher than the frequency of the external force and a critical damping ratio of 5%. The figure shows the total response of the system with a blue line and the steady state response with a red line. The response is shown as the ratio of the vibratory response deformation of the system, $u(t)$, to the static deformation, $(u_{st})_0$, that would occur if the maximum amplitude of the force were applied to the system as a static load. This ratio is furthermore referred to as the deformation response factor, R_d, and is similarly defined for the velocity response, R_v, and the acceleration response, R_a.

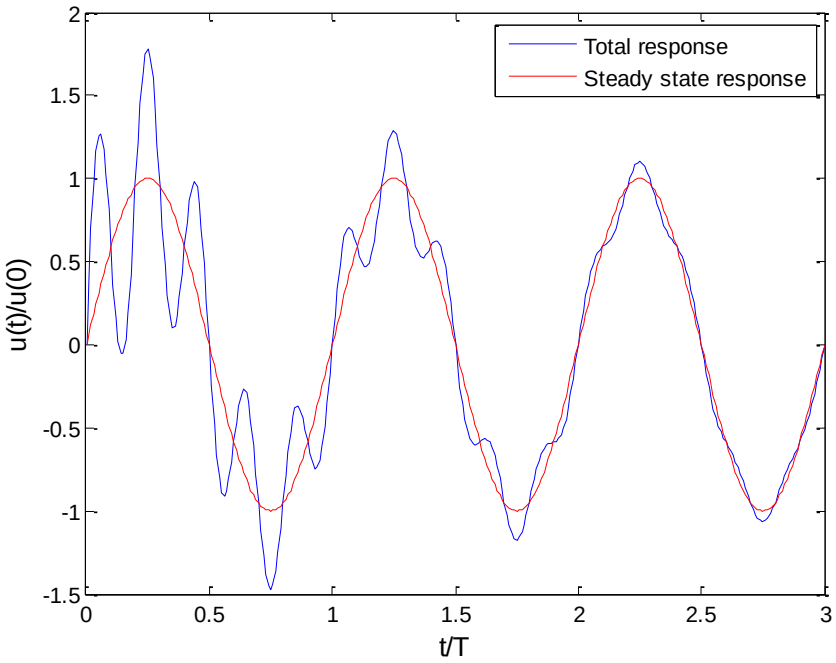

Figure 2.3: Forced vibration of a SDOF system due to a sinusoidal external force. ω/ω_n = 0,2, ζ = 0,05.

The difference between the total response and the steady state response is known as the transient component referring to that it is a temporary state of vibration that decays due to the damping of the system until a steady state of vibration is reached at the forcing frequency (Chopra, 2006).

As seen in Figure 2.3, the maximum response may take place in the transient state (Gil-Martín et al., 2012), with a higher deformation response than the deformation caused by the equivalent static load of the maximum amplitude of the force. The total response of the system is highly dependent on the frequency of the external force and the maximum response is achieved by an external force with an excitation frequency close to or equal to the natural frequency of the system. When the forcing frequency is same as the natural frequency of the system the deformation response amplitude increases with each vibrational cycle in the transient state. The amplitude does however not increase indefinitely due to the damping of the system which lowers each amplitude increase and leads the amplitude to a bound value in a steady state vibration where the deformation response factor, R_d, becomes equal to $1/(2\zeta)$ (Chopra, 2006).

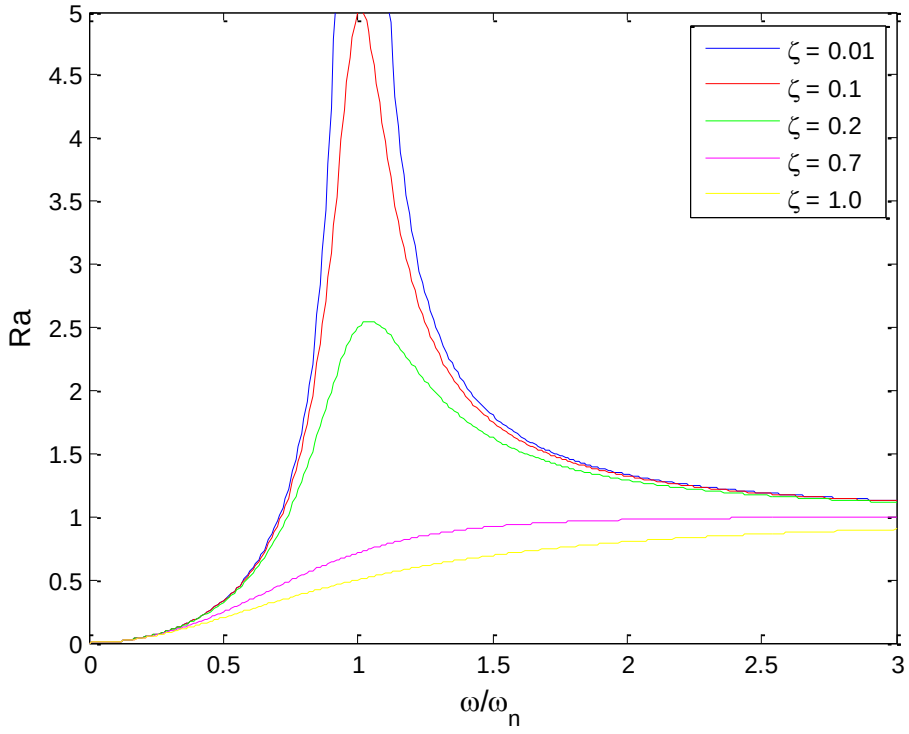

Figure 2.4: Acceleration response factors as a function of the frequency ratio for variously damped systems.

The impact of damping on the response of a SDOF system is shown by the frequency response curves in Figure 2.4, where acceleration response factors are shown for systems with various critical damping ratios excited by harmonic forces of various forcing frequencies. It shows the great difference of the response for different forcing frequencies, where the acceleration response factor is largest for forcing frequencies close to the natural frequency.

The frequency of the external excitation where the largest response occurs is referred to as the resonant frequency. Due to the influence of system damping, the resonant frequency is not equal to the natural frequency of the system. The acceleration resonant frequency is slightly higher than the natural frequency. The highest value of the acceleration response factor occurs at the respective resonant frequency and is evaluated as (Chopra, 2006):

$$\boldsymbol{R_a = \frac{1}{2\zeta\sqrt{1-\zeta^2}}} \qquad \textbf{(2.7)}$$

For a system with unknown damping, the frequency response curve of the deflection response factor, R_d, can be used to evaluate the critical damping ratio. If the forcing frequencies of deflection amplitude of $1/\sqrt{2}$ of the resonant amplitude are identified as ω_a and ω_b the critical damping ratio can be evaluated by the expression:

$$\boldsymbol{\zeta = \frac{\omega_b - \omega_a}{2\omega_n}} \qquad \textbf{(2.8)}$$

This property of the frequency response curve is referred to as the half-power bandwidth (Chopra, 2006) and is shown graphically in Figure 2.5.

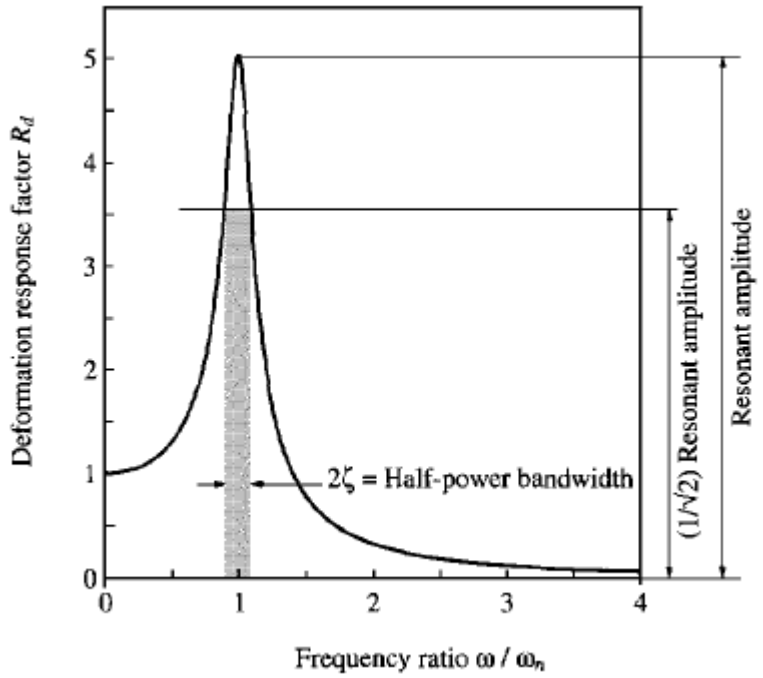

Figure 2.5: The half-power bandwidth (Chopra, 2006).

For more complex structures, such as multi-story buildings, the SDOF concept is insufficient and a more detailed model is implemented, i.e. the multi degree of freedom(MDOF) system .

From a structural engineering perspective, a simple model of a MDOF system can be thought of as many lumped masses, m_i, supported by massless columns, each with certain stiffness, k_i, and damping, c_i, as shown in Figure 2.6 (a) for a system with two degrees of freedom.

Again, the simplest MDOF system can also be expressed as two or more serial connected mass-spring-damper SDOF systems, as previously described, connected together as shown in Figure 2.6 (b). The MDOF systems shown in Figure 2.6 are capable of two independent displacements where the two masses are able to move independently in the direction of the springs and the system is therefore referred to as a two degree of freedom system.

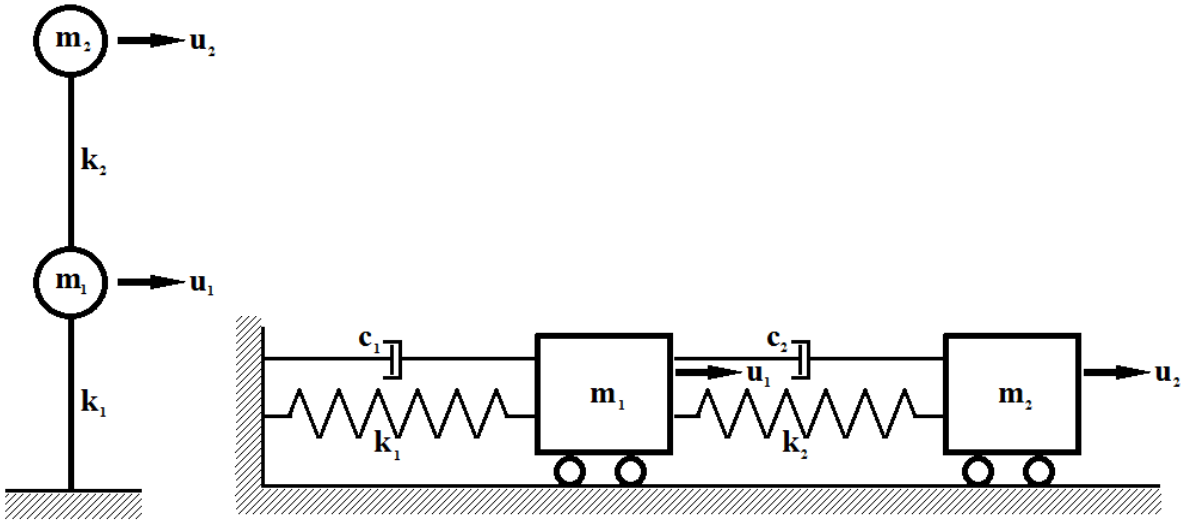

(a) **(b)**

Figure 2.6: MDOF systems. (a) Lumped masses and columns system and (b) A mass spring damper system.

The equation of motion for a free vibration of a MDOF system can be expressed as:

$$[\boldsymbol{M}]\{\ddot{\boldsymbol{u}}\} + [\boldsymbol{C}]\{\dot{\boldsymbol{u}}\} + [\boldsymbol{K}]\{\boldsymbol{u}\} = \boldsymbol{0} \qquad \textbf{(2.9)}$$

where $[M]$ is a mass matrix, $[C]$ is a damping matrix and $[K]$ is a stiffness matrix for the structure. $\{\ddot{u}\}$ is the acceleration vector, $\{\dot{u}\}$ the velocity vector and $\{u\}$ the displacement vector of the structure (Chopra, 2006).

The equation of motion for a forced vibration of a MDOF system can be expressed as:

$$[\boldsymbol{M}]\{\ddot{\boldsymbol{u}}\} + [\boldsymbol{C}]\{\dot{\boldsymbol{u}}\} + [\boldsymbol{K}]\{\boldsymbol{u}\} = \boldsymbol{P} \qquad \textbf{(2.10)}$$

where P is the external force acting on the structure (Chopra, 2006).

The MDOF system can oscillate in various characteristic deflection shapes where each characteristic deflected shape is called a natural mode of vibration or a mode shape (Chopra, 2006). As the number of degrees of freedom is evaluated by the number of independent displacements possible in the system, the system has equally many natural modes of vibration as it has degrees of freedom.

The MDOF structure has different dynamic parameters for each mode shape. For most structures the greatest response occurs in the first few modes, i.e. the ones with the lowest natural frequencies. The natural frequencies of the MDOF system can be evaluated for each mode of vibration by the eigenvalue problem:

$$[\boldsymbol{k} - \boldsymbol{\omega_n}^2\boldsymbol{m}]\boldsymbol{\phi_n} = \boldsymbol{0} \qquad \textbf{(2.11)}$$

where k is the stiffness vector, ω_n is the natural frequency for each vibration mode, m is the mass vector and ϕ_n is the mode shape vector for the desired vibration mode (Chopra, 2006). The natural periods and critical damping ratios for each mode of vibration are evaluated similarly as for the SDOF system previously described.

An example of the different mode shapes or modes of vibration is shown in Figure 2.7 where the two modes of vibration for a two degree of freedom system, such as the one shown in Figure 2.6 (a), are demonstrated.

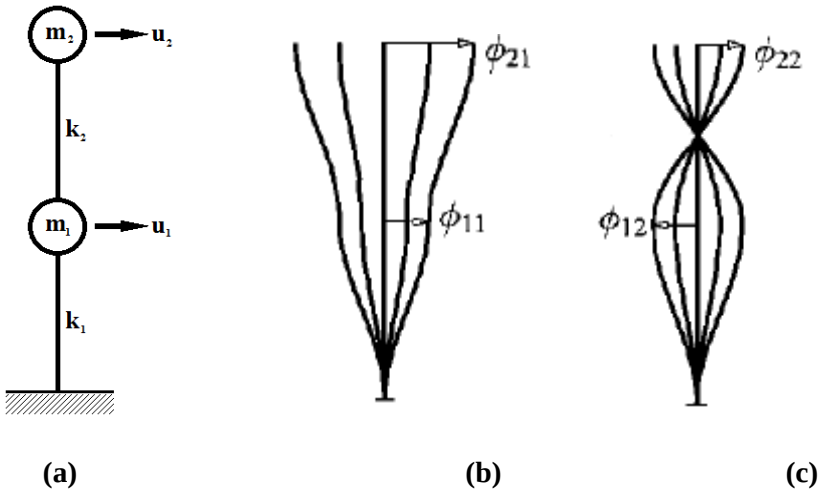

Figure 2.7: The two mode shapes of a two degree of freedom system. (a) Lumped masses and columns system, (b) first mode of vibration, (c) second mode of vibration. The different lines represent the displacements at different times in one vibration cycle (Chopra, 2006).

For MDOF systems such as buildings or bridges, the main sources of vibration and dynamic response are wind and earthquake excitations. Excitation by wind- and earthquake action have different effects on different structures. The earthquake action has relatively stronger effect on low rise buildings with relatively high natural frequencies whereas the wind action has relatively more effect on tall buildings with lower natural frequencies (Holmes, 2007). This is described graphically in Figure 2.8. Further description of the earthquake and wind induced excitations is the subject matter of the following chapters.

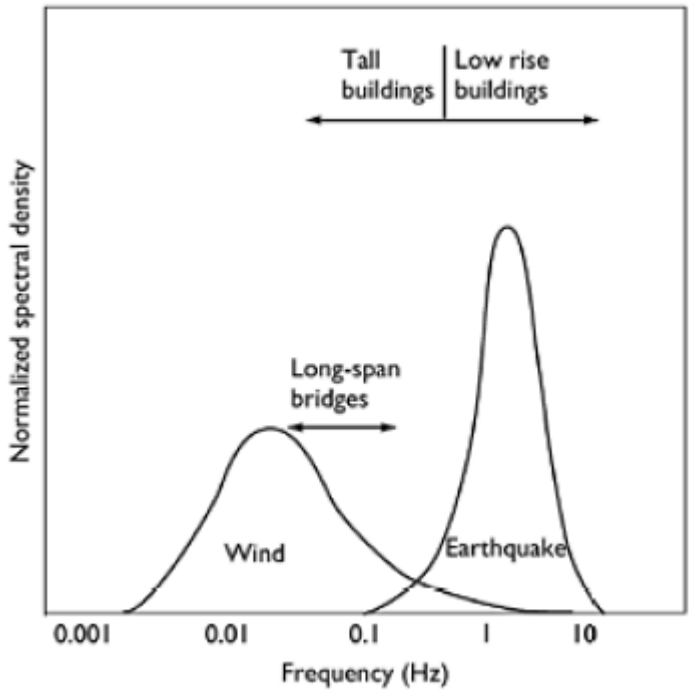

Figure 2.8: Relative effect of wind and earthquake loads to structures of various natural frequencies (Holmes, 2007).

2.2. Wind excitations

The wind is a highly turbulent phenomenon. The turbulence is due to three dimensional vortices within the flow, travelling in the air at the mean wind velocity, generating variations in the wind velocities which results in fluctuating wind loads acting on buildings and a potential to excite a dynamic structural response, especially if the structure has a relatively low natural frequency and damping (Holmes, 2007).

The wind velocity is generally treated as a stationary random process where the mean component can be separated from the fluctuating component. The wind velocity is then expressed as:

$$\boldsymbol{U(x,y,z,t) = \bar{U}(z) + u'(x,y,t)} \qquad \textbf{(2.12)}$$

The mean wind velocity, $\bar{U}(z)$, is considered to be time independent at each height level, *z*, while the fluctuating component, $u'(x,y,z,t)$, is both dependent on time and position. The turbulence, u', can be further split up into along-wind, across-wind and vertical components of velocity.

When wind acts on a building it causes varying force or pressure on the building which causes the building to respond dynamically. If the characteristics of the wind are known, a gust

spectral density can be evaluated and used to evaluate the aerodynamic force spectral density. While taking into account the buildings modal properties the aerodynamic force spectral density is used to evaluate the response spectral density of a building which determines the response of the structure to wind excitations.

This can be demonstrated by an example of a response spectral density of as the one shown in Figure 2.9. The response of the structure can be split into two categories: On one hand, a background response which can be described as an almost static response caused by wind action at frequencies lower than the natural frequency of the structure; On the other hand a resonant response which is a dynamic response caused by wind excitation at frequencies close to the natural frequencies of the structure. The resonant response of an anonymous MDOF system is segregated by the hatched peaks in Figure 2.9.

It depends on the structure whether the background response or the resonant response plays a larger role. With increasing height and slenderness and decreasing natural frequency of a structure, the resonant response becomes an increasing part of the response. For a structure where the resonant response is dominating, the instantenous response of a building under wind load does not only depend on the instantaneous wind gust hitting the building but also on the time history of the wind induced response and how the response states superimpose (Holmes, 2007).

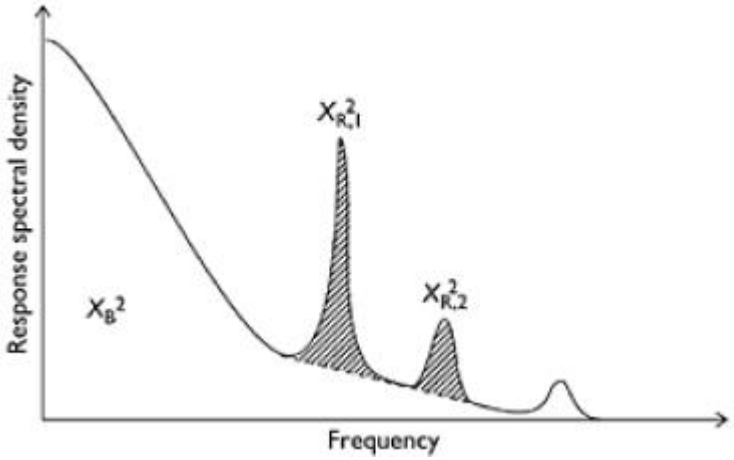

Figure 2.9: An example of a response spectral density of a structure under wind load (Holmes, 2007).

The wind does not only induce structural vibrations in the direction of the wind (along-wind response), but it will also cause the structure to vibrate perpendicular to the wind direction (across wind response) and as well as inducing torsional building vibrations.

For a tall building the across wind response may often become greater than the along wind response if the aspect ratio of the cross section is such that the side of the building paralell to the wind direction are significantly larger than the sides of the building perpendicular to the wind direction (Gu & Quan, 2004).

The wind induced response prediction procedures of three design codes, the Eurocode EN 1991-1-4, ASCE design code and AIJ design code, are discussed in Chapter 6 and described in detail in Appendx B.

2.3. Earthquake excitations

An earthquake can be described as a strong ground motion, triggered by seismic waves from an occurrence of a fault rupture. The seismic waves can be categorized into two groups, body waves and surface waves. The body waves travel inside the earth and are of two types. One type of a body wave is the pressure wave (P wave) which is a longitudinal wave that causes tension and compression of the body it travels through. The P waves have the greatest travel velocity and are the first waves to reach any certain place and are therefore often referred to as primary waves. The other type of body waves is a shear wave (S wave) which occurs perpendicular to a P wave, causing a up and down and side to side motion of the body. The S waves have less travel velocity than the P waves and arrive later at a certain location. They are therefore often referred to as secondary waves (Kramer, 1996).

As the name implies the surface waves travel along the earth surface. The surface waves are also of two types, Rayleigh waves and Love waves. The Rayleigh waves cause an up and down ground motion while the Love waves cause a side to side motion of the ground. The surface waves have less travel velocity than the body waves and therefore they reach a particular site after the P and S waves (Kramer, 1996). The S waves and the surface waves carry the most energy and have therefore greater impact on the structures than P waves (Shinozuka, Deodatis, Zhang, & Papageorgiou, 1999).

A building, or other structure, excited by seismic waves is assumed to move with the surface of the ground and the dynamic forcing is therefore created by the interaction of the structural mass and the acceleration of the ground. The equation of motion for a SDOF system under seismic action is generally expressed as:

$$\boldsymbol{m\ddot{u} + c\dot{u} + ku = -m\ddot{u}_g(t)} \qquad \textbf{(2.13)}$$

where $\ddot{u}_g$ is the ground acceleration (Chopra, 2006). The forces acting on a system, such as the one in Figure 2.1 (a), are therefore due to the relative displacement of the mass to the ground caused by the ground acceleration and although it is not an actual external force it can be thought of as an external force, equal to $-m\ddot{u}_g(t)$, acting on a stationary system in the opposite direction to the ground acceleration (Chopra, 2006). It is then seen that an increased mass of a system leads to an increase in the dynamic forcing.

If equation (2.13) is divided by the mass, *m*, it results in the equation:

$$\ddot{\boldsymbol{u}} + 2\boldsymbol{\zeta}\boldsymbol{\omega_n}\dot{\boldsymbol{u}} + \boldsymbol{\omega_n^2}\boldsymbol{u} = -\ddot{\boldsymbol{u}}_{\boldsymbol{g}}(\boldsymbol{t}) \qquad \textbf{(2.14)}$$

which demonstrates that the response of a system due to an earthquake induced ground acceleration only depends on the natural frequency, ω_n, of the system and its critical damping ratio, ζ (Chopra, 2006). It should though be noted that these parameters are both mass and stiffness dependent as previously shown in chapter 2.1.

As the earthquake excitation is a random process the differential equations of motion can be solved with numerical integration methods such as the Newmark's method (Chopra, 2006).

2.4. Human comfort and serviceability of buildings against vibrations

When a structure undergoes a wind load it is bound to move to some degree. The turbulence of the wind induces acceleration response of the structure, which can be felt by the people working or living in the building. A reasonably low acceleration response of a building may not affect occupants of a building, as they might either not notice it or simply accept it. However, for higher levels of acceleration response, the occupants may feel discomfort, their work ability may be restricted and they may even feel fear and motion sickness.

While the wind induced response of a building is generally not likely to affect the integrity of the structure it is desirable to place limits on the magnitude of structural motion as it can otherwise restrict the serviceability of the building through human discomfort.

The assessment of human perception and comfort levels due to wind induced motion is dealt with in terms of acceleration response as that is the parameter that people are most sensitive to and are more likely to sense rather than displacement or velocity of motion.

Human comfort criteria's have been put forward in international design codes and standards where limits are defined for the response acceleration, based on a certain return period and the natural frequency of the structure, since it is the natural frequency of the structure determines

the frequency of wind induced building motion. Figure 2.10 shows an example of the human comfort criteria for tall buildings defined by the international standards: ISO 6897:1984 and ISO 10137:2007, the design code of the Architectural Institute of Japan and a couple of researchers (Kwok, Hitchcock, & Burton, 2009).

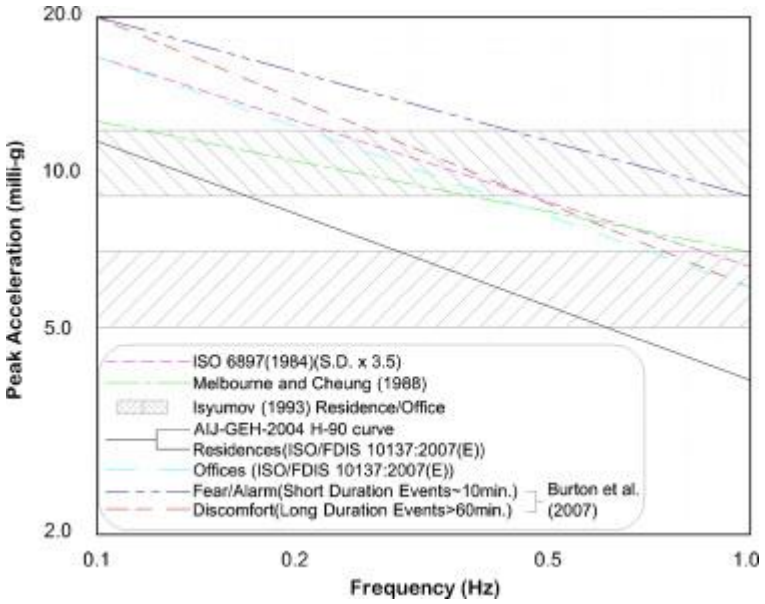

Figure 2.10: The human comfort criteria for tall buildings of the international standards ISO 6897:1984 and ISO 10137:2007, the design code of the Architectural Institute of Japan and a couple of researches on the human comfort issue (Kwok et al., 2009).

The various human comfort and acceleration perception criteria's have been developed by multiple researches and studies which can be grouped into three main categories: Firstly, full scale field experiments of building inhabitants in wind excited tall buildings where the building is equipped with accelerometers and the acceleration perception is evaluated by surveys carried out during or shortly after a wind excitation of the building or by the use of a special button that the occupants push when motion is perceived. Secondly, testing of humans in motion simulators or shake tables where the acceleration and frequency of the excitation can be controlled. At last, tests conducted on people in real buildings excited using artificial means, such as by counter rotating masses (Kwok et al., 2009).

The different study methods have different advantages and different trends of results. The full scale field experiments of wind excited tall buildings have shown the frequency dependency of the occupant acceleration perception (Kwok et al., 2009) which have also been confirmed by motion simulator tests (Burton, Kwok, Hitchcock, & Denoon, 2006). An advantage of the field experiments in wind excited buildings over the other type of studies is the possibility of

long term on going experiments that can reveal more information as it has been seen that tolerance of vibration increases with time (Kwok et al., 2009). These experiments have furthermore demonstrated that for long lasting wind induced excitation the perception tolerance is lower, suggesting that the standard deviation acceleration is a better measure of comfort level than the peak acceleration while the peak value of acceleration is on the other hand a good measure of fear triggered by a wind induced vibration (Kwok et al., 2009). It has also been seen that the field experiments in wind excited buildings typically results in higher level of acceleration perception than for test in motion simulators or shake tables which is attributed to the occupants in the field buildings being preoccupied by some unrelated tasks rather than being fully aware of the on-going test as the people in the motion simulator. It has therefore been seen that the motion perception level increases if the building inhabitants are focused on their own tasks (Kwok et al., 2009). To avoid this difference, the participants of a motion simulator test have often been requested to carry out certain tasks during the experiments. The primary disadvantage of the experiments on artificially excited buildings is that the vibration generators are only able to generate sinusoidal excitation but not random vibration as experienced in wind excited buildings. This is however a possibility in the motion simulators, as they can produce recorded excitation of real wind induced response of buildings (Morava, Haskett, Chadwick, & Wates, 2010).

If a wind induced response of a building breaches the human comfort criteria's and the building inhabitants do not tolerate the perceived motion there are ways to reduce the vibration of the building. The wind induced response of a building can be reduced by the use of external damping devices(Tamura, 1998).

2.5. Dynamic properties and structural modelling of buildings

A system identification is a process conducted to evaluate the modal parameters of a structure, such as the natural frequencies and critical damping ratios. The modal parameters represent the dynamic characteristics of a structure and control how the structure responds to a dynamic load. The system identification process is shown schematically in Figure 2.11.

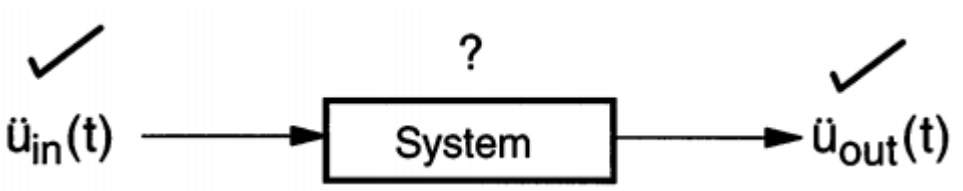

Figure 2.11: The system identification process (Stewart, Seed, & Fenves, 1998).

The system identification can be carried out using both the known input load and the output response. This is suitable for erthquake records, where the ground acceleration has been recorded at the basement or ground level along with the resposne of the structure at higher level in the structure. The system identification process can also be carried out using only the output response, which is useful for analysing wind excitation records where the wind load, or the input, can not be recorded specifically and is generally considered as a white noise signal.

The modal properties of a structure can be extracted through the use of a power spectral density where each peak of the power spectral density plot reflects each mode of vibration. The natural frequency of each mode of vibration is determined as the highest value of the peak and the critical damping ratio evaluation is based on the amplitude and width of the peak as explained in chapter 2.1 for the half-power bandwidth method. An example of a power spectral density plot is shown in Figure 2.12.

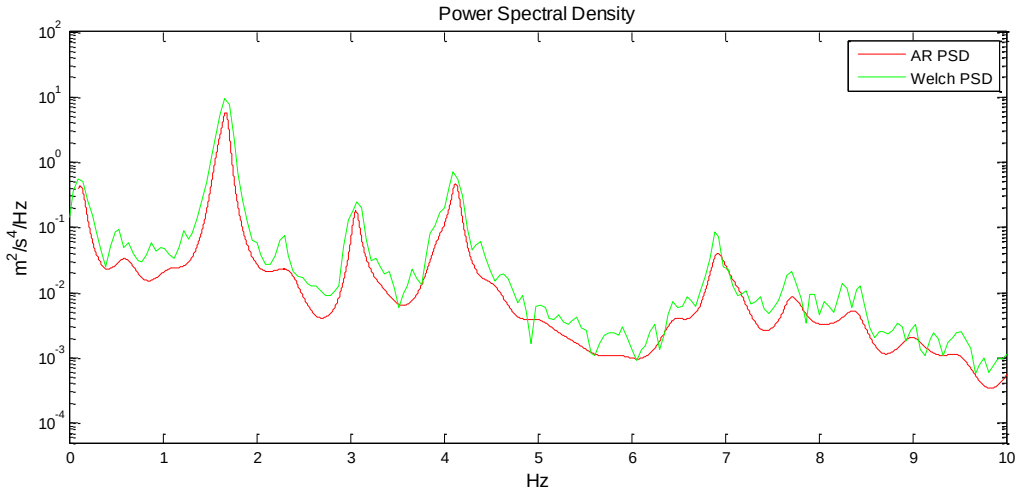

Figure 2.12: An example of a power spectral density plot.

A power spectral density can be evaluated in two different ways, with a parametric procedure, such as an auto regressive analysis, where the dynamic excitation and response are fitted to certain model or with a non-parametric procedure, such as a Fourier analysis (Spyers-Ashby,

Bain, & Roberts, 1998). The auto regressive analysis relates the output time series to an input time series as shown by the equation:

$$y_n = x_n - \sum_{j=1}^{p} a_j y_{n-j} \quad \textbf{(2.15)}$$

where y_n are the output time series, x_n are the input time series, a_j are the auto regressive poles or coefficients and p is the auto regressive model order or number of auto regressive poles (Owen, Eccles, Choo, & Woodings, 2001). The model order used in an auto regressive analysis is an important factor as it dictates the quantity of information that can be evaluated from the input time series. With to low model order, some information might be lost but with too high model order the results might contain unreal peaks (Owen et al., 2001).

For buildings that are expected to undergo considerable dynamic response it is important to be able to estimate the dynamic parameters of the building realistically as the natural frequencies of structures have significant impact on the dynamic response. It has been shown that environmental influences such as heavy rain, high temperatures, amplitude of excitation and response have an impact on natural frequencies of structures (Clinton, Bradford, & Heaton, 2005).

To interpret and extend the information provided by full scale recordings of building response to various excitations a detailed structural model is required as such recordings are only provided for a limited number of locations in a building and only provide information on limited number of response parameters.

It is also essential to be able to estimate the wind induced acceleration response and the natural frequency of the structure during the structural design phase of a tall building to ensure both the comfort of the inhabitants and the safety of the building itself. To obtain a reasonably accurate natural frequency of a structure it is often necessary to make a numerical model such as a finite-element model, especially in a case of a complex structure that does not fit the conditions assumed by simplified guidelines found in design codes.

3. The case studied

This chapter gives an overview of the observed building and its monitoring system along with a brief presentation of the recorded acceleration response of the building, both during wind and earthquake induced excitation. The available meteorological data from the storm events corresponding to the wind induced recordings is also introduced.

3.1. The building

The observed building is a 14 storey high office building, along with a 2 storey basement or underground parking area, built in the years 1975 – 1981 (Þrastardóttir & Gunnarsdóttir, 2006; Ásgeirsson & Sveinsson, 1974; (Hagverk, 1976) and is referred to as the Commerce building in Reykjavík. The overall height of the structure is 52,3 m, of which 6,5 m belong to the basement.

The main construction material is reinforced concrete. The structural system is mainly composed of shear walls and waffle slabs for the upper floors and shear walls, columns and flat slabs for the two basement floors. The building includes two concrete cores, one extending throughout the whole height of the structure, a bit west of the centre, containing stairways and elevators, and the other ranging from the basement to the 11th floor, a bit east of the centre. According to the structural drawings, the concrete used in the building is mostly of the type S-200 which should correspond to C20/25 concrete in Eurocode EN 1992-1-1:2004 (*Eurocode 2: EN 1992-1-1*, 2004).

The geometry of the structure is quite complex as the floor plans vary with changes along the height of the building as seen in Figure 3.1. The street levels are different from north of the building to the south of the building, with the street level at the north side of the building being at the 1st floor while the street level at the south side being the 2nd basement floor as seen in Figure 3.2.

Figure 3.1: The observed building.

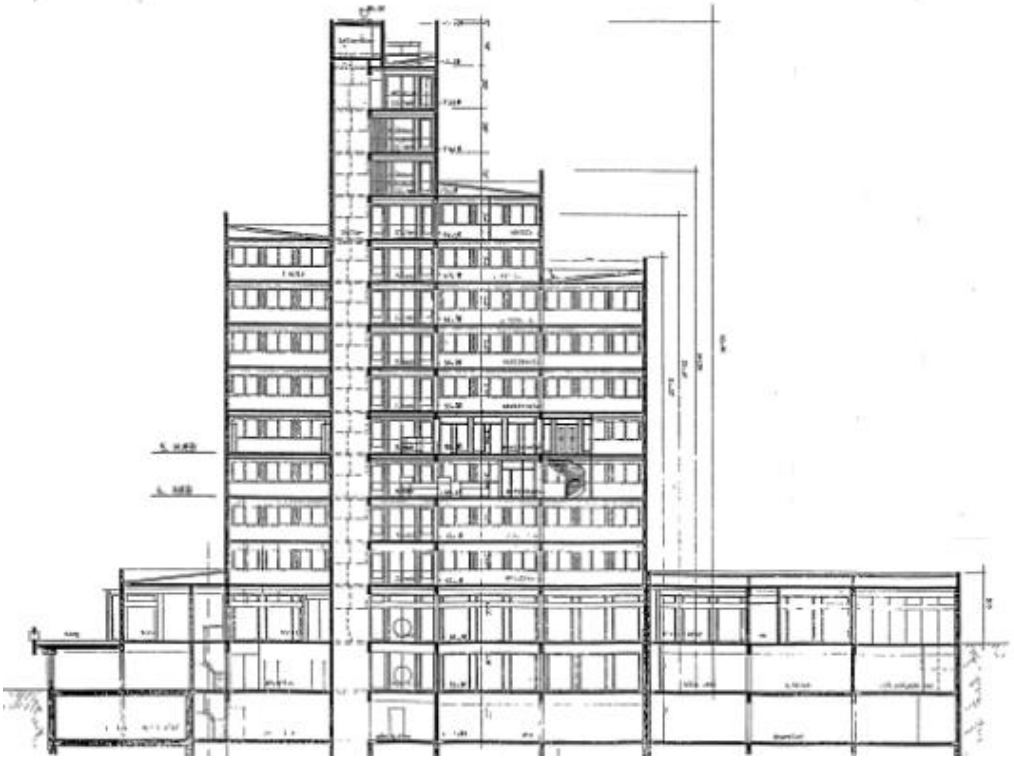

Figure 3.2: Vertical cross section of the building (Björnsson, 1998).

Figure 3.3 show the difference in horizontal cross sections of the building from the 2nd to 13th floor. The 1st floor and the basement floors are considerably larger than the upper floors and the 14th floor is a bit smaller than the floors beneath and is mainly for the elevator motors and the ventilation system equipment.

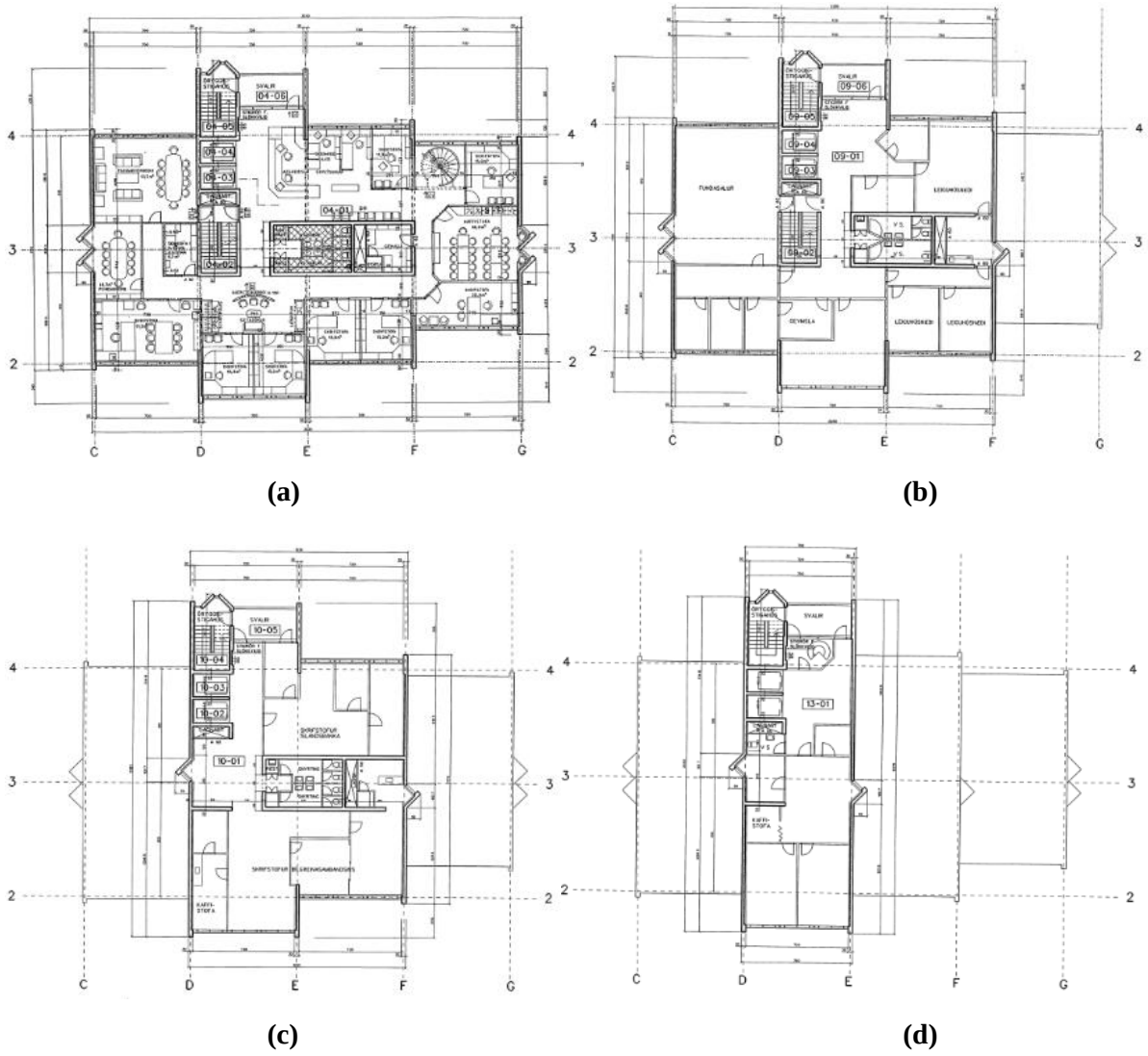

Figure 3.3: Horizontal cross sections of the building. (a) 2nd to 8th floor, (b) 9th floor, (c) 10th floor and (d) 11th to 13th floor (Sveinsson, 1996).

The alignment of the building is in such a way that the front sides of the building face the NNE and SSW directions approximately, or about 20° from east of north. For simplicity purposes the alignment of the building or its basic directions will hereafter be referred to as N-S and E-W.

3.2. Material properties of concrete

One of the key material properties for stiffness evaluation is the modulus of Elasticity. To verify the modulus of elasticity of the concrete, ultrasonic pulse velocity measurements were carried out in the building. To perform the measurements, an instrument called “PUNDIT” manufactured by CNS Instruments Ltd. PUNDIT is an abbreviation of “Portable Ultrasonic Non-destructive Digital Indicating Tester” and as the name suggests, it is particularly suitable to explore the properties of concrete in the buildings serviceability state as it has no damaging impact on the concrete. The instrument emits ultrasonic pulse wave of 54 kHz from a transmitter, through the material being tested, to a receiver and measures the travelling time of the wave. The instrument and an example of the basic method of its use are shown in Figure 3.4.

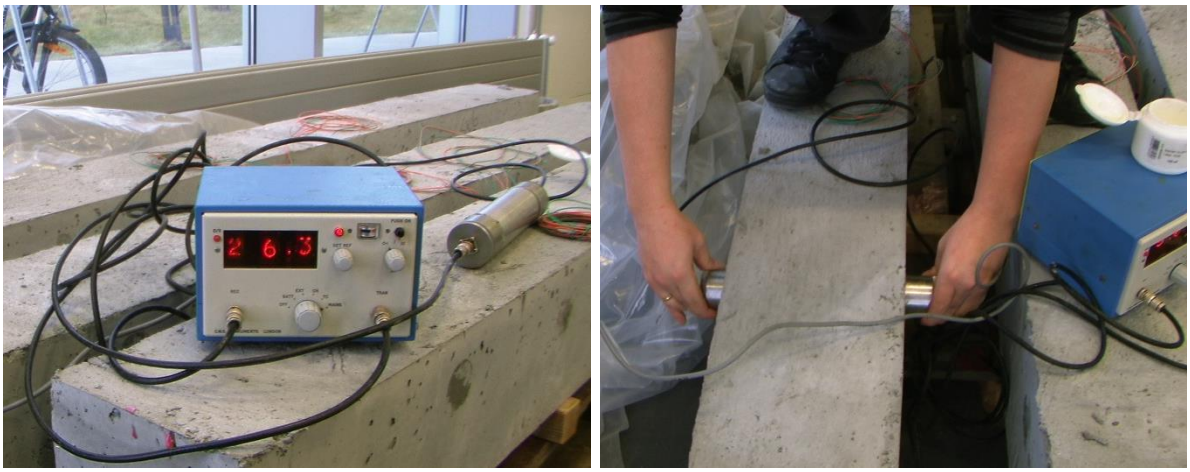

Figure 3.4: Example of the instrument in use.

Knowing the travelling time and length between the transmitter and receiver allows for the calculation of the longitudinal pulse velocity, V_L. Then the modulus of elasticity, E, of the concrete can be calculated by the following equation:

$$\boldsymbol{E = \frac{V_L^2 \rho (1+\nu)(1-2\nu)}{1-\nu}} \qquad \textbf{(3.1)}$$

The concrete is assumed to have a density, ρ, of 2500 kg/m^3 and a Poisson ratio, ν, of 0,2. The measurements were performed on the walls of the staircase core of the first few floors, the concrete of the upper floors is assumed to have equivalent properties.

The results from the measurements are shown in Table 3.1. The average value of E is found to be 19,6 GPa, which is considerably lower than the anticipated value of about 30 GPa. However, it is also seen that for the lower basement values for modulus of elasticity of about

30 GPa can be found, whereas the concrete at the upper floors has clearly lower modulus of elasticity of about 15 GPa on average.

The measurements were performed on concrete walls with very rough surface which could influence the results and due to the great thickness of the basement walls and limited access in the building the measurements were made around concrete corners instead of right through the walls which would have been the ideal approach.

Table 3.1: Results of ultrasonic pulse velocity measurements and calculation of modulus of elasticity of the concrete

x	Time	Distance	Velocity	Poisson's ratio	Density	E
	μs	mm	m/s	-	kg/m^3	GPa
Lower basement	50,0	176,7	3534	0,2	2500	28,10
Lower basement	35,0	132,3	3780	0,2	2500	32,15
Lower basement	48,3	129,5	2681	0,2	2500	16,17
Upper basement	55,0	141,4	2571	0,2	2500	14,87
1. floor	55,0	141,4	2571	0,2	2500	14,87
2. floor	58,5	151,3	2586	0,2	2500	15,05
3. floor	56,5	151,3	2678	0,2	2500	16,13
		Average	**2914**		**Average**	**19,6**

3.3. The monitoring system

The monitoring system of the structure is managed by the Earthquake Engineering Research Centre of the University of Iceland (EERC-UI). The system was installed in the building in January 1989 and has been in operation for over 24 years as this thesis is written. It consists of 8 acceleration sensors, located at three levels in the building. In the basement there is a tri-axial accelerometer, recording the three components of ground acceleration. On the 8th floor two uni-axial accelerometers are located at the staircase/elevator core, measuring acceleration in the N-S and E-W directions. On the 14th floor three uni-axial accelerometers are located. One is placed above the elevator core measuring acceleration in the N-S direction. It is placed more or less directly above the accelerometers on the 8th floor. The other two are located in opposite corners, one in the N-E corner and the other in the S-W corner, measuring acceleration in the E-W direction. The purpose of locating the 14th floor E-W accelerometers in opposite corners is to be able to identify the torsion of the 14th floor. Figure 3.5 shows the arrangement of the monitoring system.

Hereafter the 14th floor accelerometers may be referred to as 14th floor X component 1 or X sensor 1 (E-W accelerometer in S-W corner), 14th floor X component 2 or X sensor 2 (E-W accelerometer in N-E corner) and 14th floor Y component or Y sensor (N-S accelerometer).

The accelerometers are of the forced balance type from Kinemetrics Inc. The data acquisition system has a sampling frequency of 200 Hz and starts to collect data once the acceleration on the 14th floor reaches a certain trigger level. At first the trigger was set at 0,3% g, in February 1990 the trigger level was raised to 0,4% g and in February 1994 the trigger level was raised again to 0,5% g which is the trigger level that has been used up to the present time. The reason for those changes to the trigger level is that the available capacity to store recorded data is rather limited in the current aquistion system. If the data are not collected and cleared frequently enough from the available memory, the data acquisition system may be unable to store more data. This occures for example during wind storms, when the trigger level can be repeatedly exceeded during the duration of the storm, which may last for several hours.

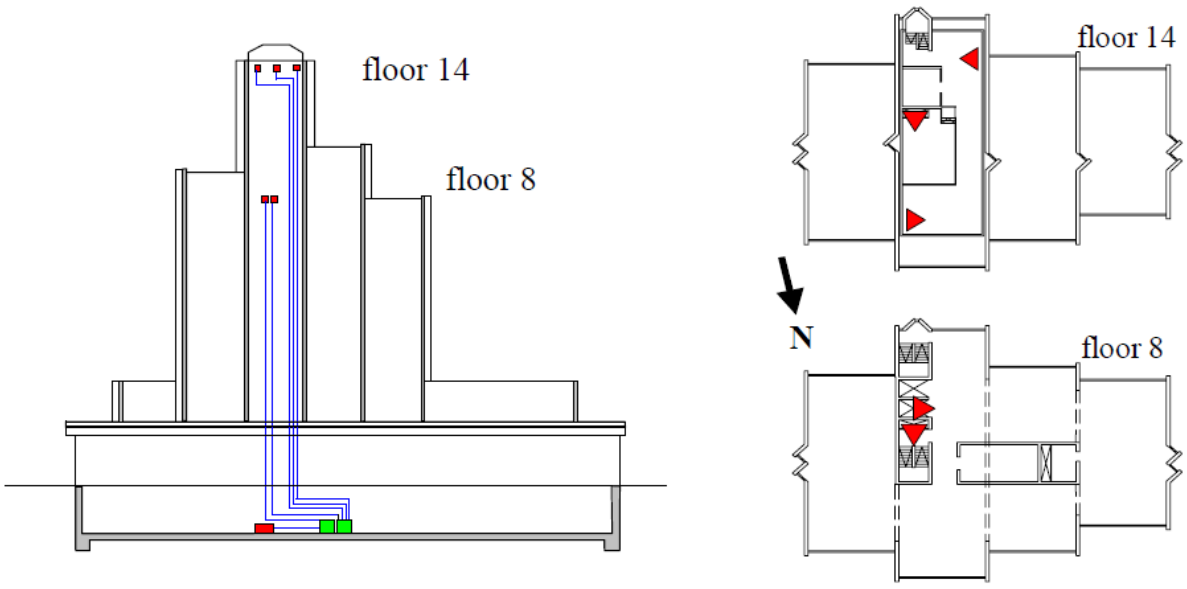

Figure 3.5: Monitoring system arrangement. Vertical section to the left and floor plans showing the location of sensors (Snæbjörnsson & Sigurbjörnsson, 2006).

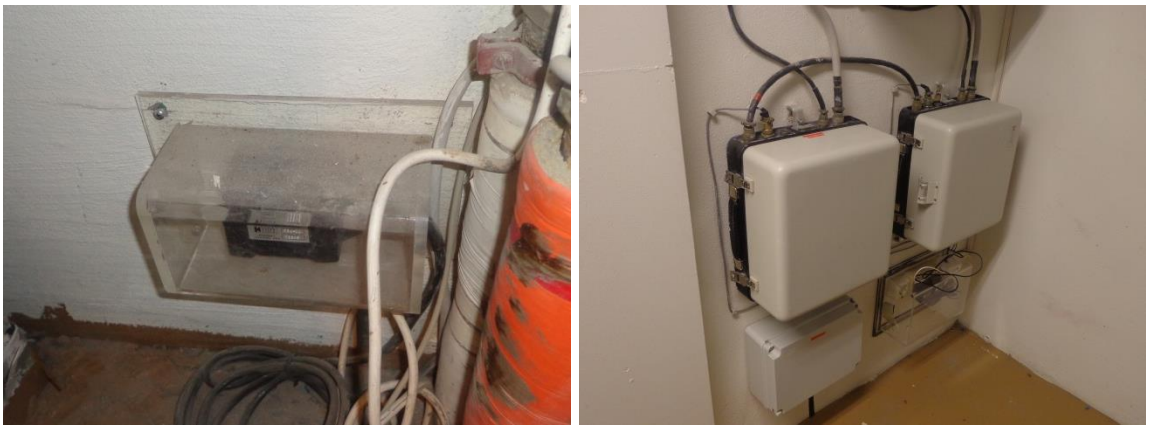

(a) **(b)**

Figure 3.6: Monitoring system. (a) Uni-axial accelerometer at the 8th floor. (b) Tri-axial accelerometer in the basement and data acquistion equipment.

3.4. Earthquake induced acceleration data and seismic information

Over the course of the last 24 years the monitoring system has recorded a great amount of earthquake induced acceleration records. The earthquakes used for analysis in this thesis are the three largest earthquakes recorded along with one aftershock earthquake that occurred 5 minutes after the largest earthquake plus four other earthquake events from recent years. The three large earthquakes all have an epicentre east-southeast of the building with a distance of 45 km or more. Therefore the other smaller earthquakes were chosen as supplementary data as their epicenters are closer to the building and from south and southwest of the building. This gives the possibility to see if there is a notable difference in the response of the building due to the different angle of incidence of the earthquake excitation. The locations of the earthquake epicenters are shown in Figure 3.7 and Figure 3.8, along with the location of the building.

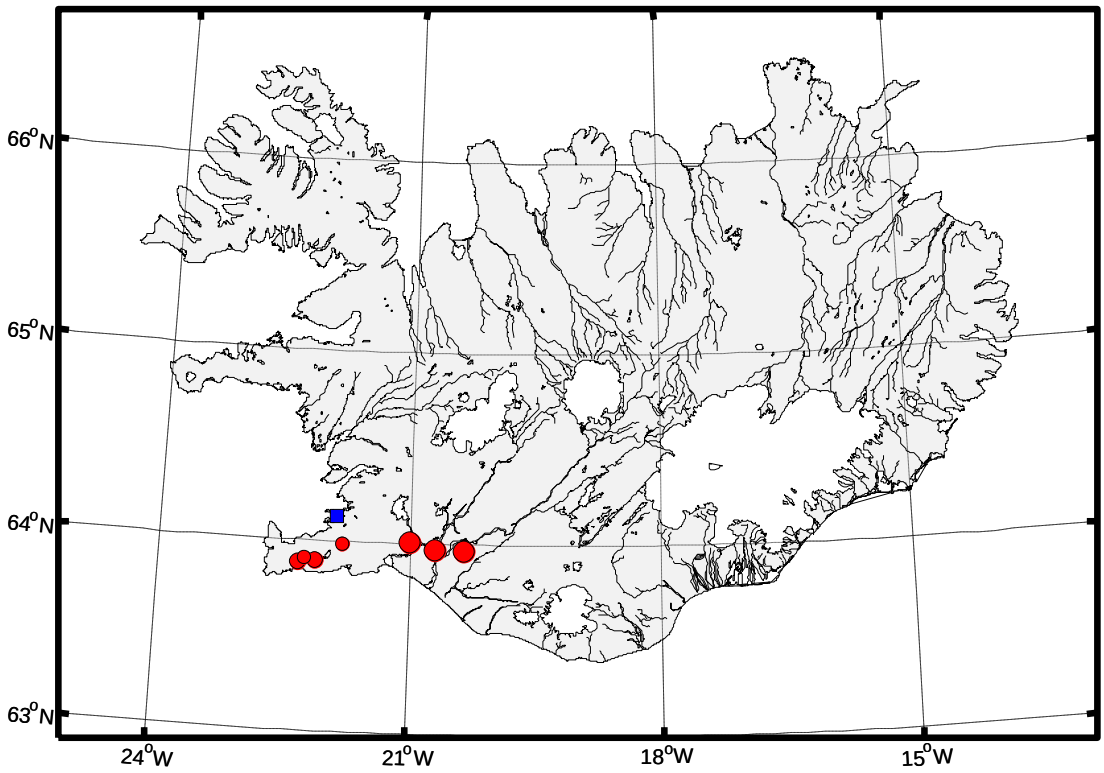

Figure 3.7: A map of Iceland showing the location of the epicentres of the chosen earthquakes (red dots) and the building observed (blue square). The size of the red dots represent the relative magnitude difference of the earthquakes.

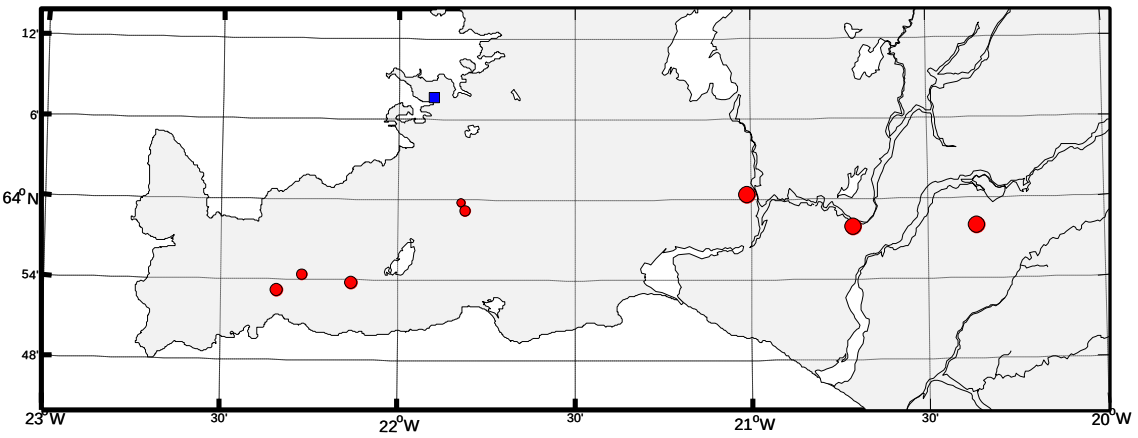

Figure 3.8: A closer view of the location of the epicentres of the chosen earthquakes (red dots) and the building observed (blue square). The size of the red dots represent the relative magnitude difference of the earthquakes.

The chosen earthquakes have a magnitude between 3,6 and 6,5. The date, magnitude and location of the earthquakes are tabulated in Table 3.2.

Table 3.2: The earthquakes chosen for further analysis

Date and time		Magnitude	Latitude	Longitude	Distance	Location descripton
		M_w	degrees	degrees	km	
17.6.2000	15:40	6,5	63,97	-20,36	76,9	East-SouthEast of building
17.6.2000	15:45	4,5	63,90	-22,13	25,7	SouthWest of building
21.6.2000	00:51	6,4	63,97	-20,71	60,5	East-SouthEast of building
29.5.2008	15:45	6,3	64,01	-21,01	45,3	East-SouthEast of building
29.5.2009	21:33	4,7	63,89	-22,34	34,4	SouthWest of building
30.5.2009	13:35	4,3	63,91	-22,27	30,6	SouthWest of building
1.3.2012	00:29	3,6	64,00	-21,82	15,1	South of building
1.3.2012	01:02	4,2	63,99	-21,81	16,3	South of building

The time series of the recorded responses were provided by the EERC-UI and further information of the earthquakes, such as magnitudes and epicentre locations were gathered from the European Strong-Motion Database website (Ambraseys, Smit, Sigbjornsson, Suhadolc, & Margaris, 2002) and the IMO website ("Archive of ShakeMaps," 2011). The highest peak acceleration recorded at the 14^{th} floor was 213,8 cm/s^2 and largest peak ground acceleration was 37,8 cm/s^2 during the main earthquake of June 17, 2000. Due to a fault in the monitoring system, the basement sensors were not active during the earthquake of May 29, 2008 and only the response acceleration at the 8^{th} and 14^{th} floor was recorded in that event.

An example of recorded earthquake induced response time series are shown in Figure 3.9. The time series are recorded during the largest earthquake, occurring June 17, 2000.

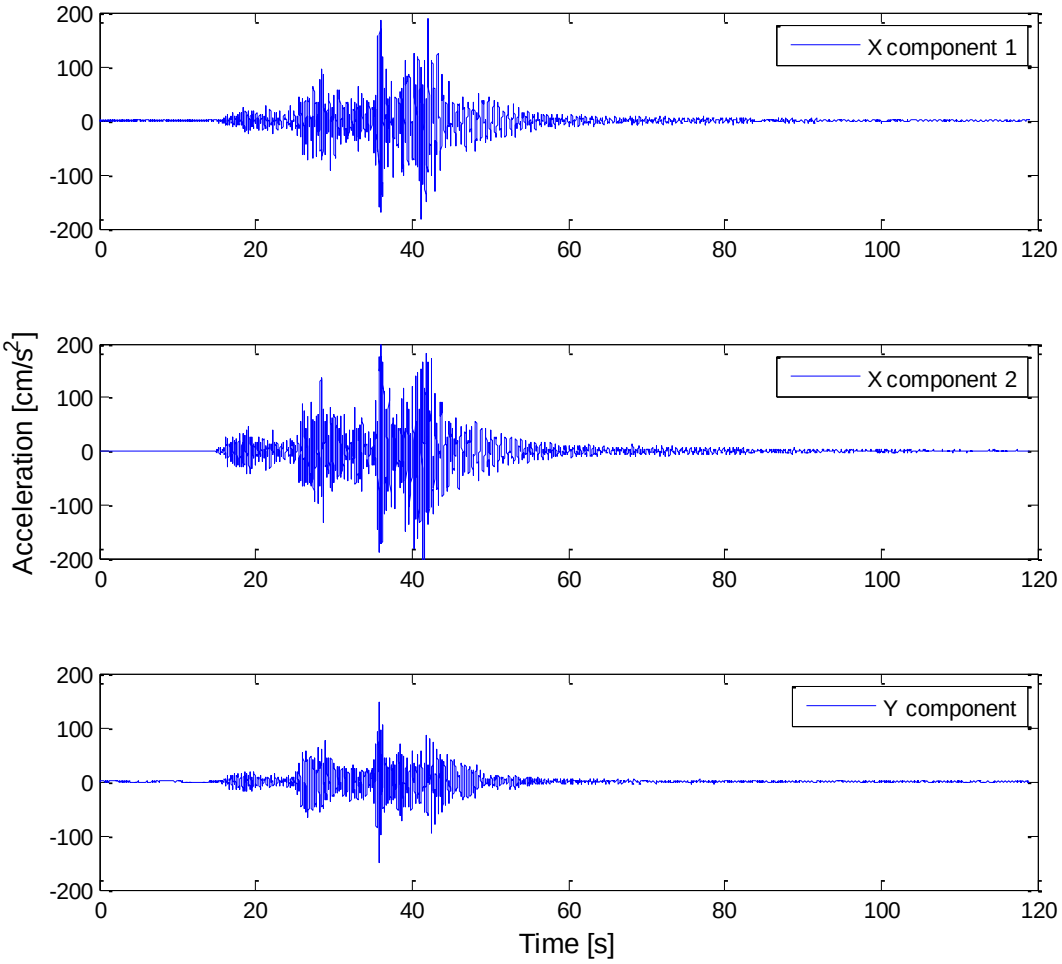

Figure 3.9: Earthquake response time series of June 17, 2000.

3.5. Wind induced acceleration data and meteorological information

During the last 24 years the monitoring system has recorded a large amount of wind induced acceleration response data. Between 1990 and 2011, 55 wind storms had triggered the monitoring system, most of them creating several recordings. The data from all except the latest four of these storms had been previously processed and linked to weather data for the given time of each storm by the supervisor of this thesis (Snæbjörnsson, 2006). For the latest 20 storms, the response time series, recorded by the monitoring system of the building, were provided by the EERC-UI. All of the recordings from those 20 storms were used in the analysis presented in the following Chapters. The highest peak to peak response of the building, recorded at the 14th floor, was 18,2 cm/s^2 in a storm that occurred January 27, 1998.

The impact of the wind induced acceleration is herein measured as peak to peak acceleration and displayed in the units of cm/s^2. When acceleration is monitored, the sampling frequency is very important. With lower sampling frequency it is likely to measure lower peak as the

sampling points are fewer, and with higher sampling frequency it is more likely to measure higher peak as there are more sampling points. Therefore it is alleged that using only a single extreme peak value for each segment or recording is not a very reliable parameter for comfort criteria evaluation.

A peak to peak measure is the difference between the highest peak to the lowest peak and with that approach the abnormal extreme high peak or low peak that could skew the time series is evened out and the resulting values should give better consistency and representation of the impact of the wind storms. An example of a peak to peak measure is shown in Figure 3.10 where the distance between the maximum value and the minimum value, shown by the red circles, is calculated.

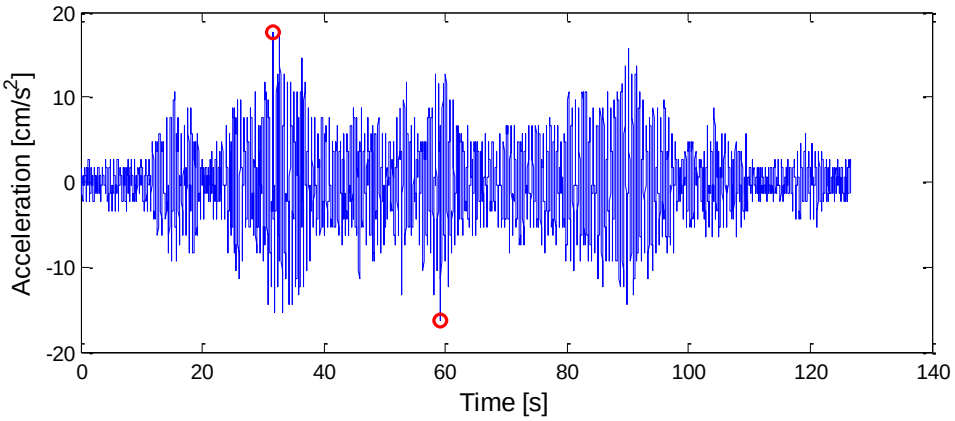

Figure 3.10: Example of the peak to peak method.

An example of a wind induced response time series are shown in Figure 3.11. The time series are recorded during the strongest storm of the monitoring period, occurring on January 27, 1998. To get an idea of the much greater intensity of the earthquake induced response recorded in the building the time series of the wind induced response in Figure 3.11 can be compared to the time series of the earthquake induced response in Figure 3.9.

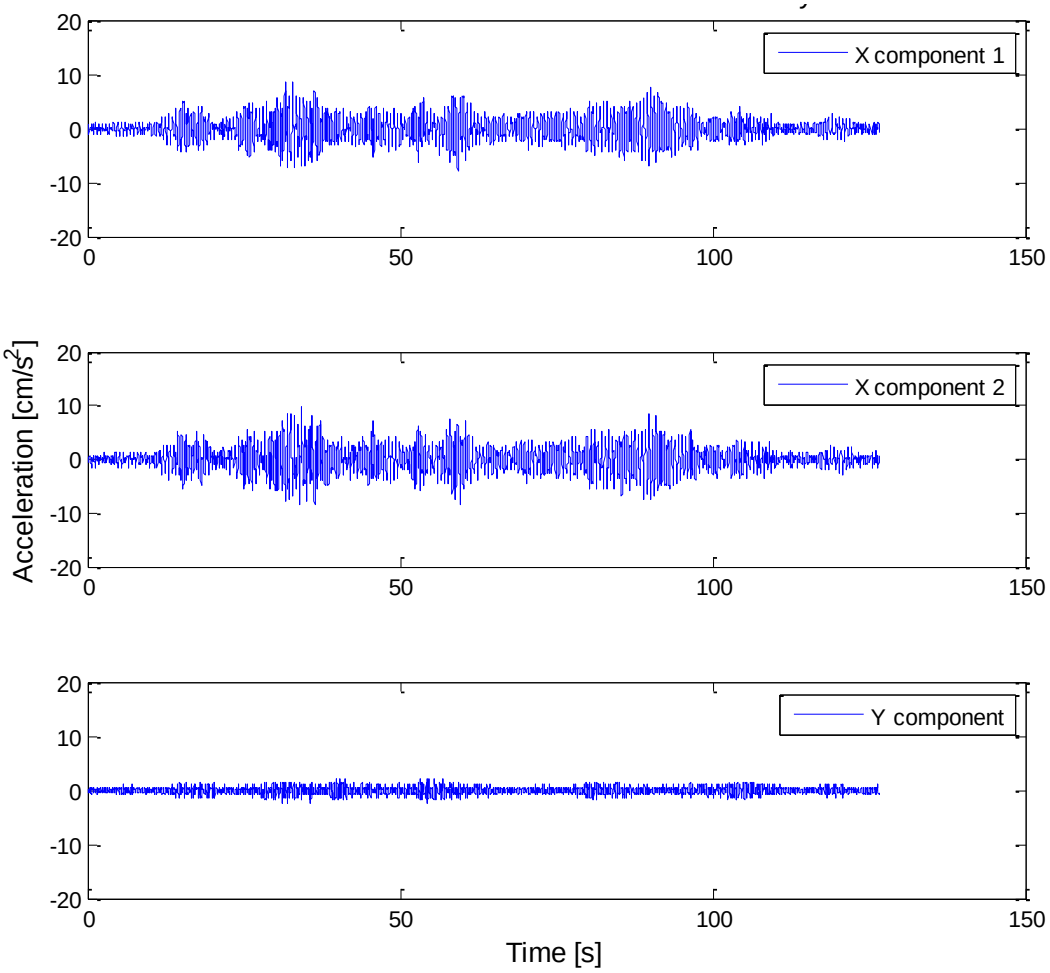

Figure 3.11: Wind induced response time series of 27. January 1998.

The building itself is not equipped with an anemometer but meteorological data were provided by the Icelandic meteorological office (IMO) located about 500 m southwest of the building. The location of the IMO in relation to the observed building is showed in Figure 3.12. The data provided are from January 1, 1990 to April 2, 2013.

The absence of a locally installed anemometer is a certain drawback as it is not possible to correlate wind velocity and acceleration response for the eddy embracing and acting on the building at the time of triggered acceleration event. The anemometer at the IMO should however give a good idea of the average and peak conditions at the building as it is located fairly close.

Figure 3.12: Aerial picture from Google Earth showing the location of the IMO anemometer mast in relation to the building. IMO mast in the lower red circle, building in the upper red circle.

The wind data used for further analysis are accumulated every third hour and contain the following information:

- The average wind direction of the first 10 minutes of every third hour at 10 m height.
- The average wind velocity of the first 10 minutes of every third hour at 10 m height.
- The maximum 10 minute average wind velocity at 10 m height during each 3 hour period.
- The maximum gust wind velocity at 10 m height during each 3 hour period.

Figure 3.13 shows the monthly and annual maximum 10 minute mean wind velocity at 10 m height. It shows a time dependent decrease in wind velocity over the past 24 years with the maximum 10 minute mean wind velocity at 10 m height undergoing a decrease of 0,3 m/s at average per year. Potentially, these changes in recorded peak wind velocity can, at least partly, be traced to increased vegetation and building density in the neighbourhood of the IMO site, influencing the surface roughness characteristics of the wind fetch and thereby affecting the wind profile.

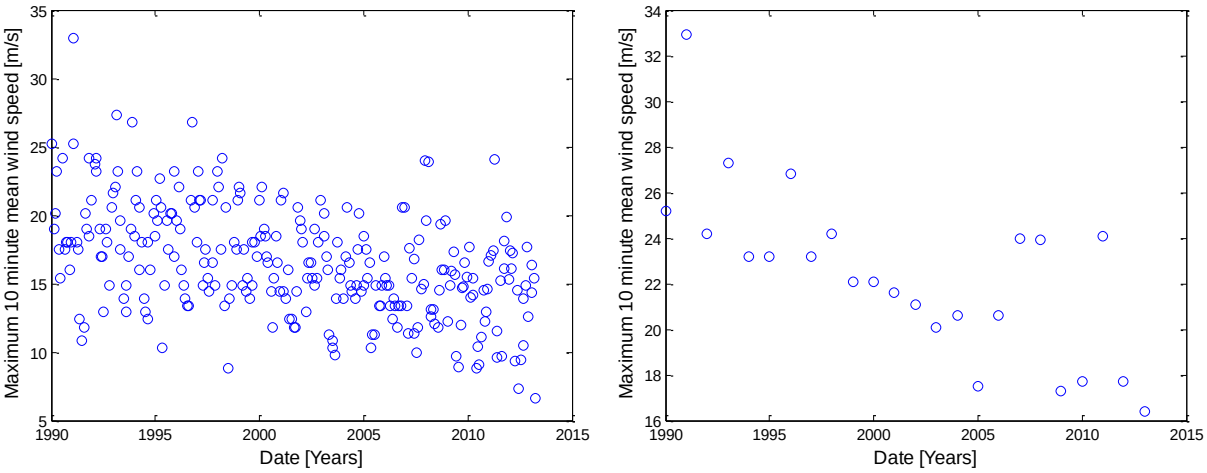

(a) **(b)**

Figure 3.13: Maximum 10 minute mean wind velocity at 10 m height during the monitoring period. (a) monthly maximum wind velocities, (b) annual maximum wind velocities.

The gust factor, the ratio of the maximum gust wind velocity and the 10 minute mean wind velocity, were evaluated for the strongest storm of each month for the entire monitoring period. The gust factors are shown in Figure 3.14 showing a slight increase over the monitoring period. The average gust factor is 1,45 and the standard deviation of the gust factors is 0,164. This increase in gust factor, and thereby turbulence intensity, is also indicative of the influence of increased vegetation and building intensity and thereby increased surface roughness in the vicinity of the IMO site.

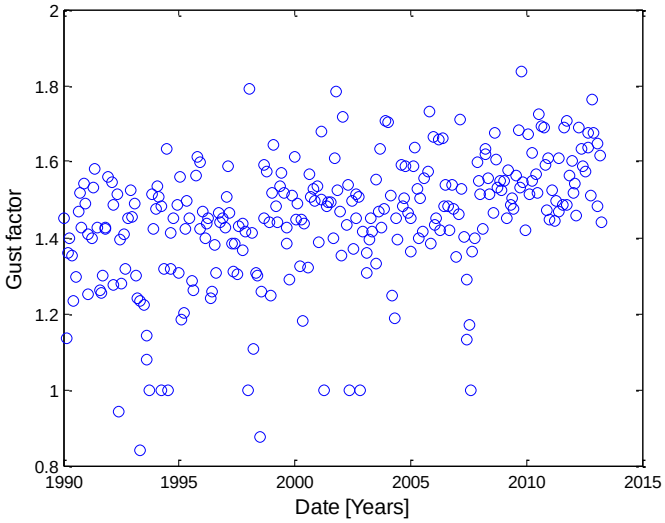

Figure 3.14: Gust factors evaluated for the strongest wind of each month.

The anticipated maximum 10 minute wind velocities at 10 m height for return periods of 1, 5, 10 and 50 years are tabulated in Table 3.3. The wind velocities of 5, 10 and 50 year return periods were evaluated from the IMO data with use of Gumbel‘s method of extreme value distribution (Holmes, 2007) but that method is not capable of predicting the 1 year return period wind velocity. Therefore, the wind velocity with an averege of 1 year return period is determined as being 62% of the 50 year return period wind velocity, in accordance with the international standard ISO 6897:1984 (Snæbjörnsson & Ingólfsson, 2013).

Table 3.3: 10 minute mean wind velocities of 1, 5 ,10 and 50 year return periods

Return period	Wind velocity
years	m/s
1	20,7
5	25,6
10	28,0
50	33,4

It should be noted that the values in Table 3.3 could be a slight overestimate of the future wind velocities as the values are evaluated from all the annual maximum wind velocities and the gradual decrease in wind velocities shown in Figure 3.13, is not taken into account.

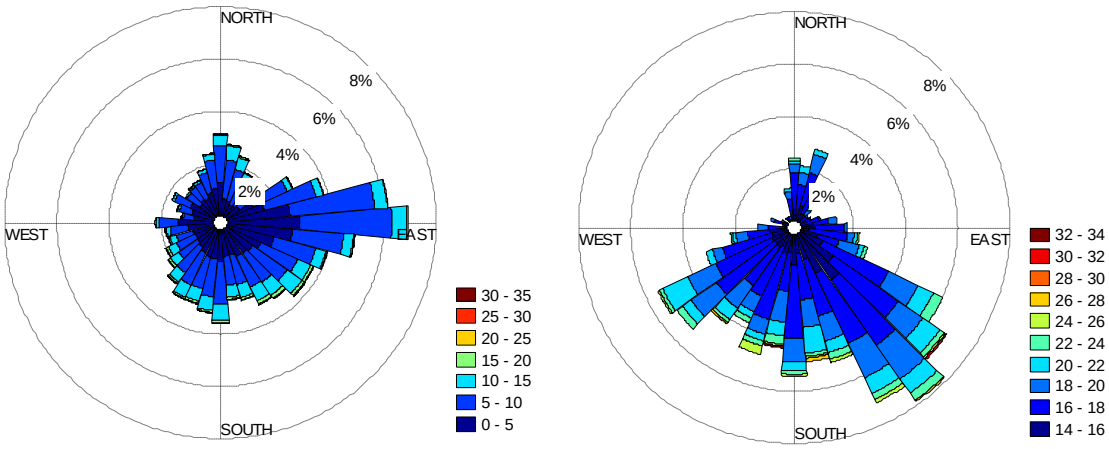

(a) **(b)**

Figure 3.15: Wind roses for the IMO site. (a) All wind velocities. (b) Wind velocities over 15 m/s.

The meteorological data shows that the most common winds at the IMO site come from the east. As shown in Figure 3.15, the stronger winds, those that are of more interest and have wind velocities over 15 m/s, are mostly from the south-west, south and south-east.

The highest maximum 10 minute average wind velocity observed at 10 m height was 32,9 m/s and occurred on February 3, 1991, between 12 and 15 pm.

4. Analysing recorded acceleration data

This chapter presents the analysis of the recorded wind and earthquake induced acceleration response of the building carried out to gain a better understanding of the behaviour of the building during wind and earthquake induced excitations. This chapter also includes the system identification process to evaluate the natural frequencies and critical damping ratio's using the time series recorded during both the wind and earthquake excitations.

4.1. Acceleration data

To gain a better understanding of the behaviour of the building, the wind induced acceleration, both in the along and across wind directions, is compared to the wind velocity at the time of the recorded response. The earthquake induced acceleration response is examined at basement level, the 8^{th} and the 14^{th} floor to evaluate the acceleration magnification along the height of the structure.

4.1.1 Wind induced acceleration.

To open the possibility to analyse the acceleration of the building in the direction of the wind, first of all the wind induced acceleration data are categorized into two groups. One category includes data recorded when the mean wind direction is within the E-W directional sector and the other category contains data recorded when the mean wind direction is within the N-S sector. The categories represent wind acting on either of the two main sides of the building, i.e. along the North-South axis or the East-West axis. Each category has a wind direction range of 45°. The categorization is shown visually in Figure 4.1. These categories capture 43 of the recorded storms and the distribution is shown in Figure 4.2. Although the categorized wind directions are only half of the possible wind directions, most of the storms that trigger the monitoring system fall into these two categories as they capture the wind directions that the building is most sensitive to, which is when the wind acts perpendicular to either face of the rectangular cross section of the building.

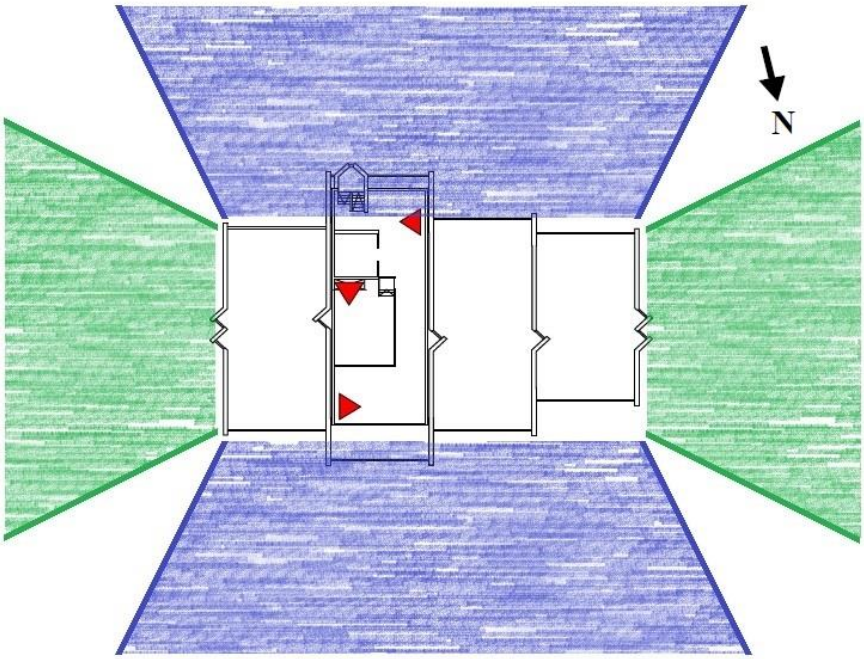

Figure 4.1: Wind directions categorized. Green zones are the E-W directions and the blue zones are the N-S directions.

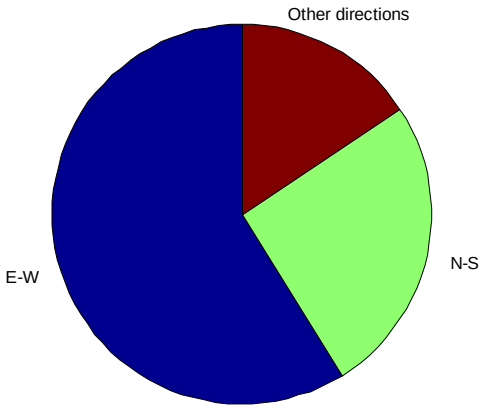

Figure 4.2: Distribution of categorized wind directions.

Although more of the stronger wind storms act in the south-west, south and south-east directions as show in Figure 3.15, most of the storms that have triggered the monitoring system act in the E-W directions. This can be explained by the characteristics of the structure, which has less resistance to vibrations in the E-W direction across the weaker axis of the top floors. This is demonstrated in chapter 5, where it is shown that the first mode of vibration is in the E-W direction. This also indicates that the building response is more sensitive to along-wind action across the wider face of the top floors, than to across wind acceleration when the wind is acting in the N-S directions.

With the wind induced acceleration categorized by wind direction, the peak to peak acceleration, along the wind direction, of each storm is compared to the maximum 10 minute mean wind velocity of the storm. The acceleration perpendicular to the wind direction, the across wind acceleration, is also an interesting thing to observe. In Figure 4.3 and Figure 4.4 both the along- and across wind acceleration is plotted against the maximum 10 minute mean wind velocity. These plots show that for wind blowing in the E-W directions, the along wind acceleration has larger impact than the across wind acceleration but with wind blowing in the N-S directions the across wind acceleration plays a bigger role. An explanation for this is the structure and geometry of the building, especially the top tower, i.e. floors 11 to 14. The stiffness of the top tower is much greater in the N-S direction than in the E-W direction. The east and west sides are significantly longer than the north and south sides, so when the wind acts on the tower from the E-W directions, the wind hits a larger area which leads to greater along wind acceleration, but when the wind acts on the tower from the N-S directions the larger surface of the east and west sides leads to a greater across wind acceleration. This is in line with the response prediction based on the design code published by the Architectural Institute of Japan (*AIJ Recommendations for Loads on Buildings*, 2005) as described in chapter 6.1.

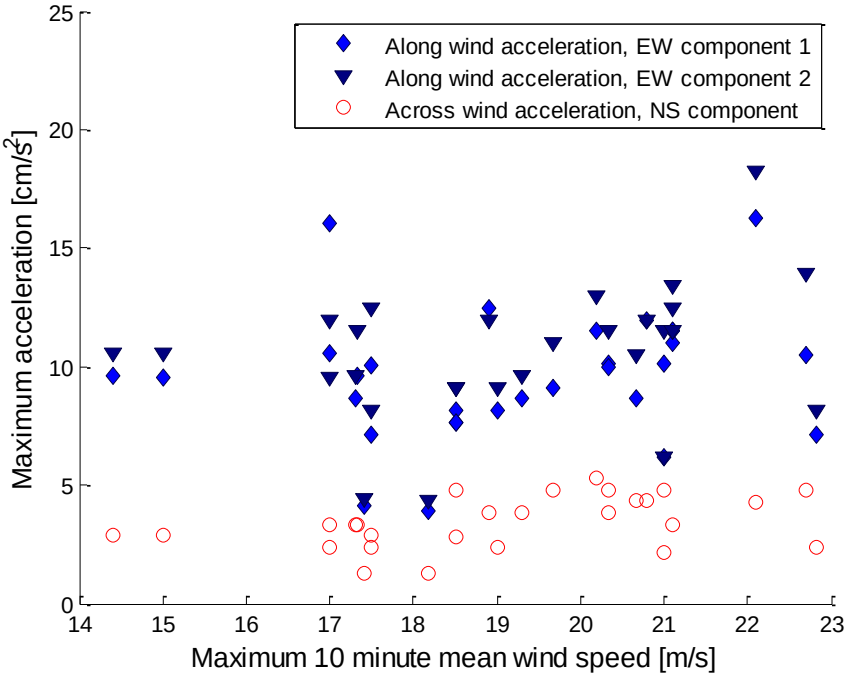

Figure 4.3: Along and across wind responses for wind acting in the E-W directions.

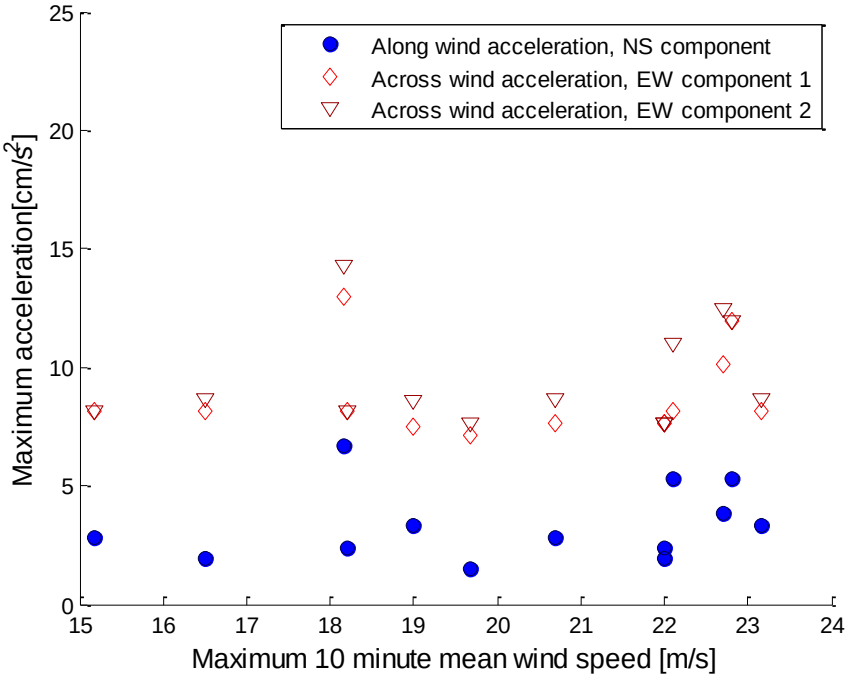

Figure 4.4: Along and across wind responses for wind acting in the N-S directions.

The ratio between the along wind acceleration and the across wind acceleration is fairly consistent for each wind direction. For wind in the E-W directions the along wind acceleration is at average roughly 3 times the across wind acceleration and for wind in the N-S directions the along wind acceleration is at average roughly one third of the across wind acceleration. The mean, maximum and minimum ratio between the along- and across wind acceleration is tabulated in Table 4.1.

Table 4.1: Along and across wind acceleration ratio

Acceleration ratio (Along/Across)		
	EW wind	NS wind
Mean	3,07	0,36
Standard deviation	0,66	0,10
Minimum	1,59	0,19
Maximum	4,98	0,65

In Figure 4.3 and Figure 4.4 the wind induced peak-to-peak acceleration levels do not show much correlation to the wind velocity, though slight correlation is noticeable for wind from the E-W directions. This can partly be explained by the wide variety of wind directions categorized as E-W direction or N-S direction, and the importance of the incidence angle for the amplitude of response. For some of the low acceleration levels recorded for high mean

wind velocities, the wind direction is far from being perpendicular to building face, similarly for some of the high acceleration levels observed for low wind velocities, the wind direction is quite close to being perpendicular to the building face.

Additional factor in explaining the lack of correlation between wind velocity and acceleration response, may be the fact that the lowest natural frequency of the building is about 1.7 Hz (see Chapter 4.2), whereas truly wind sensitive structures have a natural frequency below 1 Hz. Looking at the power spectral density function of the wind, e.g. the Eurocode spectrum as shown in Figure 4.5, it is seen that the energy of the wind has less impact on buildings with high natural frequencies than on structures with lower natural frequencies. The Smáratorg tower, which is a higher and more slender building with a natural frequency of 0,6 Hz, shows much better correlation between wind induced acceleration and wind velocity (Snæbjörnsson & Ingólfsson, 2013). When the wind power spectral density for these two buildings are plotted as a function of wind velocity, as shown in Figure 4.6, it is seen that the wind velocity has much more impact on the response of the structure with the lower natural frequency, Smáratorg tower, than on the structure with the higher frequency, i.e. the building studied.

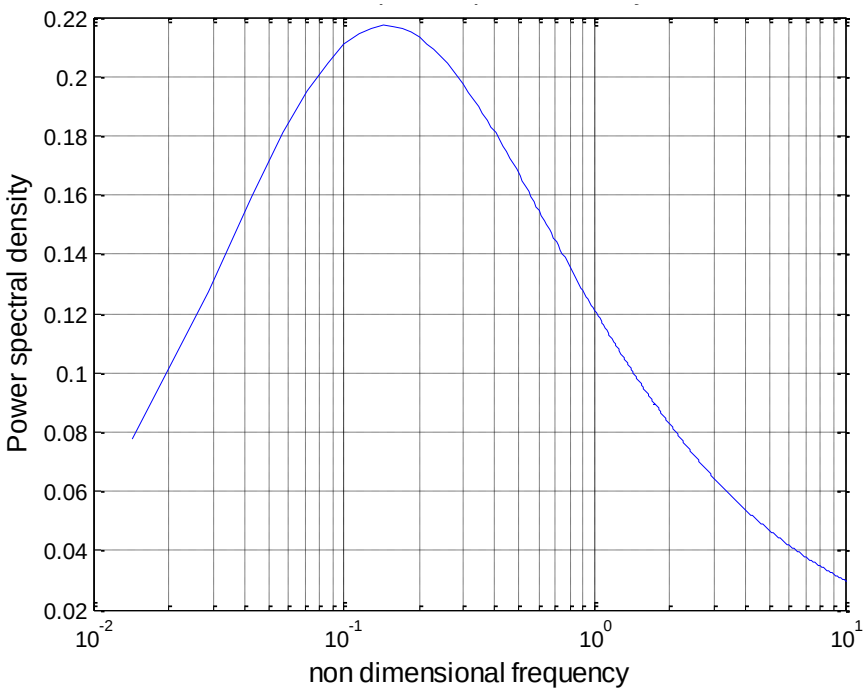

Figure 4.5: Eurocode wind power spectral density as a function of f*U/ L.

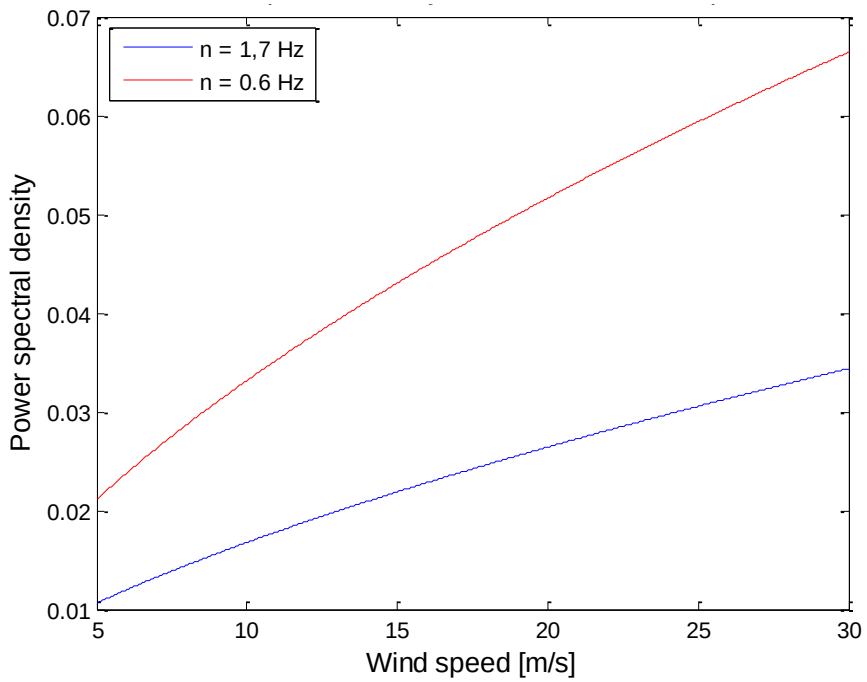

Figure 4.6: Comparison of power spectral density as a function of wind velocity for a building with natural frequency of 1,7 Hz and a building with natural frequency of 0,6 Hz.

Yet another factor of the poor correlation might be that the wind velocities are not monitored at the building itself but at the IMO site some 500 m away, as explained in Chapter 3.3. The reference wind velocity is therefore not the instantanious wind velocity at the time when the response occurs, but the maximum 10 minute mean wind velocity observed at some instance during the same 3 hour time window as the triggered recording of the acceleration response.

4.1.2 Seismic acceleration

As discussed in Chapter 3.4, eight earthquake records were selected for studying the earthquake induced response of the building. A further overview of the selected earthquakes is given in Figure 4.7 to Figure 4.9. The figures show the magnitude and recorded peak acceleration in relation to the distance to the earthquake epicenters and the peak acceleration in relation to the magnitude of the earthquakes. The acceleration values are the absolute maximum values for each direction, east-west and north-south, obtained from the time-series and the plotted values are on the one hand the peak ground acceleration recorded in the basement of the building and on the other hand the peak response acceleration recorded at the 14th floor. These values do not represent a total horizontal acceleration component but the highest value of both sensors recording in the east-west and the highest value of the north-south sensor and it should be emphasized that both of those peak values of acceleration are

not expected to occur at the exact same time. Although Figure 4.8 seems to indicate that the peak acceleration grows with longer distance to the epicenters, which is of course not the general case, it is important to see in Figure 4.7 that the earthquakes whose epicenters are the furthest away from the building were generally of greater magnitude than those with epicenters closer to the building.

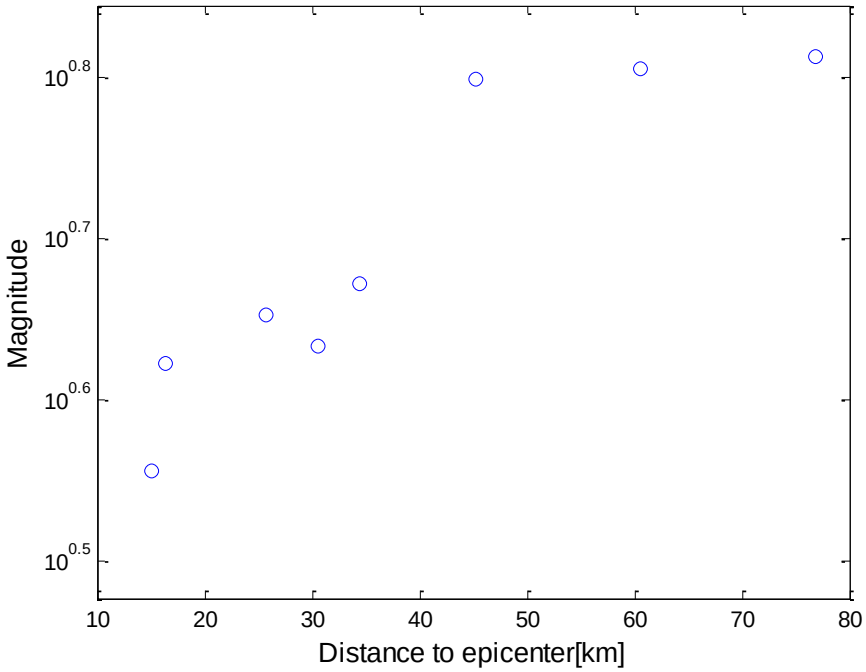

Figure 4.7: Earthquake magnitude in relation to distance to epicenters.

In Table 4-2, the peak ground acceleration and response acceleration at the 14th floor is listed. The table shows the response magnification ratio, i.e. the ratio between the peak response acceleration and the peak ground acceleration, which is ranging from 3,7 to 6,9 except for the June 17. aftershock, with an epicentre about 25 km southwest of the building, which is certainly not in line with the magnification ratios for the other selected earthquakes and has a large magnification ratio of 13,2 in the east-west direction but only 2,6 for the north-south direction. By looking closely at the time series from the June 17, aftershock it was found that the high magnification ratio is not caused by any strange or unrealistic peak. For the stronger earthquakes with epicenters southeast of the building the magnification ratio in the east – west direction is on the higher end of that range but the magnification ratio in the north – south direction on the lower range. For the weaker earthquakes with epicenters south and southwest of the building the magnification ratio in the east – west direction is on the lower end of the

range and the magnification ratio in the north south direction mostly on the higher end of the range.

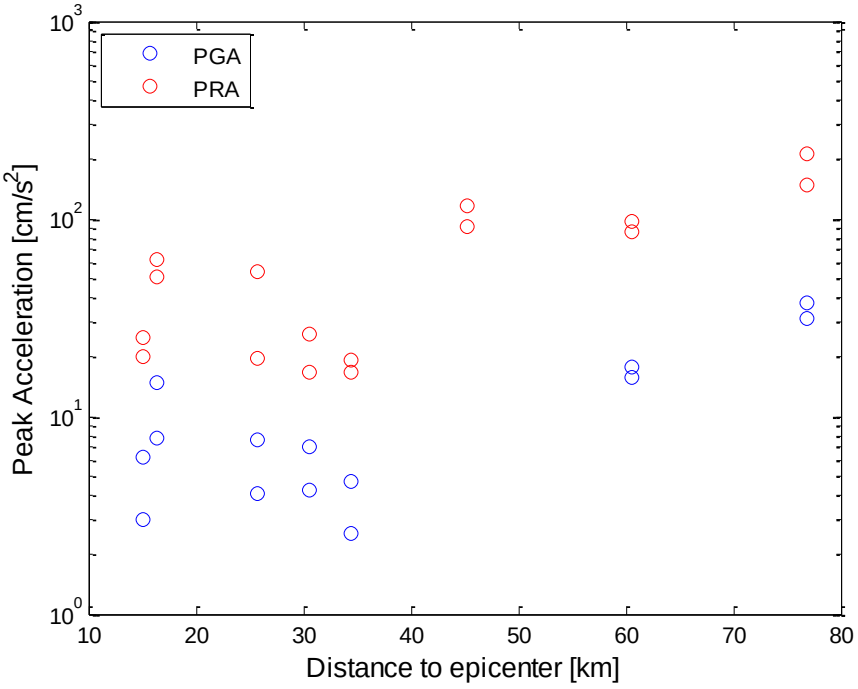

Figure 4.8: Peak acceleration in relation to distance to epicenters. Blue dots represent the peak ground acceleration and red dots represent the peak response acceleration of the top floor.

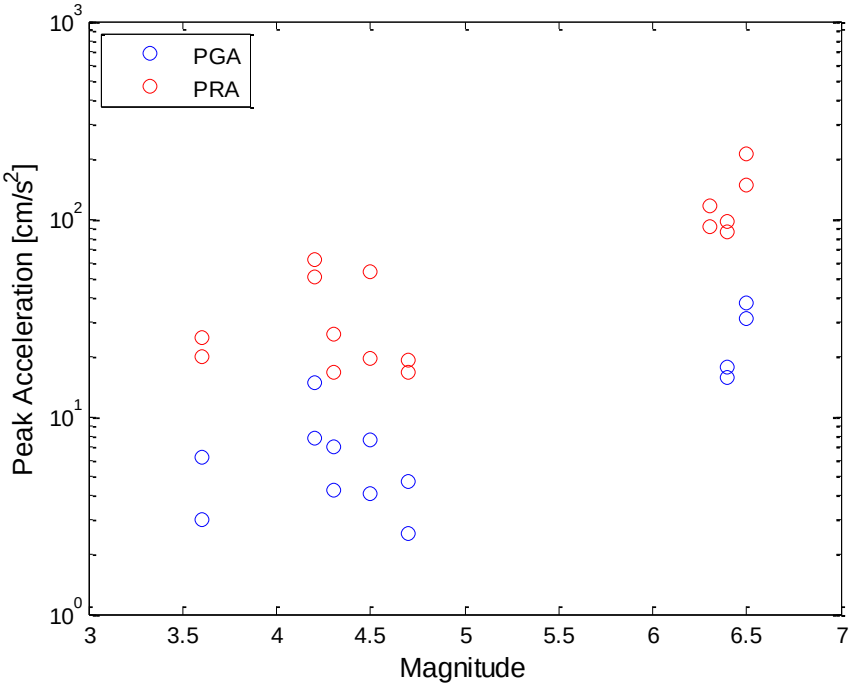

Figure 4.9: Peak acceleration in relation to earthquake magnitude. Blue dots represent the peak ground acceleration and red dots represent the peak response acceleration of the top floor.

Table 4.2: Peak acceleration at ground and at top floor and magnification ratios

Date	Magnit.	Dist.	Peak ground acc. in EW	Peak ground acc. in NS	Peak response acc. in EW	Peak response acc. in NS	Magnifi-cation ratio in EW	Magnifi-cation ratio in NS
	M_w	km	cm/s^2	cm/s^2	cm/s^2	cm/s^2		
17.6.2000	6,5	76,9	31,0	37,8	213,8	149,3	6,9	3,9
17.6.2000	4,5	25,7	4,1	7,6	53,7	19,6	13,2	2,6
21.6.2000	6,4	60,5	15,9	17,9	97,5	85,5	6,1	4,8
29.5.2008	6,3	45,3	-	-	115,5	91,5	-	-
29.5.2009	4,7	34,4	4,7	2,6	19,4	16,7	4,1	6,5
30.5.2009	4,3	30,6	7,1	4,3	26,3	16,9	3,7	4,0
1.3.2012	3,6	15,1	6,2	3,0	25,3	19,9	4,1	6,6
1.3.2012	4,2	16,3	14,7	7,8	61,9	50,6	4,2	6,5

A likely explanation for the difference in magnification ratios seen in Table 4.2, are the different mode shapes of vibration, as shown in chapter 5.2, induced by forcing in different directions as the seismic waves hit the building site.

Figure 4.10 shows the magnification of the seismic acceleration throughout the building more graphically and it also shows the magnification from the basement to the 8th floor. The colour classification of the earthquakes in the figure is made to separate the earthquakes from the east of the building, whose p-waves hit the building perpendicular to the west side of the building, from the earthquakes from south and southwest of the building, whose p-waves hit the building close perpendicular to the south side of the building. The figure does however not seem to demonstrate difference in the response of the building depending on the location of the earthquake and the directionality of the earthquake waves.

For acceleration in the east-west direction, the best fit was a quadratic curve but for the north-south direction the best fit was a straight line. This is due to the nature of the structure, as the floor plans vary with height. At the lowest floors the stiffness of an individual floor is greater in the east-west direction than the north-south direction but with increasing height the stiffness of each floor becomes greater in the north-south direction in relation to the stiffness in the east-west direction. Therefore the building is relatively stiffer in the north-south direction at the highest floors than for the lower floors which results in less acceleration magnification throughout the building in the north-south direction and therefore a semi-linear relation is seen between PGA and PRA. On the other hand the stiffness in the east-west direction becomes relatively weaker with height due to the decreasing floor width in the east-

west direction with height. Therefore the relation between PGA and PRA in the east-west direction is better represented by a quadratic curve.

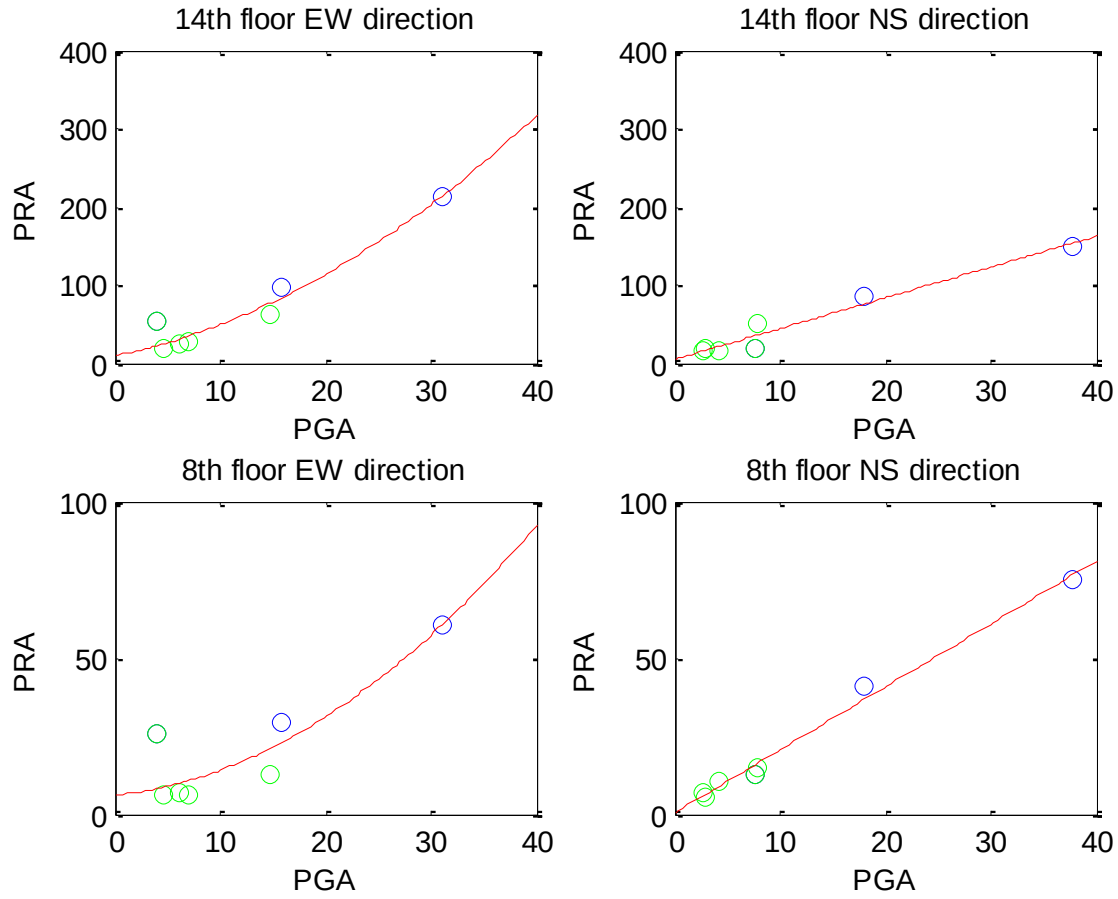

Figure 4.10: Peak response acceleration on the 8th and the 14th floor as a function of peak ground acceleration. Blue dots represent the stronger earthquakes from east of the building, green dots represent the smaller earthquakes from south and southwest of the building. Red lines are the best fit through the points.

The figure specifies even further how unique the June 17. aftershock is compared to the other earthquakes as it induces almost as much acceleration on the 8th floor in the east-west direction as an earthquake with roughly 4 times higher ground acceleration.

Using the best fit curves and lines of Figure 4.10 the PGA during the May 29. 2008 earthquake is estimated as 20,2 cm/s^2 in the east-west direction and 23,8 cm/s^2 in the north-west direction. This estimate is based on the recorded response at the 14th floor in both the east-west and north-south direction along with the recorded response in the north-west direction at the 8th floor. Unfortunately the response in the east-west direction at the 8th floor

is missing along with the ground level response, as all four channels were sampled by the same data acquisition unit.

4.2. System identification

The natural frequencies and critical damping ratios of the building were evaluated by a power spectral density analysis. The power spectral density was determined in two different ways, on the one hand with an autoregressive analysis and on the other hand with a fast Fourier transform analysis. Both methods estimate a power spectral density from the time series that the natural frequencies and critical damping ratios are evaluated from. The natural frequencies are taken at the maximum value of resonance and the critical damping ratio is evaluated with the half-power bandwidth method (Chopra, 2006).

4.2.1 Autoregressive analysis

An important factor in the autoregressive analysis is the autoregressive model order. To find an appropriate model order, an autoregressive power spectral density for a test record was evaluated using the Burg algorithm (Spyers-Ashby et al., 1998) and different model orders. The power spectral densities were plotted up and compared as shown in Figure 4.11. Based on the figure, it was decided that a model order of 500 provides acceptable accuracy, as it identifies the higher natural frequencies without showing unreal peaks.

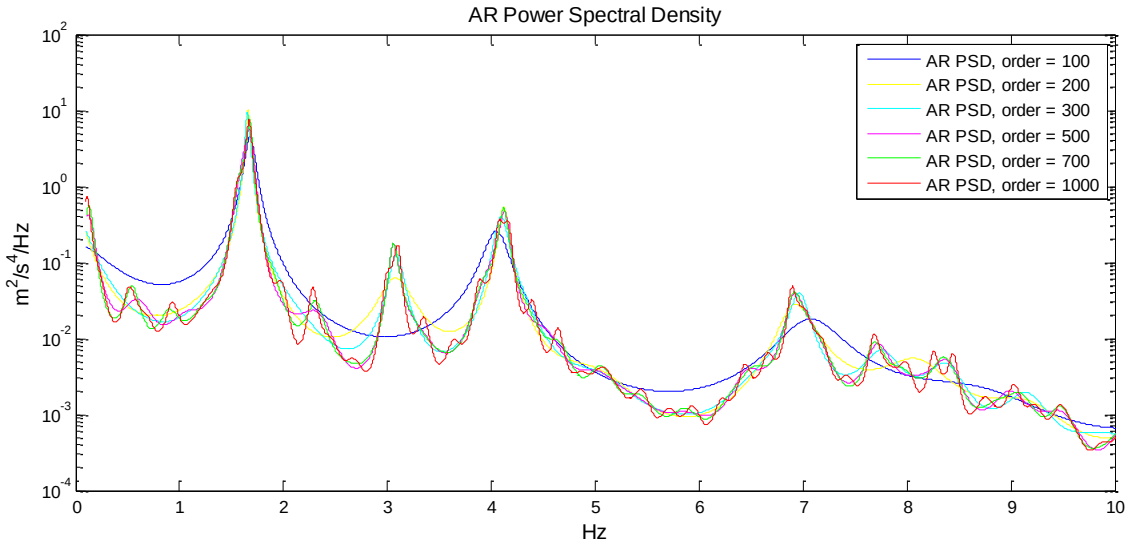

Figure 4.11: Autoregressive power spectral density of various model orders. Storm of 11. December 2008.

When looking at individual storm time-series and the natural frequency and critical damping ratio for the first mode of vibration, is estimated by an autoregressive model of various orders the results show different trends depending on the different time-series as shown in Figure 4.12. As the results do not necessarily stabilize with increasing model order, the determination of the suitable model order can be difficult.

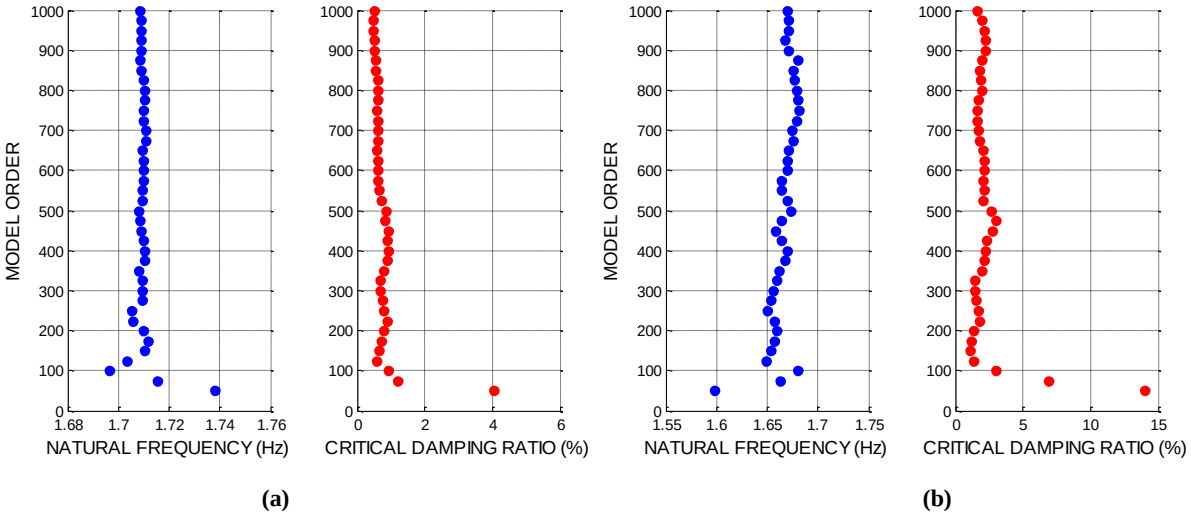

(a) **(b)**

Figure 4.12: Natural frequency and critical damping ratio of two different time series, estimated with various autoregressive model orders. (a) storm event of January 27, 1998, the strongest storm recorded, (b) storm event of December 11, 2008.

Therefore, to determine if 500 is a suitable order of the autoregressive model, the average natural frequency and critical damping ratio for the first two modes of vibration was estimated with model orders of 200 to 1000 with an interval of 25 and compared to the natural frequency and critical damping estimated by the model order of 500. The results of the comparison are shown in Table 4.3 and Table 4.4.

The comparison of the natural frequency and critical damping ratios of the autoregressive model order of 500 and the average values of natural frequency and critical damping ratios determined with the autoregressive model of order varying from 200 to 1000 is also shown graphically in Figure 4.13 and Figure 4.14.

Table 4.3: A comparison of the natural frequencies for the first two modes estimated by autoregressive model of order 500 and of order from 200 – 1000. For model order ranging from 200 – 1000 the average value is displayed.

Date	Model order of 500			Model order from 200 - 1000		
	Mode 1		Mode 2	Mode 1		Mode 2
	X Sensor 1	X Sensor 2	Y Sensor	X Sensor 1	X Sensor 2	Y Sensor
	Hz	Hz	Hz	Hz	Hz	Hz
30.12.1997	1,72	1,72	2,31	1,72	1,72	2,31
27.1.1998	1,71	1,71	2,31	1,71	1,71	2,31
3.6.1998	1,69	1,69	2,31	1,71	1,71	2,31
16.1.1999	1,72	1,73	2,33	1,73	1,72	2,33
31.12.1999	1,69	1,69	2,32	1,69	1,69	2,31
2.12.2002	1,67	1,67	2,28	1,67	1,67	2,29
2.12.2002	1,68	1,67	2,28	1,68	1,68	2,28
9.2.2003	1,68	1,68	2,27	1,68	1,68	2,28
15.2.2003	1,70	1,70	2,28	1,70	1,70	2,29
5.11.2006	1,69	1,69	2,27	1,68	1,68	2,27
21.12.2006	1,68	1,68	2,29	1,68	1,68	2,29
10.12.2007	1,70	1,70	2,31	1,70	1,70	2,31
13.12.2007	1,68	1,68	2,29	1,68	1,68	2,29
22.1.2008	1,68	1,67	2,32	1,67	1,67	2,32
8.2.2008	1,67	1,67	2,29	1,67	1,67	2,29
11.12.2008	1,67	1,68	2,27	1,67	1,67	2,26
9.10.2009	1,66	1,66	2,27	1,67	1,67	2,26
5.3.2011	1,65	1,66	2,26	1,65	1,66	2,09
10.4.2011	1,66	1,64	2,25	1,65	1,64	2,25
8.10.2011	1,65	1,65	2,25	1,65	1,65	2,25
Average	**1,68**	**1,68**	**2,29**	**1,68**	**1,68**	**2,28**
Median	1,68	1,68	2,29	1,68	1,68	2,29
Standard deviation	0,02	0,02	0,02	0,02	0,02	0,05

Table 4.4: A comparison of the critical damping ratios for the first two modes estimated by autoregressive model of order 500 and of order from 200 – 1000. For model order ranging from 200 – 1000 the average is displayed.

	Model order of 500			Model order from 200 - 1000		
	Mode 1		Mode 2	Mode 1		Mode 2
Date	**X Sensor 1**	**X Sensor 2**	**Y Sensor**	**X Sensor 1**	**X Sensor 2**	**Y Sensor**
	Damping %	Damping %	Damping %	Damping %	Damping %	Damping %
30.12.1997	0,94	0,98	2,34	1,46	1,46	1,65
27.1.1998	0,94	0,86	2,39	0,67	0,67	1,51
3.6.1998	0,96	0,83	8,64	3,03	2,90	2,17
16.1.1999	1,60	1,57	2,03	1,14	1,13	1,59
31.12.1999	1,03	0,86	1,12	0,45	0,46	1,39
2.12.2002	0,52	0,55	1,50	0,55	0,59	1,42
2.12.2002	2,50	2,88	0,49	0,80	0,83	1,62
9.2.2003	0,85	0,82	8,59	0,58	0,56	0,74
15.2.2003	1,44	1,21	1,09	0,83	0,84	0,78
5.11.2006	1,18	1,39	3,51	2,48	2,26	1,64
21.12.2006	0,70	0,68	1,40	0,54	0,50	0,74
10.12.2007	1,61	1,64	7,10	1,28	1,02	0,84
13.12.2007	1,36	1,59	7,04	1,75	1,38	0,64
22.1.2008	0,81	0,83	1,26	0,75	0,59	0,69
8.2.2008	1,57	1,37	1,62	1,05	1,04	0,55
11.12.2008	1,25	1,34	1,46	1,95	1,85	1,27
9.10.2009	1,54	1,55	1,62	1,51	1,50	1,15
5.3.2011	8,40	1,51	8,58	2,87	1,51	2,75
10.4.2011	1,50	1,65	4,01	2,80	1,50	1,55
8.10.2011	1,94	2,06	1,47	1,02	0,92	1,37
Average	**1,63**	**1,31**	**3,36**	**1,38**	**1,18**	**1,30**
Median	1,31	1,35	1,83	1,09	1,03	1,38
Standard deviation	1,62	0,53	2,81	0,82	0,62	0,54

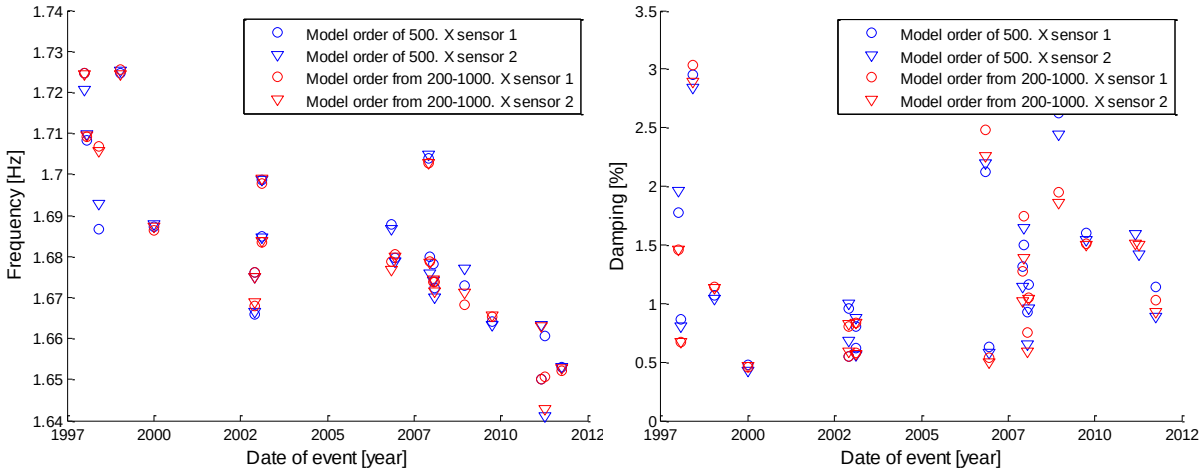

(a) **(b)**

Figure 4.13: Comparison of (a) natural frequencies and (b) critical damping ratios for the first mode of vibration.

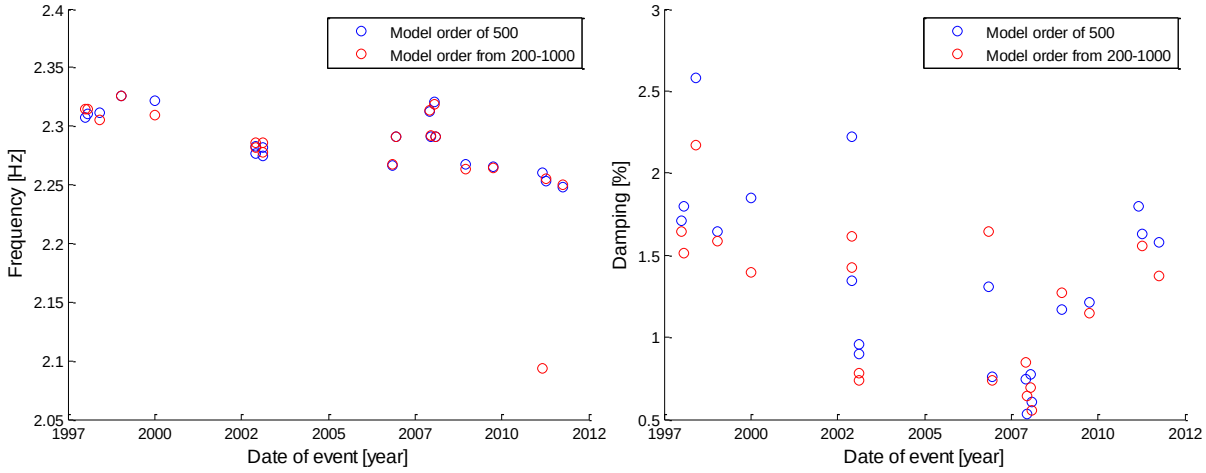

(a) **(b)**

Figure 4.14: Comparison of (a) natural frequencies and (b) critical damping ratios for the second mode of vibration.

Tables 4.3 and 4.4, along with Figures 4.13 and 4.14 verify that a model order of 500 is suitable for further use and it is therefore used to estimate the natural frequencies and critical damping ratios of the first six modes of vibration of the structure. There are however a few anomalies in the natural frequencies as seen in Figure 4.13 and Figure 4.14, most noteworthy in the results of time series from 5. March 2011 where the average of the results of model order ranging from 200 to 1000 is a bit off in comparison to the results of model order of 500. When looking at the analysis of that particular time series it is seen that the natural frequency for the second mode of vibration is, for unknown reason, quite dramatically lower than the

anticipated value for model order from 200 to 400, which skews the average a bit. This is shown in Figure 4.15.

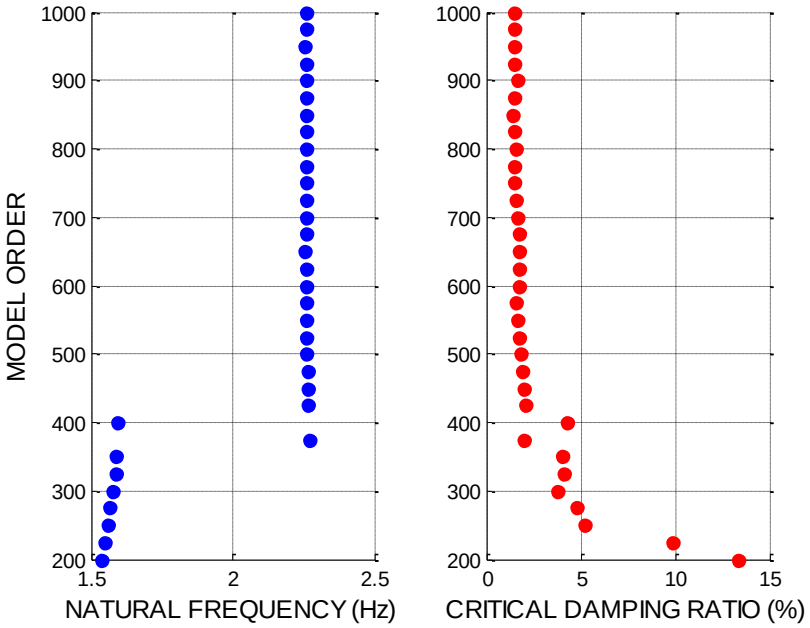

Figure 4.15: Natural frequency and critical damping for the second mode of vibration analysed by the autoregressive analysis for model order varying from 200 – 1000 of a time series of 5. March 2011.

The modes of vibration are not all detected with the same degree of accuracy by all of the 14th floor sensors. This is due to the different forcing characteristics of the excitation. The first mode is detected by the X components, the second mode by the Y component, the third mode is detected by all three sensors, the forth mode is detected by the X component and the fifth and sixth mode is detected by all three sensors. Where the natural frequency and critical damping ratio is detected by more than one sensor, the results are displayed separately.

When looking at the standard deviation of the natural frequencies and critical damping ratio for various model orders from 200 to 1000, both cases show a slight trend of decrease in variance with longer duration of the recorded time series. The difference in variance of the results depending on the model order as shown in Figure 4.12 could therefore be related to the difference in duration, as the time series from the storm in January 1998 has about 1.77 times longer duration, and therefore much more data points than the time series recorded in a storm in December 2008.

The standard deviation of the natural frequencies and critical damping ratio for model orders from 200 to 1000 for the first and second mode of vibration as a function of time series duration are shown in Figure 4.16 and Figure 4.17 respectively.

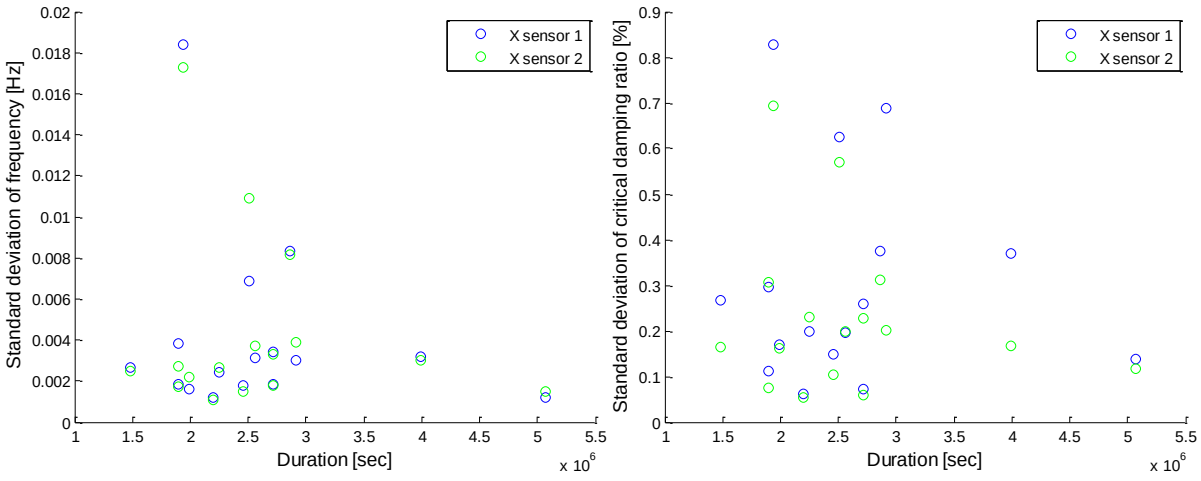

(a) **(b)**

Figure 4.16: Standard deviation of (a) natural frequencies and (b) critical damping ratios for model order for various model orders for the first mode of vibration.

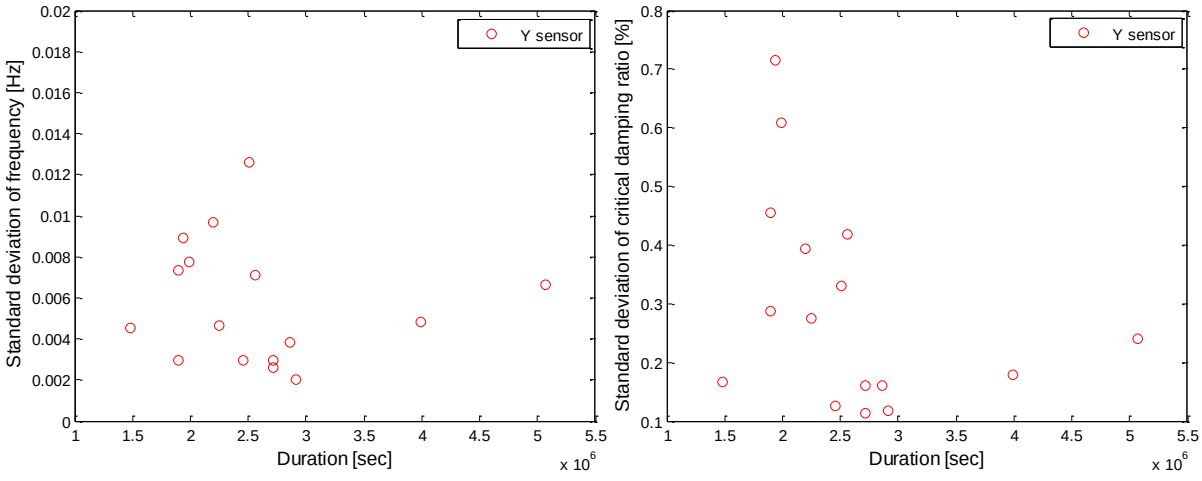

(a) **(b)**

Figure 4.17: Standard deviation of (a) natural frequencies and (b) critical damping ratios for model order for various model orders for the second mode of vibration.

In Table 4.5 and Table 4.6 the natural frequencies and critical damping ratios for the first six modes of vibration are listed, estimated by an autoregressive spectral analysis using a model of order 500 for all time-series from 1997 to 2011. Where the mode of vibration is detected by multiple sensors the tables show the average of the results from the sensors that detect the mode of vibration depending on the particular mode shape as explained earlier in this chapter.

The natural frequencies and critical damping ratios of the first six modes of vibration are also shown graphically in Figures 4.19 through 4.23, as a function of the date of the storm events. The figures display the results separately for each mode of vibration and the particular sensor that is able to detect that specific mode of vibration.

Table 4.5: Natural frequencies of the first six modes of vibration evaluated by the autoregressive analysis

Date	Mode 1	Mode 2	Mode 3	Mode 4	Mode 5	Mode 6
	Hz	Hz	Hz	Hz	Hz	Hz
30.12.1997	1,72	2,31	3,14	4,23	7,17	7,85
27.1.1998	1,71	2,31	3,15	4,22	7,11	7,78
3.6.1998	1,69	2,31	3,17	4,15	7,11	8,15
16.1.1999	1,73	2,33	3,16	4,23	7,27	7,86
31.12.1999	1,69	2,32	3,13	4,22	6,94	7,80
2.12.2002	1,67	2,28	3,10	4,17	7,04	7,72
2.12.2002	1,68	2,28	3,08	4,15	6,89	7,74
9.2.2003	1,68	2,27	3,12	4,17	7,11	7,83
15.2.2003	1,70	2,28	3,13	4,15	6,96	7,81
5.11.2006	1,69	2,27	3,08	4,13	6,94	7,89
21.12.2006	1,68	2,29	3,08	4,15	6,97	7,75
10.12.2007	1,70	2,31	3,13	4,21	6,97	7,89
13.12.2007	1,68	2,29	3,13	4,17	7,03	7,97
22.1.2008	1,68	2,32	3,12	4,19	7,03	7,72
8.2.2008	1,67	2,29	3,13	4,13	6,95	7,81
11.12.2008	1,67	2,27	3,08	4,12	6,92	7,71
9.10.2009	1,66	2,27	3,05	4,15	6,90	7,77
5.3.2011	1,66	2,26	3,07	4,10	6,39	7,78
10.4.2011	1,65	2,25	3,07	4,06	6,83	7,72
8.10.2011	1,65	2,25	3,04	4,11	6,87	7,70
Average	**1,68**	**2,29**	**3,11**	**4,16**	**6,97**	**7,81**
Median	1,68	2,29	3,12	4,15	6,97	7,79
Standard deviation	0,02	0,02	0,04	0,04	0,17	0,10

Table 4.6: Critical damping ratios of the first six modes of vibration evaluated by the autoregressive analysis

Date	Mode 1	Mode 2	Mode 3	Mode 4	Mode 5	Mode 6
	%	%	%	%	%	%
30.12.1997	1,87	1,71	1,42	0,96	5,01	4,96
27.1.1998	0,83	1,80	1,44	0,90	3,89	9,08
3.6.1998	2,90	2,58	1,31	0,90	5,34	3,17
16.1.1999	1,06	1,64	1,31	1,59	2,62	4,10
31.12.1999	0,45	1,85	1,47	0,94	1,10	4,01
2.12.2002	0,61	1,34	0,53	0,53	2,76	6,17
2.12.2002	0,98	2,22	2,47	2,69	0,50	5,65
9.2.2003	0,59	0,96	1,25	0,84	6,39	4,42
15.2.2003	0,84	0,90	2,37	1,33	1,15	2,56
5.11.2006	2,16	1,31	1,24	1,29	4,84	4,71
21.12.2006	0,60	0,76	1,54	0,69	4,00	5,75
10.12.2007	1,23	0,75	1,05	1,62	4,05	3,88
13.12.2007	1,57	0,53	1,16	1,48	3,78	4,45
22.1.2008	0,79	0,78	0,64	0,82	2,12	7,24
8.2.2008	1,06	0,61	1,10	1,47	1,53	5,50
11.12.2008	2,53	1,17	1,56	1,29	3,30	4,20
9.10.2009	1,57	1,21	1,13	1,54	3,31	8,06
5.3.2011	2,43	1,79	2,46	4,95	7,45	1,81
10.4.2011	2,26	1,63	1,24	1,57	3,64	5,42
8.10.2011	1,01	1,58	1,43	2,00	1,46	2,99
Average	**1,37**	**1,36**	**1,41**	**1,47**	**3,41**	**4,91**
Median	1,06	1,33	1,31	1,31	3,47	4,58
Standard deviation	0,73	0,54	0,50	0,94	1,78	1,75

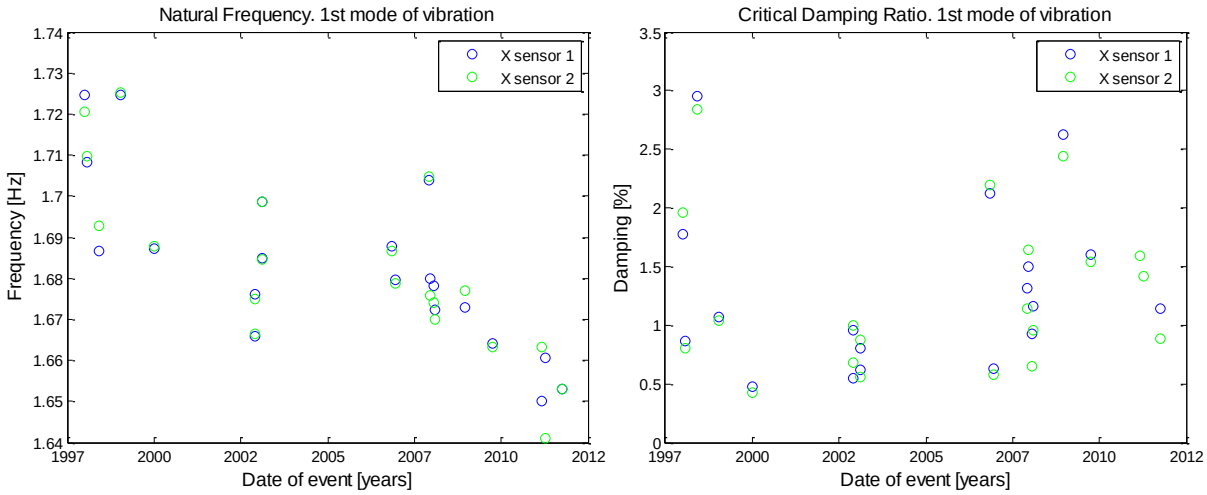

Figure 4.18: Natural frequencies and critical damping ratios for the first mode of vibration evaluated by the autoregressive analysis.

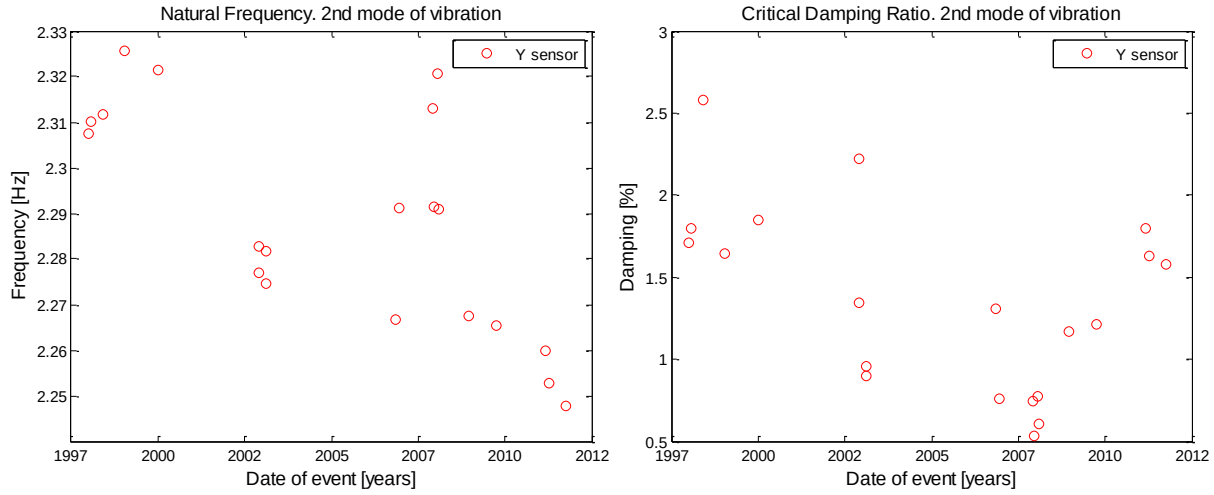

Figure 4.19: Natural frequencies and critical damping ratios for the second mode of vibration evaluated by the autoregressive analysis.

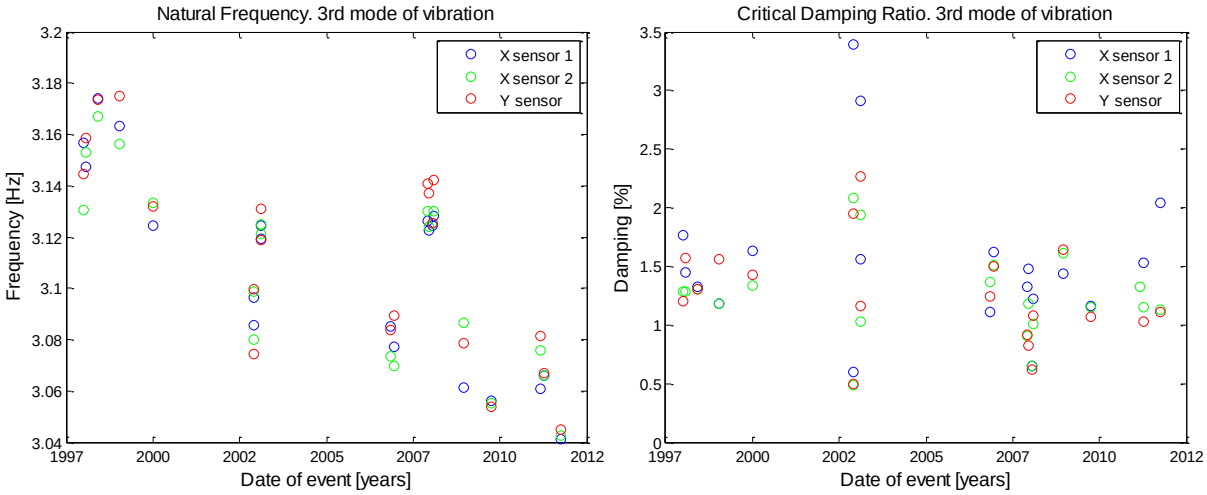

Figure 4.20: Natural frequencies and critical damping ratios for the third mode of vibration evaluated by the autoregressive analysis.

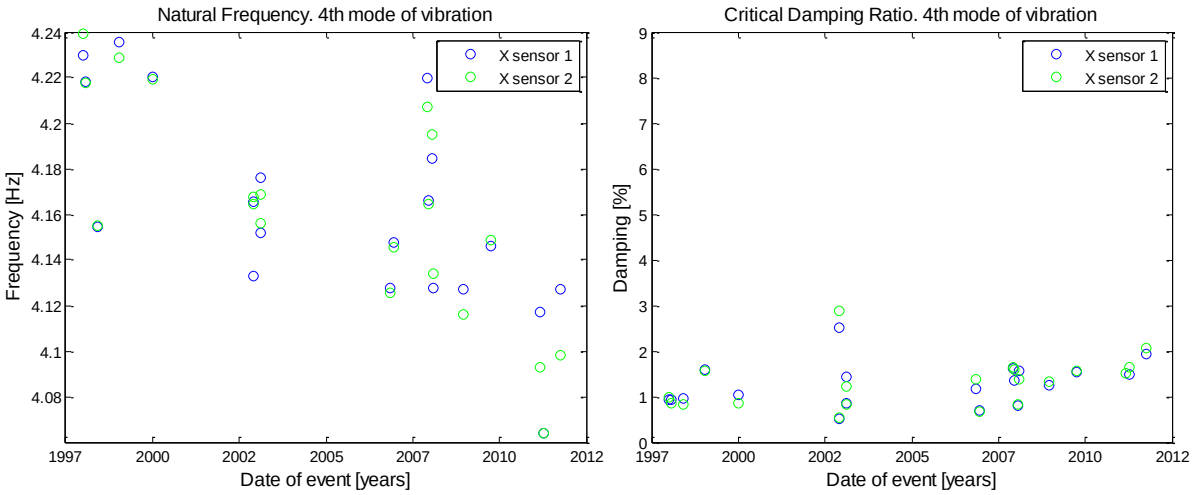

Figure 4.21: Natural frequencies and critical damping ratios for the fourth mode of vibration evaluated by the autoregressive analysis.

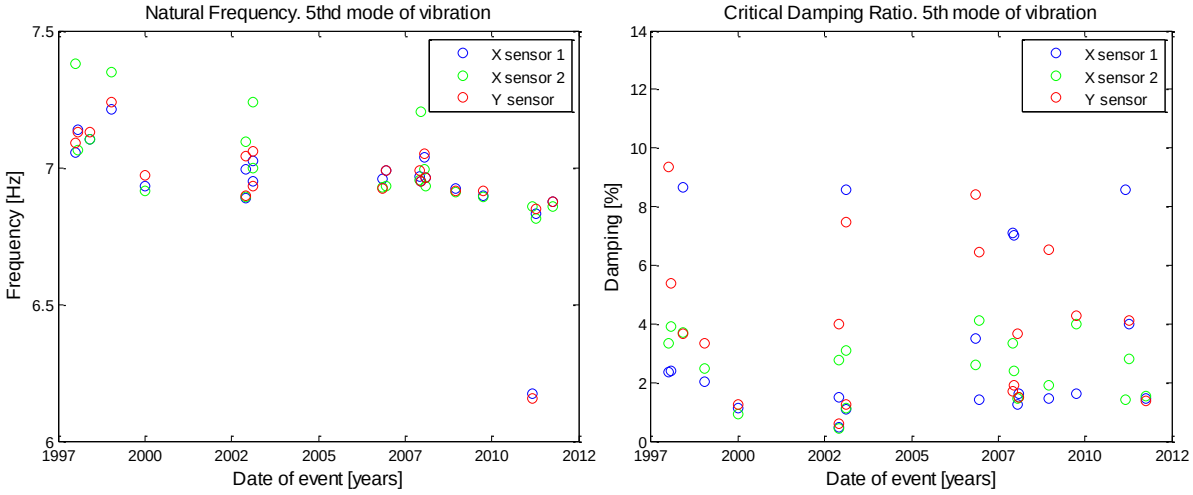

Figure 4.22: Natural frequencies and critical damping ratios for the fifth mode of vibration evaluated by the autoregressive analysis.

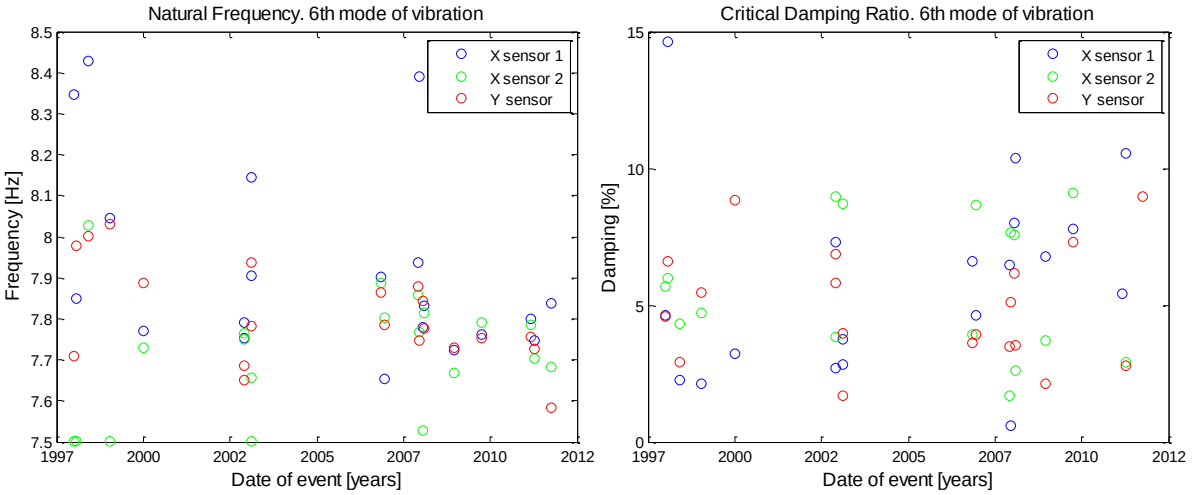

Figure 4.23: Natural frequencies and critical damping ratios for the sixth mode of vibration evaluated by the autoregressive analysis.

4.2.2 Fast Fourier transform analysis

In the fast Fourier transform the power spectral density is estimated with the Welch method where the each time-series is divided into segments with an overlap of 50%. A power spectral density is evaluated from 8192 sample points of each segment and then averaged to get the final power spectral density of the time-series (Alkan & Yilmaz, 2007). The natural frequencies and critical damping ratios, evaluated by the fast Fourier transform analysis are listed in Table 4.7 and Table 4.8. Where multiple sensors detected a mode of vibration the results were averaged as before.

The natural frequencies and critical damping ratios of the first six modes of vibration are also shown graphically in the Figures 4.24 through 4.29, as a function of the date of the storm events. The figures display the results separately for each mode of vibration and the particular sensor that is able to detect that specific mode of vibration.

Table 4.7: Natural frequencies of the first six modes of vibration evaluated by the fast Fourier transform analysis

Date	Mode 1	Mode 2	Mode 3	Mode 4	Mode 5	Mode 6
	Hz	Hz	Hz	Hz	Hz	Hz
30.12.1997	1,73	2,32	3,15	4,25	7,16	7,76
27.1.1998	1,71	2,32	3,17	4,20	7,10	7,83
3.6.1998	1,71	2,29	3,17	4,17	7,13	8,03
16.1.1999	1,73	2,32	3,15	4,22	7,26	8,01
31.12.1999	1,68	2,29	3,10	4,22	6,94	7,80
2.12.2002	1,66	2,29	3,10	4,17	7,03	7,76
2.12.2002	1,68	2,27	3,10	4,15	6,88	7,76
9.2.2003	1,68	2,27	3,13	4,15	7,10	7,83
15.2.2003	1,71	2,29	3,14	4,16	6,97	7,93
5.11.2006	1,68	2,27	3,08	4,13	7,03	7,85
21.12.2006	1,68	2,29	3,09	4,15	6,99	7,83
10.12.2007	1,71	2,32	3,13	4,20	6,98	7,87
13.12.2007	1,68	2,29	3,13	4,15	7,01	7,98
22.1.2008	1,68	2,32	3,13	4,17	7,03	7,71
8.2.2008	1,68	2,29	3,15	4,15	6,94	7,80
11.12.2008	1,68	2,27	3,10	4,10	6,91	7,71
9.10.2009	1,66	2,27	3,05	4,15	6,92	7,76
5.3.2011	1,67	2,27	3,08	4,10	6,62	7,76
10.4.2011	1,64	2,25	3,05	4,04	6,82	7,75
8.10.2011	1,66	2,22	3,05	4,10	6,88	7,67
Average	**1,69**	**2,29**	**3,11**	**4,16**	**6,99**	**7,82**
Median	1,68	2,29	3,11	4,15	6,99	7,80
Standard deviation	0,02	0,03	0,04	0,05	0,13	0,10

Table 4.8: Critical damping ratios of the first six modes of vibration evaluated by the fast Fourier transform analysis

Date	Mode 1	Mode 2	Mode 3	Mode 4	Mode 5	Mode 6
	%	%	%	%	%	%
30.12.1997	3,55	2,71	2,55	1,72	4,33	8,29
27.1.1998	1,72	2,23	1,57	1,47	2,97	3,59
3.6.1998	5,81	4,54	2,85	2,26	6,50	6,57
16.1.1999	4,26	3,49	3,28	2,19	3,33	5,48
31.12.1999	3,45	3,23	3,78	2,01	1,48	5,82
2.12.2002	3,40	3,19	1,94	1,49	3,08	7,31
2.12.2002	3,87	3,37	4,99	2,54	1,31	5,44
9.2.2003	2,83	2,24	2,12	1,43	6,39	3,80
15.2.2003	4,27	2,90	6,15	2,17	1,99	3,68
5.11.2006	4,30	3,20	2,40	1,71	4,22	3,36
21.12.2006	3,12	2,41	2,69	1,63	4,21	4,92
10.12.2007	2,14	2,05	1,89	1,20	2,60	5,70
13.12.2007	3,44	2,17	1,79	1,85	5,41	2,88
22.1.2008	5,11	3,65	3,01	2,55	3,38	5,46
8.2.2008	3,28	2,07	2,26	2,14	2,15	6,07
11.12.2008	3,57	2,35	2,69	1,75	2,57	5,79
9.10.2009	1,66	1,30	0,68	1,75	3,14	3,56
5.3.2011	3,44	1,33	3,93	1,33	6,44	10,10
10.4.2011	2,35	0,96	1,40	1,73	5,01	3,55
8.10.2011	1,89	1,89	0,87	2,44	1,19	3,67
Average	**3,37**	**2,56**	**2,64**	**1,87**	**3,58**	**5,25**
Median	3,44	2,38	2,48	1,75	3,23	5,45
Standard deviation	1,06	0,87	1,29	0,39	1,64	1,81

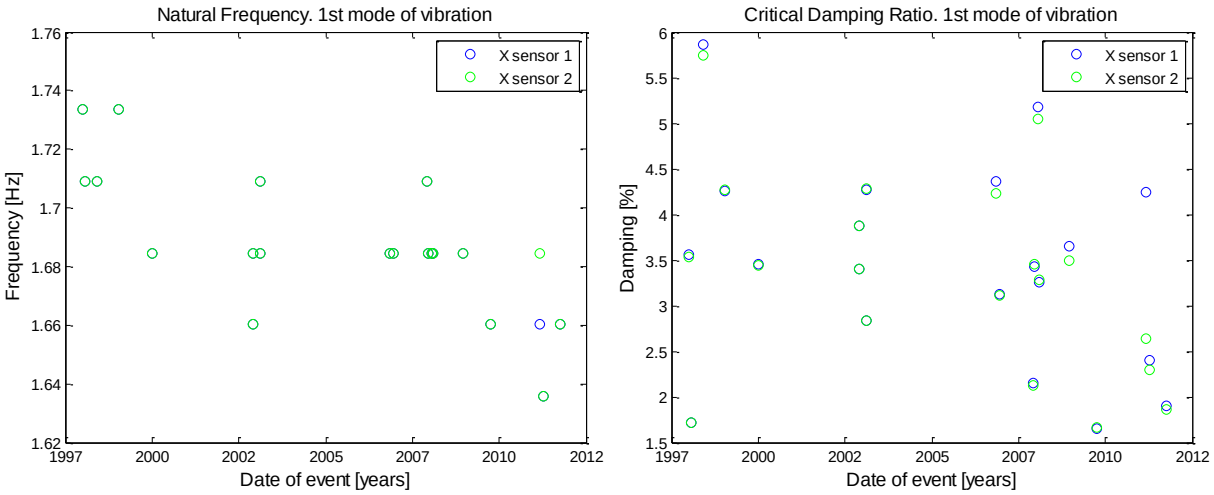

Figure 4.24: Natural frequencies and critical damping ratios for the first mode of vibration evaluated by the fast Fourier transform analysis.

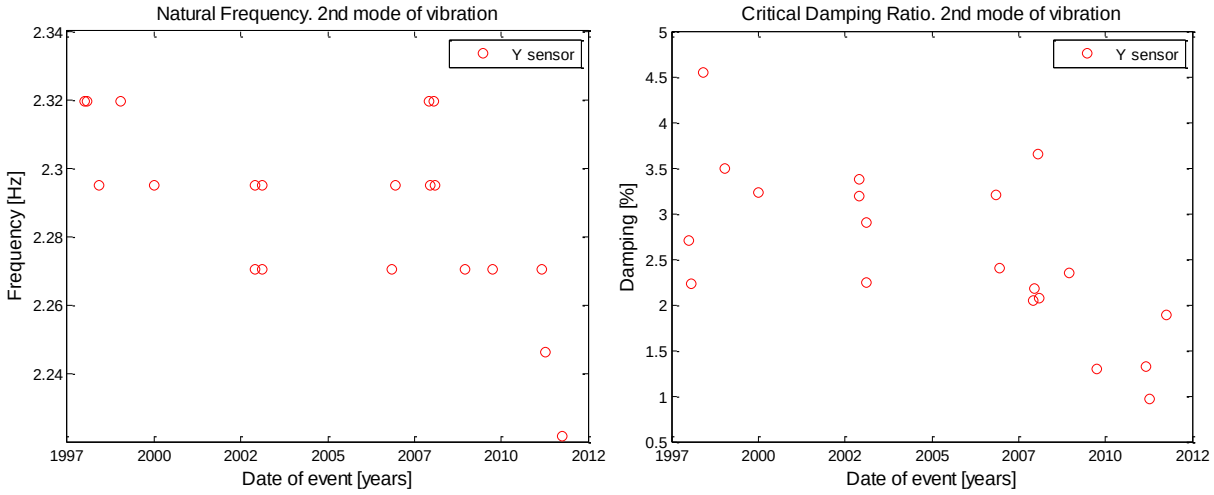

Figure 4.25: Natural frequencies and critical damping ratios for the second mode of vibration evaluated by the fast Fourier transform analysis.

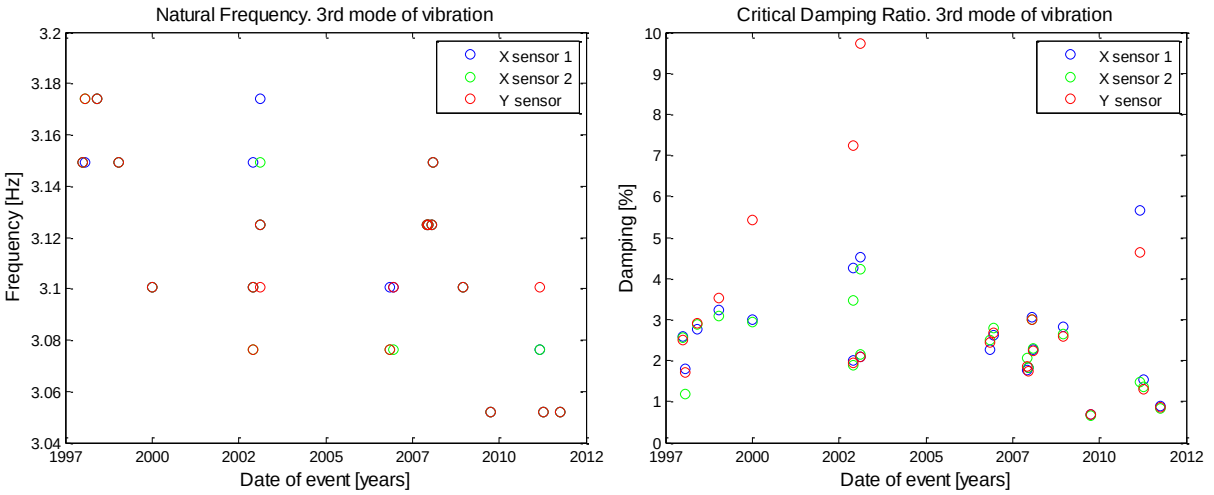

Figure 4.26: Natural frequencies and critical damping ratios for the third mode of vibration evaluated by the fast Fourier transform analysis.

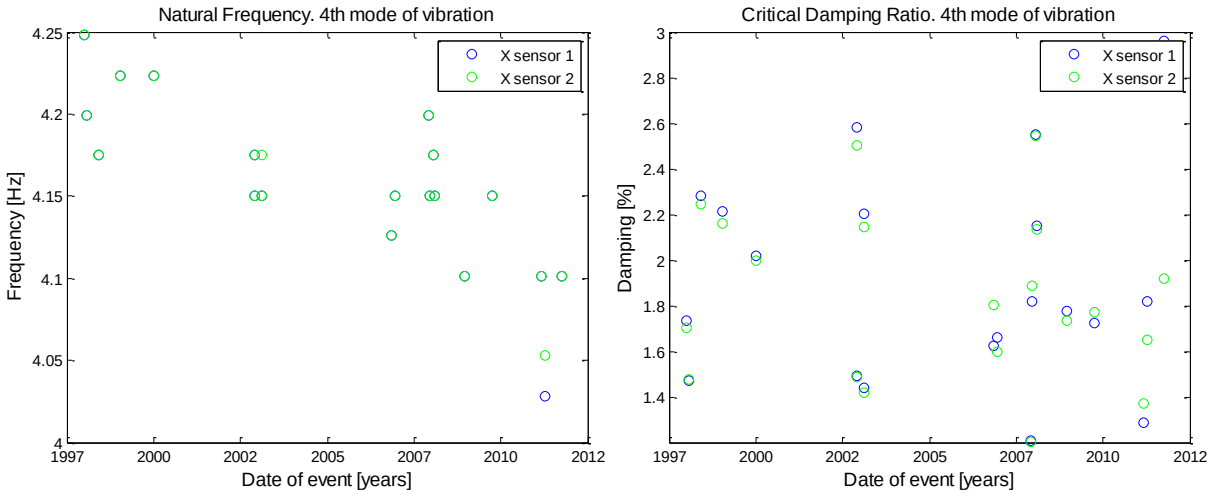

Figure 4.27: Natural frequencies and critical damping ratios for the fourth mode of vibration evaluated by the fast Fourier transform analysis.

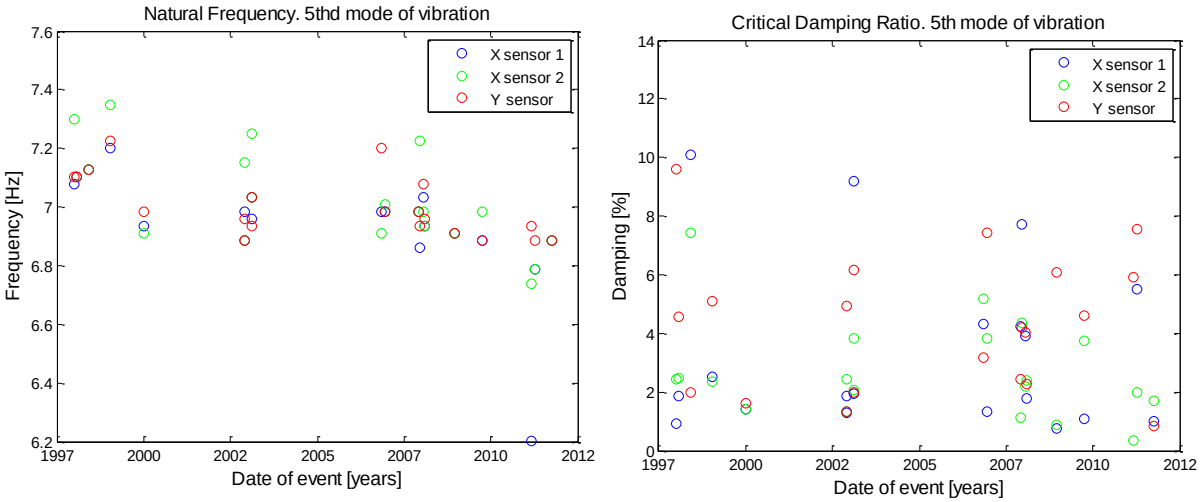

Figure 4.28: Natural frequencies and critical damping ratios for the fifth mode of vibration evaluated by the fast Fourier transform analysis.

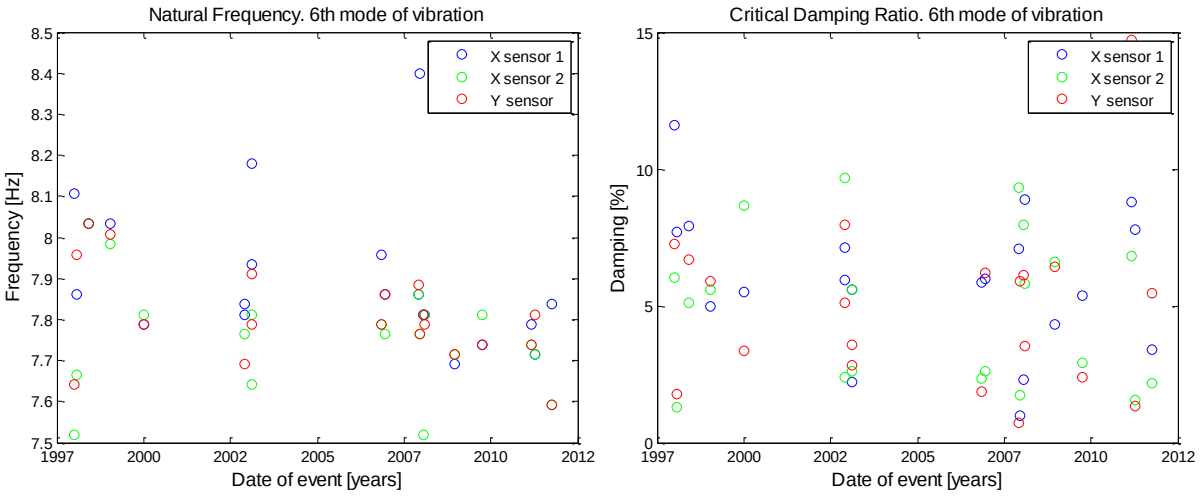

Figure 4.29: Natural frequencies and critical damping ratios for the sixth mode of vibration evaluated by the fast Fourier transform analysis.

A comparison of the results from the two methods show an extremely similar results for the average natural frequencies but the average critical damping ratio varies considerably as shown in Table 4.9 and Table 4.10. The difference of the critical damping ratios is largest for the first mode of vibration and then decreases gradually for the higher modes of vibration. The power spectral density is however made of much less points in the fast Fourier transform analysis, leading to much smaller resolution than in the autoregressive analysis and could therefore be considered less accurate, especially for damping estimation purposes. The fact that using the FFT approach, the natural frequencies of any specific mode of vibration have been evaluated as the exact same value for numerous different time-series, something that was not seen in the autoregressive analysis. This is due to the limited resolution in frequency in the fast Fourier transform analysis. Examples of the power spectral densities estimates from both methods are shown in Figure 4.30 and Figure 4.31 for a better understanding of the different results of the two methods.

Table 4.9: Comparison of the average natural frequencies

Method	Mode 1	Mode 2	Mode 3	Mode 4	Mode 5	Mode 6
	Hz	Hz	Hz	Hz	Hz	Hz
Autoregressive	1,68	2,29	3,11	4,16	6,97	7,81
Fast Fourier Transform	1,69	2,29	3,11	4,16	6,99	7,82
Difference	0,3%	0,0%	0,1%	-0,1%	0,2%	0,1%

Table 4.10: Comparison of the average critical damping ratios

Method	Mode 1	Mode 2	Mode 3	Mode 4	Mode 5	Mode 6
	%	%	%	%	%	%
Autoregressive	1,37	1,36	1,41	1,47	3,41	4,91
Fast Fourier Transform	3,37	2,56	2,64	1,87	3,58	5,25
Difference	146,7%	89,1%	88,0%	27,1%	5,1%	7,0%

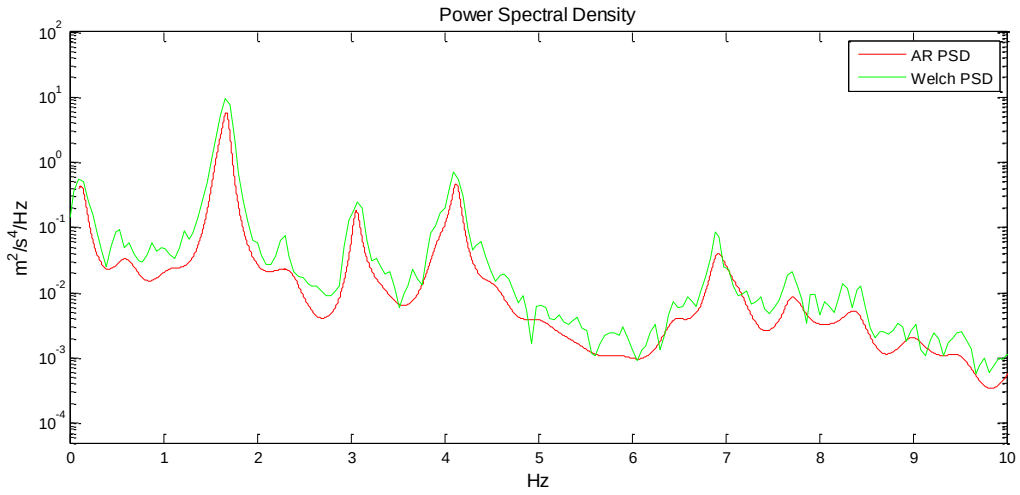

Figure 4.30: Power Spectral Density of both the autoregressive analysis and the fast Fourier transform analysis from a X sensor of time-series from 11. December 2008.

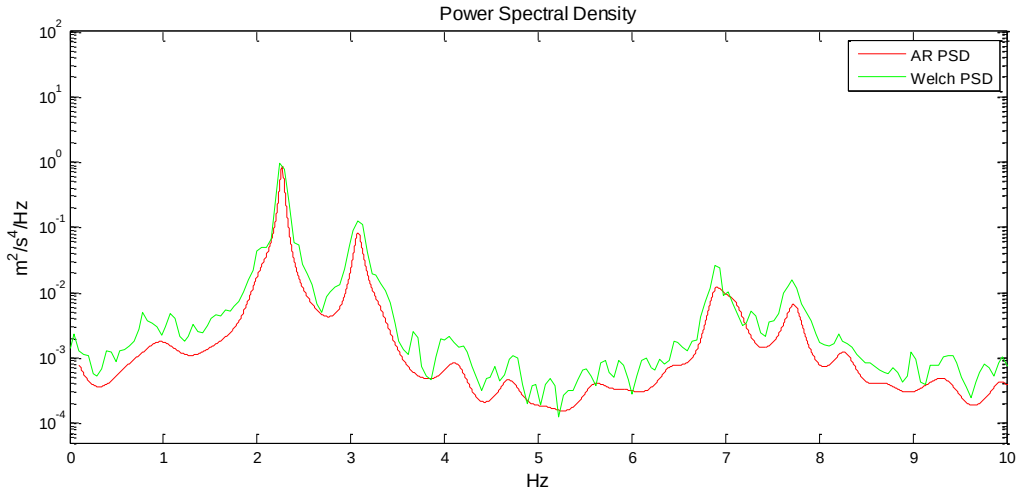

Figure 4.31: Power Spectral Density of both the autoregressive analysis and the fast Fourier transform analysis from the Y sensor of time-series from 11. December 2008.

The results of the system identification show a clear trend of decrease in the natural frequencies with time for all the modes of vibration observed. This evolution of the natural frequencies seems to have been taken place without any visible damage to the structure. This has previously been studied for this particular building for both earthquake and wind excitations showing similar results for the behaviour of the natural frequencies which are now shown to follow the same trend of reduced stiffness with time. (Snæbjörnsson & Sigurbjörnsson, 2006).

The relation between the amplitude of acceleration response and the natural frequencies was studied for the wind induced response time series. However, there were no clear suggestions of amplitude dependency of the natural frequencies as shown in Figure 4.32.

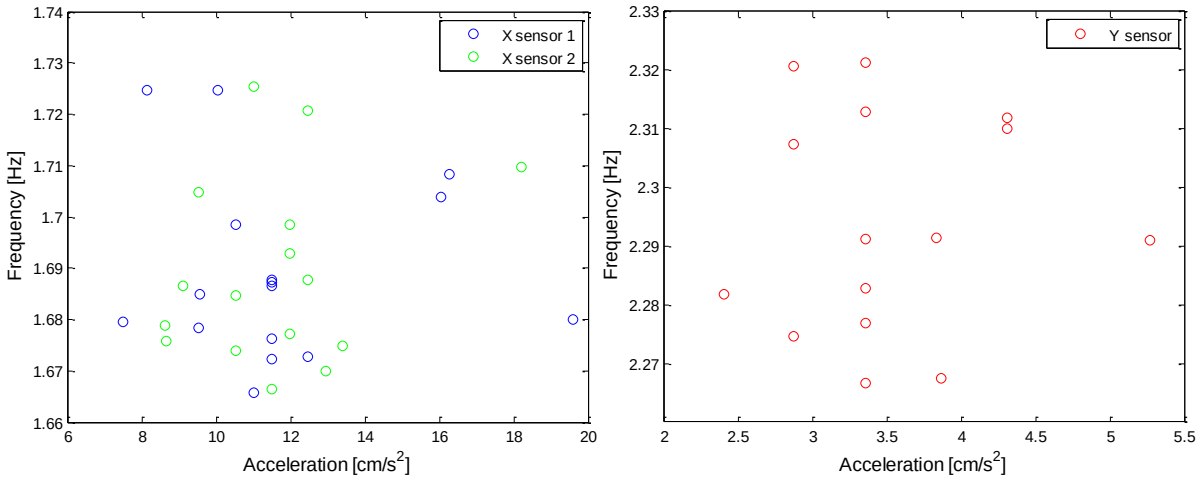

Figure 4.32: Natural frequency as a function of response acceleration for a) the E-W components and b) for the N-S components.

4.2.3 Autoregressive analysis of earthquake induced excitation

In addition to the system identification based on the time-series of the wind induced responses, the natural frequencies and critical damping ratios were also evaluated from the time-series of the earthquake responses with the autoregressive method. As the earthquake induced response time series are shorter than those of the wind induced response, it was deemed not useful to analyse the time series with a fast Fourier transform analysis as the frequency resolution was low enough for the wind induced response due to short time series. The natural frequencies and critical damping ratios are listed in Table 4.11 and Table 4.12 and shown graphically in Figure 4.33 through Figure 4.38.

Table 4.11: Natural frequencies of the first six modes of vibration based on the earthquake time-series and evaluated by the autoregressive analysis

Date	Mode 1	Mode 2	Mode 3	Mode 4	Mode 5	Mode 6
	Hz	Hz	Hz	Hz	Hz	Hz
17.6.2000	1,66	2,24	3,05	4,02	6,75	7,66
17.6.2000	1,68	2,09	3,38	4,04	6,86	7,66
21.6.2000	1,67	2,26	3,50	4,16	7,47	7,56
29.5.2008	1,63	2,21	3,06	3,97	7,30	7,52
29.5.2009	1,58	2,20	3,19	3,95	7,23	7,89
30.5.2009	1,64	2,22	3,18	3,99	6,73	7,69
1.3.2012	1,63	2,21	3,16	4,06	6,94	7,95
1.3.2012	1,64	2,22	3,21	3,89	7,26	7,52
Average	**1,64**	**2,20**	**3,22**	**4,01**	**7,07**	**7,68**
Median	1,64	2,21	3,19	4,01	7,08	7,66
Standard deviation	0,03	0,05	0,14	0,07	0,26	0,15

Table 4.12: Critical damping ratio of the first six modes of vibration based on the earthquake time-series and evaluated by the autoregressive analysis

Date	Mode 1	Mode 2	Mode 3	Mode 4	Mode 5	Mode 6
	%	%	%	%	%	%
17.6.2000	0,81	0,72	8,01	0,70	6,10	3,13
17.6.2000	1,24	9,61	4,83	0,51	2,43	5,20
21.6.2000	0,97	1,47	0,00	2,95	3,68	4,03
29.5.2008	1,36	2,24	8,85	1,66	4,04	6,83
29.5.2009	4,35	3,81	0,00	0,24	2,84	1,72
30.5.2009	1,04	0,54	7,04	0,78	2,60	5,45
1.3.2012	0,97	0,01	8,99	0,87	0,64	6,20
1.3.2012	4,65	0,79	0,00	0,92	3,38	2,58
Average	**1,92**	**2,40**	**4,71**	**1,08**	**3,21**	**4,39**
Median	1,14	1,13	5,93	0,83	3,11	4,61
Standard deviation	1,50	2,95	3,85	0,80	1,46	1,70

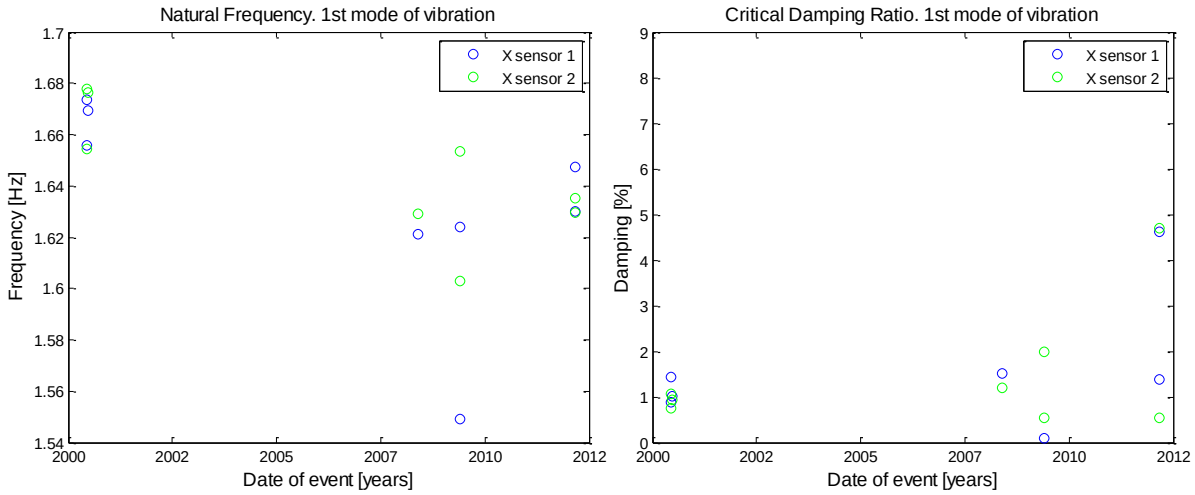

Figure 4.33: Natural frequencies and critical damping ratios for the first mode of vibration based on the earthquake time-series and evaluated by the autoregressive analysis.

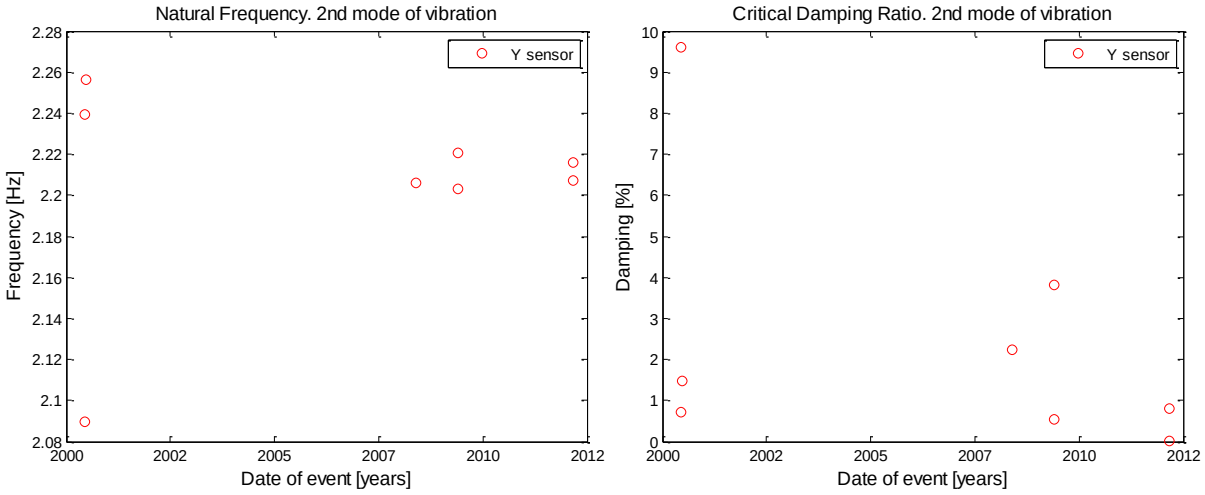

Figure 4.34: Natural frequencies and critical damping ratios for the second mode of vibration based on the earthquake time-series and evaluated by the autoregressive analysis.

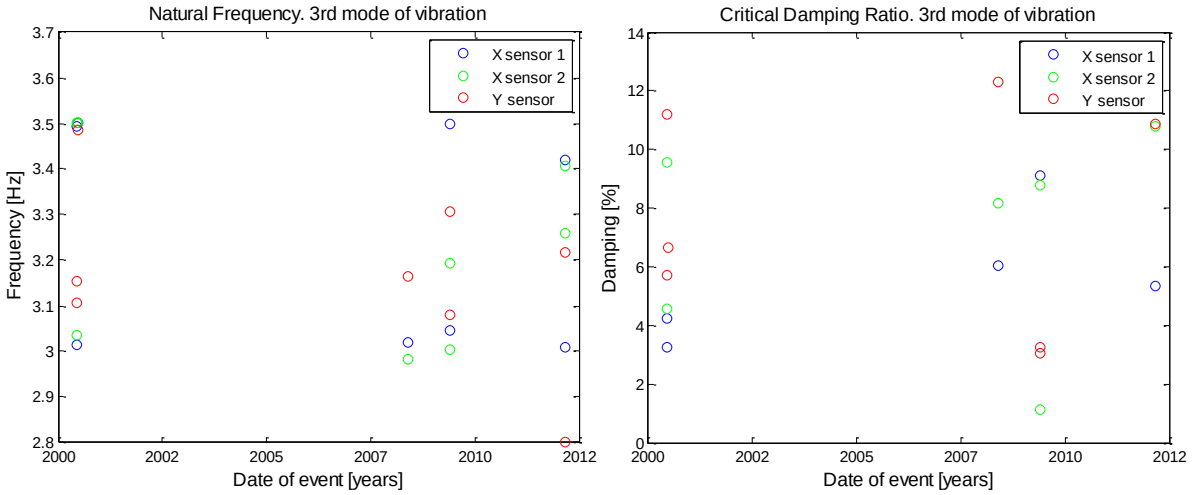

Figure 4.35: Natural frequencies and critical damping ratios for the third mode of vibration based on the earthquake time-series and evaluated by the autoregressive analysis.

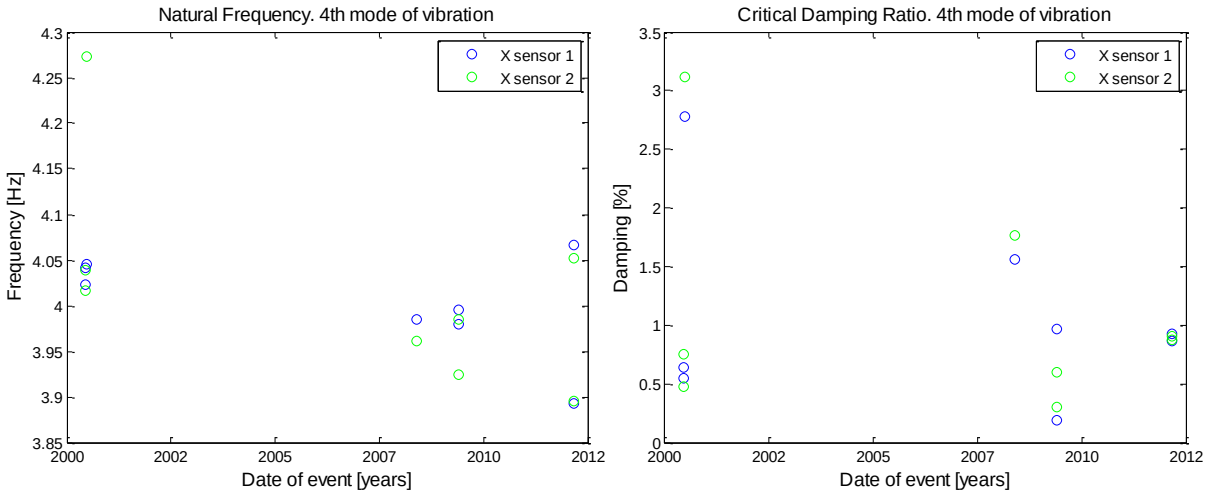

Figure 4.36: Natural frequencies and critical damping ratios for the fourth mode of vibration based on the earthquake time-series and evaluated by the autoregressive analysis.

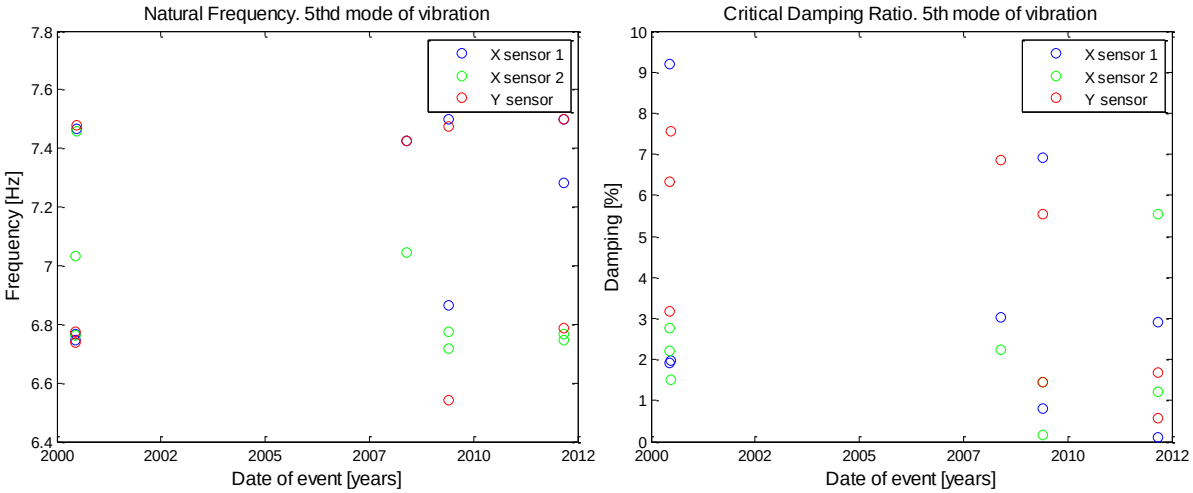

Figure 4.37: Natural frequencies and critical damping ratios for the fifth mode of vibration based on the earthquake time-series and evaluated by the autoregressive analysis.

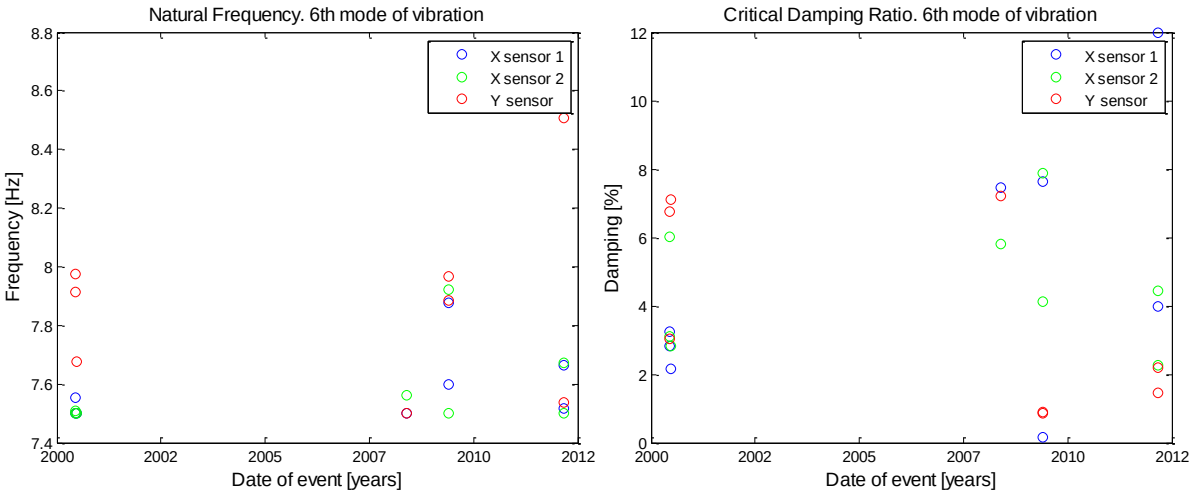

Figure 4.38: Natural frequencies and critical damping ratios for the sixth mode of vibration based on the earthquake time-series and evaluated by the autoregressive analysis.

A comparison of the results from the wind data and the earthquake data shows only a slight difference in the natural frequencies but quite a big difference in the critical damping ratios as shown in Table 4.13 and Table 4.14. The biggest difference in the critical damping ratios occur in the first three modes of vibration, while there is much less difference in the higher three modes. This could indicate different behaviour of the structure in earthquake induced excitation than in wind induced excitation where the vibration is mostly in the top-tower. An example of the different power spectral density from a wind induced excitation and an earthquake induced excitation is shown in Figure 4.39 and Figure 4.40. These power spectral densities are though only evaluated from a single time-series each so the figures are not necessarily representing the true difference in behaviour of the building to the different source of excitation.

Table 4.13: A comparison of the natural frequencies evaluated from the earthquake and wind data

Data Type	Mode 1	Mode 2	Mode 3	Mode 4	Mode 5	Mode 6
	Hz	Hz	Hz	Hz	Hz	Hz
EQ data	1,64	2,20	3,22	4,01	7,07	7,68
Wind data	1,68	2,29	3,11	4,16	6,97	7,81
Difference	2,6%	3,6%	-3,5%	3,6%	-1,4%	1,7%

Table 4.14: A comparison of the critical damping ratios evaluated from the earthquake and wind data

Data Type	Mode 1	Mode 2	Mode 3	Mode 4	Mode 5	Mode 6
	%	%	%	%	%	%
EQ data	1,92	2,40	4,71	1,08	3,21	4,39
Wind data	1,37	1,36	1,41	1,47	3,41	4,91
Difference	-40,8%	-77,0%	-235,3%	26,6%	5,8%	10,5%

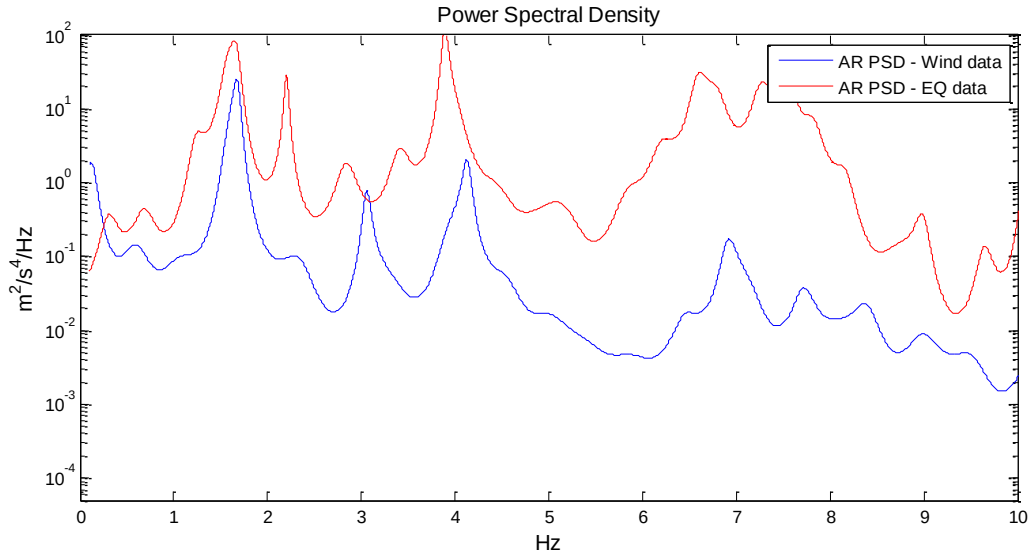

Figure 4.39: Power Spectral Density of both wind induced excitation and earthquake induced excitation evaluated from a X sensor with the autoregressive method. Wind data from December 11, 2008 and earthquake data from May 29, 2008.

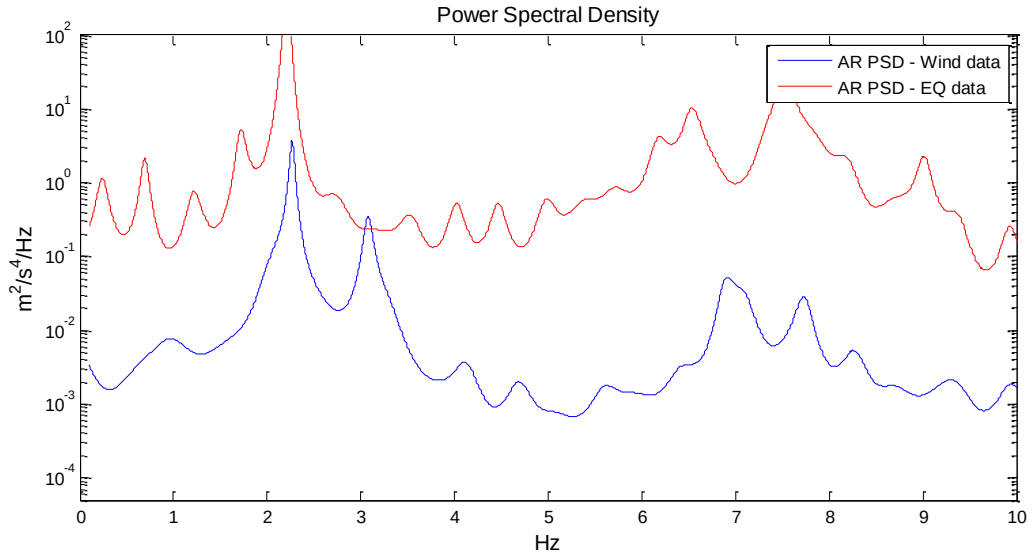

Figure 4.40: Power Spectral Density of both wind induced excitation and earthquake induced excitation evaluated from a Y sensor with the autoregressive method. Wind data from December 11, 2008 and earthquake data from May 29, 2008.

The natural frequencies evaluated from the earthquake response time-series do show signs of stiffness decrease with time. However, the validity of this behaviour is affected by the fact thata only eight time-series used for the analysis. The different intensity and impact of the earthquakes could also be distorting the time dependency of the natural frequencies as they also depend on the magnitude of acceleration as shown in Figure 4.41, where the natural frequencies seem to decrease with increased response acceleration.

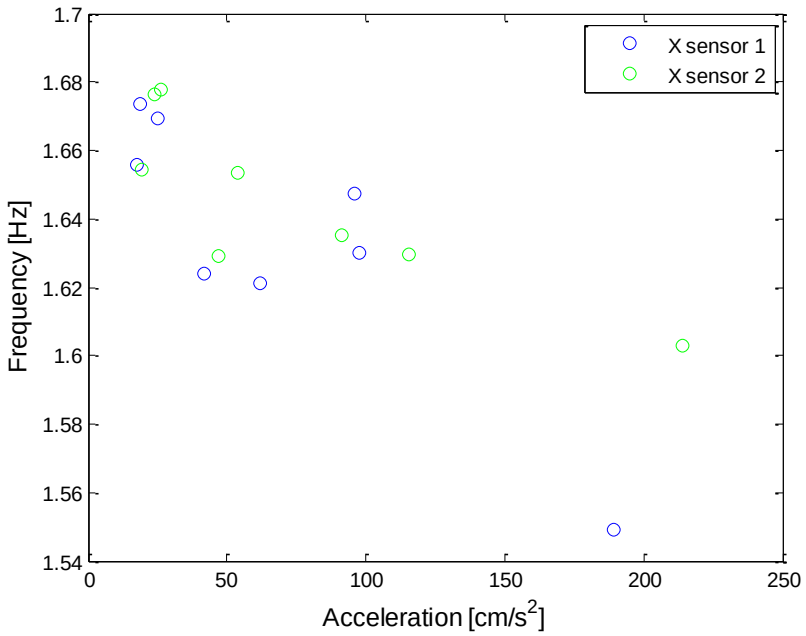

Figure 4.41: Natural frequency for the first mode of vibration as a function of response acceleration based on the earthquake data.

5. Finite element modelling

To interpret and extend the information provided by the full scale recordings of the building response to the environmental excitations a finite element model of the building was prepared. This chapter describes the finite element modelling process and presents some key results.

5.1. The modelling process

The finite element modelling of the building is carried out using the finite element software SAP2000, version 14.0.0 (*SAP 2000*, 2010). The software is a practical general purpose structural analysis program that can perform various analyses, from a simple static 2D frame analysis to a complicated 3D non-linear dynamic analysis.

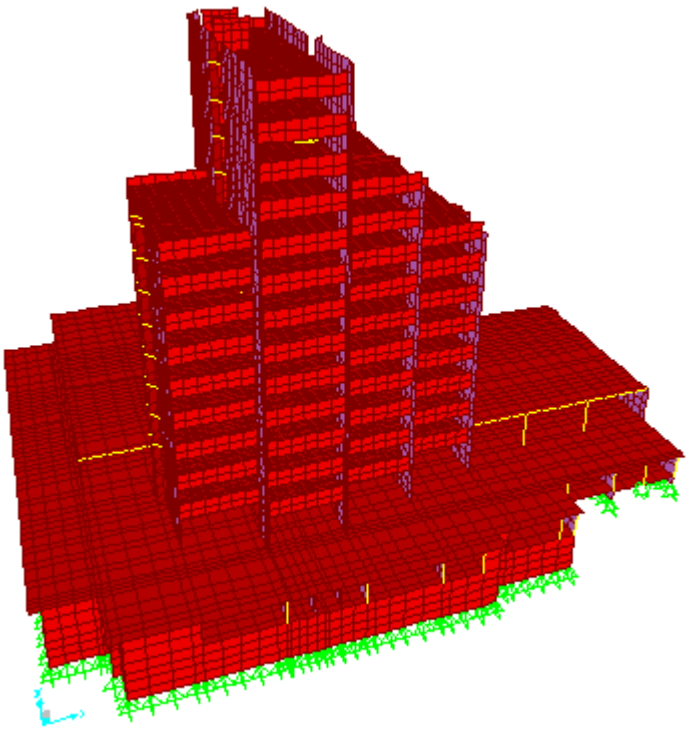

Figure 5.1: 3D view of the model in SAP2000

The finite element model of the building is shown in Figure 5.1. It is based on the available architectural and structural drawings (Ásgeirsson & Sveinsson, 1974; Hagverk, 1976), along with on-site measurements to verify the dimensions of structural elements and the modulus of elasticity of the concrete. It is important to make appropriate assumptions in the construction of a model like this to achieve good correspondence between the natural frequencies of the

model and the natural frequencies from the recorded full-scale data. Therefore it is important to take into account the true characteristics of the floor slabs, the core wall openings, possible stiffness contribution from non-structural elements as well as applying realistic material properties (Kim, Yu, Kim, & Kim, 2009).

The model consists of all the elements of the building that contribute to stiffness, such as the reinforced concrete walls, beams, columns and slabs. The foundation is included in the model in the form of shell elements that reach 1,0 m further down than the bottom slab. The boundary conditions of the foundations, both walls and columns, allow rotation but no translation.

As previously stated the concrete used in the building is, according to the structural drawings, mostly of the type S-200 which corresponds to C20/25 concrete in current codes. The modulus of elasticity of C20/25 concrete is E_{cm} = 30 GPa, according to Eurocode (*Eurocode 2: EN 1992-1-1*, 2004). The modulus of elasticity used in the model is however 19,6 GPa as found by on site measurement on site as described in chapter 3.1. The density of the concrete is assumed to be ρ = 2500kg/m^3 and the poisson's ratio v = 0,2.

The imposed live load on the floor slabs is assumed to be about 50 kg/m^2 which should represent a realistic load at normal condition (Kumar, 2002). A simple way to introduce this additional mass in the model is to increase the density of the slab. The densities of the floor slabs are listed in Table 5.1.

Table 5.1: Density of slabs in the model

Slab type	Thickness	Density
	mm	kg/m^3
Waffle slab	140	2850
Core slab	210	2740
Basement slab	36	2640

The top floor of the building is structured mainly from steel frames instead of concrete and is not included in the model by stiffness elements as it is not contributing to the overall stiffness of the building. It is however included as added mass in the model. The steel frames weigh about 5000 kg and with the extra weight of the top floor it is estimated to weigh roughly 50 kg/m^2, similar to the imposed live load and therefore the density is modelled in the same way as for the other waffle slabs. The concrete walls and slabs are modelled as shells. The slabs on the 2nd floor and above are "waffle slabs" or "two-way ribbed slabs". A waffle slab is a thin

concrete slab on top of multiple perpendicular concrete beams. The beams of the slab are arranged tighter in one direction, resulting in different stiffness of the slab along its two perpendicular directions. The benefits of using waffle slabs are that they are much stiffer than flat plate of equal weight and the increased stiffness results in smaller deflections and the ability to cover large spans with reduced self-weight (Abdul-Wahab & Khalil, 2000).

In an attempt to ease the modelling process and the processing of the software it was attempted to model the waffle slabs as flat slabs by making a flat slab elements that were equivalent to the waffle slab. To test the suitability of this modelling approach, a model was made of a square waffle slab, 6 by 6 m, and another model of a flat slab of the same size and weight. The properties of the flat slab elements were then adjusted to match the dynamic properties of the waffle slabs. To do so the modulus of elasticity was decreased as the flat slab was to stiff. These two models are shown in Figure 5.2. Then another pair of models were made for another aspect ratio, now 12 by 6 m. For this case, using the previous properties of the equivalent flat slab elements, the dynamic properties of the two slabs did not match as the flat slab was not stiff enough. Therefore, it was decided to model the waffle slabs in the building as a thin flat concrete slab on top of concrete beams. This method achieved more accurate modelling of the size and shape of the waffle slabs with less or equal effort.

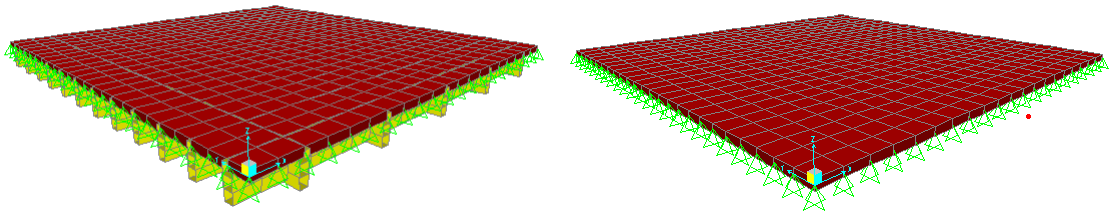

Figure 5.2: 3D view of the waffle slab and flat slab models in SAP2000.

The FE-software was used to calculate the first 12 modes of vibration. The natural frequencies evaluated by the initial model, without any calibration through comparison with the natural frequency values determined based on the recorded data, are listed in Table 5.2. Following the evaluation a calibration procedure was initiated, as discussed further in section 5.2

Table 5.2: Natural periods and frequencies evaluated by the initial model

Mode	Period	Frequency
	s	Hz
1	0,646	1,549
2	0,491	2,038
3	0,378	2,645
4	0,245	4,088
5	0,152	6,574
6	0,137	7,315
7	0,125	7,969
8	0,121	8,288
9	0,103	9,720
10	0,062	16,071
11	0,059	16,983
12	0,048	20,855

5.2. Calibration of the FE model

Calibration of the model for the case at hand, primarily involves modifications of the modulus of elasticity. The initial model showed somewhat less stiffness than the recorded data and by increasing the modulus of elasticity the results of the modal analysis corresponded reasonably well with the results from the system identification of the full-scale data. As the measurements of the modulus of elasticity of the concrete indicates higher modulus of elasticity at the basement and lower at higher floors, the modulus of elasticity used in the calibration process of the model was set 30 GPa for the basement floors, 23 GPa for the middle floors, the 1^{st} to 8^{th} floors and 18 GPa for the top floors, the 9^{th} to 14^{th} floors. The lower modulus of elasticity of the top floors than the floors below was necessary to achieve the right modal properties for the higher modes of vibration without having much affect to the modal properties of the first modes of vibration as the 4^{th} to 6^{th} mode of vibration take place predominantly in the top floors.

To verify the improvement of the model, a time history analysis was performed to get a modal response that could be compared to a recorded time series. The time history used was acceleration recorded at the building during a 6,4 magnitude earthquake, located about 60 km south-east of the building, from June 21 2000. The computed acceleration time history and recorded time history at the 14^{th} floor are plotted together and shown in Figure 5.3 and a closer look for a shorter interval is given in Figure 5.4. A comparison of the Fourier amplitude spectra was also carried out and is shown in Figure 5.6.

With the results of the modal analysis and the time history analysis of the model at hand, it was seen that the model gives a good simulation of the real behaviour of the building. Therefore no further modifications to the model were judged to be necessary, such as modifications to the boundary conditions or the mass distribution of the building.

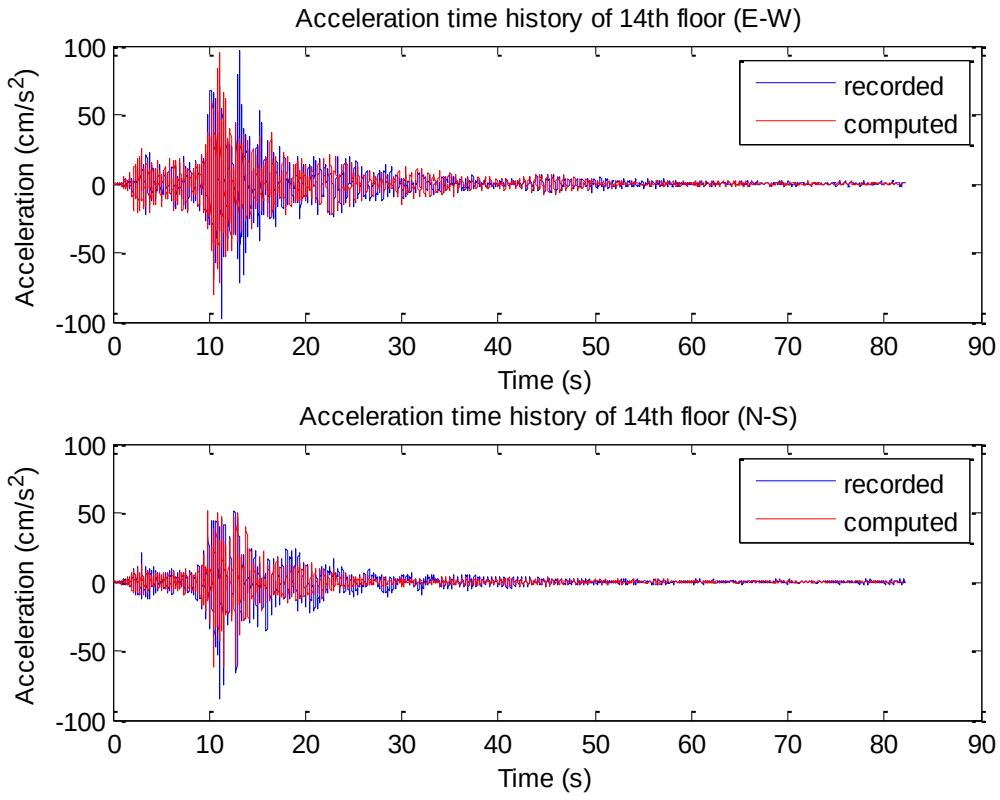

Figure 5.3: Computed and recorded time history acceleration at 14th floor.

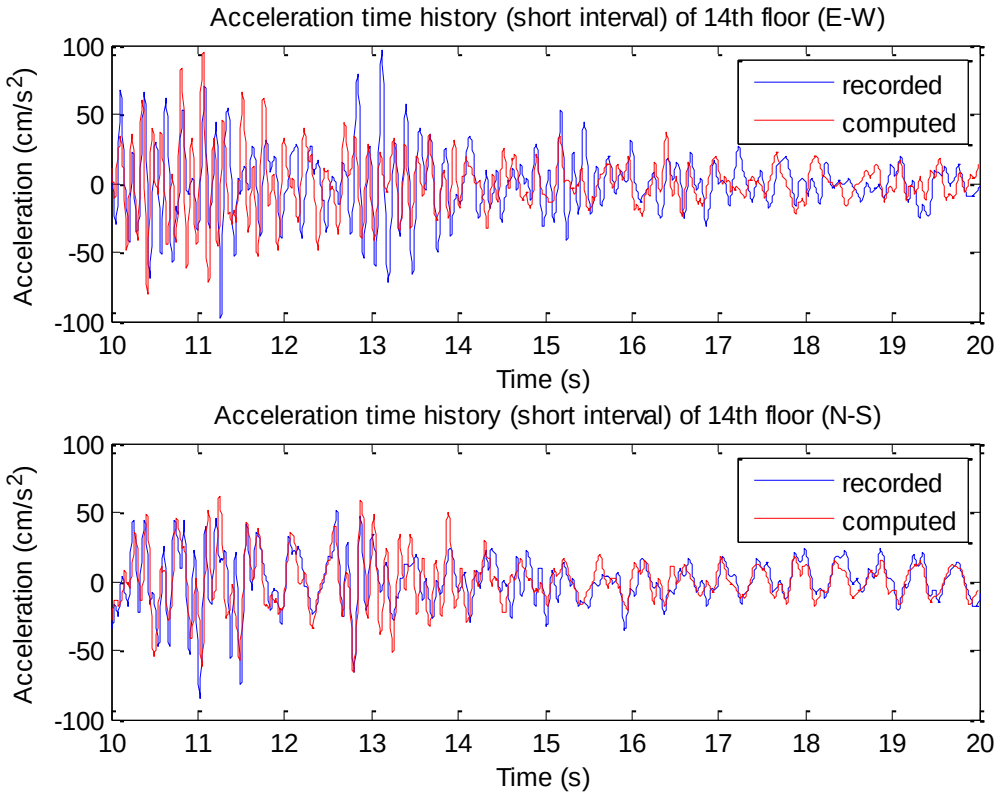

Figure 5.4: Short interval of the computed and recorded time history acceleration at 14th floor.

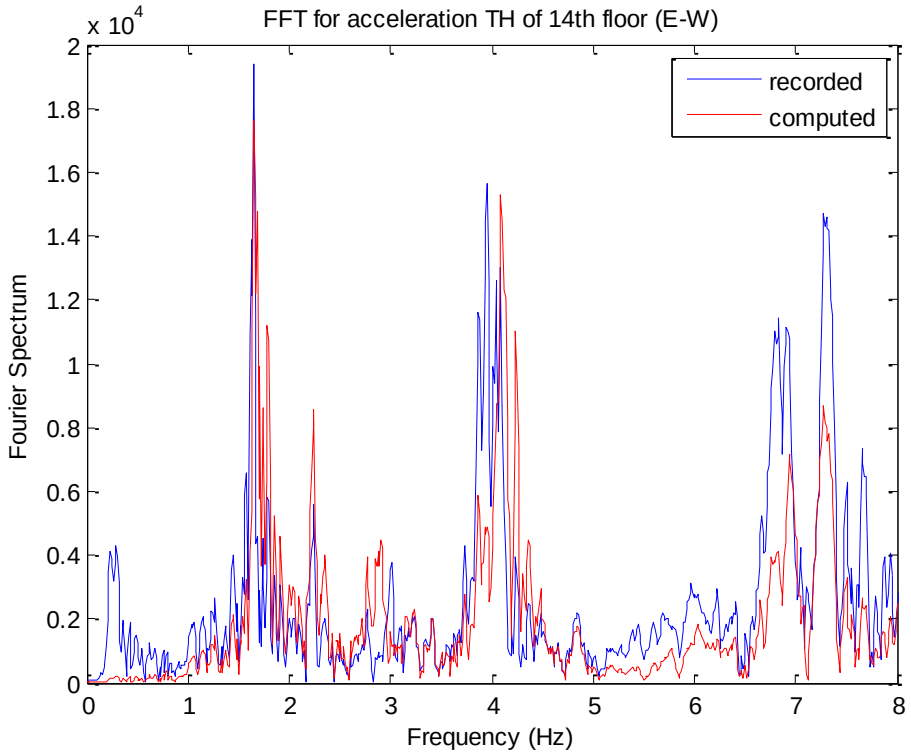

Figure 5.5: Fourier amplitude spectra of the acceleration time history of the 14th floor. Vibration in the E-W direction.

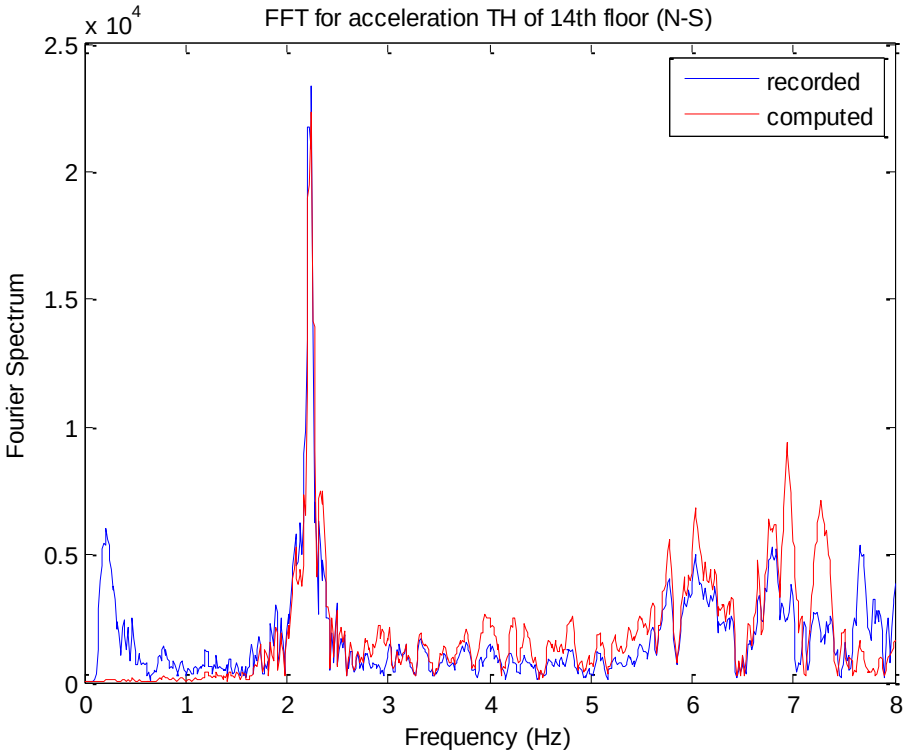

Figure 5.6: Fourier amplitude spectra of the acceleration time history of the 14th floor. Vibration in the N-S direction.

The natural frequencies and periods of the 12 modes of the calibrated model, calculated by the software, are shown in Table 5.3.

Table 5.3: Natural periods and frequencies evaluated by the calibrated model

Mode	Period	Frequency
□	s	Hz
1	0,591	1,692
2	0,445	2,249
3	0,347	2,881
4	0,240	4,173
5	0,144	6,959
6	0,128	7,821
7	0,117	8,572
8	0,116	8,656
9	0,095	10,509
10	0,055	18,089
11	0,053	18,722
12	0,045	22,198

A comparison of the natural frequencies of the finite element model and the average values of natural frequencies evaluated by the system identification of chapter 4.2 is shown in Table 5.4. It shows how the model resembles the wind data very closely except for the third mode of vibration which is the only clear torsional mode.

Table 5.4: Comparison of the natural frequencies evaluated by the finite element model and the system identification

Data type / Analysis	Mode 1	Mode 2	Mode 3	Mode 4	Mode 5	Mode 6
	Hz	Hz	Hz	Hz	Hz	Hz
Finite element model	1,69	2,25	2,88	4,17	6,96	7,82
Wind data / AR	1,68	2,29	3,11	4,16	6,97	7,81
Wind data / FFT	1,69	2,29	3,11	4,16	6,99	7,82
EQ data / AR	1,64	2,20	3,22	4,01	7,07	7,68

The first six mode shapes are shown graphically in Figure 5.8 with a 3-D view of the building and a cross section of the 8th floor showing a scaled deflection. The first mode is predominantly translation in the E-W direction and the second mode is predominantly translation in the N-S direction, while the third mode is rotation about the centre core. The fourth mode is a vibration in the E-W direction, predominantly in the 11.-14. floor of the tower. The fifth mode is a vibration in the N-S direction with torsion, predominantly in the 11.-14. floor of the tower. The sixth mode is a translation in the E-W direction with some rotation also predominantly in the uppermost 4 floors. The higher modes are somewhat more complex. All the modes are however influenced by torsion to some extent due to the asymmetry of the cores and the complexity of the geometry of the structure.

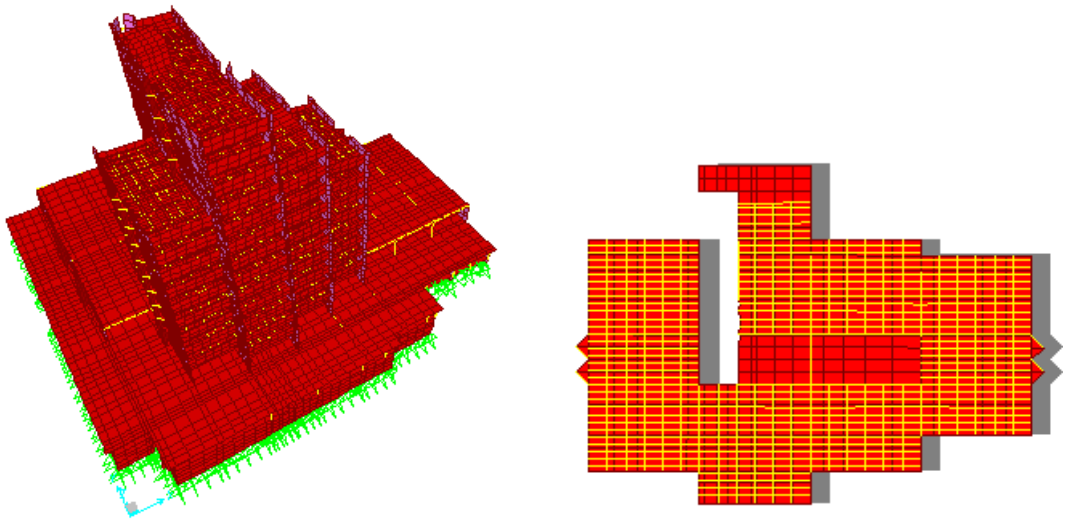

(a) 1st mode shape

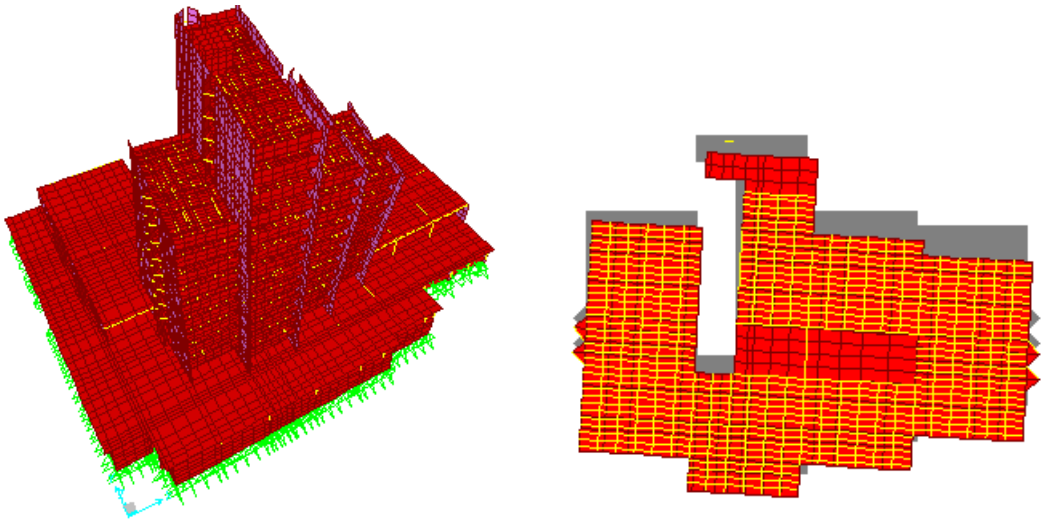

(b) 2nd mode shape

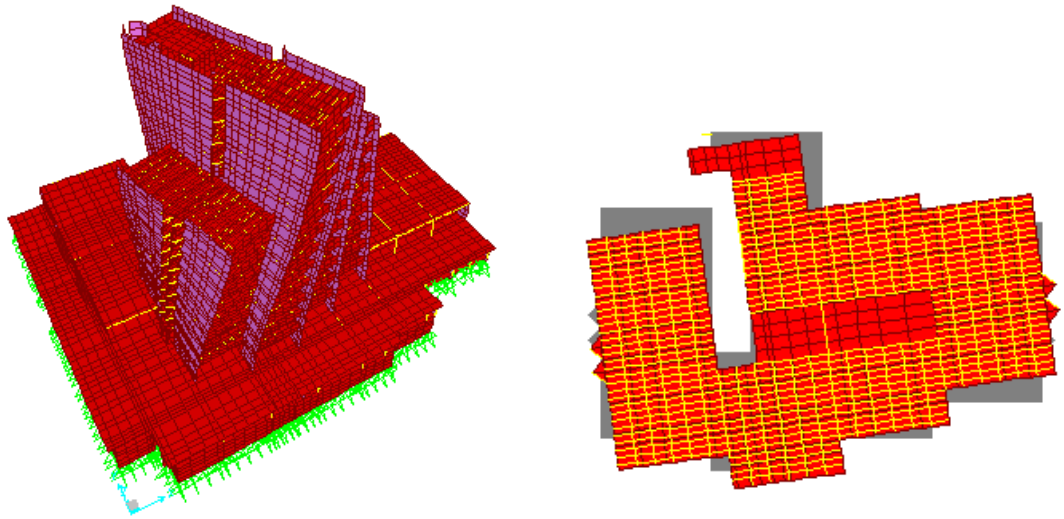

(c) 3rd mode shape

Figure 5.7: First three mode shapes of the finite element model.

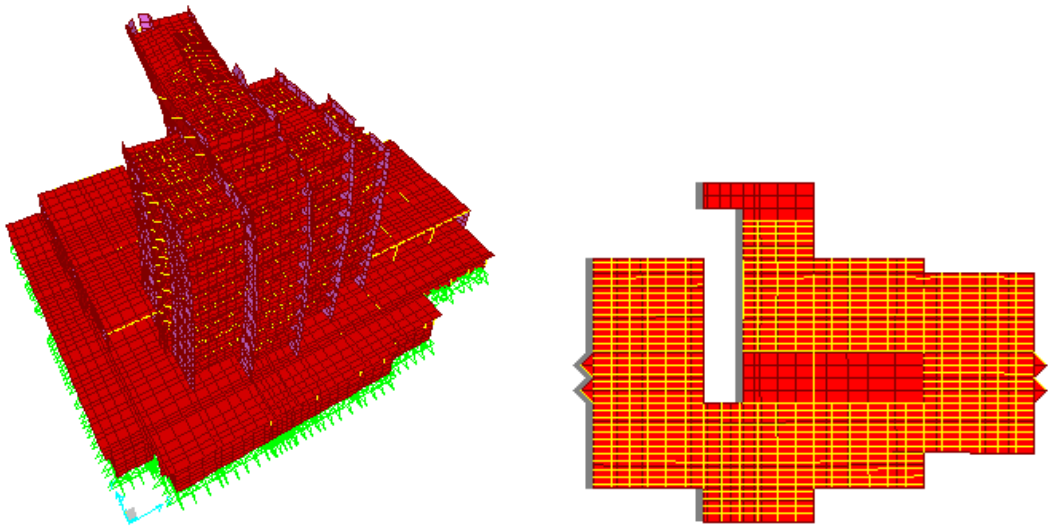

(d) 4th mode shape

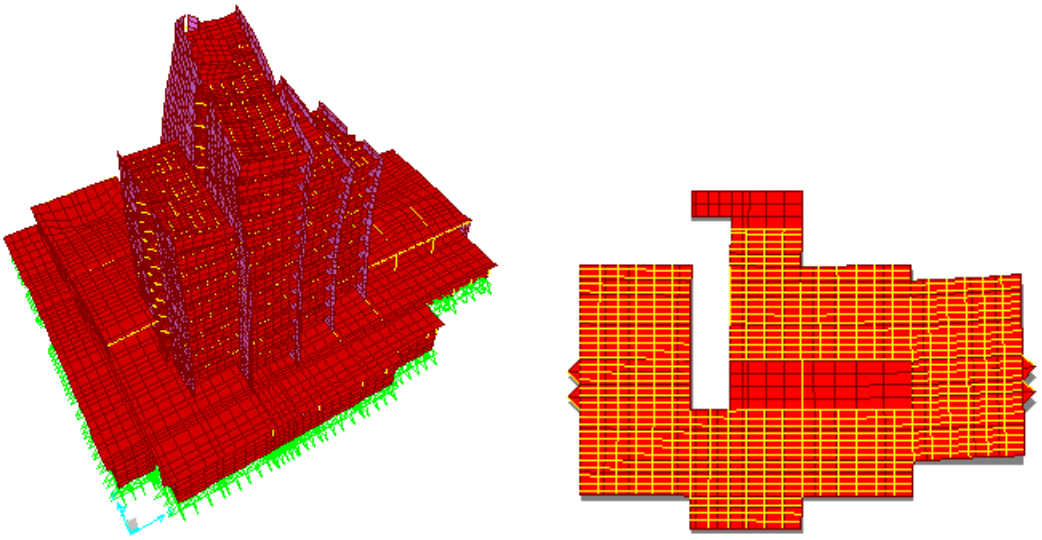

(e) 5th mode shape

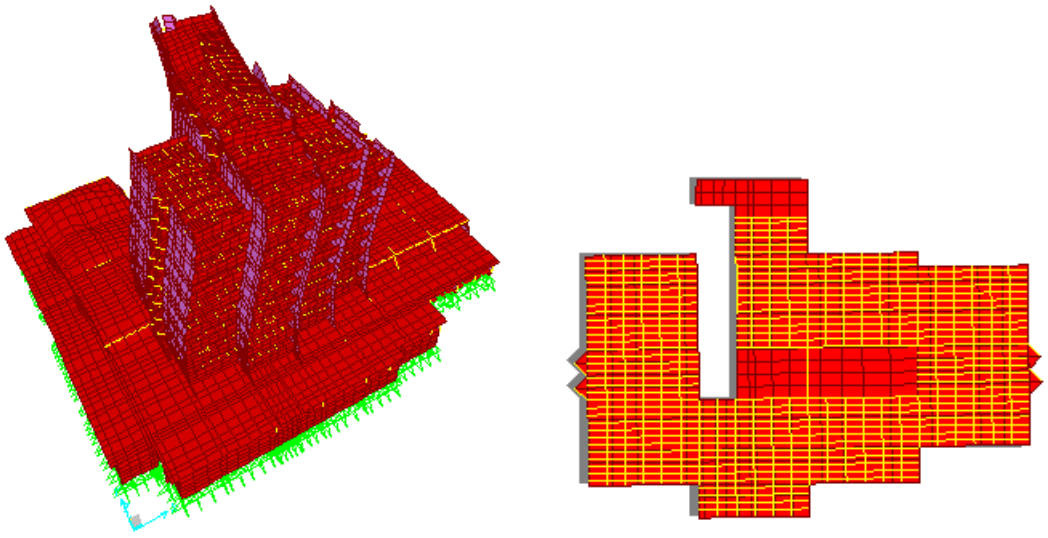

(f) 6th mode shape

Figure 5.8: Mode shapes 4 to 6 of the finite element model.

6. Human comfort and serviceability of buildings against vibration

In this chapter the simplified response prediction based on three international design codes are discussed. The design codes used are the European design code, Eurocode 1991-1-4 (*Eurocode 1: EN 1991-1-4*, 2004), the American design code, presented by the American Society of Civil Engineers (ASCE) (Structural Engineering Institute, 2006) and the Japanese design code, presented by the Architectural Institute of Japan (AIJ) (AIJ Recommendations for Loads on Buildings, 2005). The human comfort criteria's of the AIJ and the international standard ISO 10137 (*ISO 10137*, 2007), published by the International Organization for Standardization are presented and compared to the recorded response.

6.1. Response prediction based on design code procedures

The geometry of the observed structure is quite complex but the design codes provide methods which are based on more simple and predictable structures, such as buildings with rectangular cross section of constant size. When following the design code procedures it is therefore necessary to simplify the geometry and/or structural behavior of more complex buildings.

A key wind loading parameter is for instance the area of the building that is under wind action. For the case being studied herein, the wind loading area of the building sides facing easterly and westerly directions is defined as the total height of the building, 48,9 m, times the width of the middle tower, 24,3 m. For the sides facing the north and south directions, the area under wind load is taken as the area facing the wind without the extra width of the bottom floors. The width of the sides of the building facing the north and south directions, used in the design code procedures, is therefore taken as the wind loaded area divided by the total height of the building resulting in an average width of about 24,1 m. The active wind loaded areas of the building are shown graphically in Figure 6.1.

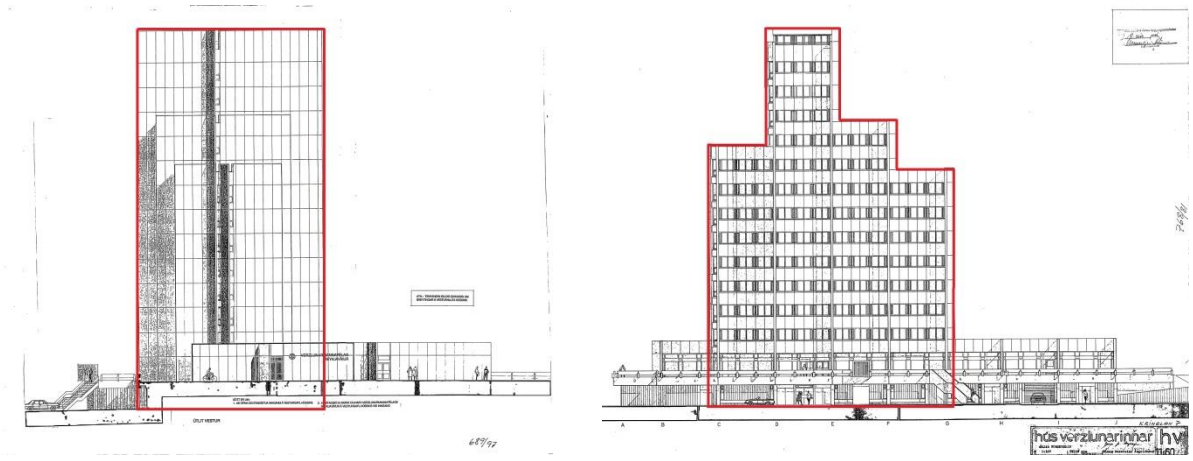

(a) **(b)**

Figure 6.1: Wind loaded area as used in the simplified design code procedures marked with the red regions. (a) sides facing the east and west directions, (b) sides facing the north and south directions (drawings from Ásgeirsson & Sveinsson, 1974).

Through these definitions of equvilent area of each building face, the building could even be described as a square tower with all sides of equal width. In reality that description does not fit the building as for the lower floors the sides facing the east and west directions are about twice the length of the sides facing the north and south direction but for the highest floors the sides facing the north and south directions are about three times the length of the sides facing the east and west directions.

The design codes take account to the roughness of the environment and for the observed building rather smooth terrain categories are chosen, characterized by flat, open terrain with low vegetation and scattered structures. Although the building is located in the small city of Reykjvik, the size, density and height of the built-up area is much less than for big cities around the world and therefore the terrain roughness parameters can not be chosen based on the city category in the code, but rather needs to represent the true conditons at the building site(Snæbjörnsson, 2002). It is assumed that there are no hills, ridges or cliffs affecting the wind at the building site so where it is appropriate the topography factors are set to 1.

The modal parameters used in the design code procedures are taken from the finite element model and the system identification process. The mode shapes and natural frequencies are taken from the finite element model and the critical damping ratios are assumed to be 2% for the first two modes of vibration based on the varying results of the system identification.

The design codes assume that the mode shape of the structure can be represented by the equation:

$$\boldsymbol{\Phi} = \left(\frac{\boldsymbol{Z}}{\boldsymbol{H}}\right)^{\boldsymbol{\beta}} \qquad \textbf{(6.1)}$$

While the mode shapes have been evaluated by the finite element model the mode shape exponent, β, is used in further calculations in the ASCE and AIJ design codes. The mode shape exponent is therefore estimated based on the mode shape evaluated by the finite element model. As shown in Figure 6.2 the two mode shapes are quite different. The first mode shape is a vibration in the E-W direction and resembles a parabolic shape and may be considered to have a mode shape exponent of 2. The second mode shape is a vibration in the N-S direction and resembles more a linear shape with a mode shape exponent of 1. The mode shapes are however quite more complex than what can be estimated with the design code equations. The mode shapes can be explained with the nature of the structure. The two basement floors of the structure are very stiff in relation to the upper floors, for the lower floors above the basement the structure is stiffer in the E-W directions relative to the N-S direction but as the floor plans vary with increasing height the structure becomes stiffer in the N-S direction relative to the E-W direction at the top floors.

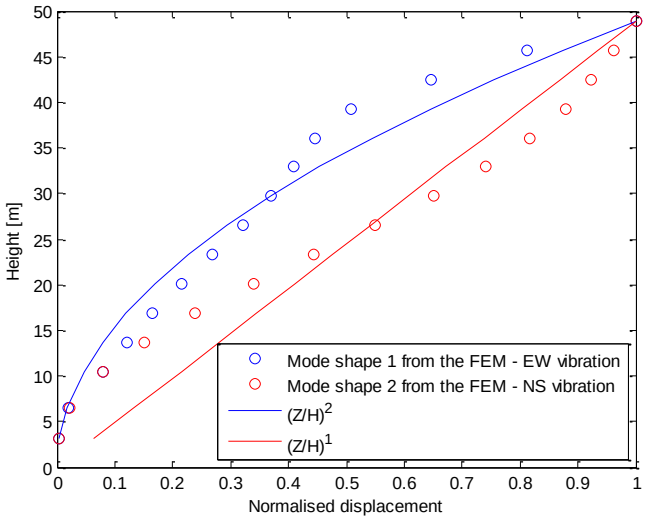

Figure 6.2: Mode shapes of the first two modes of vibration.

The Eurocode and ASCE design codes only offer a procedure to evaluate the along wind response of the structure while the AIJ design code offers procedures to evaluate the along wind-, across wind- and the torsional response.

6.1.1 Eurocode EN 1991-1-4 response prediction

In Eurocode EN 1991-1-4 there are two different methods to estimate the maximum anticipated along wind acceleration response. On the one hand there is a method in Annex B and on the other hand there is a method in Annex C in the design code which is quite a bit more detailed than the previous one. In both methods the along wind acceleration response is evaluated by estimating the standard deviation of the characteristic along wind acceleration and multiplying it with a peak factor.

The peak along wind response acceleration, evaluated with the method presented in EN 1991-1-4 Annex B is shown in Figure 6.3 for 10 minute mean wind velocity at 10 m height above ground ranging from 0 to 35 m/s. A detailed description of the code procedure to evaluate the along wind response is published in Appendix B1.

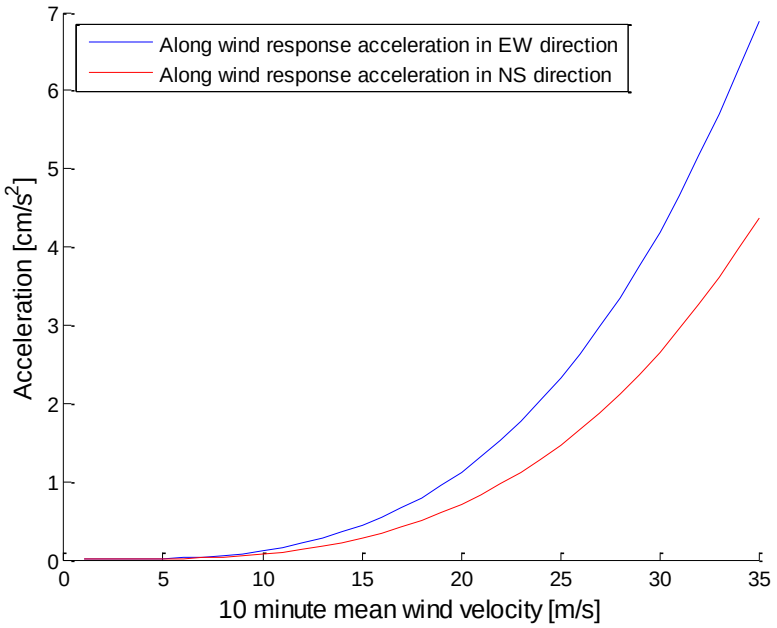

Figure 6.3: Along wind acceleration response, evaluated with EN 1991-1-4 Annex B.

The peak along wind acceleration, evaluated with the method presented in EN 1991-1-4 Annex C is shown in Figure 6.4 for 10 minute mean wind velocity at 10 m height above ground ranging from 0 to 35 m/s.

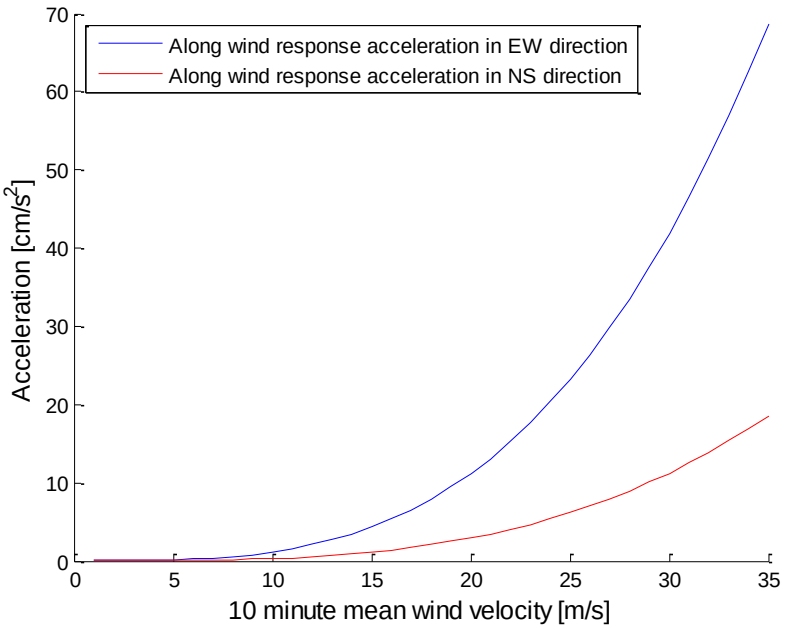

Figure 6.4: Along wind acceleration response, evaluated with EN 1991-1-4 Annex C.

The greatest difference of how the along wind acceleration response is determined in EN 1991-1-4 Annex C to Annex B is how the method of Annex C takes account to the mode shape of the along wind vibration of the building when determining the resonance response factor. A detailed description of the Eurocode Annex C procedure to evaluate the along wind response is published in Appendix B2.

Figure 6.5 shows the results of using the two different procedures to estimate the along wind acceleration response of the building, presented in EN 1991-1-4. The figure demonstrates the great difference in results with the Annex C method predicting much higher values of acceleration with increased wind velocity than the Annex B method. It also shows greater dependence on the direction of along wind response for the building using the Annex C method than when using the Annex B method. This difference can be explained by the different mode shapes for the first two modes of vibration.

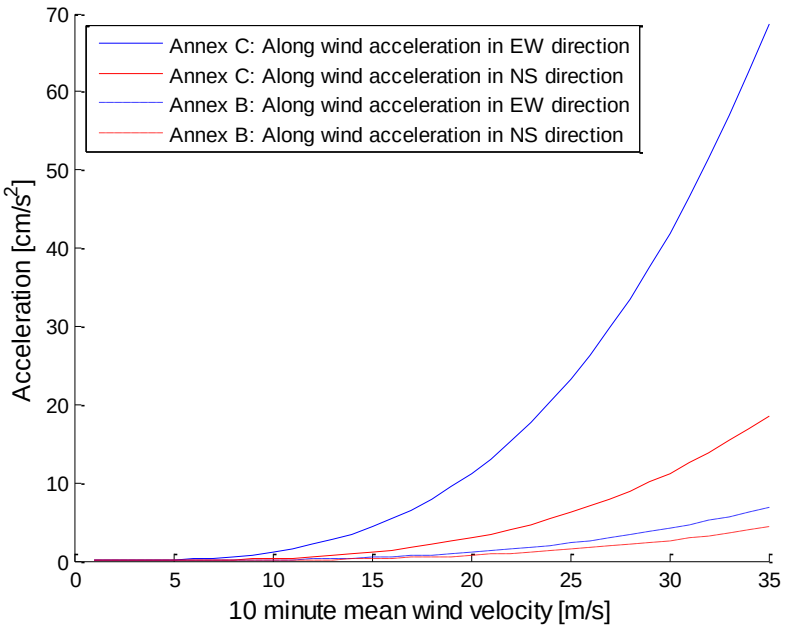

Figure 6.5: Comparison of the two different procedures to predict the anticipated along wind acceleration response, presented in EN 1991-1-4.

6.1.2 ASCE design code response prediction

Similarly to the Eurocode EN 1991-1-4 the ASCE design code estimates the peak response acceleration of the structure by evaluating the root mean square of the response acceleration and multiplying it with a peak factor of acceleration. A detailed description of the ASCE code procedure to evaluate the along wind response, accurately as presented in the design code, is published in Appendix B3.

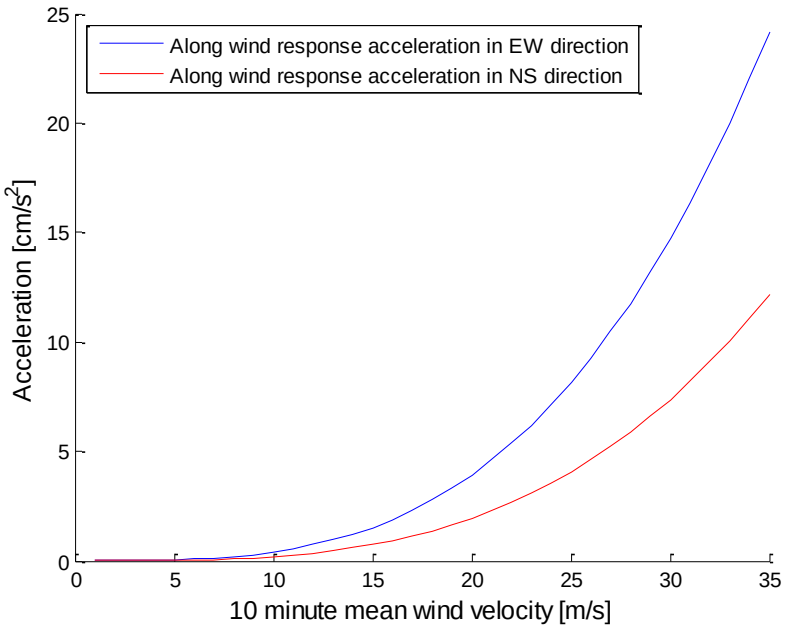

Figure 6.6: Along wind acceleration response, evaluated with the ASCE procedure.

The peak along wind acceleration, evaluated with the method presented in ASCE is shown in Figure 6.6 for 10 minute mean wind velocity at 10 m height above ground ranging from 0 to 35 m/s.

6.1.3 AIJ design code response prediction

Different from the Eurocode EN 1991-1-4 and the ASCE design code, the AIJ design code does not estimate the standard deviation of the response acceleration and then evaluates the peak response acceleration by multiplying it with a certain peak factor, but evaluates the peak response acceleration with an expression containing a peak factor similarly to the other two design codes considered.

The AIJ design code also includes procedures to estimate across wind acceleration response, unlike the Eurocode EN 1991-1-4 and the ASCE design code presenting only a procedure to estimate the along wind acceleration response.

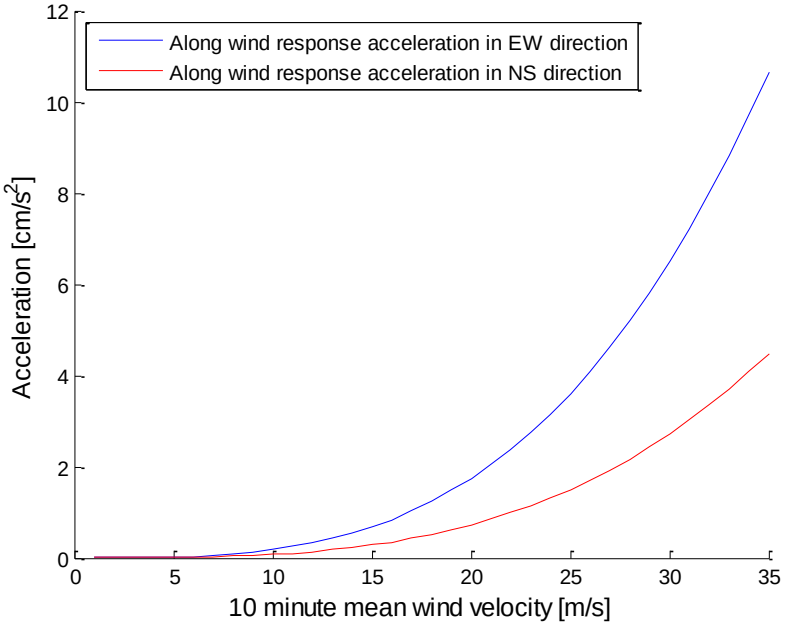

Figure 6.7: Along wind acceleration response, evaluated with the AIJ procedure.

The peak along wind acceleration, evaluated with the method presented in AIJ is shown in Figure 6.7 for 10 minute mean wind velocity at 10 m height above ground ranging from 0 to 35 m/s. A detailed description of the AIJ code procedure to evaluate the along wind response is published in Appendix B4.

The peak across wind acceleration response is shown in Figure 6.8, along with the peak along wind acceleration response, evaluated with the method presented in AIJ, for wind acting in the east-west direction. The same is shown in Figure 6.9 for wind acting in the north-south direction. In both cases the reference wind is the 10 minute mean wind velocity at 10 m height above ground, ranging from 0 to 35 m/s. A detailed description of the AIJ code procedure to evaluate the across wind response is published in Appendix B5.

Interestingly the AIJ design code response prediction, expects high impact of the across wind acceleration response, especially for wind acting in the north-south direction. For wind acting in the north-south direction, the AIJ design code predicts far greater impact of the across wind response than the along wind response. This corresponds to the geometry of the structure, especially the top tower, and the mode shapes of the first two modes of vibration, demonstrating the shift of stiffness along the height of the structure.

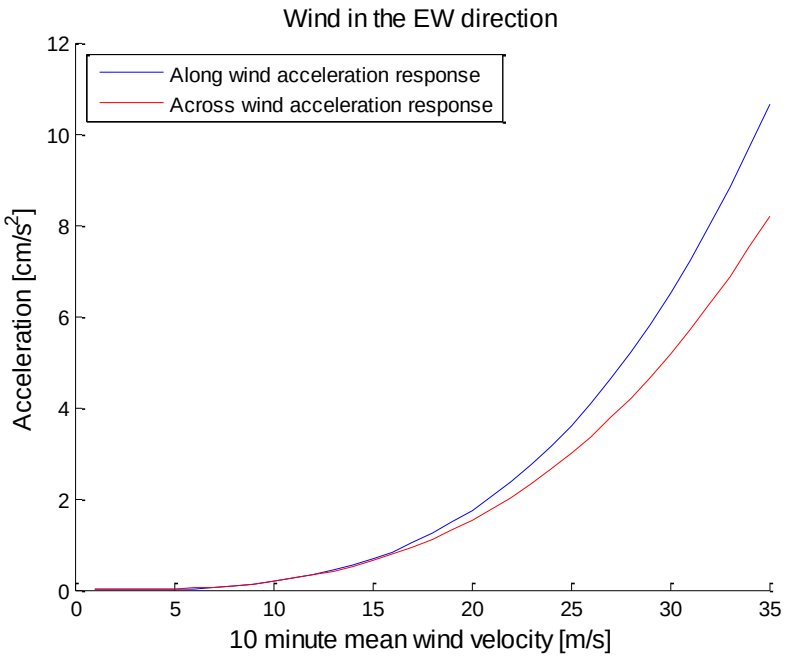

Figure 6.8: Along wind and across wind acceleration response for wind acting in the EW direction, evaluated with the AIJ procedure.

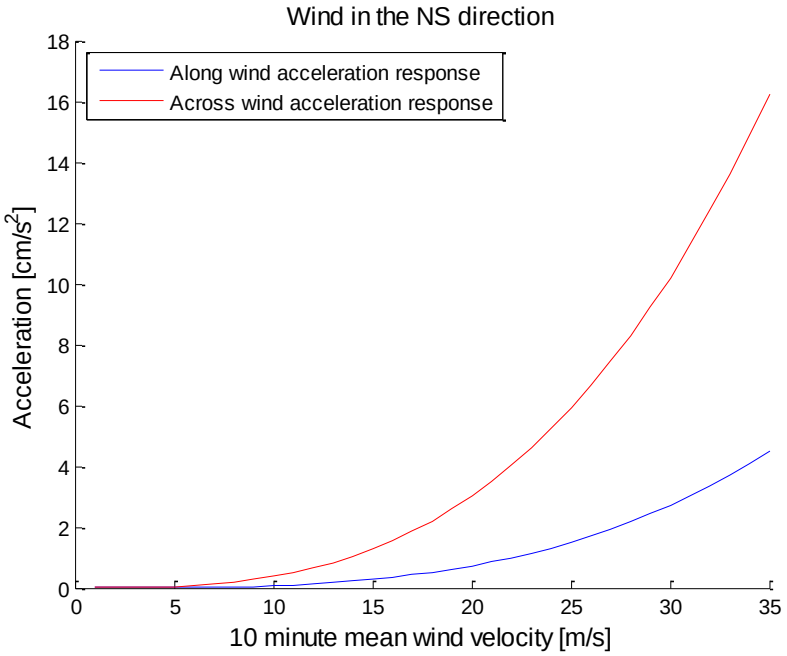

Figure 6.9: Along wind and across wind acceleration response for wind acting in the NS direction, evaluated with the AIJ procedure.

6.1.4 Comparison of the design code results

Figure 6.10 shows the results of the along wind acceleration response predictions from the simplified design code procedures, along with all the recorded, wind induced, response of the building. The recorded acceleration response values have been modified, as they have been multiplied with ½ to get a sort of absolute value instead of a peak to peak value as described in Chapter 3.5, to make the recorded response comparable to the predictions of the design codes. It is therefore assumed that the absolute maximum acceleration response value of each wind storm is similar to the absolute minimum acceleration response value.

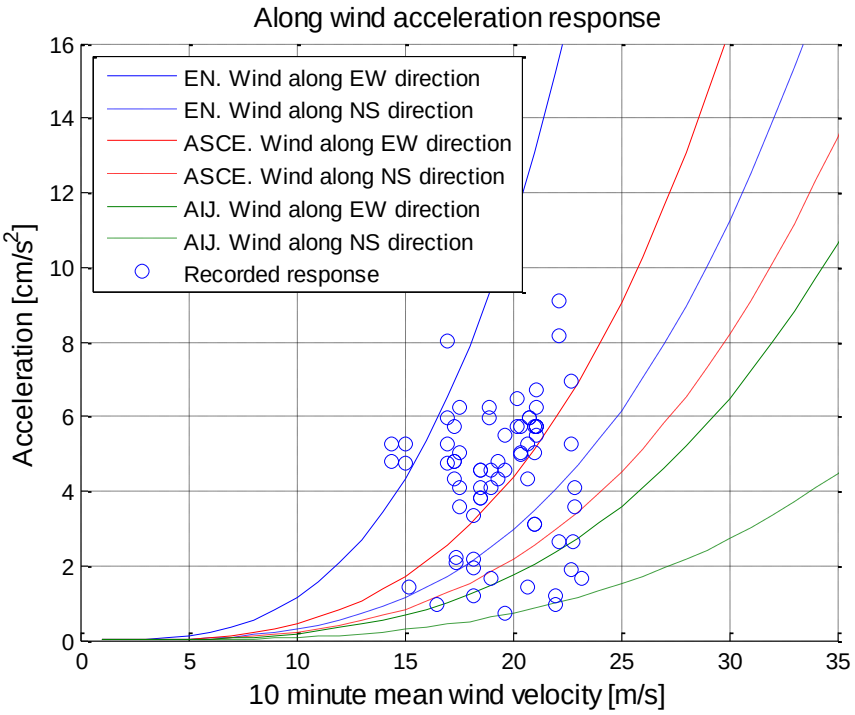

Figure 6.10: Along wind response predictions of the design codes along with the recorded response.

Figure 6.10 shows the clear difference of the design code predictions of the along wind acceleration response. All three design codes predict greater along wind response for wind acting in the east-west direction than for wind acting in the north-south direction, which corresponds to the recorded wind response as noted in Section 4.1.1. This is due to the geometry of the structure, as the first mode of vibration is in the east-west direction and the second mode of vibration is in the north-south direction and the fact that these two mode shapes have a very different character as previously described.

Figure 6.11 and Figure 6.12 show the results of the design code predictions for each wind direction separately. They include the along wind response prediction of all three codes along with the across wind response prediction of the AIJ code and the recorded wind induced response, categorized as either along wind response or across wind response.

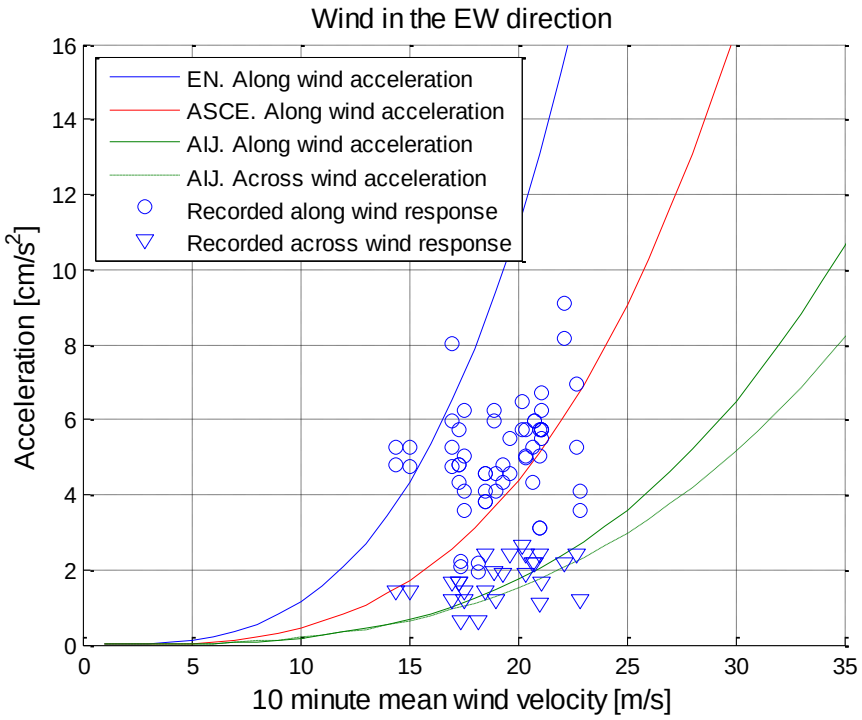

Figure 6.11: Response predictions of the design codes along with the recorded response for wind acting in the east-west direction.

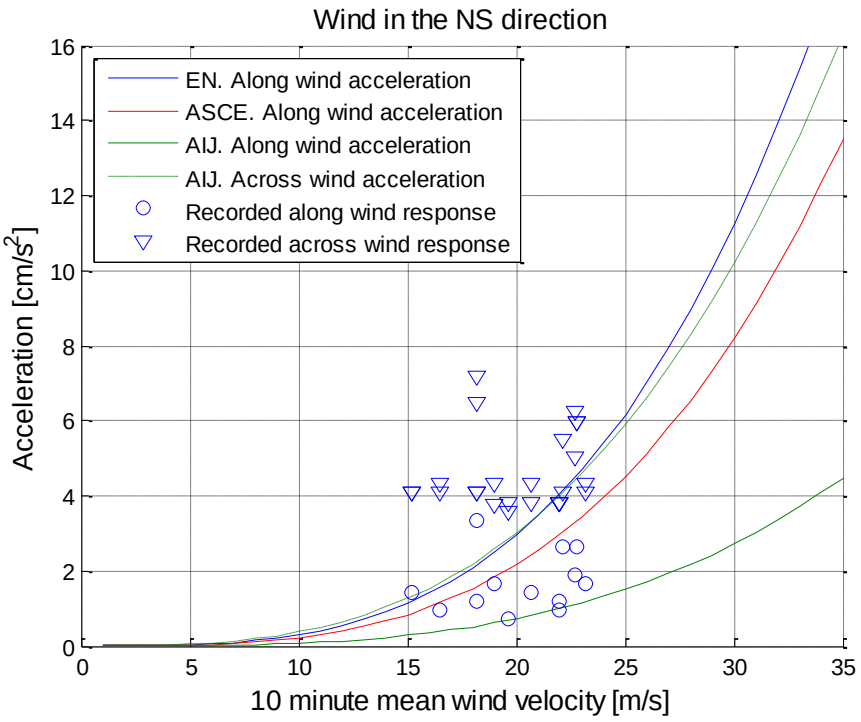

Figure 6.12: Response predictions of the design codes along with the recorded response for wind acting in the north-south direction.

The Eurocode EN 1991-1-4 Annex C procedure predicts the greatest along wind response of the design codes considered. For the recorded along wind response, it seems to be quite representative for the maximum along wind response, although there are a few points of recorded response of higher values than predicted by the Eurocode. The Eurocode EN 1991-1-4 prediction of along wind response acceleration does however grow quite rapidly with increasing wind velocity and with no recorded wind response for 10 minute mean wind velocity at 10 m height over 23 m/s it is difficult to assess whether the Eurocode, and the other design codes under consideration, predict the behaviour of the building well for high wind velocities. For wind acting in the north-south direction, where the across wind response is greater than the along wind response, the Eurocode along wind response prediction is much less than most of the recorded across wind acceleration values at lower wind velocities. It is however not justifiable to compare the Eurocode prediction of response to the recorded across wind response as the Eurocode does not offer procedures to predict the across wind response.

The ASCE procedure for evaluation of the along wind response acceleration results in lower values of response acceleration than the procedure of the Eurocode. The predicted response is close to the average recorded along wind response, a bit lower than the average for wind acting in the east-west direction and a bit higher than the average for wind acting in the north-

south direction. As for the Eurocode, the ASCE code does not include any procedure to evaluate the across wind response acceleration and thus can not be compared to the recorded across wind response.

The AIJ procedure to determine the maximum along wind response acceleration results in the lowest values of response acceleration of the design codes under consideration. The predicted along wind response is lower than all except one recorded along wind response so the AIJ code is clearly not representing a realistic behaviour of the building. The AIJ code predicts the across wind response much better than the along wind response when comparing the predictions of the design code to the recorded response although the maximum across wind response prediction values are a bit lower than the average recorded across wind responses, for wind acting in either direction.

Although all three design codes base their response prediction on the same basic theory, the theory and evaluation procedures are simplified in a different way. When seeking to assess what leads to the difference in results of the design code procedures, it seems that the resonance factors, which are evaluated based on the modal parameters of the structure, play a large role as shown in Figure 6.13 where the resonance factors, evaluated by the design codes, are compared. It shows how the along wind response prediction of the design codes are proportional to the resonance factors.

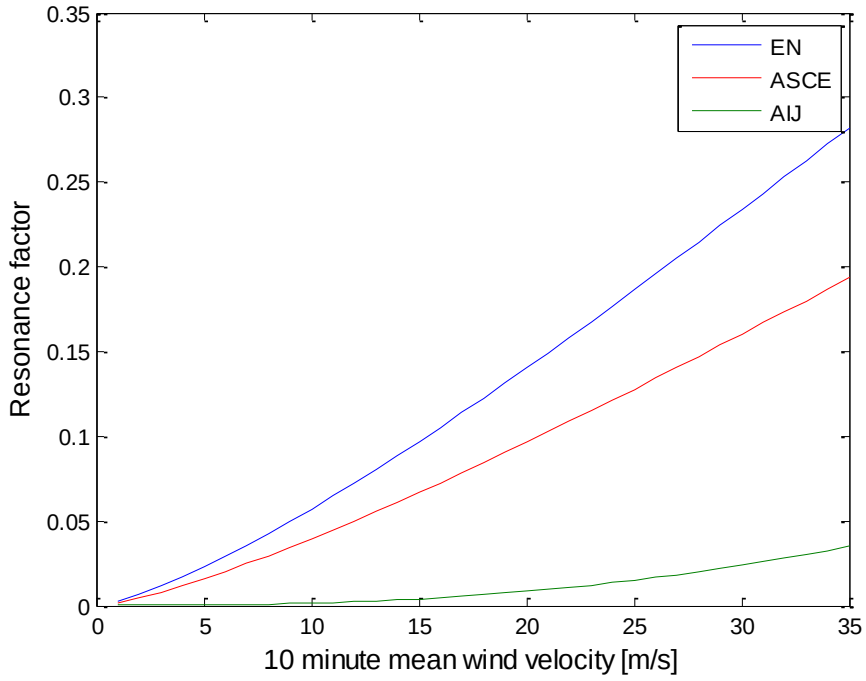

Figure 6.13: Comparison on the resonance factor evaluation of the design codes.

6.2. Comfort criteria's for building vibrations according to design codes

The Eurocode and the ASCE design code do not present their own human comfort criteria in terms of the maximum tolerated acceleration response. The AIJ code presents a human comfort criteria in the AIJ Guidelines for the Evaluation of Habitability to Building Vibration, AIJ-GBV-2004 (Tamura, Kawai, Uematsu, Okada, & Ohkuma, 2004), which is used in comparison to the recorded and predicted response of the building along with a comfort criteria presented in the international standard ISO 10137:2007.

The human comfort criteria's of the AIJ-GBV-2004 and the ISO 10137:2007 take account to the natural frequency of the structure and are applicable for wide variety of buildings, with natural frequency ranging from 0,06 Hz to 5 Hz, unlike the previous versions of both codes, the AIJ-GBV-1991 and the ISO 6897:1984, which were only applicable for taller buildings with natural frequency limited to up to 1 Hz. The comfort criteria's of both codes specify the maximum tolerated acceleration for a 10 minute mean wind velocity with a 1 year return period, which is about 21 m/s for the site in question, as noted in Chapter 3.5

The AIJ human comfort criteria's are shown in Figure 6.14. The five curves, marked H-10, H-30, H-50, H-70 and H-90 represent the percentage of perception probability, where it is

assumed that 10% of a building inhabitant's car perceive a motion when the acceleration response is above the H-10 curve and so on for the other curves.

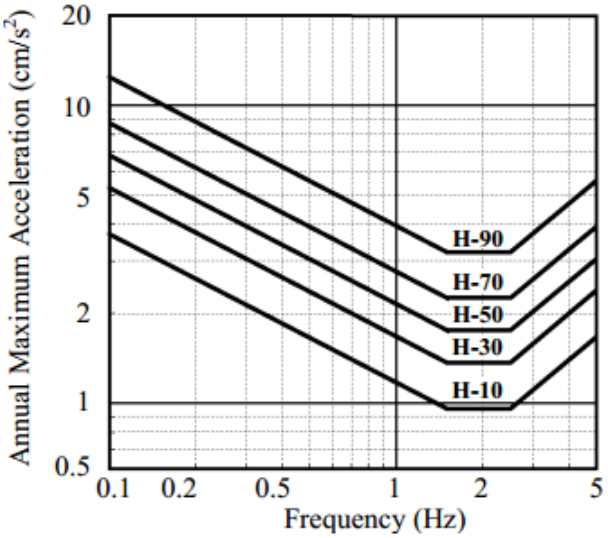

Figure 6.14: Human comfort criteria presented in AIJ-GBV-2004 for wind induced acceleration response of one year return period. The curves are marked with a persentage of a probability of vibration perception (Tamura et al., 2004).

The AIJ-GBV-2004 does not specify which curve represents an appropriate criterion for office buildings. The previous code, the AIJ-GBV-1991, with different human comfort criteria (Tamura, Ohkuma, Okada, & Kanda, 1999) did recommend a criteria for office building which resembles the H-70 curve the most so that curve is used in comparison to the response of the building and for a more liberal criteria the H-90 curve is also examined, indicating that the peak acceleration response with a one year return period should not be greater than about 2,2 or 3,1 cm/s^2 according to the H-70 and H-90 curves respectively for wind velocities of 21 m/s or less.

The ISO 10137 sets different serviceability criteria for office buildings than for residence buildings as it demands 1/3 more stability of the residence buildings. The human comfort criteria of the ISO 10137 standard against wind induced acceleration response is shown in Figure 6.15.

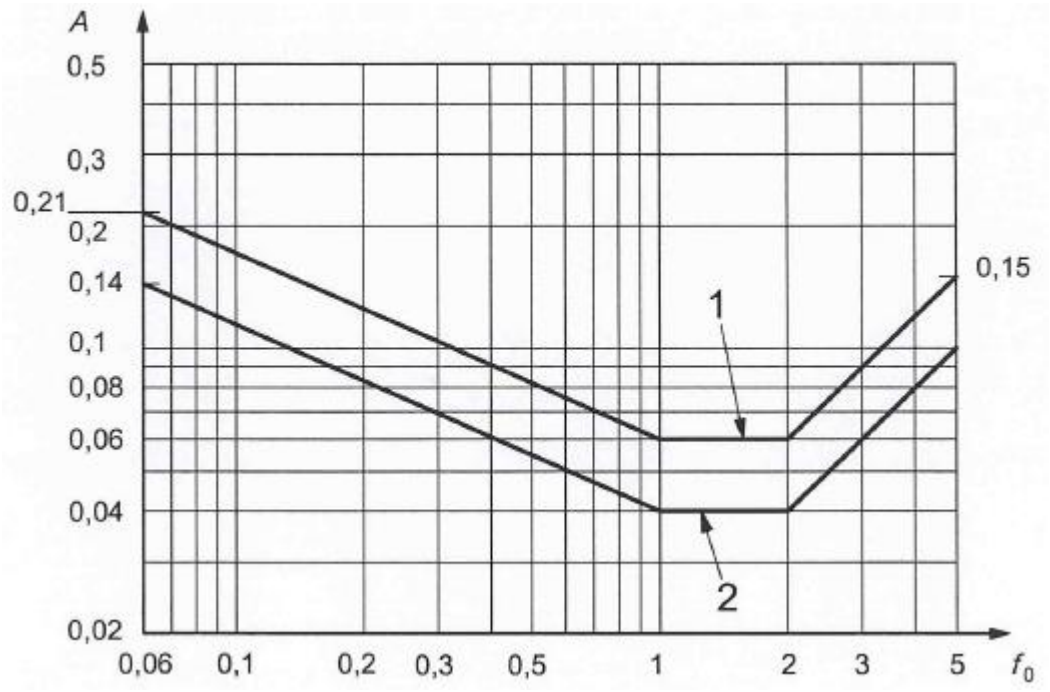

Figure 6.15: Human comfort criteria presented in ISO 10137:2007 for wind induced acceleration response of one year return period. The upper curve, marked with „1“, represents the criteria for office buildings and the lower curve, marked with „2“, represents the criteria for residence buildings. The peak acceleration is measured in m/s^2 and the natural frequency in Hz (*ISO 10137,* 2007).

According to the ISO 10137 comfort criteria, the peak acceleration response with a one year return period should not be greater than 6 cm/s^2 for wind velocities of 21 m/s or less.

It is noteworthy that as the observed building has a first natural frequency of about 1,7 Hz it falls into a group of buildings that have the lowest critical acceleration level of both codes, as the strictest acceleration criteria is given for structures with the first natural frequency ranging from about 1,4 to 2,4 Hz in the AIJ code and 1 to 2 Hz in the ISO code.

Figure 6.16 and Figure 6.17 show the great difference of the comfort criteria’s of the AIJ-GBV-2004 and the ISO 10137:2007 as the criteria’s are plotted along with the design code response prediction and the recorded response of the building for wind velocity in the east-west and north-south directions respectively. It shows that for wind velocities lower than 21 m/s, the wind velocity of 1 year return period, the acceleration response of the vast majority of records was over both of the AIJ criteria’s and a few times the recorded acceleration response was over the ISO criteria. It is therefore clear that the building does not fulfill the human comfort criteria of neither code considered. It should though be reaffirmed that each recorded wind storm result in three values on the figure, either two for along wind response

and one for across wind response or two for across wind response and one for along wind response, as a result of the three accelerometers at the 14th floor, two in the east-west direction and one in the north-west direction. It should also be noted that the 10 minute mean wind velocity has on many occasions been higher than the evaluated wind velocity for 1 year return period, as shown in chapter 3.4 and on the figures showing the recorded response.

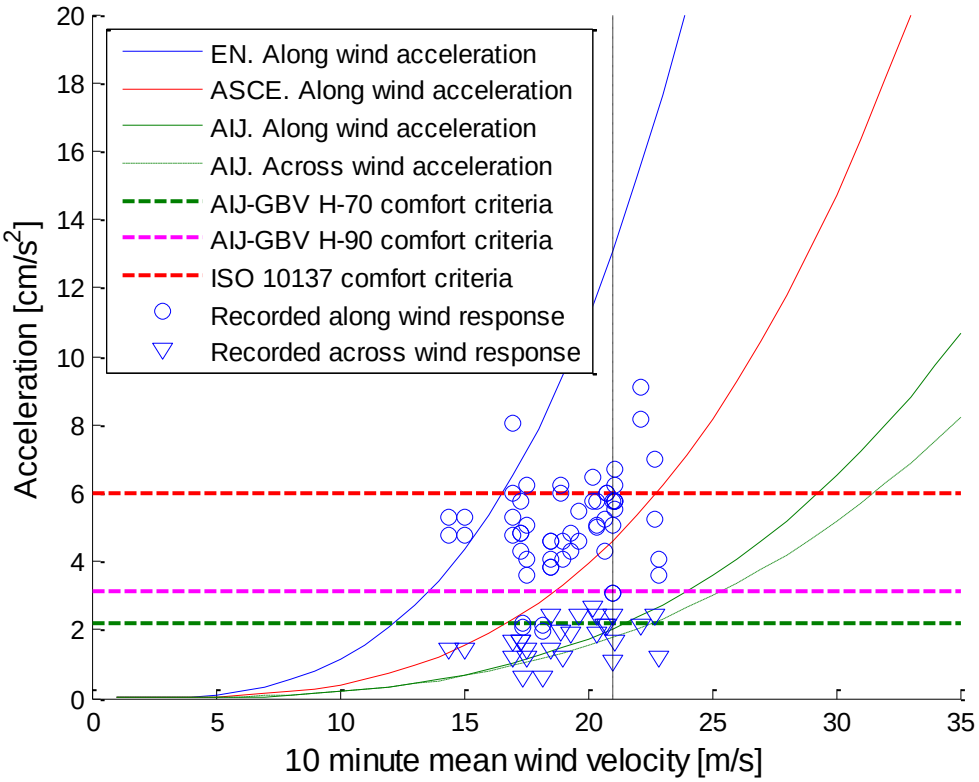

Figure 6.16: Comparison of the comfort criteria's of AIJ-GBV-2004 and ISO 10137:2007, design code prediction and recorded wind induced vibration for wind in the east-west directions. The vertical line at 21 m/s represents the maximum mean wind velocity expected every year.

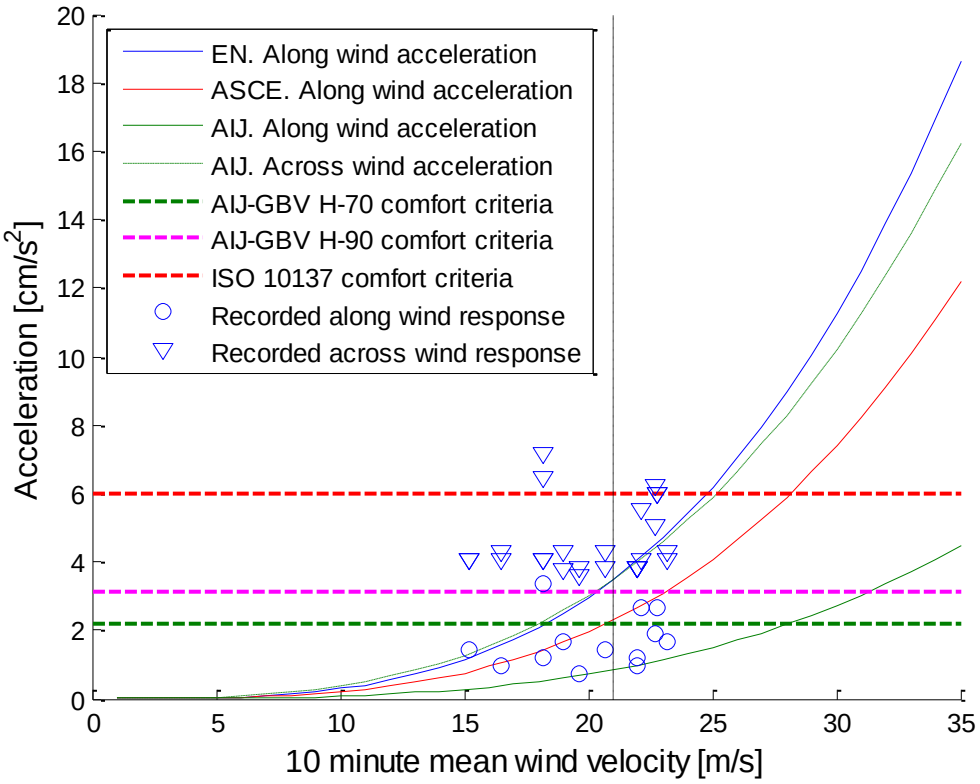

Figure 6.17: Comparison of the comfort criteria's of AIJ-GBV-2004 and ISO 10137:2007, design code prediction and recorded wind induced vibration for wind in the north-south directions. The vertical line at 21 m/s represents the maximum mean wind velocity expected every year.

In the 19 year monitoring period used in the analysis where the recorded wind induced response has been linked to the wind speed at the given time, from the year 1990 to 2008, with only a few short unfortunate pauses in monitoring, there have been recorded 51 wind storms strong enough to trigger the monitoring system. Of those 51 storms, regardless of wind speed, 40 storms have breached the human comfort criteria of the AIJ design code, based on the H-90 curve, assuming that over 90 % of the building inhabitants have perceived motion 40 times in the 19 year monitoring history. Over the same period only 10 storms have breached the human comfort criteria of the ISO 10137 code, taking no account to the wind speed. As the human comfort criteria's of the codes are based on the wind speed of one year reoccurrence the number of storms breaching the criteria's can be put into perspective by evaluating the average number of criteria breaches over the monitoring period. Over these 19 years the ISO 10137 comfort criteria has been breached at average about 0,53 times per year, or about every two years. Over the same period the AIJ comfort criteria has been breached at average about 2,11 times a year. In that perspective, it can be inferred that the building does not breach the human comfort criteria presented by the ISO 10137.

A comparison of the design code response prediction to the comfort criteria's is also shown in Figure 6.16 and Figure 6.17 where it is seen that only the Eurocode EN 1991-1-4 predicts the response to breach the human comfort criteria presented by the ISO 10137 code for wind velocity of one year return period or 21 m/s and is assumed to be for wind velocity in the east-west direction. Both of the AIJ comfort criteria's, the H-70 and H-90 criteria's, are breached by all three design codes response predictions for the same wind velocity.

7. Conclusion and final remarks

This chapter gives a brief review of the tasks and summaries the main findings of the thesis. It also reflects on a few unanswered questions that could be the subjects of further researches.

7.1. Review of tasks and main findings

The building that was examined is a 14 storey tall, reinforced concrete, office building. Along with the two floor basement, the total height of the structure is about 52,3 m. With a quite complex geometry of the structure, the dynamic behaviour of the structure may not be completely predictable at first sight. The building is equipped with a monitoring system, which has been used to record the acceleration response of the structure due to wind and earthquake excitations since 1989.

The wind induced response, recorded with the monitoring system installed in the building, was analysed along with the additional weather data from the Icelandic meteorological office (IMO). It was found that the acceleration response of the building showed poor correlation to the wind velocity. The lack of correlation between the wind velocity and acceleration response might be due to the wind velocity not being recorded at the building itself but at the IMO site about 500 m away or the way the data are categorized, with a possibility of 45° variety of wind direction in each wind direction category. Partly, the lack of correlation between wind action and acceleration response can be traced to the high natural frequency of the building. By studying the power spectral density of the along wind velocity, it is seen that the energy of the wind is less influenced by the wind velocity for structures with natural frequencies of 1.7 Hz as for the first mode of vibration of the building, than for structures with natural frequencies below 1 Hz.

The building was shown to respond strongly in the across wind direction with the wind acting in the north-south directions. At average the along wind response was seen to be about 3 times the across wind acceleration response for wind acting in the east-west direction while for wind acting the north-south direction the along wind response was seen to be only about one third of the across wind response at average. The difference on the along and across wind response for the different wind directions is due to the geometry of the building, the slenderness of the top floors where the sides facing the east-west directions are about four times wider than the sides facing the north-south directions. As opposed to the top floors aspect ratio, the bottom floors, i.e. floors 2 to 8, have about four times wider sides facing the

north-south directions than the east-west directions. This results in a structure relatively much stiffer in the east-west directions at the bottom than in the north-south directions and completely the opposite in the top floors. This shift in stiffness along the height of the structure promotes the possibility of strong response of the building in the across wind direction for wind acting in the north-south directions.

The earthquake induced response time series were analysed to evaluate the magnification ratios, the ratio of the peak response recorded at the top floor to the peak response recorded in the basement. The magnification ratios were seen to range from 3,7 to 6,9 except for one earthquake event, which is an aftershock from the June 17. 2000, where the magnification ratios were 13,2 and 2,6 in the east-west directions and the north-west directions respectively for unknown reasons. Peak response acceleration at the top floor was seen to increase exponentially with increased acceleration at the basement level in the east-west directions, but close to linearly in the north-south directions.

A system identification was carried out to evaluate the natural frequencies and critical damping ratios. In the system identification process, two different methods were used to evaluate the power spectral densities, the non-parametric fast Fourier method and the parametric auto regressive method. All the response time series available were used in the system identification process, 20 time series of wind induced response and 8 of earthquake induced response, although for the time series of the earthquake induced responses, only the auto regressive analysis method was used due to the short time series.

The system identification resulted in very similar results for the natural frequencies which can be seen in Table 4.9 where the results for the natural frequencies of both methods of analysis for the wind induced response time series are compared and in Table 4.13 where the results of the natural frequencies evaluated with the auto regressive method for wind and earthquake induced response are compared.

The critical damping ratios were seen to vary considerably. When the results of both analysis methods for the wind induced response time series were compared, the difference in results of the critical damping ratios between the two methods were greatest for the first modes of vibration but the variablity was reduced for the higher modes of vibration as shown in Table 4.10. When the results of the auto regressive analysis of wind and earthquake induced response were compared, the greatest difference of the critical damping ratios were for the first three modes of vibration as shown in Table 4.14.

From all three sets of system identification, the natural frequencies were seen to decrease with time. This evolution in natural frequencies seems to have undergone without damage to the structure. From the analysis of the earthquake induced response time series, the decrease in natural frequencies seem to depend on the amplitude of the response as the natural frequency of the first mode of vibration is seen to decrease with increased response amplitude in Figure 4.41.

A finite element modelling of the building was carried out with the use of the finite element software SAP2000 to interpret and extend the information gathered by the full scale recordings. The finite element model gave further understanding of the dynamic behaviour of the building as the modes of vibration were seen visually. It showed the difference of the first two mode shapes which are translations in the east-west directions and north-south directions respectively, and how the first mode shape resembles a parabolic shape while the second mode shape resembles a linear shape which further explains the difference in along and across wind response for different wind directions and the difference in magnification ratios of the earthquake response, recorded in different directions of the building as previously noted.

The finite element model was calibrated by using various modulus of elasticity along the height of the building, 30 GPa for the basement floors, 23 GPa for the 1^{st} to 8^{th} floor and 18 GPa for the 9^{th} to 14^{th} floor. The calibrated model showed great correlation in natural frequencies to the full scale recordings for the first six modes, except for the third mode of vibration which is a clear torsional vibration where the finite element model showed a bit to low natural frequency. It was nonetheless decided that the model was sufficiently accurate for the purpose at hand.

Using the simplified procedures of design codes, the predicted response of the building was evaluated and compared to the full scale recordings. Three design codes were used, the European design code, Eurocode 1991-1-4, the American design code, presented by the American Society of Civil Engineers (ASCE) and the Japanese design code, presented by the Architectural Institute of Japan (AIJ).

The three design code predictions gave very different results to each other. The Eurocode predicted the greatest along wind response, matching relatively well the maximum recorded along wind response but with very rapid growth in predicted response with increased wind velocity. The ASCE design code gave lower results than the Eurocode and was close to representing the average recorded along wind response. The AIJ design code predicted the

lowest values of response of the three design code, clearly missing out on the realistic behaviour of the along wind response. The AIJ code was however the only design code of the three to present a procedure to evaluate the across wind response and gave higher values of across wind response than along wind response for wind acting in the north-south directions as had been shown previously with the full scale recordings. The values of predicted across wind response of the AIJ code were nonetheless not high enough to represent the across wind response recorded in the building. The Eurocode and the ASCE design code were missing out on the across wind response as their procedures did not evaluate the across wind response and the along wind response evaluated was well below the recorded across wind response for wind acting in the north-south directions.

The human comfort criteria's of the AIJ and the international standard ISO 10137 published by the International Organization for Standardization were presented and compared to the recorded response. Both of the criteria's are based on wind velocity of one year return period, which is assumed to be about 21 m/s. The AIJ code human comfort criteria's limits the wind induced response to 2,2 m/s^2 and 3,1 m/s^2 representing a perception of 70 % and 90% of the building inhabitants respectively. The human comfort criteria of the ISO 10137 limits the wind induced response to 6 m/s^2. The recorded response of the building was shown to be above the criteria's of both codes on numerous occasions for the given wind velocity of one year return period. When looking at the whole monitoring history however, the recorded response does only breach the ISO 10137 comfort criteria once every two years at average, but the AIJ comfort criteria is breached at average twice a year. In that perspective it can be said that the building fulfills the human comfort criteria of the ISO 10137 code.

7.2. Recommendations for further research

In the working process of the thesis, some questions arose that were not answered and could possibly be the subject of further researches.

The evolution of the natural frequencies is an interesting issue and could possibly by the focus point of further research, concentrating more on the cause of the decrease.

The difference in results of the response predictions evaluated with the design code procedures drew attention and it could be interesting to gain further understanding of the difference in the simplified procedures by evaluating the predicted response for various buildings by these procedures.

As the building is equipped with the monitoring system as previously described it has the potential to further examine the human comfort of the people working in the building during wind induced response, especially as the recorded acceleration response has on numerous occasions been above the human comfort criteria's presented in the ISO 10137 code and the AIJ code. The comfort of the workers could be evaluated with surveys during or shortly after an event of considerably strong winds.

References

Abdul-Wahab, H., & Khalil, M. (2000). Rigidity and Strength of Orthotropic Reinforced Concrete Waffle Slabs. *Journal of Structural Engineering*, *126*(2), 219–227. doi:10.1061/(ASCE)0733-9445(2000)126:2(219)

Alkan, A., & Yilmaz, A. S. (2007). Frequency domain analysis of power system transients using Welch and Yule–Walker AR methods. *Energy Conversion and Management*, *48*(7), 2129–2135. doi:10.1016/j.enconman.2006.12.017

Ambraseys, N., Smit, P., Sigbjornsson, R., Suhadolc, P., & Margaris, B. (2002). *Internet-Site for European Strong-Motion Data*. European Commission, Research-Directorate General, Environment and Climate Programme. Retrieved from http://www.isesd.hi.is/ESD_Local/frameset.htm

Archive of ShakeMaps. (2011). *Veðurstofa Íslands*. Retrieved December 19, 2013, from http://hraun.vedur.is/ja/alert/shake/archive/2011.html

Burton, M., Kwok, K., Hitchcock, P., & Denoon, R. (2006). Frequency dependence of human response to wind-induced building motion. *Journal of Structural Engineering*, *132*(2), 296–303. doi:10.1061/(ASCE)0733-9445(2006)132:2(296)

Chopra, A. K. (2006). *Dynamics of Structures* (3rd ed.). New Jersey: Prentice Hall.

Clinton, J. F., Bradford, S. C., & Heaton, T. H. (2005). Variations in the Natural Frequencies of Millikan Library Caused by Weather and Small Earthquakes. In *Structures Congress 2005* (pp. 1–11). American Society of Civil Engineers. Retrieved from http://ascelibrary.org/doi/abs/10.1061/40753%28171%2990

Gil-Martín, L. M., Carbonell-Márquez, J. F., Hernández-Montes, E., Aschheim, M., & Pasadas-Fernández, M. (2012). Dynamic magnification factors of SDOF oscillators under harmonic loading. *Applied Mathematics Letters*, *25*(1), 38–42. doi:10.1016/j.aml.2011.07.005

Gu, M., & Quan, Y. (2004). Across-wind loads of typical tall buildings. *Journal of Wind Engineering and Industrial Aerodynamics*, *92*(13), 1147–1165. doi:10.1016/j.jweia.2004.06.004

Holmes, J. D. (2007). *Wind Loading of Structures* (2nd ed.). Abingdon: CRC Press.

Kim, J. Y., Yu, E., Kim, D. Y., & Kim, S.-D. (2009). Calibration of analytical models to assess wind-induced acceleration responses of tall buildings in serviceability level. *Engineering Structures*, *31*(9), 2086–2096. doi:10.1016/j.engstruct.2009.03.010

Kramer, S. L. (1996). *Geotechnical earthquake engineering*. Upper Saddle River, N.J.: Prentice Hall.

Kumar, S. (2002). Live loads in office buildings: point-in-time load intensity. *Building and Environment*, *37*(1), 79–89. doi:10.1016/S0360-1323(00)00074-3

Kwok, K. C. S., Hitchcock, P. A., & Burton, M. D. (2009). Perception of vibration and occupant comfort in wind-excited tall buildings. *Journal of Wind Engineering and Industrial Aerodynamics*, *97*(7–8), 368–380. doi:10.1016/j.jweia.2009.05.006

Morava, B., Haskett, T., Chadwick, A., & Wates, E. (2010). Assessment of Occupant Comfort in Wind-Sensitive Buildings Using a Six-Degree-of-Freedom Motion Simulator. In *Structures Congress 2010* (pp. 2972–2980). American Society of Civil Engineers. Retrieved from http://ascelibrary.org/doi/abs/10.1061/41130%28369%29268

Owen, J. S., Eccles, B. J., Choo, B. S., & Woodings, M. A. (2001). The application of auto–regressive time series modelling for the time–frequency analysis of civil engineering structures. *Engineering Structures*, *23*(5), 521–536. doi:10.1016/S0141-0296(00)00059-6

Shinozuka, M., Deodatis, G., Zhang, R., & Papageorgiou, A. S. (1999). Modeling, synthetics and engineering applications of strong earthquake wave motion. *Soil Dynamics and Earthquake Engineering*, *18*, 209–228. doi:10.1016/S0267-7261(98)00045-1

Snæbjörnsson, J. Þ. (2002, September). *Full- and model scale study of wind effects on a medium-rise building in a built up area* (Doctoral Thesis). Norwegian University of Science and Technology, Trondheim, Norway.

Snæbjörnsson, J. Þ., & Ingólfsson, E. Þ. (2013). Full-Scale Monitoring of the Dynamic Behavior of a 20 story RC Building. Presented at the The 12th Americas Conference on Wind Engineering, Seattle, Washington, USA.

Snæbjörnsson, J. Þ., & Sigurbjörnsson, R. (2006). Monitoring the dynamics of a concrete building enduring earthquake and wind excitation. Presented at the First European Conference of Earthquake Engineering and Seismology, Geneva, Switzerland.

Spyers-Ashby, J. M., Bain, P. G., & Roberts, S. J. (1998). A comparison of fast fourier transform (FFT) and autoregressive (AR) spectral estimation techniques for the analysis of tremor data. *Journal of Neuroscience Methods*, *83*(1), 35–43. doi:10.1016/S0165-0270(98)00064-8

Stewart, J. P., Seed, R. B., & Fenves, G. L. (1998). *Empirical evaluation of inertial soil-structure interaction effects (Report)*. Pacific Earthquake Engineering Research Center.

Tamura, Y. (1998). Application of damping devices to suppress wind-induced responses of buildings. *Journal of Wind Engineering and Industrial Aerodynamics*, *74–76*, 49–72. doi:10.1016/S0167-6105(98)00006-3

Tamura, Y., Kawai, H., Uematsu, Y., Okada, H., & Ohkuma, T. (2004). Documents for wind resistant design of buildings in Japan. In *Workshop on Regional Harmonization of Wind Loading and Wind Environmental Specifications in Asia-Pacific Economies (APEC-WW)* (pp. 61–84). Retrieved from http://www.wind.arch.t-kougei.ac.jp/APECWW/Report/2004/JAPANa.pdf

Tamura, Y., Ohkuma, T., Okada, H., & Kanda, J. (1999). Wind loading standards and design criteria in Japan. *Journal of Wind Engineering and Industrial Aerodynamics*, *83*(1–3), 555–566. doi:10.1016/S0167-6105(99)00101-4

Þrastardóttir, D. K., & Gunnarsdóttir, G. G. (2006). *Húsakönnun*. Reykjavík: Minjasafn Reykjavíkur.

Computer programs references

MATLAB (Version 7.12.0.635 (R2011a)). (2011). The MathWorks, Inc. Retrieved from http://www.mathworks.se/products/matlab/

SAP 2000 (Version 14). (2010). Computers and Structures, Inc. Retrieved from http://www.csiamerica.com/sap2000

Design codes and standards references

AIJ Recommendations for Loads on Buildings. (2005). Architectural Istitute of Japan. Retrieved from http://www.aij.or.jp/jpn/symposium/2006/loads/loads.htm

Eurocode 1: Actions on structures - General actions - Part 1-4: Wind actions. (2004). Brussel: European Committee for Standardization.

Eurocode 2: Design of concrete structures - Part 1-1: General rules and rules for buildings. (2004). Brussel: European Committee for Standardization.

ISO 10137:2007, Bases for design of structures - Serviceability of buildings against vibration. (2007). Geneva: ISO.

Structural Engineering Institute. (2006). *Minimum design loads for buildings and other structures*. Virginia: American Society of Civil Engineers/Structural Engineering Institute.

Drawings references

Ásgeirsson, E. Þ., & Sveinsson, I. (1974). *Hús verzlunarinnar: Arkitektateikningar*. Reykjavik.

Björnsson, P. Ö. (1998). *Hús verslunarinnar, Kringlunni 7: Arkitektateikningar*. Reykjavik.

Hagverk. (1976). *Hús verzlunarinnar: Verkfræðiteikningar*. Reykjavik.

Sveinsson, I. (1996). *Hús verslunarinnar: Arkitektateikningar*. Reykjavik.

Appendix A

In this appendix the calculations and analysis performed in Matlab is presented. These calculations consists of analysis of meteorological, wind and earthquake data, the system identification process, validation of the finite element model, predictions of wind induced response based on the simplified design code procedures and assessment of human comfort.

A1: Analysis of meteorological data

In this Matlab code the analysis of the meteorological data is performed, mainly in relation to Chapter 3.

```
%-------------------------------------------------------------------------
% This routine compares the human comfort criteria's presented by the AIJ
% and ISO 10137 codes to the response predicted by the Eurocode, the ASCE
% design code and the AIJ design code, and the recorded response provided
% by the Earthquake Engineering Research Center along with meteorological
% data provided by the Icelandic Meteorolocical Office
%
% Written by: Örvar Jónsson
%-------------------------------------------------------------------------

%% Comfort criteria

AIJc70 = 2.2; % AIJ H-70 criteria: 2,2 cm/s^2
AIJc90 = 3.1; % AIJ H-90 criteria: 3,1 cm/s^2
ISOc = 6;   % ISO criteria: 6 cm/s^2

% Loading recorded response
load max10mwindx; load max10mwindy; load windaccx1; load windaccx2;
load windaccy; load acrossaccx1; load acrossaccx2; load acrossaccy;

% Recorded response converted from peak-to-peak values to absolute values
windaccx1 = windaccx1/2;
windaccx2 = windaccx2/2;
windaccy = windaccy/2;
acrossaccx1 = acrossaccx1/2;
acrossaccx2 = acrossaccx2/2;
acrossaccy = acrossaccy/2;

figure
hold on
plot([0 35],[AIJc70 AIJc70],'--','color',[0 0.5 0],'linewidth',2)    % AIJ
guidelines
plot([0 35],[AIJc90 AIJc90],'--','color',[1 0 1],'linewidth',2)    % AIJ
guidelines
plot([0 35],[ISOc ISOc],'--r','linewidth',2)    % ISO guidelines
plot(max10mwindy,windaccy,'o')                  % Recorded along response
plot(max10mwindy,acrossaccx1,'v')               % Recorded across response
plot(max10mwindy,acrossaccx2,'v')               % Recorded across response
plot(max10mwindx,windaccx1,'o')                 % Recorded along response
plot(max10mwindx,windaccx2,'o')                 % Recorded along response
plot(max10mwindx,acrossaccy,'v')                % Recorded across response
plot([21 21],[0 12],'--k')                      % 1 year return period wind
velocity
hold off
legend('AIJ-GBV H-70','AIJ-GBV H-90','ISO 10137',...
    'Recorded along wind response','Recorded across wind response',...
    'location','northwest')
fs = 12;
xlabel('10 minute mean wind velocity [m/s]','fontsize',fs)
ylabel('Acceleration [cm/s^2]','fontsize',fs)


%% Counting storms that breach the criteria's+
```

```
% AIJ H-90
% wind in EW direction
aijcritx = zeros(length(max10mwindx),3);
aijcrity = zeros(length(max10mwindy),3);
for i = 1:length(max10mwindx)
    aijcritx(i,1) = windaccx1(i,1)>AIJc90;
    aijcritx(i,2) = windaccx2(i,1)>AIJc90;
    aijcritx(i,3) = acrossaccy(i,1)>AIJc90;
end
% Wind in NS direction
for i = 1:length(max10mwindy)
    aijcrity(i,1) = windaccy(i,1)>AIJc90;
    aijcrity(i,2) = acrossaccx1(i,1)>AIJc90;
    aijcrity(i,3) = acrossaccx2(i,1)>AIJc90;
end
% Number of responses higher than criteria
aijcritxnum = sum(sum(aijcritx')>0);
aijcritynum = sum(sum(aijcrity')>0);
aijcritnum = aijcritxnum + aijcritynum

% ISO
% Wind in EW direction
isocritx = zeros(length(max10mwindx),3);
isocrity = zeros(length(max10mwindy),3);
for i = 1:length(max10mwindx)
    isocritx(i,1) = windaccx1(i,1)>ISOc;
    isocritx(i,2) = windaccx2(i,1)>ISOc;
    isocritx(i,3) = acrossaccy(i,1)>ISOc;
end
% Wind in NS direction
for i = 1:length(max10mwindy)
    isocrity(i,1) = windaccy(i,1)>ISOc;
    isocrity(i,2) = acrossaccx1(i,1)>ISOc;
    isocrity(i,3) = acrossaccx2(i,1)>ISOc;
end
% Number of responses higher than criteria
isocritxnum = sum(sum(isocritx')>0);
isocritynum = sum(sum(isocrity')>0);
isocritnum = isocritxnum + isocritynum


%% Comfort criteria compared to design code estimations

EN_HV
ASCE_HV
AIJ_HV

% Wind in EW
figure
hold on
plot(V10,acc_along_C(:,1),'b') % EC C along wind EW

plot(Vm,a_max_EW,'r') % ASCE along wind EW

plot(U0,aDmaxEW,'color',[0 0.5 0]) % AIJ along wind EW
plot(U0,aLmaxEW,'-.','color',[0 0.5 0]) % AIJ across wind EW

plot([0 35],[AIJc70 AIJc70],'--','color',[0 0.5 0],'linewidth',2)    % AIJ
guidelines
```

```
plot([0 35],[AIJc90 AIJc90],'--','color',[1 0 1],'linewidth',2)    % AIJ
guidelines
plot([0 35],[ISOc ISOc],'--r','linewidth',2)    % ISO guidelines

plot(max10mwindx,windaccx1,'o')
plot(max10mwindx,acrossaccy,'v')
plot(max10mwindx,windaccx2,'o')

plot([21 21],[0 20],'--k')    % 1 year return period wind velocity

hold off
ylim([0 20]); xlim([0 35]);
fs = 12;
title('Wind in the EW direction','fontsize',fs)
legend('EN. Along wind acceleration',...
    'ASCE. Along wind acceleration',...
    'AIJ. Along wind acceleration',...
    'AIJ. Across wind acceleration',...
    'AIJ-GBV H-70 comfort criteria','AIJ-GBV H-90 comfort criteria',...
    'ISO 10137 comfort criteria',...
    'Recorded along wind response',...
    'Recorded across wind response','location','northwest')
xlabel('10 minute mean wind velocity [m/s]','fontsize',fs)
ylabel('Acceleration [cm/s^2]','fontsize',fs)

%% Wind in NS direction

figure
hold on
plot(V10,acc_along_C(:,2),'b') % EC C along wind NS

plot(Vm,a_max_NS,'r') % ASCE along wind Ns

plot(U0,aDmaxNS,'color',[0 0.5 0]) % AIJ along wind NS
plot(U0,aLmaxNS,'-.','color',[0 0.5 0]) % AIJ across wind NS

plot([0 35],[AIJc70 AIJc70],'--','color',[0 0.5 0],'linewidth',2)    % AIJ
guidelines
plot([0 35],[AIJc90 AIJc90],'--','color',[1 0 1],'linewidth',2)    % AIJ
guidelines
plot([0 35],[ISOc ISOc],'--r','linewidth',2)    % ISO guidelines

plot(max10mwindy,windaccy,'o')
plot(max10mwindy,acrossaccx1,'v')
plot(max10mwindy,acrossaccx2,'v')

plot([21 21],[0 20],'--k')                      % 1 year return period wind
velocity

hold off
grid on
ylim([0 20]); xlim([0 35]);
fs = 12;
title('Wind in the NS direction','fontsize',fs)
legend('EN. Along wind acceleration',...
    'ASCE. Along wind acceleration',...
    'AIJ. Along wind acceleration',...
    'AIJ. Across wind acceleration',...
    'AIJ-GBV H-70 comfort criteria','AIJ-GBV H-90 comfort criteria',...
```

```
    'ISO 10137 comfort criteria',...
    'Recorded along wind response',...
    'Recorded across wind response','location','northwest')
xlabel('10 minute mean wind velocity [m/s]','fontsize',fs)
ylabel('Acceleration [cm/s^2]','fontsize',fs)
```

A2: Analysis of wind data

In this Matlab code, the analysis of the recorded wind induced response is performed, mainly in relation to Chapter 4.

```
%-------------------------------------------------------------------------
% This routine analyses the wind induced response of the building from
% recorded data provided by the Earthquake Engineering Research Center
% along with meteorological data provided by the Icelandic Meteorolocical
% Office
%
% The routine analyses and presents the following:
% - categorizes the wind induced responses into groups based on the wind
%   direction
% - the along and across wind response in relation to wind direction and
%   velocity
% - the eurocode wind power spectral density
%
% Written by: Örvar Jónsson
%-------------------------------------------------------------------------

gogn = xlsread('HV_90_96_pikkad.xls',1,'B7:Z262');
gogn(:,7:9) = gogn(:,7:9)*9.81; % Converted from g's to cm/s^2

% loading data from 1997 - 2008
wind97_08
gogn(end+1:end+16,:) = 0;
gogn(end-15:end,1) = [37:52];
gogn(end-15:end,7:9) = Mx;
gogn(end-15:end,13:16) = W(:,7:10);
gogn(end-15:end,21) = W(:,9);
gogn(end-15:end,25) = W(:,7);

N = 52; % Number of events

windacc = zeros(N-1,1);
meanwind = zeros(N-1,1);
knots2ms = 0.514444;


for i = 1:N-1
    for j = i:length(gogn)
        if gogn(j,1) == i+1 %first record not included
            %B = gogn(j,7);
            if gogn(j,7) > windacc(i,1)
                windacc(i) = gogn(j,7);
                meanwind(i) = gogn(j,21);
            end
        end
    end
end

%% Categorizing data based on wind direction

% Building alignment
ydir = 20; % y alignment
xdir = 110; % x alignment
```

```
% wind directions of the y direction category
% 157.5° to 202.5°   plus HVydir     = 177.5° to 222.5°
% 337.5° to 22.5°        plus HVydir     = 357.5° to 42.5°
ydirmin(1,1) = ydir - 22.5;
if ydirmin(1,1) < 0
    ydirmin(1,1) = ydirmin(1,1) + 360;
end
ydirmin(2,1) = ydirmin(1,1) + 180;
if ydirmin(2,1) > 360
    ydirmin(2,1) = ydirmin(2,1) - 360;
end

ydirmax(1,1) = ydir + 22.5;
if ydirmax(1,1) > 360
    ydirmax(1,1) = ydirmax(1,1) - 360;
end
ydirmax(2,1) = ydirmax(1,1) + 180;
if ydirmax(2,1) > 360
    ydirmax(2,1) = ydirmax(2,1) - 360;
end

% wind directions of the x direction category
% 247.5° to 292.5°  plus HVydir      = 267.5° to 312.5°
% 67.5° to 112.5°   plus HVydir      = 87.5° to 132.5°
xdirmin(1,1) = xdir - 22.5;
if xdirmin(1,1) < 0
    xdirmin(1,1) = xdirmin(1,1) + 360;
end
xdirmin(2,1) = xdirmin(1,1) + 180;
if xdirmin(2,1) > 360
    xdirmin(2,1) = xdirmin(2,1) - 360;
end

xdirmax(1,1) = xdir + 22.5;
if xdirmax(1,1) > 360
    xdirmax(1,1) = xdirmax(1,1) - 360;
end
xdirmax(2,1) = xdirmax(1,1) + 180;
if xdirmax(2,1) > 360
    xdirmax(2,1) = xdirmax(2,1) - 360;
end

% Picking out x direction data
gognx = zeros(size(gogn));
for i = 1:length(gogn)
    if gogn(i,13) >= xdirmin(1,1) && gogn(i,13) <= xdirmax(1,1)
        gognx(i,:) = gogn(i,:);% Tek alla línuna
    elseif gogn(i,13) >= xdirmin(2,1) && gogn(i,13) <= xdirmax(2,1)
        gognx(i,:) = gogn(i,:);% Tek alla línuna
    end
end

for i=length(gognx):-1:1
    if gognx(i,1) == 0
        gognx(i,:) = [];
    end
end

% Picking out y direction data
gogny = zeros(size(gogn));
```

```
for i = 1:length(gogn)
    if gogn(i,13) >= ydirmin(1,1) && gogn(i,13) <= 360
        gogny(i,:) = gogn(i,:);% the whole line
    elseif gogn(i,13) >= 0 && gogn(i,13) <= ydirmax(1,1)
        gogny(i,:) = gogn(i,:);% the whole line
    elseif gogn(i,13) >= ydirmin(2,1) && gogn(i,13) <= ydirmax(2,1)
        gogny(i,:) = gogn(i,:);% the whole line
    end
end

for i=length(gogny):-1:1
    if gogny(i,1) == 0
        gogny(i,:) = [];
    end
end

%% Distribution of wind directions triggering the monitoring system

figure
pie([30,13,8],{'E-W','N-S','Other directions'})
title('Distribution of wind directions','fontsize',14)

%% Peak acceleration values of response in each storm event categorized

N = 52; % Number of events
windaccx1 = zeros(N,1);
meanwindx1 = zeros(N,1);
windaccx2 = zeros(N,1);
meanwindx2 = zeros(N,1);
windaccy = zeros(N,1);
meanwindy = zeros(N,1);

% Acceleration response of the 14th floor. EW south (X sensor 1)
% Peak values of each storm event along with wind velocity located
for i = 1:N
    for j = 1:length(gognx)
        if gognx(j,1) == i
            if gognx(j,7) > windaccx1(i,1)
                windaccx1(i) = gognx(j,7);
                meanwindx1(i) = gognx(j,15)*0.51444444;
            end
        end
    end
end
% Deleting zeros
for i=length(windaccx1):-1:1
    if windaccx1(i) == 0
        windaccx1(i) = [];
        meanwindx1(i) = [];
    end
end

% Acceleration response of the 14th floor. EW north (X sensor 2)
% Peak values of each storm event along with wind velocity located
for i = 1:N
    for j = 1:length(gognx)
        if gognx(j,1) == i
            %B = gogn(j,7);
            if gognx(j,8) > windaccx2(i,1)
                windaccx2(i) = gognx(j,8);
```

```
                meanwindx2(i) = gognx(j,15)*0.51444444;
            end
        end
    end
end
% Deleting zeros
for i=length(windaccx2):-1:1
    if windaccx2(i) == 0
        windaccx2(i) = [];
        meanwindx2(i) = [];
    end
end

% Acceleration response of the 14th floor. NS (Y sensor)
% Peak values of each storm event along with wind velocity located
for i = 1:N
    for j = 1:length(gogny)
        if gogny(j,1) == i
            if gogny(j,9) > windaccy(i,1)
                windaccy(i) = gogny(j,9);
                meanwindy(i) = gogny(j,15)*0.51444444;
            end
        end
    end
end
% Deleting zeros
for i=length(windaccy):-1:1
    if windaccy(i) == 0
        windaccy(i) = [];
        meanwindy(i) = [];
    end
end

%% Maximum 10minute mean wind velocity of each storm picked
max10mwindx = zeros(N,1);
max10mwindy = zeros(N,1);

for i = 1:N
    for j = 1:length(gognx)
        if gognx(j,1) == i
            if gognx(j,21) > max10mwindx(i,1)
                max10mwindx(i) = gognx(j,21);
            end
        end
    end
end
% Deleting zeros
for i=length(max10mwindx):-1:1
    if max10mwindx(i) == 0
        max10mwindx(i) = [];
    end
end

for i = 1:N
    for j = 1:length(gogny)
        if gogny(j,1) == i
            if gogny(j,21) > max10mwindy(i,1)
                max10mwindy(i) = gogny(j,21);
            end
        end
    end
end
```

```
end
% Deleting zeros
for i=length(max10mwindy):-1:1
    if max10mwindy(i) == 0
        max10mwindy(i) = [];
    end
end

%% Along wind response plotted agains wind velocity
figure
plot(max10mwindx,windaccx1,'o')
fs = 12;
title('Acceleration of 14th floor in the EW direction. EW component
1','FontSize',fs)
xlabel('Maximum 10 minute mean wind velocity of [m/s]','FontSize',fs)
ylabel('Maximum acceleration of [cm/s^2]','FontSize',fs)

figure
plot(max10mwindx,windaccx2,'o')
fs = 12;
title('Acceleration of 14th floor in the EW direction. EW component
2','FontSize',fs)
xlabel('Maximum 10 minute mean wind velocity of [m/s]','FontSize',fs)
ylabel('Maximum acceleration of [cm/s^2]','FontSize',fs)

figure
plot(max10mwindy,windaccy,'o')
fs = 12;
title('Acceleration of 14th floor in the NS direction','FontSize',fs)
xlabel('Maximum 10 minute mean wind velocity of [m/s]','FontSize',fs)
ylabel('Maximum acceleration of [cm/s^2]','FontSize',fs)


%% Across response
% locating responses in x direction of winds acting in y direction
acrossaccx1 = zeros(N,1);
acrossaccx2 = zeros(N,1);
acrossaccy = zeros(N,1);

for i = 1:N
    for j = 1:length(gogny)
        if gogny(j,1) == i
            if gogny(j,7) > acrossaccx1(i,1)
                acrossaccx1(i) = gogny(j,7);
            end
        end
    end
end
% Deleting zeros
for i=length(acrossaccx1):-1:1
    if acrossaccx1(i) == 0
        acrossaccx1(i) = [];
    end
end

for i = 1:N
    for j = 1:length(gogny)
        if gogny(j,1) == i
            if gogny(j,8) > acrossaccx2(i,1)
                acrossaccx2(i) = gogny(j,8);
```

```
            end
        end
    end
end
% Deleting zeros
for i=length(acrossaccx2):-1:1
    if acrossaccx2(i) == 0
        acrossaccx2(i) = [];
    end
end

for i = 1:N
    for j = 1:length(gognx)
        if gognx(j,1) == i
            if gognx(j,9) > acrossaccy(i,1)
                acrossaccy(i) = gognx(j,9);
            end
        end
    end
end
% Deleting zeros
for i=length(acrossaccy):-1:1
    if acrossaccy(i) == 0
        acrossaccy(i) = [];
    end
end

% Plotting across response as a function of maximum 10 minute mean wind
velocity
figure
plot(max10mwindy,acrossaccx1,'o')
fs = 12;
title('Across acceleration of 14th floor with wind blowing in the NS
direction. EW component 1','FontSize',fs)
xlabel('Maximum 10 minute mean wind velocity of [m/s]','FontSize',fs)
ylabel('Maximum across acceleration of [cm/s^2]','FontSize',fs)

figure
plot(max10mwindy,acrossaccx2,'o')
fs = 12;
title('Across acceleration of 14th floor with wind blowing in the NS
direction. EW component 2','FontSize',fs)
xlabel('Maximum 10 minute mean wind velocity of [m/s]','FontSize',fs)
ylabel('Maximum across acceleration of [cm/s^2]','FontSize',fs)

figure
plot(max10mwindx,acrossaccy,'o')
fs = 12;
title('Across acceleration of 14th floor with wind blowing in the EW
direction. NS component','FontSize',fs)
xlabel('Maximum 10 minute mean wind velocity of [m/s]','FontSize',fs)
ylabel('Maximum across acceleration of [cm/s^2]','FontSize',fs)


%% Along and across wind responses plotted together

limy = max([max(windaccx1) max(windaccx2) max(windaccy)...
    max(acrossaccx1) max(acrossaccx2) max(acrossaccy)]);

% Wind in ESE-WNW (x)
```

```
figure
hold on
plot(max10mwindx,windaccx1,'d','markeredgecolor',[0 0
0.3],'markerfacecolor',[0 0 1])
plot(max10mwindx,windaccx2,'v','markeredgecolor',[0 0
0.3],'markerfacecolor',[0 0 0.5])
plot(max10mwindx,acrossaccy,'o','markeredgecolor','r')
hold off
title('Acceleration of 14th floor with wind blowing in the EW
direction','FontSize',fs)
xlabel('Maximum 10 minute mean wind velocity [m/s]','FontSize',fs)
ylabel('Maximum acceleration [cm/s^2]','FontSize',fs)
legend('Along wind acceleration, EW component 1',...
    'Along wind acceleration, EW component 2','Across wind acceleration, NS
component')
ylim([0 ceil(limy*1.35)])

% Wind in NNE-SSW (y)
figure
hold on
plot(max10mwindy,windaccy,'o','markeredgecolor',[0 0
0.3],'markerfacecolor','b')
plot(max10mwindy,acrossaccx1,'d','markeredgecolor',[1 0 0])
plot(max10mwindy,acrossaccx2,'v','markeredgecolor',[0.6 0 0])
hold off
title('Acceleration of 14th floor with wind blowing in the NS
direction','FontSize',fs)
xlabel('Maximum 10 minute mean wind velocity [m/s]','FontSize',fs)
ylabel('Maximum acceleration[cm/s^2]','FontSize',fs)
legend('Along wind acceleration, NS component',...
    'Across wind acceleration, EW component 1','Across wind acceleration,
EW component 2')
ylim([0 ceil(limy*1.35)])

%% Comparison of amplitude of along and across resposnes

figure
plot(max10mwindx,windaccx1./acrossaccy,'o')
hold on
plot(max10mwindx,windaccx2./acrossaccy,'o')

figure
plot(max10mwindy,windaccy./acrossaccx1,'o')
hold on
plot(max10mwindy,windaccy./acrossaccx2,'o')

windaccx_mean = mean([windaccx1 windaccx2]')';
acrossaccx_mean = mean([acrossaccx1 acrossaccx2]')';
Ratio_Al_Ac_EW = mean(windaccx_mean./acrossaccy)
Ratio_Al_Ac_NS = mean(windaccy./acrossaccx_mean)

%% Wind spectrum
%EC spectrum
n = 0.001:0.001:10;
Lt = 300;
zt = 200;
z0 = 0.03;
z = 45; %elevation of the 14th floor
alfa = 0.67+0.05*log(z0);
L = Lt*(z/zt)^alfa;
```

```
U20 = 10; %20m/s
fL = n.*L/U20;
SL = 6.8*fL./((1+10.2*fL).^(5/3));
figure
semilogx(fL,SL)
xlim([0.01 10])
grid on
fs = 12;
title('Eurocode wind power spectral density function','FontSize',fs)
xlabel('non dimensional frequency','FontSize',fs)
ylabel('Power spectral density','FontSize',fs)

% Comparison of wind psd for buildings of different natural frequencies
n_HV = 1.7;
n_ST = 0.6;
Um_vek = 5:0.01:30;
fL_HV = n_HV*L./Um_vek;
SL_HV = 6.8*fL_HV./((1+10.2*fL_HV).^(5/3));
fL_ST = n_ST*L./Um_vek;
SL_ST = 6.8*fL_ST./((1+10.2*fL_ST).^(5/3));

figure
plot(Um_vek,SL_HV,'b')
hold on
plot(Um_vek,SL_ST,'r')
fs = 12;
title('Power spectral density as a function of wind
velocity','FontSize',fs)
xlabel('Wind velocity [m/s]','FontSize',fs)
ylabel('Power spectral density','FontSize',fs)
legend('n = 1,7 Hz','n = 0.6 Hz','location','northwest')

%% Time series of the strongest storm (peak2peak)

load Wind_data_new\HM19980127013300.mat
io0 = io0*0.4790; % converted to cm/s^2
dt = 1/200;
timi = 0:dt:length(io0)*dt-dt;
figure
fs=12;
subplot(3,1,1); plot(timi,io0(:,1)); legend('X component 1'); ylim([-20
20]); xlim([0 150]);
title('Acceleration recorded in wind storm 27. January 1998','fontsize',fs)
subplot(3,1,2); plot(timi,io0(:,2)); legend('X component 2'); ylim([-20
20]); xlim([0 150]);
ylabel('Acceleration [cm/s^2]','fontsize',fs)
subplot(3,1,3); plot(timi,io0(:,3)); legend('Y component'); ylim([-20 20]);
xlim([0 150]);
xlabel('Time [s]','fontsize',fs)

[mina mint] = min(io0(:,1));
[maxa maxt] = max(io0(:,1));
figure
plot(timi,io0(:,1))
hold on
plot(timi(mint),mina,'ro','linewidth',2)
plot(timi(maxt),maxa,'ro','linewidth',2)
title('Example of peak to peak measure of acceleration','fontsize',fs)
ylabel('Acceleration [cm/s^2]','fontsize',fs)
xlabel('Time [s]','fontsize',fs)
```

A3: Analysis of earthquake data

In this Matlab code the analysis of the recorded earthquake induced response is performed, mainly in relation to Chapter 4.

```
%-------------------------------------------------------------------------
% This routine analyses the earthquake induced response of the building
% from recorded data provided by the Earthquake Engineering Research Center
% and further information from the European Strong-Motion Database
%
% The routine analyses and presents the following:
% - general statistics of the chosen earthquakes
% - the peak acceleration response of the 14th and 8th floor as a function
%   of the peak ground acceleration
%
% Written by: Örvar Jónsson
%-------------------------------------------------------------------------

%% Properties of chosen earthquakes

% magnitude vs distance
Dist = [76.9 25.7 60.5 45.3 34.4 30.6 15.1 16.3]; % without 17june 2.
According to excel table
Magnitude = [6.5 4.5 6.4 6.3 4.7 4.3 3.6 4.2]; % without 17june 2
figure
semilogy(Dist,Magnitude,'o')
ylim([3 7])
fs = 12;
%title('','FontSize',fs)
xlabel('Distance to epicenter[km]','FontSize',fs)
ylabel('Magnitude','FontSize',fs)

% acc vs distance
Dist_Gr = [76.9 25.7 60.5 34.4 30.6 15.1 16.3];
Mag_Gr = [6.5 4.5 6.4 4.7 4.3 3.6 4.2];
PGA_EW=[31.04 4.1 15.91 4.68 7.06 6.18 14.69];
PGA_NS=[37.81 7.6 17.91 2.58 4.26 3.00 7.79];
PRA_EW=[213.78 53.7 97.54 115.50 19.37 26.30 25.27 61.95];
PRA_NS=[149.32 19.6 85.45 91.54 16.72 16.87 19.93 50.64];

figure
semilogy(Dist_Gr,PGA_EW,'bo')
hold on
semilogy(Dist,PRA_EW,'ro')
semilogy(Dist_Gr,PGA_NS,'bo')
semilogy(Dist,PRA_NS,'ro')
fs = 12;
%title('','FontSize',fs)
xlabel('Distance to epicenter [km]','FontSize',fs)
ylabel('Peak Acceleration [cm/s^2]','FontSize',fs)
legend('PGA','PRA','location','northwest')

figure
semilogy(Mag_Gr,PGA_EW,'bo')
hold on
semilogy(Magnitude,PRA_EW,'ro')
semilogy(Mag_Gr,PGA_NS,'bo')
semilogy(Magnitude,PRA_NS,'ro')
xlim([3 7])
```

```
fs = 12;
%title('','FontSize',fs)
xlabel('Magnitude','FontSize',fs)
ylabel('Peak Acceleration [cm/s^2]','FontSize',fs)
legend('PGA','PRA','location','northwest')

%% PGA vs PRA
% EW og NS seperately
% Max value of x components used, EW

% Maximum responses
load hm20000617154037.mat
maxresp170600x = max(abs(acc(:,1:2))); maxresp170600x =
max(maxresp170600x);
maxresp170600y = max(abs(acc(:,3))); maxresp170600y = max(maxresp170600y);
maxresp170600y8 = max(abs(acc(:,4))); maxresp170600y8 =
max(maxresp170600y8);

load hm20000617154516.mat
maxresp170600_2x = max(abs(acc(:,1:2))); maxresp170600_2x =
max(maxresp170600_2x);
maxresp170600_2y = max(abs(acc(:,3))); maxresp170600_2y =
max(maxresp170600_2y);
maxresp170600_2y8 = max(abs(acc(:,4))); maxresp170600_2y8 =
max(maxresp170600_2y8);

load hm20000621005158.mat
maxresp210600x = max(abs(acc(:,1:2))); maxresp210600x =
max(maxresp210600x);
maxresp210600y = max(abs(acc(:,3))); maxresp210600y = max(maxresp210600y);
maxresp210600y8 = max(abs(acc(:,4))); maxresp210600y8 =
max(maxresp210600y8);

load hm200805291545.mat
maxresp290508x = max(abs(acc(:,1:2))); maxresp290508x =
max(maxresp290508x);
maxresp290508y = max(abs(acc(:,3))); maxresp290508y = max(maxresp290508y);
maxresp290508y8 = max(abs(acc(:,4))); maxresp290508y8 =
max(maxresp290508y8);

load HM20090529213349.mat
maxresp290509x = max(abs(Acc(:,1:2))); maxresp290509x =
max(maxresp290509x);
maxresp290509y = max(abs(Acc(:,3))); maxresp290509y = max(maxresp290509y);
maxresp290509y8 = max(abs(Acc(:,4))); maxresp290509y8 =
max(maxresp290509y8);

load HM20090530133520.mat
maxresp300509x = max(abs(Acc(:,1:2))); maxresp300509x =
max(maxresp300509x);
maxresp300509y = max(abs(Acc(:,3))); maxresp300509y = max(maxresp300509y);
maxresp300509y8 = max(abs(Acc(:,4))); maxresp300509y8 =
max(maxresp300509y8);

load HM20120301002903.mat
maxresp010312x = max(abs(Acc(:,1:2))); maxresp010312x =
max(maxresp010312x);
maxresp010312y = max(abs(Acc(:,3))); maxresp010312y = max(maxresp010312y);
maxresp010312y8 = max(abs(Acc(:,4))); maxresp010312y8 =
max(maxresp010312y8);
```

```
load HM20120301010251.mat
maxresp010312_2x = max(abs(Acc(:,1:2))); maxresp010312_2x =
max(maxresp010312_2x);
maxresp010312_2y = max(abs(Acc(:,3))); maxresp010312_2y =
max(maxresp010312_2y);
maxresp010312_2y8 = max(abs(Acc(:,4))); maxresp010312_2y8 =
max(maxresp010312_2y8);

%PGA's and 8th floor x
load hs20000617154057.mat
PGA170600x = max(abs(acc(:,1:2))); PGA170600x = max(PGA170600x);
PGA170600y = max(abs(acc(:,3))); PGA170600y = max(PGA170600y);
maxresp170600x8 = max(abs(acc(:,4))); maxresp170600x8 =
max(maxresp170600x8);

load hs20000617154535.mat
PGA170600_2x = max(abs(acc(:,1:2))); PGA170600_2x = max(PGA170600_2x);
PGA170600_2y = max(abs(acc(:,3))); PGA170600_2y = max(PGA170600_2y);
maxresp170600_2x8 = max(abs(acc(:,4))); maxresp170600_2x8 =
max(maxresp170600_2x8);

load hs20000621005200.mat
PGA210600x = max(abs(acc(:,1:2))); PGA210600x = max(PGA210600x);
PGA210600y = max(abs(acc(:,3))); PGA210600y = max(PGA210600y);
maxresp210600x8 = max(abs(acc(:,4))); maxresp210600x8 =
max(maxresp210600x8);

load HS20090529213340.mat
PGA290509x = max(abs(Acc(:,1:2))); PGA290509x = max(PGA290509x);
PGA290509y = max(abs(Acc(:,3))); PGA290509y = max(PGA290509y);
maxresp290509x8 = max(abs(Acc(:,4))); maxresp290509x8 =
max(maxresp290509x8);

load HS20090530133512.mat
PGA300509x = max(abs(Acc(:,1:2))); PGA300509x = max(PGA300509x);
PGA300509y = max(abs(Acc(:,3))); PGA300509y = max(PGA300509y);
maxresp300509x8 = max(abs(Acc(:,4))); maxresp300509x8 =
max(maxresp300509x8);

load HS20120301002853.mat
PGA010312x = max(abs(Acc(:,1:2))); PGA010312x = max(PGA010312x);
PGA010312y = max(abs(Acc(:,3))); PGA010312y = max(PGA010312y);
maxresp010312x8 = max(abs(Acc(:,4))); maxresp010312x8 =
max(maxresp010312x8);

load HS20120301010241.mat
PGA010312_2x = max(abs(Acc(:,1:2))); PGA010312_2x = max(PGA010312_2x);
PGA010312_2y = max(abs(Acc(:,3))); PGA010312_2y = max(PGA010312_2y);
maxresp010312_2x8 = max(abs(Acc(:,4))); maxresp010312_2x8 =
max(maxresp010312_2x8);

% values loaded in vectors (without 2008)
MaxRespx = [0 maxresp170600x maxresp170600_2x maxresp210600x maxresp290509x
maxresp300509x maxresp010312x maxresp010312_2x];
PGAx = [0 PGA170600x PGA170600_2x PGA210600x PGA290509x PGA300509x
PGA010312x PGA010312_2x];
MaxRespy = [0 maxresp170600y maxresp170600_2y maxresp210600y maxresp290509y
maxresp300509y maxresp010312y maxresp010312_2y];
```

```
PGAy = [0 PGA170600y PGA170600_2y PGA210600y PGA290509y PGA300509y
PGA010312y PGA010312_2y];

MaxRespx8 = [0 maxresp170600x8 maxresp170600_2x8 maxresp210600x8
maxresp290509x8 maxresp300509x8 maxresp010312x8 maxresp010312_2x8];
MaxRespy8 = [0 maxresp170600y8 maxresp170600_2y8 maxresp210600y8
maxresp290509y8 maxresp300509y8 maxresp010312y8 maxresp010312_2y8];


% Plotted
figure
hold on
plot(PGAx(1:8),MaxRespx(1:8),'bo')
plot(PGAy(1:8),MaxRespy(1:8),'go')
plot(PGAx(1:8),MaxRespx8(1:8),'rx')
plot(PGAy(1:8),MaxRespy8(1:8),'cx')
xlabel('PGA')
ylabel('Peak response acceleration')

Px = polyfit(PGAx,MaxRespx,2);
Py = polyfit(PGAy,MaxRespy,1);
Px8 = polyfit(PGAx,MaxRespx8,2);
Py8 = polyfit(PGAy,MaxRespy8,1);
d = linspace(0,40,100);
Polyx = Px(1).*d.^2+Px(2).*d+Px(3);
Polyy = Py(1).*d+Py(2);
Polyx8 = Px8(1).*d.^2+Px8(2).*d+Px8(3);
Polyy8 = Py8(1).*d+Py8(2);

figure
fs = 10;
subplot(2,2,1); plot(PGAx(2:4),MaxRespx(2:4),'bo'); hold on
plot(PGAx(3),MaxRespx(3),'go');
plot(PGAx(5:8),MaxRespx(5:8),'go'); plot(d,Polyx,'r')
title('14th floor EW direction','FontSize',fs)
xlabel('PGA','FontSize',fs)
ylabel('PRA','FontSize',fs)
ylim([0 400])
xlim([0 40])

subplot(2,2,2); plot(PGAy(2:4),MaxRespy(2:4),'bo'); hold on
plot(PGAy(3),MaxRespy(3),'go');
plot(PGAy(5:8),MaxRespy(5:8),'go'); plot(d,Polyy,'r')
title('14th floor NS direction','FontSize',fs)
xlabel('PGA','FontSize',fs)
ylabel('PRA','FontSize',fs)
ylim([0 400])

subplot(2,2,3); plot(PGAx(2:4),MaxRespx8(2:4),'bo'); hold on
plot(PGAx(3),MaxRespx8(3),'go');
plot(PGAx(5:8),MaxRespx8(5:8),'go'); plot(d,Polyx8,'r')
title('8th floor EW direction','FontSize',fs)
xlabel('PGA','FontSize',fs)
ylabel('PRA','FontSize',fs)

subplot(2,2,4); plot(PGAy(2:4),MaxRespy8(2:4),'bo'); hold on
plot(PGAy(3),MaxRespy8(3),'go');
plot(PGAy(5:8),MaxRespy8(5:8),'go'); plot(d,Polyy8,'r')
title('8th floor NS direction','FontSize',fs)
xlabel('PGA','FontSize',fs)
```

```
ylabel('PRA','FontSize',fs)

%% Timeseries of June 17th earthquake plotted

load hm20000617154037.mat
dt = 1/200;
timi = 0:dt:length(acc)*dt-dt;
figure
fs=12;
subplot(3,1,1); plot(timi,acc(:,1)); legend('X component 1'); ylim([-200
200]);
title('Acceleration recorded in earthquake 17. June 2000','fontsize',fs)
subplot(3,1,2); plot(timi,acc(:,2)); legend('X component 2'); ylim([-200
200]);
ylabel('Acceleration [cm/s^2]','fontsize',fs)
subplot(3,1,3); plot(timi,acc(:,3)); legend('Y component'); ylim([-200
200]);
xlabel('Time [s]','fontsize',fs)
```

A4: System identification using the auto regressive analysis method

In these Matlab codes the system identification is performed using both the autoregressive and the fast Fourier transform method to evaluate the power spectral densities. In addition, two Matlab functions are presented that are used to determine the natural frequencies and damping based on the power spectral densities.

An autoregressive method of system identification

```
%-------------------------------------------------------------------------
% This routine performs a system identification, using an autoregressive
% analysis to evaluate power spectral densities from the wind induced
% response of the building from recorded data provided by the Earthquake
% Engineering Research Center
%
% The routine analyses and presents the following:
% - natural frequencies and critical damping ratios of the first six modes
%   of vibration
%
% Written by: Örvar Jónsson
%-------------------------------------------------------------------------

cd('Wind_data_new');  % Set accordingly
List = dir('*.mat');
% peak1 = zeros(numel(List),3);
% peak2 = zeros(numel(List),3);
order = 500;
NF = zeros(numel(List),14);
DR = zeros(numel(List),14);

for iFile = [1 numel(List)-3:numel(List)] % data marked as io1, 1997 and
2009-2011
    matName = List(iFile).name;
    load(matName);
    [nf1s1,dr1s1] =
NaturalfrequencyCriticalDampingRatio_mov1_2(io1(:,1),order,200);
    [nf1s2,dr1s2] =
NaturalfrequencyCriticalDampingRatio_mov1_2(io1(:,2),order,200);
    [nf2s3,dr2s3] =
NaturalfrequencyCriticalDampingRatio_mov1_2(io1(:,3),order,200);
    [nf3s1,dr3s1] =
NaturalfrequencyCriticalDampingRatio_mov3(io1(:,1),order,200);
    [nf3s2,dr3s2] =
NaturalfrequencyCriticalDampingRatio_mov3(io1(:,2),order,200);
    [nf3s3,dr3s3] =
NaturalfrequencyCriticalDampingRatio_mov3(io1(:,3),order,200);
    [nf4s1,dr4s1] =
NaturalfrequencyCriticalDampingRatio_mov4(io1(:,1),order,200);
    [nf4s2,dr4s2] =
NaturalfrequencyCriticalDampingRatio_mov4(io1(:,2),order,200);
    [nf5s1,dr5s1] =
NaturalfrequencyCriticalDampingRatio_mov5(io1(:,1),order,200);
    [nf5s2,dr5s2] =
NaturalfrequencyCriticalDampingRatio_mov5(io1(:,2),order,200);
    [nf5s3,dr5s3] =
NaturalfrequencyCriticalDampingRatio_mov5(io1(:,3),order,200);
```

```
    [nf6s1,dr6s1] =
NaturalfrequencyCriticalDampingRatio_mov6(io1(:,1),order,200);
    [nf6s2,dr6s2] =
NaturalfrequencyCriticalDampingRatio_mov6(io1(:,2),order,200);
    [nf6s3,dr6s3] =
NaturalfrequencyCriticalDampingRatio_mov6(io1(:,3),order,200);

    NF(iFile,1) = nf1s1; NF(iFile,2) = nf1s2; NF(iFile,3) = nf2s3;...
        NF(iFile,4) = nf3s1; NF(iFile,5) = nf3s2; NF(iFile,6) = nf3s3;...
        NF(iFile,7) = nf4s1; NF(iFile,8) = nf4s2;...
        NF(iFile,9) = nf5s1; NF(iFile,10) = nf5s2; NF(iFile,11) = nf5s3;...
        NF(iFile,12) = nf6s1; NF(iFile,13) = nf6s2; NF(iFile,14) = nf6s3;
    DR(iFile,1) = dr1s1; DR(iFile,2) = dr1s2; DR(iFile,3) = dr2s3;...
        DR(iFile,4) = dr3s1; DR(iFile,5) = dr3s2; DR(iFile,6) = dr3s3;...
        DR(iFile,7) = dr4s1; DR(iFile,8) = dr4s2;...
        DR(iFile,9) = dr5s1; DR(iFile,10) = dr5s2; DR(iFile,11) = dr5s3;...
        DR(iFile,12) = dr6s1; DR(iFile,13) = dr6s2; DR(iFile,14) = dr6s3;
end

for iFile = 2:numel(List)-4 %data marked as io0 1998-2008
    matName = List(iFile).name;
    load(matName);
    [nf1s1,dr1s1] =
NaturalfrequencyCriticalDampingRatio_mov1_2(io0(:,1),order,200);
    [nf1s2,dr1s2] =
NaturalfrequencyCriticalDampingRatio_mov1_2(io0(:,2),order,200);
    [nf2s3,dr2s3] =
NaturalfrequencyCriticalDampingRatio_mov1_2(io0(:,3),order,200);
    [nf3s1,dr3s1] =
NaturalfrequencyCriticalDampingRatio_mov3(io0(:,1),order,200);
    [nf3s2,dr3s2] =
NaturalfrequencyCriticalDampingRatio_mov3(io0(:,2),order,200);
    [nf3s3,dr3s3] =
NaturalfrequencyCriticalDampingRatio_mov3(io0(:,3),order,200);
    [nf4s1,dr4s1] =
NaturalfrequencyCriticalDampingRatio_mov4(io0(:,1),order,200);
    [nf4s2,dr4s2] =
NaturalfrequencyCriticalDampingRatio_mov4(io0(:,2),order,200);
    [nf5s1,dr5s1] =
NaturalfrequencyCriticalDampingRatio_mov5(io0(:,1),order,200);
    [nf5s2,dr5s2] =
NaturalfrequencyCriticalDampingRatio_mov5(io0(:,2),order,200);
    [nf5s3,dr5s3] =
NaturalfrequencyCriticalDampingRatio_mov5(io0(:,3),order,200);
    [nf6s1,dr6s1] =
NaturalfrequencyCriticalDampingRatio_mov6(io0(:,1),order,200);
    [nf6s2,dr6s2] =
NaturalfrequencyCriticalDampingRatio_mov6(io0(:,2),order,200);
    [nf6s3,dr6s3] =
NaturalfrequencyCriticalDampingRatio_mov6(io0(:,3),order,200);

    NF(iFile,1) = nf1s1; NF(iFile,2) = nf1s2; NF(iFile,3) = nf2s3;...
        NF(iFile,4) = nf3s1; NF(iFile,5) = nf3s2; NF(iFile,6) = nf3s3;...
        NF(iFile,7) = nf4s1; NF(iFile,8) = nf4s2;...
        NF(iFile,9) = nf5s1; NF(iFile,10) = nf5s2; NF(iFile,11) = nf5s3;...
        NF(iFile,12) = nf6s1; NF(iFile,13) = nf6s2; NF(iFile,14) = nf6s3;
    DR(iFile,1) = dr1s1; DR(iFile,2) = dr1s2; DR(iFile,3) = dr2s3;...
        DR(iFile,4) = dr3s1; DR(iFile,5) = dr3s2; DR(iFile,6) = dr3s3;...
        DR(iFile,7) = dr4s1; DR(iFile,8) = dr4s2;...
        DR(iFile,9) = dr5s1; DR(iFile,10) = dr5s2; DR(iFile,11) = dr5s3;...
        DR(iFile,12) = dr6s1; DR(iFile,13) = dr6s2; DR(iFile,14) = dr6s3;
```

```
end

% Storm properties
ap2p = zeros(numel(List),3);          % p2p acceleration
duration = zeros(numel(List),1);      % duration [sec]
sF = 200;                             % Sampling frequency [Hz]

for iFile = [1 numel(List)-3:numel(List)] %open io1 files
    matName = List(iFile).name;
    load(matName);
    ap2p(iFile,:) = (max(io1)-min(io1))*0.4790;
    duration(iFile) = length(io1(:,1))*sF;
end

for iFile = 2:numel(List)-4 %open io0 files
    matName = List(iFile).name;
    load(matName);
    ap2p(iFile,:) = (max(io0)-min(io0))*0.4790;
    duration(iFile) = length(io0(:,1))*sF;
end
cd ..

exdates = xlsread('dates_97_11.xlsx',1,'A1:A20');
matdates = x2mdate(exdates,0);
matdatesstr = datestr(matdates);

% Write SI results in an excel file
xlswrite('SI_AR_allsensors',NF,1);
xlswrite('SI_AR_allsensors',DR,2);

fs=12
%MODE1
figure
plot(matdates,NF(:,1),'bo')
hold on
plot(matdates,NF(:,2),'go')
title('Natural Frequency. 1st mode of vibration','fontsize',fs)
xlabel('Date of event [years]','fontsize',fs); ylabel('Frequency
[Hz]','fontsize',fs);
legend('X sensor 1','X sensor 2')
datetick('x','yyyy')

figure
plot(matdates,DR(:,1)*100,'bo')
hold on
plot(matdates,DR(:,2)*100,'go')
title('Critical Damping Ratio. 1st mode of vibration','fontsize',fs)
xlabel('Date of event [years]','fontsize',fs); ylabel('Damping
[%]','fontsize',fs);
legend('X sensor 1','X sensor 2')
datetick('x','yyyy')

%MODE2
figure
plot(matdates,NF(:,3),'ro')
title('Natural Frequency. 2nd mode of vibration','fontsize',fs)
xlabel('Date of event [years]','fontsize',fs); ylabel('Frequency
[Hz]','fontsize',fs);
legend('Y sensor')
datetick('x','yyyy')
```

```
figure
plot(matdates,DR(:,3)*100,'ro')
title('Critical Damping Ratio. 2nd mode of vibration','fontsize',fs)
xlabel('Date of event [years]','fontsize',fs); ylabel('Damping
[%]','fontsize',fs);
legend('Y sensor')
datetick('x','yyyy')

%MODE3
figure
plot(matdates,NF(:,4),'bo')
hold on
plot(matdates,NF(:,5),'go')
plot(matdates,NF(:,6),'ro')
title('Natural Frequency. 3rd mode of vibration','fontsize',fs)
xlabel('Date of event [years]','fontsize',fs); ylabel('Frequency
[Hz]','fontsize',fs);
legend('X sensor 1','X sensor 2','Y sensor')
datetick('x','yyyy')

figure
plot(matdates,DR(:,4)*100,'bo')
hold on
plot(matdates,DR(:,5)*100,'go')
plot(matdates,DR(:,6)*100,'ro')
title('Critical Damping Ratio. 3rd mode of vibration','fontsize',fs)
xlabel('Date of event [years]','fontsize',fs); ylabel('Damping
[%]','fontsize',fs);
legend('X sensor 1','X sensor 2','Y sensor')
datetick('x','yyyy')

%MODE4
figure
plot(matdates,NF(:,7),'bo')
hold on
plot(matdates,NF(:,8),'go')
title('Natural Frequency. 4th mode of vibration','fontsize',fs)
xlabel('Date of event [years]','fontsize',fs); ylabel('Frequency
[Hz]','fontsize',fs);
legend('X sensor 1','X sensor 2')
datetick('x','yyyy')

figure
plot(matdates,DR(:,7)*100,'bo')
hold on
plot(matdates,DR(:,8)*100,'go')
title('Critical Damping Ratio. 4th mode of vibration','fontsize',fs)
xlabel('Date of event [years]','fontsize',fs); ylabel('Damping
[%]','fontsize',fs);
legend('X sensor 1','X sensor 2')
datetick('x','yyyy')

%MODE5
figure
plot(matdates,NF(:,9),'bo')
hold on
plot(matdates,NF(:,10),'go')
plot(matdates,NF(:,11),'ro')
title('Natural Frequency. 5thd mode of vibration','fontsize',fs)
```

```
xlabel('Date of event [years]','fontsize',fs); ylabel('Frequency
[Hz]','fontsize',fs);
legend('X sensor 1','X sensor 2','Y sensor')
datetick('x','yyyy')

figure
plot(matdates,DR(:,9)*100,'bo')
hold on
plot(matdates,DR(:,10)*100,'go')
plot(matdates,DR(:,11)*100,'ro')
title('Critical Damping Ratio. 5th mode of vibration','fontsize',fs)
xlabel('Date of event [years]','fontsize',fs); ylabel('Damping
[%]','fontsize',fs);
legend('X sensor 1','X sensor 2','Y sensor')
datetick('x','yyyy')

%MODE6
figure
plot(matdates,NF(:,12),'bo')
hold on
plot(matdates,NF(:,13),'go')
plot(matdates,NF(:,14),'ro')
title('Natural Frequency. 6th mode of vibration','fontsize',fs)
xlabel('Date of event [years]','fontsize',fs); ylabel('Frequency
[Hz]','fontsize',fs);
legend('X sensor 1','X sensor 2','Y sensor')
datetick('x','yyyy')

figure
plot(matdates,DR(:,12)*100,'bo')
hold on
plot(matdates,DR(:,13)*100,'go')
plot(matdates,DR(:,14)*100,'ro')
title('Critical Damping Ratio. 6th mode of vibration','fontsize',fs)
xlabel('Date of event [years]','fontsize',fs); ylabel('Damping
[%]','fontsize',fs);
legend('X sensor 1','X sensor 2','Y sensor')
datetick('x','yyyy')


% Natural frequencies vs peak to peak acceleration
figure
plot(ap2p(1:16,1),NF(1:16,1),'bo')
hold on
plot(ap2p(1:16,2),NF(1:16,2),'go')
xlabel('Acceleration [cm/s^2]','fontsize',fs); ylabel('Frequency
[Hz]','fontsize',fs);
legend('X sensor 1','X sensor 2')

figure
plot(ap2p(1:16,3),NF(1:16,3),'ro')
xlabel('Acceleration [cm/s^2]','fontsize',fs); ylabel('Frequency
[Hz]','fontsize',fs);
legend('Y sensor')
```

A fast Fourier transform method of system identification

```
%-------------------------------------------------------------------------
% This routine performs a system identification, using a fast Fourer
% transform analysis to evaluate power spectral densities from the wind
% induced response of the building from recorded data provided by the
% Earthquake Engineering Research Center
%
% The routine analyses and presents the following:
% - natural frequencies and critical damping ratios of the first six modes
%   of vibration
%
% Written by: Örvar Jónsson
%-------------------------------------------------------------------------

cd('Wind_data_new');  % Set accordingly
List = dir('*.mat');

NFw = zeros(numel(List),14);
DRw = zeros(numel(List),14);

sF = 200;
NFFT = 8192; % Number of FFT points used to calculate the PSD estimate

for iFile = [1 numel(List)-3:numel(List)] %data marked as io1, 1997 and
2009-2011
    matName = List(iFile).name;
    load(matName);
    [Pxx_w,F_w] = pwelch(io1(:,1),[],[],NFFT,sF);
    Pxx_w = Pxx_w'; F_w = F_w';
    [d,fo,fup,flp,Smax] = damping_mov1_2(F_w,Pxx_w); NFw(iFile,1) = fo;
DRw(iFile,1) = d;
    [d,fo,fup,flp,Smax] = damping_mov3(F_w,Pxx_w); NFw(iFile,4) = fo;
DRw(iFile,4) = d;
    [d,fo,fup,flp,Smax] = damping_mov4(F_w,Pxx_w); NFw(iFile,7) = fo;
DRw(iFile,7) = d;
    [d,fo,fup,flp,Smax] = damping_mov5(F_w,Pxx_w); NFw(iFile,9) = fo;
DRw(iFile,9) = d;
    [d,fo,fup,flp,Smax] = damping_mov6(F_w,Pxx_w); NFw(iFile,12) = fo;
DRw(iFile,12) = d;

    [Pxx_w,F_w] = pwelch(io1(:,2),[],[],NFFT,sF);
    Pxx_w = Pxx_w'; F_w = F_w';
    [d,fo,fup,flp,Smax] = damping_mov1_2(F_w,Pxx_w); NFw(iFile,2) = fo;
DRw(iFile,2) = d;
    [d,fo,fup,flp,Smax] = damping_mov3(F_w,Pxx_w); NFw(iFile,5) = fo;
DRw(iFile,5) = d;
    [d,fo,fup,flp,Smax] = damping_mov4(F_w,Pxx_w); NFw(iFile,8) = fo;
DRw(iFile,8) = d;
    [d,fo,fup,flp,Smax] = damping_mov5(F_w,Pxx_w); NFw(iFile,10) = fo;
DRw(iFile,10) = d;
    [d,fo,fup,flp,Smax] = damping_mov6(F_w,Pxx_w); NFw(iFile,13) = fo;
DRw(iFile,13) = d;

    [Pxx_w,F_w] = pwelch(io1(:,3),[],[],NFFT,sF);
    Pxx_w = Pxx_w'; F_w = F_w';
    [d,fo,fup,flp,Smax] = damping_mov1_2(F_w,Pxx_w); NFw(iFile,3) = fo;
DRw(iFile,3) = d;
    [d,fo,fup,flp,Smax] = damping_mov3(F_w,Pxx_w); NFw(iFile,6) = fo;
DRw(iFile,6) = d;
```

```
    [d,fo,fup,flp,Smax] = damping_mov5(F_w,Pxx_w); NFw(iFile,11) = fo;
DRw(iFile,11) = d;
    [d,fo,fup,flp,Smax] = damping_mov6(F_w,Pxx_w); NFw(iFile,14) = fo;
DRw(iFile,14) = d;
end

for iFile = 2:numel(List)-4 %data marked as io0, 1998-2008
    matName = List(iFile).name;
    load(matName);
    [Pxx_w,F_w] = pwelch(io0(:,1),[],[],NFFT,sF);
    Pxx_w = Pxx_w'; F_w = F_w';
    [d,fo,fup,flp,Smax] = damping_mov1_2(F_w,Pxx_w); NFw(iFile,1) = fo;
DRw(iFile,1) = d;
    [d,fo,fup,flp,Smax] = damping_mov3(F_w,Pxx_w); NFw(iFile,4) = fo;
DRw(iFile,4) = d;
    [d,fo,fup,flp,Smax] = damping_mov4(F_w,Pxx_w); NFw(iFile,7) = fo;
DRw(iFile,7) = d;
    [d,fo,fup,flp,Smax] = damping_mov5(F_w,Pxx_w); NFw(iFile,9) = fo;
DRw(iFile,9) = d;
    [d,fo,fup,flp,Smax] = damping_mov6(F_w,Pxx_w); NFw(iFile,12) = fo;
DRw(iFile,12) = d;

    [Pxx_w,F_w] = pwelch(io0(:,2),[],[],NFFT,sF);
    Pxx_w = Pxx_w'; F_w = F_w';
    [d,fo,fup,flp,Smax] = damping_mov1_2(F_w,Pxx_w); NFw(iFile,2) = fo;
DRw(iFile,2) = d;
    [d,fo,fup,flp,Smax] = damping_mov3(F_w,Pxx_w); NFw(iFile,5) = fo;
DRw(iFile,5) = d;
    [d,fo,fup,flp,Smax] = damping_mov4(F_w,Pxx_w); NFw(iFile,8) = fo;
DRw(iFile,8) = d;
    [d,fo,fup,flp,Smax] = damping_mov5(F_w,Pxx_w); NFw(iFile,10) = fo;
DRw(iFile,10) = d;
    [d,fo,fup,flp,Smax] = damping_mov6(F_w,Pxx_w); NFw(iFile,13) = fo;
DRw(iFile,13) = d;

    [Pxx_w,F_w] = pwelch(io0(:,3),[],[],NFFT,sF);
    Pxx_w = Pxx_w'; F_w = F_w';
    [d,fo,fup,flp,Smax] = damping_mov1_2(F_w,Pxx_w); NFw(iFile,3) = fo;
DRw(iFile,3) = d;
    [d,fo,fup,flp,Smax] = damping_mov3(F_w,Pxx_w); NFw(iFile,6) = fo;
DRw(iFile,6) = d;
    [d,fo,fup,flp,Smax] = damping_mov5(F_w,Pxx_w); NFw(iFile,11) = fo;
DRw(iFile,11) = d;
    [d,fo,fup,flp,Smax] = damping_mov6(F_w,Pxx_w); NFw(iFile,14) = fo;
DRw(iFile,14) = d;
end

% Average of each mode
NFwelch = zeros(20,6);
NFwelch(:,1) = mean(NFw(:,1:2)')';
NFwelch(:,2) = NFw(:,3);
NFwelch(:,3) = mean(NFw(:,4:6)')';
NFwelch(:,4) = mean(NFw(:,7:8)')';
NFwelch(:,5) = mean(NFw(:,9:11)')';
NFwelch(:,6) = mean(NFw(:,12:14)')';

DRwelch = zeros(20,6);
DRwelch(:,1) = mean(DRw(:,1:2)')';
DRwelch(:,2) = DRw(:,3);
DRwelch(:,3) = mean(DRw(:,4:6)')';
```

```
DRwelch(:,4) = mean(DRw(:,7:8)')';
DRwelch(:,5) = mean(DRw(:,9:11)')';
DRwelch(:,6) = mean(DRw(:,12:14)')';

% Storm properties
ap2p = zeros(numel(List),3);        % p2p acceleration
duration = zeros(numel(List),1);    % duration [sec]
sF = 200;                           % Sampling frequency [Hz]

for iFile = [1 numel(List)-3:numel(List)] %open io1 files
    matName = List(iFile).name;
    load(matName);
    ap2p(iFile,:) = (max(io1)-min(io1))*0.4790;
    duration(iFile) = length(io1(:,1))*sF;
end

for iFile = 2:numel(List)-4 %open io0 files
    matName = List(iFile).name;
    load(matName);
    ap2p(iFile,:) = (max(io0)-min(io0))*0.4790;
    duration(iFile) = length(io0(:,1))*sF;
end

exdates = xlsread('dates_97_11.xlsx',1,'A1:A20');
matdates = x2mdate(exdates,0);
matdatesstr = datestr(matdates);

cd ..

% Write SI results in an excel file
xlswrite('SI_FFT_Welch',NFwelch,1);
xlswrite('SI_FFT_Welch',DRwelch,2);

% Plotting natural frequency and critical damping ratio for each mode
stormprop
fs=12;
%MODE1
figure
plot(matdates,NFw(:,1),'bo')
hold on
plot(matdates,NFw(:,2),'go')
title('Natural Frequency. 1st mode of vibration','fontsize',fs)
xlabel('Date of event [years]','fontsize',fs); ylabel('Frequency
[Hz]','fontsize',fs);
legend('X sensor 1','X sensor 2')
datetick('x','yyyy')

figure
plot(matdates,DRw(:,1)*100,'bo')
hold on
plot(matdates,DRw(:,2)*100,'go')
title('Critical Damping Ratio. 1st mode of vibration','fontsize',fs)
xlabel('Date of event [years]','fontsize',fs); ylabel('Damping
[%]','fontsize',fs);
legend('X sensor 1','X sensor 2')
datetick('x','yyyy')

%MODE2
figure
plot(matdates,NFw(:,3),'ro')
```

```
title('Natural Frequency. 2nd mode of vibration','fontsize',fs)
xlabel('Date of event [years]','fontsize',fs); ylabel('Frequency
[Hz]','fontsize',fs);
legend('Y sensor')
datetick('x','yyyy')

figure
plot(matdates,DRw(:,3)*100,'ro')
title('Critical Damping Ratio. 2nd mode of vibration','fontsize',fs)
xlabel('Date of event [years]','fontsize',fs); ylabel('Damping
[%]','fontsize',fs);
legend('Y sensor')
datetick('x','yyyy')

%MODE3
figure
plot(matdates,NFw(:,4),'bo')
hold on
plot(matdates,NFw(:,5),'go')
plot(matdates,NFw(:,6),'ro')
title('Natural Frequency. 3rd mode of vibration','fontsize',fs)
xlabel('Date of event [years]','fontsize',fs); ylabel('Frequency
[Hz]','fontsize',fs);
legend('X sensor 1','X sensor 2','Y sensor')
datetick('x','yyyy')

figure
plot(matdates,DRw(:,4)*100,'bo')
hold on
plot(matdates,DRw(:,5)*100,'go')
plot(matdates,DRw(:,6)*100,'ro')
title('Critical Damping Ratio. 3rd mode of vibration','fontsize',fs)
xlabel('Date of event [years]','fontsize',fs); ylabel('Damping
[%]','fontsize',fs);
legend('X sensor 1','X sensor 2','Y sensor')
datetick('x','yyyy')

%MODE4
figure
plot(matdates,NFw(:,7),'bo')
hold on
plot(matdates,NFw(:,8),'go')
title('Natural Frequency. 4th mode of vibration','fontsize',fs)
xlabel('Date of event [years]','fontsize',fs); ylabel('Frequency
[Hz]','fontsize',fs);
legend('X sensor 1','X sensor 2')
datetick('x','yyyy')

figure
plot(matdates,DRw(:,7)*100,'bo')
hold on
plot(matdates,DRw(:,8)*100,'go')
title('Critical Damping Ratio. 4th mode of vibration','fontsize',fs)
xlabel('Date of event [years]','fontsize',fs); ylabel('Damping
[%]','fontsize',fs);
legend('X sensor 1','X sensor 2')
datetick('x','yyyy')

%MODE5
figure
```

```
plot(matdates,NFw(:,9),'bo')
hold on
plot(matdates,NFw(:,10),'go')
plot(matdates,NFw(:,11),'ro')
title('Natural Frequency. 5thd mode of vibration','fontsize',fs)
xlabel('Date of event [years]','fontsize',fs); ylabel('Frequency
[Hz]','fontsize',fs);
legend('X sensor 1','X sensor 2','Y sensor')
datetick('x','yyyy')

figure
plot(matdates,DRw(:,9)*100,'bo')
hold on
plot(matdates,DRw(:,10)*100,'go')
plot(matdates,DRw(:,11)*100,'ro')
title('Critical Damping Ratio. 5th mode of vibration','fontsize',fs)
xlabel('Date of event [years]','fontsize',fs); ylabel('Damping
[%]','fontsize',fs);
legend('X sensor 1','X sensor 2','Y sensor')
datetick('x','yyyy')

%MODE6
figure
plot(matdates,NFw(:,12),'bo')
hold on
plot(matdates,NFw(:,13),'go')
plot(matdates,NFw(:,14),'ro')
title('Natural Frequency. 6th mode of vibration','fontsize',fs)
xlabel('Date of event [years]','fontsize',fs); ylabel('Frequency
[Hz]','fontsize',fs);
legend('X sensor 1','X sensor 2','Y sensor')
datetick('x','yyyy')

figure
plot(matdates,DRw(:,12)*100,'bo')
hold on
plot(matdates,DRw(:,13)*100,'go')
plot(matdates,DRw(:,14)*100,'ro')
title('Critical Damping Ratio. 6th mode of vibration','fontsize',fs)
xlabel('Date of event [years]','fontsize',fs); ylabel('Damping
[%]','fontsize',fs);
legend('X sensor 1','X sensor 2','Y sensor')
datetick('x','yyyy')
```

A function of autoregressive analysis to evaluate natural frequencies

```
% m-function: NaturalfrequencyCriticalDampingRatio.m
%
% Purpose
%       To estimate viscous damping ratio
%       and natural frequency from power
%       spectral density and plot the results
%       as a function of model order
%
% Input parameters
%       data  - time series (1D array)
%       order - model order (1D array)
%       sF    - sampling frequency (Hz)
%
% Output parameters
%       dmpng - critical damping ratio
%       nfreq - natural frequency (Hz)
%       plots showing natural frequency
%               and critical damping ratio
%               as a function of model order
%
% Function required
%       daming.m
%
% Written by Ragnar Sigbjörnsson / 5 March 2011.m

function [nfreq,dmpng] =
NaturalfrequencyCriticalDampingRatio(data,order,sF),

timeseries = data - mean(data);

Frng  = 0.1:0.0001:sF/2;
dmpng = zeros(length(order),1);
nfreq = zeros(length(order),1);

for i = 1:length(order);
    [Px,F] = pburg(timeseries,order(i),Frng,sF);
    [d,fo,fup,flp,Smax] = damping(F,Px);
    dmpng(i) = d;
    nfreq(i) = fo;
end;

% StandardDeviation_PS = sqrt(2*sum(Px)*(F(2)-F(1))) % one-sided spectral
% density
% StandardDeviation_ts = std(timeseries)

figure('Color','w')

fs = 12;
ms = 20;

subplot(121)
line(nfreq,order,'Color','b','LineStyle','none','Marker','.','MarkerSize',m
s)
box off
xlabel('NATURAL FREQUENCY (Hz)','FontSize',fs)
ylabel('MODEL ORDER','FontSize',fs)
grid
```

```
subplot(122)
plot(100*dmpng,order,'Color','r','LineStyle','none','Marker','.','MarkerSiz
e',ms)
box off
xlabel('CRITICAL DAMPING RATIO (%)','FontSize',fs)
grid

% figure('Color','w')
% normplot(100*dmpng)
% xlabel('CRITICAL DAMPING RATIO (%)','FontSize',fs)
% % ylabel('PROBABILITY','FontSize',fs)
% axis square

% END
```

A function to evaluate critical damping ratios

```
% m-function: damping.m
%
% Purpose
%       To estimate viscous damping ratio
%       and natural frequency from power
%       spectral density
%
% Input parameters
%       f  - frequency vector (Hz)
%       Sx - spectral density
%
% Output parameters
%       d        - critical damping ratio
%       fo       - natural frequency
%       fup, flp - frequencies corresponding to the half power pont
%       Smax     - max value of spectral density (in the range considered)
%
% Written by Ragnar Sigbjörnsson / 5 March 2011

function [d,fo,fup,flp,Smax] = damping(f,Sx)

F1 = 0.5;
F2 = 2.8;
FF1 = find(f > F1);
FF1 = FF1(1);
FF2 = find(f > F2);
FF2 = FF2(1);
[Smax,I] = max(Sx(1,FF1:FF2));
I = I+FF1-1;

% F1 = 0.2; % Starting point of frequency analysis [Hz]
% FF1 = find(f==F1);
% [Smax,I] = max(Sx(1,FF1:end)); % peak picking (only the biggest peak
selected)
fo  = f(I);          % natural frequency
flp = interp1(Sx(fix(0.8*I):I),f(fix(0.8*I):I),Smax/2); % 1st half power
point
fup = interp1(Sx(I:fix(1.2*I)),f(I:fix(1.2*I)),Smax/2); % 2nd half power
point
d   = 0.5*(fup-flp)/fo; % critical damping ratio (approximation)

%d   = ((fup/fo)^2 - (flp/fo)^2)/4; % exact

% END
```

A5: Comparison of recorded response to calculations based on the finite element model for validation of the calibrated FEM

In this Matlab code, calculations based on the finite element model are compared to the recorded response in order to validate the calibration of the finite element model are performed.

```
%-------------------------------------------------------------------------
%
% The routine evaluates the earthquake response of a structure
% based on an acceleration at its base
%
% The routine requires the following data:
% - Ground accleration timeseris (gracc.mat)
% - Modal parameters (eigin_J1.m):
%   natural frequencies, mode shapes, damping ratio, participation factors
%
% Written by: Jonas Thor Snaebjornsson
% Edited by: Örvar Jónsson
%-------------------------------------------------------------------------

fs=200; % sampling frequency
npfa = 16384; %4x4096 sirka
% Picking out the relevant time frame of ground motion
start = 2800; %ca 3000                  % Earthquake starts
finish = start+npfa-1;

% Measured acceleration at 8th & 14th floor
% 14SU 14NO 14MI 8NS
% x(E-W), y(N-S)
load hm20000621005158.mat
acc14x1 = acc(start:finish,1);
acc14x2 = acc(start:finish,2);
acc14y  = acc(start:finish,3);
acc08y  = acc(start:finish,4);

% Displacements at 8th and 14th floor
dis14x1 = dis(start:finish,1);
dis14x2 = dis(start:finish,2);
dis14y  = dis(start:finish,3);
dis08y  = dis(start:finish,4);

% Ground acceleration components:
% -1NS  -1UN  -1AV  08AV
% x(E-W), y(N-S) and z(vertical)
load hs20000621005200.mat
agy = acc(start:finish,1);
agz = acc(start:finish,2);
agx = acc(start:finish,3);
acc08x = acc(start:finish,4);

[cnr,rnr] = size(agx);

% Defining the time axis for excitation and response
dt=1/fs;
if rem(npfa,2)==0,
  tmax=(npfa-1)*dt;
```

```
else
  tmax=npfa*dt;
end
t=0:dt:tmax;
t=t';            % time axis

% Defining the frequency axis
df=1/(tmax+dt);
fmax=(npfa/2)*df;
fmax_=df-fmax;
f=[0:df:fmax,fmax_:df:-df];
f=f';

% Evaluating the Fourier transform for acceleration
Ax=fft(agx,npfa);
Ay=fft(agy,npfa);
Az=fft(agz,npfa);

%--------------------------------------------------------------------------
%  Loading the modal parameters evaluated with SAP2000

% Natural Frequencies
F = xlsread('modal8.xlsx',4,'E4:E15');
F = F';

%   Critical damping ratio
Zi = [1.2 1.7 2 1.5 3 6 5 5 5 5 5 5]*0.01;

% Mode shapes [m]
O = xlsread('disp8.xlsx',1,'F4:H55');
O = O([13:24,25:36,37:48,1:12,],:)'; % Modal case

Ox = zeros(4,12);
Ox(1,:) = O(1,1:12); Ox(2,:) = O(1,13:24);
Ox(3,:) = O(1,25:36); Ox(4,:) = O(1,37:48);

Oy = zeros(4,12);
Oy(1,:) = O(2,1:12); Oy(2,:) = O(2,13:24);
Oy(3,:) = O(2,25:36); Oy(4,:) = O(2,37:48);

Oz = zeros(4,12);
Oz(1,:) = O(3,1:12); Oz(2,:) = O(3,13:24);
Oz(3,:) = O(3,25:36); Oz(4,:) = O(3,37:48);
%   n = number of measurement locations
%   m = number of modes included in analysis
% Modal Participation Factors  [kN-s2]
P = xlsread('modal8.xlsx',3,'E4:G15');
Px = P(:,1);
Py = P(:,2);
Pz = P(:,3);

[r,i3]=size(F);   % i3 = number of mode shapes included in the analysis
%--------------------------------------------------------------------------
% Locating natural frequencies (F) in the frequency vector (f)
for k=1:length(F)
   FF=F(1,k);
    a=find(f>FF);
   location(1,k)=a(1,1);
%    valur(1,k)=b;
```

```
end
%-------------------------------------------------------------------------
% Evaluating the excitation for each modal equation
%-------------------------------------------------------------------------
for i=1:i3,
Q(:,i)=-Px(i)*Ax(:)-Py(i)*Ay(:)-Pz(i)*Az(:);
end

%-------------------------------------------------------------------------
% Evaluating the frequency response function H(iw)
% and the Fourier spectrum of the response Fa(iw) in modal coordinates
%-------------------------------------------------------------------------
ii=sqrt(-1);

for i=1:1:i3

H(:,i)=(2*pi)^2*((F(i)^2 - f(:).^2) + 2*ii*Zi(i)*F(i)*f(:));
H(:,i)=H(:,i).^(-1);

Fa(:,i) = -((2*pi*f(:,1)).^2).*(H(:,i).*Q(:,i));

end
Fa=Fa';

%-------------------------------------------------------------------------
% Evaluating the Fourier spectrum of the response in global coordinates
%-------------------------------------------------------------------------
[n1,n2]=size(Ox);

for i=1:n1;
Fgx(i,:)=Ox(i,1:i3)*Fa(1:i3,:);
Fgy(i,:)=Oy(i,1:i3)*Fa(1:i3,:);
Fgz(i,:)=Oz(i,1:i3)*Fa(1:i3,:);
end
%-------------------------------------------------------------------------
% Evaluating the real response in the time domain through
% invers Fourier transform of the response in the frequency domain
%-------------------------------------------------------------------------
rax = detrend(real(ifft(Fgx')));
ray = detrend(real(ifft(Fgy')));
raz = detrend(real(ifft(Fgz')));
%-------------------------------------------------------------------------
% Evaluating the Fourier transform of the response for plotting
%-------------------------------------------------------------------------
FTx1=fft(rax(:,1));
FTy1=fft(ray(:,1));
FTz1=fft(raz(:,1));
%-------------------------------------------------------------------------

%% plotting measured acceleration time series at 14th floor

figure;
subplot(211); plot(t+0.25,acc14x1,'b'); hold on
subplot(212); plot(t+0.25,acc14y,'b'); hold on
hold on
subplot(211); plot(t,rax(:,1),'r')
legend('recorded','computed')
title(' Acceleration time history of 14th floor (E-W)')
ylabel('Acceleration (cm/s^2)')
xlabel('Time (s)')
```

```
subplot(212); plot(t,ray(:,3),'r')
legend('recorded','computed')
title(' Acceleration time history of 14th floor (N-S)')
ylabel('Acceleration (cm/s^2)')
xlabel('Time (s)')
hold off

%% plotting shorter interval of above
figure;
subplot(211); plot(t(41:4040),acc14x1(1:4000,1),'b'); hold on
subplot(212); plot(t(41:4040),acc14y(1:4000,1),'b'); hold on
subplot(211); plot(t(1:4000),rax(1:4000,1),'r')
xlim([10 20]);
title(' Acceleration time history (short interval) of 14th floor (E-W)')
legend('recorded','computed')
ylabel('Acceleration (cm/s^2)')
xlabel('Time (s)')
subplot(212); plot(t(1:4000),ray(1:4000,1),'r')
title(' Acceleration time history (short interval) of 14th floor (N-S)')
legend('recorded','computed')
xlim([10 20]);
ylabel('Acceleration (cm/s^2)')
xlabel('Time (s)')
hold off

%% Take Fourier transform of measured TH at 14th floor

FTx2=fft(acc14x1(:,1));
FTy2=fft(acc14y(:,1));

% Plotting fourier spectrum for TH at 14th floor for x-axis
figure;
plot(f(1:1000),abs(FTx2(1:1000)),'b',f(1:1000),abs(FTx1(1:1000)),'r')
xlabel('Frequency (Hz)')
ylabel('Fourier Spectrum')
title('FFT for acceleration TH of 14th floor (E-W)')
legend('recorded','computed')
xlim([0 8])

% Plotting fourier spectrum for TH at 14th floor for y-axis
figure;
plot(f(1:1000),abs(FTy2(1:1000)),'b',f(1:1000),abs(FTy1(1:1000)),'r')
xlabel('Frequency (Hz)')
ylabel('Fourier Spectrum')
title('FFT for acceleration TH of 14th floor (N-S)')
legend('recorded','computed')
xlim([0 8])
```

A6: Design code procedures to evaluate acceleration response

In these Matlab codes, the design code procedure calculations are performed to evaluate the predicted acceleration response

Eurocode procedure to evaluate acceleration response

```
%-------------------------------------------------------------------------
% Wind induced response based on the Eurocode EN 1-4 procedures.
% Wind excitation of tall buildings - Estimation of acceleration response
%-------------------------------------------------------------------------
% Structural parameters explained:
% B(m) : The projected breadth of the building
% D(m) : The projected width of the building
% H(m) : reference height
% hi(m) : Height between floors from basement to top
% Mi(kg) : Mass of each building floor
% f_1(Hz): Natural frequency for first mode across the weaker axis
% z_1 : Critical damping ratio for the mode 1
% f_2(Hz): Natural frequency for first mode across the stronger axis
% z_2 : Critical damping ratio for the mode 2
% f_3(Hz): Natural frequency for the first torsional mode of vibration
% z_3 : Critical damping ratio for the mode 3
% fi : Mode shape of the building can be evaluated as fi=(Z/H).^beta
% where beta lies within the range 1.5 to 2.0;
%
% Written by: Andri Gunnarsson
% Edited by: Jonas Thor Snaebjornsson and Örvar Jónsson
%-------------------------------------------------------------------------
% Structural parameters: Values
% Hús verslunarinnar  - The Commerce building in Reykjavik
% Heigth parameters
Z = xlsread('FEMprop.xlsx',1,'C2:C16');
H = Z(end);
% Width parameters
Atot = 1179; %m2
B = Atot/H; % average width 24,1m
D = 24.3;
Breidd = B; Dypt = D;
% Mode Shapes. 1st mode shape in each direction
MS_X = xlsread('FEMprop.xlsx',1,'D2:D16');
MS_Y = xlsread('FEMprop.xlsx',1,'E2:E16');
% Dynamic mass
M = diag(xlsread('FEMprop.xlsx',1,'I2:I16'));
Mtot=sum(diag(M));
% Natural frequencies and critical damping ratios
f1 = 1.69; z1 = 0.02; % ModeShape 1, along
f2 = 2.22; z2 = 0.02; % ModeShape 2, across
f3 = 2.86; z3 = 0.02; % ModeShape 3, torsion
% frequencies from FE model. Damping chosen 2% based on the various results
% of the SI
%
%-------------------------------------------------------------------------
%% Response of the building based on the EN 1-4 - Procedue 2 (Annex C)
% EN only presents a procedure to evaluate the along wind response
f = [f1 f2]; damp = [(z1*2*pi()) (z2*2*pi())];

% Background factor
ze = 0.6*H; % Reference height [m]
```

```
z0 = 0.05; % Roughness length [m]
alfa = 0.67+0.05*log(z0);
Lze = 300*(ze/200)^alfa; % Turbulence length [m]

% Resonance factor
V10 = 1:1:35; % Mean wind velocity at 10m height
kr = 0.19*(z0/0.05)^0.07; % terrain factor
cr = kr*log(ze/z0); % roughness factor
Vm = cr.*V10; % Windvelocity at reference height
acc_along_C = zeros(length(Vm),length(f));
R_C = zeros(length(f),length(Vm));
for i = 1:length(f);
% Values for vibration of the first two modes
if i == 1 % Vibration in EW
B = Dypt; D = Breidd; cf = 2.1;
fim = MS_X;
Ky = 1; Kz = 5/3; Gy = 1/2; Gz = 5/18; % Table C.1  Uniform for width,
Parabolic for height
B2 = 1/(1+(3/2)*sqrt((B/Lze)^2+(H/Lze)^2+((B/Lze)*(H/Lze))^2));
elseif i == 2 % Vibration in NS
B = Breidd; D = Dypt; cf = 2.1;
fim = MS_Y;
Ky = 1; Kz = 3/2; Gy = 1/2; Gz = 3/8; % Table C.1  Uniform for width,
Linear for height
B2 = 1/(1+(3/2)*sqrt((B/Lze)^2+(H/Lze)^2+((B/Lze)*(H/Lze))^2));
end
fimax = max(fim); % Mode shape on the top storie

% Total decrement of damping
%deltaS = 0.1; % structural damping
deltaS = damp(i); % structural damping
deltaD = 0; % damping due to special device
p = 1.25; % density of air [kg/m3]
%n1 = f1; % natural frequency [Hz]
n1 = f(i); % natural frequency [Hz]
%cf = 2; % force coefficient
mm=fim'*M*fim; % modal mass
Ifi=fim'*fim; % integration of modeshape squared
%me=mm/Ifi; % equivalent mass per unit length of the fundamental mode
M5 = diag(M);
me = mean(M5(11:15));
deltaA = (cf*p*B.*Vm)./(2*n1*me); % aerodynamic damping
delta = deltaS + deltaD + deltaA; % logarithmic decrement of damping
% Wind power spectral density
fl = (n1*Lze)./Vm; % non dimensional frequency
SL = (6.8.*fl)./(1+10.2.*fl).^(5/3); % wind psd
% Size reduction function
cy = 11.5; cz = 11.5; % Table C.1
phiy = (cy*B*n1)./Vm;
phiz = (cz*H*n1)./Vm;
Ks =
1./(1+sqrt((Gy.*phiy).^2+(Gz.*phiz).^2+(2/pi()*Gy.*phiy*Gz.*phiz).^2));
% Resonance factor R^2
R2 = (pi()*pi())./(2.*delta).*SL.*Ks;
% Standard deviation of along wind response evaluation
% Turbulence intensity
kl = 1.0; % Turbulence factor
co = 1.0; % Orography factor
Iv = kl/(co*log(ze/z0)); % Turbulence intensity
% reference mass and sqrt of R^2
% uref = mm/(B*D); % modal mass per area
```

```
uref = mm/(B*D); % modal mass per area
R = sqrt(R2);
% standard deviation of along wind response
sigmaa = cf*p*Iv.*Vm.^2.*R*Ky*Kz*fim(end)./(uref*fimax);
% Peak value of along response evaluated with the peak factor
v = n1; % up-crossing frequency
T = 600; % time of mean wind velocity evaluation (10 min)
kp = sqrt(2*log(v*T))+0.6/sqrt(2*log(v*T)); % peak factor
acc = kp.*sigmaa*100; % peak response [cm/s^2]
% Acceletarion response values loaded in vectors
acc_along_C(:,i) = acc;
% Resonance factors loaded into vectors
R_C(i,:) = R;
end
figure;
hold on
plot(V10,acc_along_C(:,1),'b')
plot(V10,acc_along_C(:,2),'r')
fs = 12;
legend('Along wind response acceleration in EW direction','Along wind
response acceleration in NS direction')
xlabel('10 minute mean wind velocity [m/s]','fontsize',fs)
ylabel('Acceleration [cm/s^2]','fontsize',fs)
%hold off

%% Response of the building based on the EN 1-4 - Procedue 1 (Annex B)
f = [f1 f2]; damp = [(z1*2*pi()) (z2*2*pi())];
fim = (Z'./H).^1.7; % Mode shape for all stories
fimax = max(fim); % Mode shape on the top storie

ze = 0.6*H; % Reference height [m]
z0 = 0.05; % Roughness length [m]
alfa = 0.67+0.05*log(z0);
Lze = 300*(ze/200)^alfa; % Turbulence length [m]
% Resonance factor
V10 = 1:1:35; % mean wind velocity at 10 m height
kr = 0.19*(z0/0.05)^0.07; % terrain factor
cr = kr*log(ze/z0); % roughness factor
Vm = cr.*V10; % wind velocity at reference height
acc_along_B = zeros(length(Vm),length(f));
for i = 1:length(f);
% Values for vibration of the first two modes
if i == 1 %Vibration in EW
B = Dypt; D = Breidd; cf = 2.1;
fim = MS_X;
ex = 2;
elseif i == 2 %Vibration in NS
B = Breidd; D = Dypt; cf = 2.1;
fim = MS_Y;
ex = 1;
end
% total decrement of damping
deltaS = damp(i); % structural damping
deltaD = 0; % damping due to special device
p = 1.25; % density of air [kg/m3]
n1 = f(i); % natural frequency [Hz]
mm=fim'*M*fim; % modal mass
Ifi=fim'*fim; % integration of modeshape squared
%me=mm/Ifi; % equivalent mass per unit length of the fundamental mode
M5 = diag(M);
me = mean(M5(11:15));
```

```
deltaA = (cf*p*B.*Vm)./(2*n1*me); % aerodynamic damping
delta = deltaS + deltaD + deltaA; % logarithmic decrement of damping
% Wind power spectral density
fl = (n1*Lze)./Vm; % non dimensional frequency
SL = (6.8.*fl)./(1+10.2.*fl).^(5/3); % wind psd
% aerodynamic admittance function
nh = (4.6*H.*fl)./Lze;
nb = (4.6*B.*fl)./Lze;
Rh = 1./nh-(1-exp(-2.*nh))./(2.*nh.^2);
Rb = 1./nb-(1-exp(-2.*nb))./(2.*nb.^2);
% R^2
R2 = (pi()*pi())./(2.*delta).*SL.*Rh.*Rb;
% Standard deviation of acceleration response evaluated
% Turbulence intensity
kl = 1.0; % Turbulence factor
co = 1.0; % Orography factor
Iv = kl/(co*log(ze/z0)); % Turbulence intensity
% reference massann and sqrt of R^2
%uref = mm/(B*D); % modal mass per area
R = sqrt(R2);
% ex = 1.7; % exponent of the mode shape
Kx = ((2*ex+1)*((ex+1)*(log(ze/z0)+0.5)-1))/((ex+1)^2*log(ze/z0));
% standard deviation of along wind response
sigmaa = cf*p*B*Iv.*Vm.^2.*R.*Kx*fimax./(me);
% Peak along wind resposne evaluated
v = n1; % up-crossing frequency
T = 600; % time of mean wind velocity evaluation (10 min)
kp = sqrt(2*log(v*T))+0.6/sqrt(2*log(v*T)); % peak factor
acc = kp.*sigmaa*100; % peak hröðun [cm/s^2]
% Response values loaded into vectors
acc_along_B(:,i) = acc;
end
hold on
plot(V10,acc_along_B(:,1),'--b')
plot(V10,acc_along_B(:,2),'--r')
fs = 12;
legend('Annex C: Along wind acceleration in EW direction',...
    'Annex C: Along wind acceleration in NS direction',...
    'Annex B: Along wind acceleration in EW direction',...
    'Annex B: Along wind acceleration in NS
direction','location','northwest')
xlabel('10 minute mean wind velocity [m/s]','fontsize',fs)
ylabel('Acceleration [cm/s^2]','fontsize',fs)

% Annex C results plotted seperately
figure
hold on
plot(V10,acc_along_C(:,1),'b')
plot(V10,acc_along_C(:,2),'r')
fs = 12;
legend('Along wind response acceleration in EW direction',...
    'Along wind response acceleration in NS
direction','location','northwest')
xlabel('10 minute mean wind velocity [m/s]','fontsize',fs)
ylabel('Acceleration [cm/s^2]','fontsize',fs)

% Annex C results plotted seperately
figure
hold on
plot(V10,acc_along_B(:,1),'b')
plot(V10,acc_along_B(:,2),'r')
```

```
fs = 12;
legend('Along wind response acceleration in EW direction',...
    'Along wind response acceleration in NS
direction','location','northwest')
xlabel('10 minute mean wind velocity [m/s]','fontsize',fs)
ylabel('Acceleration [cm/s^2]','fontsize',fs)
```

ASCE procedure to evaluate acceleration response

```
%-------------------------------------------------------------------------
% Wind induced response based on the ASCE code procedure.
% Wind excitation of tall buildings - Estimation of acceleration response
%-------------------------------------------------------------------------
% Structural parameters explained:
% B(m) : The projected breadth of the building
% D(m) : The projected width of the building
% H(m) : reference height
% hi(m) : Height between floors from basement to top
% Mi(kg) : Mass of each building floor
% f_1(Hz): Natural frequency for first mode across the weaker axis
% z_1 : Critical damping ratio for the mode 1
% f_2(Hz): Natural frequency for first mode across the stronger axis
% z_2 : Critical damping ratio for the mode 2
% f_3(Hz): Natural frequency for the first torsional mode of vibration
% z_3 : Critical damping ratio for the mode 3
% fi : Mode shape of the building can be evaluated as fi=(Z/H).^beta
% where beta lies within the range 1.5 to 2.0;
%
% Written by: Oliver Claxton
% Edited by: Jonas Thor Snaebjornsson and Örvar Jónsson
%-------------------------------------------------------------------------
% Structural parameters: Values
% Hús verslunarinnar  - The Commerce building in Reykjavik
% Heigth parameters
Z = xlsread('FEMprop.xlsx',1,'C2:C16');
H = Z(end);
% Width parameters
Atot = 1179; %m2
B = Atot/H; % average width 24,1m
D = 24.3;
Breidd = B; Dypt = D;
% Mode Shapes. 1st mode shape in each direction
MS_X = xlsread('FEMprop.xlsx',1,'D2:D16');
MS_Y = xlsread('FEMprop.xlsx',1,'E2:E16');
% Dynamic mass
M = diag(xlsread('FEMprop.xlsx',1,'I2:I16'));
Mtot=sum(diag(M));
% Natural frequencies and critical damping ratios
f1 = 1.69; z1 = 0.02; % ModeShape 1, along
f2 = 2.22; z2 = 0.02; % ModeShape 2, across
f3 = 2.86; z3 = 0.02; % ModeShape 3, torsion
% frequencies from FE model. Damping chosen 2% based on the various results
% of the SI
%-------------------------------------------------------------------------
%% Factors due to Exposure class C
n1 = f1; % Building natural frequency, Hz
n2 = f2;
% Table 6-2 in ASCE07-05 (metric)
alpha = 9.5; % 3-s gust-velocity power law exponent
Zg = 274.32; % Nominal height of the atmospheric boundary
% layer used in this standard.
a_Hat = (1/9.5); % Reciprocal of a
b_Hat = 1.00; % 3-s gust velocity factor
alpha_mean = (1/6.5); % Mean hourly wind-velocity power law exponent in
% Eq. 6-14
b_mean = 0.65; % Mean hourly wind velocity factor in Eq. 6-14
c = 0.2; % Turbulence intensity factor in Eq. 6-5
l = 152.4; % Integral length scale factor
```

```
epsilon = (1/5.0); % Integral length scale power law exponent in
% Eq. 6-7
z_min = 4.57; % Exposure constant
z_mean = 0.6*H; % Equivalent height of structure
hro = 1.25; % Air density

%% Factors for RMS Along-Wind Acceleration
Vm = linspace(1,35,35); % Basic 10m wind velocity
G = 1.5;
VG = Vm*G;
Vz = (z_mean/10).^alpha_mean.*VG; % mean hourly wind velocity at height z
% force coefficient
% fi = (Z'/H).^1.5; % Fundamental model shape
m1_X = MS_X'*M*MS_X; % Modal mass
m1_Y = MS_Y'*M*MS_Y; % Modal mass
Cfx = 1.35;
Iz = c*(10/z_mean)^(1/6); % Turbulence intensity
beta = 2;
K_X = 1.65^a_Hat/(a_Hat+beta+1);
beta = 1;
K_Y = 1.65^a_Hat/(a_Hat+beta+1);
%% Resonant response factor
Beta = z1; % Damping ratio, percent critical
% for buildings or other structures
Lz = l*(z_mean/10)^epsilon; % Integral length scale of turbulence
N1= (n1.*Lz./Vz); % Reduced frequency from Eq. 6-12
N2= (n2.*Lz./Vz);
Rn1 = 4.74*N1./((1+10.3*N1).^(5/3)); % value from Eq. 6- 11
Rn2 = 4.74*N2./((1+10.3*N2).^(5/3));
E = 1; % Effect of horizontal and
% vertical earthquakeinduced forces
L = D; % Horizontal dimension of a building
% measured parallel to the wind
% direction
% #1 = wind in EW
% #2 = wind in NS
% value used in Eq. 6-13
eta_h1 = 4.6*n1.*H./Vz;
eta_h2 = 4.6*n2.*H./Vz;
Rh1 = 1./eta_h1-1./(2.*eta_h1.^2).*(1-exp(-2.*eta_h1));
Rh2 = 1./eta_h2-1./(2.*eta_h2.^2).*(1-exp(-2.*eta_h2));
% values from Eq. 6-13
eta_B1 = 4.6*n1.*B*E./Vz;
eta_B2 = 4.6*n2.*D*E./Vz;
RB1 = 1./eta_B1-1./(2.*eta_B1.^2).*(1-exp(-2.*eta_B1));
RB2 = 1./eta_B2-1./(2.*eta_B2.^2).*(1-exp(-2.*eta_B2));
% values from Eq. 6-13
eta_L1 = 15.4*n1.*L./Vz;
eta_L2 = 15.4*n2.*B./Vz;
RL1 = 1./eta_L1-1./(2.*eta_L1.^2).*(1-exp(-2.*eta_L1));
RL2 = 1./eta_L2-1./(2.*eta_L2.^2).*(1-exp(-2.*eta_L2));
% Equation 6-13
R_1 = sqrt(1./Beta.*Rn1.*Rh1.*RB1.*(0.53+0.47.*RL1));
R_2 = sqrt(1./Beta.*Rn2.*Rh2.*RB2.*(0.53+0.47.*RL2));
%% RMS Along-Wind Acceleration
Sigma_1 = 0.85*MS_X(end)*hro*Dypt*H*Cfx.*Vz.^2./m1_X.*Iz*K_X.*R_1;
Sigma_2 = 0.85*MS_Y(end)*hro*Breidd*H*Cfx.*Vz.^2./m1_Y.*Iz*K_Y.*R_2;
%% Maximum Along-Wind acceleration
T = 600; % Length of time over which the minimum acceleration
% is computed, usually taken to be 3,600 s to represent 1h.
gx1 = sqrt(2*log(n1*T))+0.5772/(sqrt(2*log(n1*T)));
```

```
gx2 = sqrt(2*log(n2*T))+0.5772/(sqrt(2*log(n2*T)));
a_max_EW = Sigma_1*gx1*100;
a_max_NS = Sigma_2*gx2*100;
%open ('figure1.fig')
figure
hold on
plot(Vm,a_max_EW,'b',Vm,a_max_NS,'r');
fs = 12;
legend('Along wind response acceleration in EW direction',...
    'Along wind response acceleration in NS
direction','location','northwest')
xlabel('10 minute mean wind velocity [m/s]','fontsize',fs)
ylabel('Acceleration [cm/s^2]','fontsize',fs)
```

AIJ procedure to evaluate acceleration response

```
%-------------------------------------------------------------------------
% Wind induced response based on the AIJ code procedure.
% Wind excitation of tall buildings - Estimation of acceleration response
%-------------------------------------------------------------------------
% Structural parameters explained:
% B(m) : The projected breadth of the building
% D(m) : The projected width of the building
% H(m) : reference height
% hi(m) : Height between floors from basement to top
% Mi(kg) : Mass of each building floor
% f_1(Hz): Natural frequency for first mode across the weaker axis
% z_1 : Critical damping ratio for the mode 1
% f_2(Hz): Natural frequency for first mode across the stronger axis
% z_2 : Critical damping ratio for the mode 2
% f_3(Hz): Natural frequency for the first torsional mode of vibration
% z_3 : Critical damping ratio for the mode 3
% fi : Mode shape of the building can be evaluated as fi=(Z/H).^beta
% where beta lies within the range 1.5 to 2.0;
%
% Written by: Örvar Jónsson
% Edited by: Jonas Thor Snaebjornsson and Örvar Jónsson
%-------------------------------------------------------------------------
% Structural parameters: Values
% Hús Verslunarinnar - The Commerce building in Reykjavik
% Heigth parameters
Z = xlsread('FEMprop.xlsx',1,'C2:C16');
H = Z(end);
% Width parameters
Atot = 1179; %m2
B = Atot/H; % average width 24,1m
D = 24.3;
% Mode Shapes. 1st mode shape in each direction
MS_X = xlsread('FEMprop.xlsx',1,'D2:D16');
MS_Y = xlsread('FEMprop.xlsx',1,'E2:E16');
% Dynamic mass
M = diag(xlsread('FEMprop.xlsx',1,'I2:I16'));
Mtot=sum(diag(M));
% Natural frequencies and critical damping ratios
f1 = 1.69; z1 = 0.02; % ModeShape 1, along
f2 = 2.22; z2 = 0.02; % ModeShape 2, across
f3 = 2.86; z3 = 0.02; % ModeShape 3, torsion
% frequencies from FE model. Damping chosen 2% based on the various results
% of the SI

figure
plot(MS_X,Z,'o')
hold on
plot(MS_Y,Z,'ro')

plot((Z/H).^2,Z) % beta = 2
plot((Z/H).^1,Z,'r') % beta = 1
% beta = 2 fyrir vibration in x direction (EW)
% beta = 1 fyrir vibration in y direction (NS)
fs=12;
legend('Mode shape 1 from the FEM - EW vibration',...
    'Mode shape 2 from the FEM - NS vibration',...
    '(Z/H)^2','(Z/H)^1','location','SouthEast')
xlabel('Normalised displacement')
ylabel('Height [m]')
```

```
%-------------------------------------------------------------------------
%% Response of the building based on the AIJ code procedure
Breidd = B; Dypt = D;
% terrain category 2
Zb = 5; % according to table A6.3 for terrain category II
ZG = 350; % according to A6.3 for terrain category II
alfa = 0.15; % according to A6.3 for terrain category II
% Wind pressure
hro = 1.25; % density of air
U0 = 1:1:35;
KD = 1;
Er = 1.7*(H/ZG)^alfa; % for Zb < H < ZG
Eg = 1; % flat terrain, no hills close
EH = Er*Eg;
U50ar = 35.5;
U500ar = 41.48; % Previously evaluated wind velocity of 500 year return
period
lambdaU = U500ar./U50ar;
r = 50; % 50 year design
rkW = 0.63*(lambdaU-1)*log(r)-2.9*lambdaU+3.9;
UH = U0*KD*EH.*rkW;
% UH=linspace(1,35.5,100)
qH = 0.5*hro*UH.^2; % WindPressure
% Modal mass
MD_X = MS_X'*M*MS_X;
MD_Y = MS_Y'*M*MS_Y;
%% Along wind response: Wind in the EW direction
% Values for wind in the EW direction
B = Dypt; D = Breidd;
% Values for vibration in the EW direction
fD = f1; zD = z1;
gaD = sqrt(2*log(600*fD)+1.2);
kz = zeros(length(Z),1);
for i=1:length(Z)
if Z(i)<Zb
kz(i)=(Zb/H)^(2*alfa);
elseif Z(i)<0.8*H
kz(i)=(Z(i)/H)^(2*alfa);
elseif Z(i)>0.8*H
kz(i)=0.8^(2*alfa);
end
end
Cpe1 = 0.8*kz;
if D/B>1
Cpe2 = -0.35;
else
Cpe2 = -0.5;
end
CD = Cpe1-Cpe2;
CH = CD(end); % wind force coefficient at reference height
%Cmerktg %rms overturning moment coefficient as defined in A6.3
if H/B<1
k=0.15;
else
k=0.07;
end
IrH = 0.1*(H/ZG)^(-alfa-0.05); % Gildir ef H>Zb
EI = 1; % Taken as 1 for no close hills or ridges
Eg = 1; % Taken as 1 for no close hills or ridges
EgI = EI/Eg;
```

```
IH = IrH*EgI;
LH = 100*(H/30)^0.5; % if H>30m
Cdg = 2*IH*((0.49-0.14*alfa)/(1+(0.63*(sqrt(B*H)/LH)^0.56)/(H/B)^k));
beta = 2;
lambda = 1-0.4*log(beta);
F = (4*fD*LH./UH)./(1+71*(fD*LH./UH).^2).^(5/6);
SD = 0.9./(((1+6*(fD*H./UH).^2).^0.5).*(1+3*(fD*B./UH)));
R = 1./(1+20*fD*B./UH);
FD = (IH^2.*F.*SD.*(0.57-0.35*alfa+2.*R.*sqrt(0.053-0.042*alfa)))./Cdg^2;
RD = pi*FD/(4*zD);
aDmaxEW = 100.*(qH.*gaD*B*H*CH*Cdg*lambda.*sqrt(RD))./MD_X; %cm/s^2

%% Along wind response: Wind in the NS direction
% Values for wind in the NS direction
B = Breidd; D = Dypt;
% Values for vibration in the NS direction
fD = f2; zD = z2;
gaD = sqrt(2*log(600*fD)+1.2);
kz = zeros(length(Z),1);
for i=1:length(Z)
if Z(i)<Zb
kz(i)=(Zb/H)^(2*alfa);
elseif Z(i)<0.8*H
kz(i)=(Z(i)/H)^(2*alfa);
elseif Z(i)>0.8*H
kz(i)=0.8^(2*alfa);
end
end
Cpe1 = 0.8*kz;
if D/B>1
Cpe2 = -0.35;
else
Cpe2 = -0.5;
end
CD = Cpe1-Cpe2;
CH = CD(end); %wind force coefficient at reference height
%Cmerktg %rms overturning moment coefficient as defined in A6.3
if H/B<1
k=0.15;
else
k=0.07;
end
IrH = 0.1*(H/ZG)^(-alfa-0.05); % Gildir ef H>Zb
EI = 1; % Taken as 1 for no close hills or ridges
Eg = 1; % Taken as 1 for no close hills or ridges
EgI = EI/Eg;
IH = IrH*EgI;
LH = 100*(H/30)^0.5; % Gildir ef H>30m
Cdg = 2*IH*((0.49-0.14*alfa)/(1+(0.63*(sqrt(B*H)/LH)^0.56)/(H/B)^k));
beta = 1;
lambda = 1-0.4*log(beta);
F = (4*fD*LH./UH)./(1+71*(fD*LH./UH).^2).^(5/6);
SD = 0.9./(((1+6*(fD*H./UH).^2).^0.5).*(1+3*(fD*B./UH)));
R = 1./(1+20*fD*B./UH);
FD = (IH^2.*F.*SD.*(0.57-0.35*alfa+2.*R*sqrt(0.053-0.042*alfa)))/Cdg^2;
RD = pi*FD/(4*zD);
aDmaxNS = 100.*(qH.*gaD*B*H*CH*Cdg*lambda.*sqrt(RD))./MD_Y; %cm/s^2

%% Across wind resposne: Wind in the EW direction
% Values for wind in the EW direction
B = Dypt; D = Breidd;
```

```
% Values for vibration in the NS direction
fL = f2; zL = z2;
gaL = sqrt(2*log(600*fL)+1.2);
% the building fulfills the criteria of A6.4.1
CdL = 0.0082*(D/B)^3-0.071*(D/B)^2+0.22*(D/B);
beta = 1;
lambda = 1-0.4*log(beta);
% D/B < 3 for both wind directions. Then m=1 and beta1 and kappa1 are used
beta1 = (((D/B)^4+2.3*(D/B)^2)/(2.4*(D/B)^4-9.2*(D/B)^3+18*(D/B)^2+...
9.5*(D/B)-0.15))+0.12/(D/B);
kappa1 = 0.85;
fs1 = (0.12/((1+0.38*(D/B)^2)^0.89)).*(UH./B);
FL = (4*kappa1*(1+0.6*beta1)*beta1/pi).*((fL./fs1).^2./((1-
(fL./fs1).^2).^2+...
4*beta1^2.*(fL./fs1).^2));
RL = pi*FL./(4*zL);
aLmaxEW = 100*qH.*gaL*B*H*CdL*lambda.*sqrt(RL)./MD_Y;

%% Across wind response: Wind in the NS direction
% Values for wind in the NS direction
B = Breidd; D = Dypt;
% Values for vibration in the EW direction
fL = f1; zL = z1;
gaL = sqrt(2*log(600*fL)+1.2);
% the building fulfills the criteria of A6.4.1
CdL = 0.0082*(D/B)^3-0.071*(D/B)^2+0.22*(D/B);
beta = 2;
lambda = 1-0.4*log(beta);
% D/B < 3 for both wind directions. Then m=1 and beta1 and kappa1 are used
beta1 = (((D/B)^4+2.3*(D/B)^2)/(2.4*(D/B)^4-9.2*(D/B)^3+18*(D/B)^2+...
9.5*(D/B)-0.15))+0.12/(D/B);
kappa1 = 0.85;
fs1 = (0.12/((1+0.38*(D/B)^2)^0.89))*(UH/B);
FL = (4*kappa1*(1+0.6*beta1)*beta1/pi).*((fL./fs1).^2./((1-
(fL./fs1).^2).^2+...
4*beta1^2.*(fL./fs1).^2));
RL = pi*FL./(4*zL);
aLmaxNS = 100*qH.*gaL*B*H*CdL*lambda.*sqrt(RL)./MD_X;
%% Plotting figures
% Square root of sums
aEW = sqrt(aDmaxEW.^2+aLmaxEW.^2);
aNS = sqrt(aDmaxNS.^2+aLmaxNS.^2);
figure
hold on
plot(U0,aEW,'b')
plot(U0,aNS,'r')
hold off
grid on
fs=12;
legend('Wind along strong axis','Wind along weak axis')
xlabel('Mean wind velocity [m/s]')
ylabel('acceleration [cm/s^2]')

%Along and across resposnes for wind in EW
figure
hold on
plot(U0,aDmaxEW,'b')
plot(U0,aLmaxEW,'r')
hold off
legend('Along wind acceleration response',...
    'Across wind acceleration response','location','northwest')
```

```
title('Wind in the EW direction','fontsize',fs)
xlabel('10 minute mean wind velocity [m/s]','fontsize',fs)
ylabel('Acceleration [cm/s^2]','fontsize',fs)

% Along and across resposne for wind in NS
figure
hold on
plot(U0,aDmaxNS,'b')
plot(U0,aLmaxNS,'r')
hold off
legend('Along wind acceleration response',...
    'Across wind acceleration response','location','northwest')
title('Wind in the NS direction','fontsize',fs)
xlabel('10 minute mean wind velocity [m/s]','fontsize',fs)
ylabel('Acceleration [cm/s^2]','fontsize',fs)

% Only along wind response
figure
hold on
plot(U0,aDmaxEW,'b')
plot(U0,aDmaxNS,'r')
hold off
legend('Along wind response acceleration in EW direction',...
    'Along wind response acceleration in NS
direction','location','northwest')
xlabel('10 minute mean wind velocity [m/s]','fontsize',fs)
ylabel('Acceleration [cm/s^2]','fontsize',fs)
```

Comparison of the design code procedures of response prediction to the recorded response

```
%-------------------------------------------------------------------------
% This routine compares the results of the design code procedures of
% response prediction to the recorded response provided by the Earthquake
% Engineering Research Center along with meteorological data provided by
% the Icelandic Meteorolocical Office
%
% Written by: Örvar Jónsson
%-------------------------------------------------------------------------

% Design code results plotted together
EN_HV
ASCE_HV
AIJ_HV

figure
hold on
plot(V10,acc_along_C(:,1),'b') % EC C along wind EW
plot(V10,acc_along_C(:,2),'--b') % EC C along wind NS

plot(Vm,a_max_EW,'r') % ASCE along wind EW
plot(Vm,a_max_NS,'--r') % ASCE along wind NS

plot(U0,aDmaxEW,'color',[0 0.5 0]) % AIJ along wind EW
plot(U0,aDmaxNS,'--','color',[0 0.5 0]) % AIJ along wind NS

% Loading recorded response
load max10mwindx; load max10mwindy; load windaccx1; load windaccx2;
load windaccy; load acrossaccx1; load acrossaccx2; load acrossaccy;

% Recorded response converted from peak-to-peak values to absolute values
windaccx1 = windaccx1/2;
windaccx2 = windaccx2/2;
windaccy = windaccy/2;
acrossaccx1 = acrossaccx1/2;
acrossaccx2 = acrossaccx2/2;
acrossaccy = acrossaccy/2;

plot(max10mwindx,windaccx1,'o')
plot(max10mwindx,windaccx2,'o')
plot(max10mwindy,windaccy,'o')

hold off
grid on
ylim([0 16]); xlim([0 35]);
fs = 12;
title('Along wind acceleration response','fontsize',fs)
legend('EN. Wind along EW direction',...
    'EN. Wind along NS direction',...
    'ASCE. Wind along EW direction',...
    'ASCE. Wind along NS direction',...
    'AIJ. Wind along EW direction',...
    'AIJ. Wind along NS direction',...
    'Recorded response','location','northwest')
xlabel('10 minute mean wind velocity [m/s]','fontsize',fs)
ylabel('Acceleration [cm/s^2]','fontsize',fs)
```

```
%% Wind in EW direction

figure
hold on
plot(V10,acc_along_C(:,1),'b') % EC C along wind EW

plot(Vm,a_max_EW,'r') % ASCE along wind EW

plot(U0,aDmaxEW,'color',[0 0.5 0]) % AIJ along wind EW
plot(U0,aLmaxEW,'-.','color',[0 0.5 0]) % AIJ across wind EW

plot(max10mwindx,windaccx1,'o')
plot(max10mwindx,acrossaccy,'v')
plot(max10mwindx,windaccx2,'o')

hold off
grid on
ylim([0 16]); xlim([0 35]);
fs = 12;
title('Wind in the EW direction','fontsize',fs)
legend('EN. Along wind acceleration',...
    'ASCE. Along wind acceleration',...
    'AIJ. Along wind acceleration',...
    'AIJ. Across wind acceleration',...
    'Recorded along wind response',...
    'Recorded across wind response','location','northwest')
xlabel('10 minute mean wind velocity [m/s]','fontsize',fs)
ylabel('Acceleration [cm/s^2]','fontsize',fs)

%% Wind in NS direction

figure
hold on
plot(V10,acc_along_C(:,2),'b') % EC C along wind NS

plot(Vm,a_max_NS,'r') % ASCE along wind Ns

plot(U0,aDmaxNS,'color',[0 0.5 0]) % AIJ along wind NS
plot(U0,aLmaxNS,'-.','color',[0 0.5 0]) % AIJ across wind NS

plot(max10mwindy,windaccy,'o')
plot(max10mwindy,acrossaccx1,'v')
plot(max10mwindy,acrossaccx2,'v')


hold off
grid on
ylim([0 16]); xlim([0 35]);
fs = 12;
title('Wind in the NS direction','fontsize',fs)
legend('EN. Along wind acceleration',...
    'ASCE. Along wind acceleration',...
    'AIJ. Along wind acceleration',...
    'AIJ. Across wind acceleration',...
    'Recorded along wind response',...
    'Recorded across wind response','location','northwest')
xlabel('10 minute mean wind velocity [m/s]','fontsize',fs)
ylabel('Acceleration [cm/s^2]','fontsize',fs)
```

```
%% Resonance factors compared
% wind in EW
figure
plot(V10,R_C(1,:),'b')
hold on
plot(Vm,R_1,'r')
plot(U0,RD,'color',[0 0.5 0])
fs = 12;
legend('EN','ASCE', 'AIJ')
xlabel('10 minute mean wind velocity [m/s]','fontsize',fs)
ylabel('Resonance factor','fontsize',fs)
```

A7: Human comfort criteria's

In this Matlab code the human comfort criteria's are compared to the recorded response and the response predicted by the design codes.

```
%-------------------------------------------------------------------------
% This routine compares the human comfort criteria's presented by the AIJ
% and ISO 10137 codes to the response predicted by the Eurocode, the ASCE
% design code and the AIJ design code, and the recorded response provided
% by the Earthquake Engineering Research Center along with meteorological
% data provided by the Icelandic Meteorolocical Office
%
% Written by: Örvar Jónsson
%-------------------------------------------------------------------------

%% Comfort criteria

AIJc70 = 2.2; % AIJ H-70 criteria: 2,2 cm/s^2
AIJc90 = 3.1; % AIJ H-90 criteria: 3,1 cm/s^2
ISOc = 6;   % ISO criteria: 6 cm/s^2

% Loading recorded response
load max10mwindx; load max10mwindy; load windaccx1; load windaccx2;
load windaccy; load acrossaccx1; load acrossaccx2; load acrossaccy;

% Recorded response converted from peak-to-peak values to absolute values
windaccx1 = windaccx1/2;
windaccx2 = windaccx2/2;
windaccy = windaccy/2;
acrossaccx1 = acrossaccx1/2;
acrossaccx2 = acrossaccx2/2;
acrossaccy = acrossaccy/2;

figure
hold on
plot([0 35],[AIJc70 AIJc70],'--','color',[0 0.5 0],'linewidth',2)    % AIJ
guidelines
plot([0 35],[AIJc90 AIJc90],'--','color',[1 0 1],'linewidth',2)    % AIJ
guidelines
plot([0 35],[ISOc ISOc],'--r','linewidth',2)    % ISO guidelines
plot(max10mwindy,windaccy,'o')                  % Recorded along response
plot(max10mwindy,acrossaccx1,'v')               % Recorded across response
plot(max10mwindy,acrossaccx2,'v')               % Recorded across response
plot(max10mwindx,windaccx1,'o')                 % Recorded along response
plot(max10mwindx,windaccx2,'o')                 % Recorded along response
plot(max10mwindx,acrossaccy,'v')                % Recorded across response
plot([21 21],[0 12],'--k')                      % 1 year return period wind
velocity
hold off
legend('AIJ-GBV H-70','AIJ-GBV H-90','ISO 10137',...
    'Recorded along wind response','Recorded across wind response',...
    'location','northwest')
fs = 12;
xlabel('10 minute mean wind velocity [m/s]','fontsize',fs)
ylabel('Acceleration [cm/s^2]','fontsize',fs)


%% Counting storms that breach the criteria's+
```

```
% AIJ H-90
% wind in EW direction
aijcritx = zeros(length(max10mwindx),3);
aijcrity = zeros(length(max10mwindy),3);
for i = 1:length(max10mwindx)
    aijcritx(i,1) = windaccx1(i,1)>AIJc90;
    aijcritx(i,2) = windaccx2(i,1)>AIJc90;
    aijcritx(i,3) = acrossaccy(i,1)>AIJc90;
end
% Wind in NS direction
for i = 1:length(max10mwindy)
    aijcrity(i,1) = windaccy(i,1)>AIJc90;
    aijcrity(i,2) = acrossaccx1(i,1)>AIJc90;
    aijcrity(i,3) = acrossaccx2(i,1)>AIJc90;
end
% Number of responses higher than criteria
aijcritxnum = sum(sum(aijcritx')>0);
aijcritynum = sum(sum(aijcrity')>0);
aijcritnum = aijcritxnum + aijcritynum

% ISO
% Wind in EW direction
isocritx = zeros(length(max10mwindx),3);
isocrity = zeros(length(max10mwindy),3);
for i = 1:length(max10mwindx)
    isocritx(i,1) = windaccx1(i,1)>ISOc;
    isocritx(i,2) = windaccx2(i,1)>ISOc;
    isocritx(i,3) = acrossaccy(i,1)>ISOc;
end
% Wind in NS direction
for i = 1:length(max10mwindy)
    isocrity(i,1) = windaccy(i,1)>ISOc;
    isocrity(i,2) = acrossaccx1(i,1)>ISOc;
    isocrity(i,3) = acrossaccx2(i,1)>ISOc;
end
% Number of responses higher than criteria
isocritxnum = sum(sum(isocritx')>0);
isocritynum = sum(sum(isocrity')>0);
isocritnum = isocritxnum + isocritynum


%% Comfort criteria compared to design code estimations

EN_HV
ASCE_HV
AIJ_HV

% Wind in EW
figure
hold on
plot(V10,acc_along_C(:,1),'b') % EC C along wind EW

plot(Vm,a_max_EW,'r') % ASCE along wind EW

plot(U0,aDmaxEW,'color',[0 0.5 0]) % AIJ along wind EW
plot(U0,aLmaxEW,'-.','color',[0 0.5 0]) % AIJ across wind EW

plot([0 35],[AIJc70 AIJc70],'--','color',[0 0.5 0],'linewidth',2)    % AIJ
guidelines
```

```
plot([0 35],[AIJc90 AIJc90],'--','color',[1 0 1],'linewidth',2)    % AIJ
guidelines
plot([0 35],[ISOc ISOc],'--r','linewidth',2)    % ISO guidelines

plot(max10mwindx,windaccx1,'o')
plot(max10mwindx,acrossaccy,'v')
plot(max10mwindx,windaccx2,'o')

plot([21 21],[0 20],'--k')    % 1 year return period wind velocity

hold off
ylim([0 20]); xlim([0 35]);
fs = 12;
title('Wind in the EW direction','fontsize',fs)
legend('EN. Along wind acceleration',...
    'ASCE. Along wind acceleration',...
    'AIJ. Along wind acceleration',...
    'AIJ. Across wind acceleration',...
    'AIJ-GBV H-70 comfort criteria','AIJ-GBV H-90 comfort criteria',...
    'ISO 10137 comfort criteria',...
    'Recorded along wind response',...
    'Recorded across wind response','location','northwest')
xlabel('10 minute mean wind velocity [m/s]','fontsize',fs)
ylabel('Acceleration [cm/s^2]','fontsize',fs)

%% Wind in NS direction

figure
hold on
plot(V10,acc_along_C(:,2),'b') % EC C along wind NS

plot(Vm,a_max_NS,'r') % ASCE along wind Ns

plot(U0,aDmaxNS,'color',[0 0.5 0]) % AIJ along wind NS
plot(U0,aLmaxNS,'-.','color',[0 0.5 0]) % AIJ across wind NS

plot([0 35],[AIJc70 AIJc70],'--','color',[0 0.5 0],'linewidth',2)    % AIJ
guidelines
plot([0 35],[AIJc90 AIJc90],'--','color',[1 0 1],'linewidth',2)    % AIJ
guidelines
plot([0 35],[ISOc ISOc],'--r','linewidth',2)    % ISO guidelines

plot(max10mwindy,windaccy,'o')
plot(max10mwindy,acrossaccx1,'v')
plot(max10mwindy,acrossaccx2,'v')

plot([21 21],[0 20],'--k')                      % 1 year return period wind
velocity

hold off
grid on
ylim([0 20]); xlim([0 35]);
fs = 12;
title('Wind in the NS direction','fontsize',fs)
legend('EN. Along wind acceleration',...
    'ASCE. Along wind acceleration',...
    'AIJ. Along wind acceleration',...
    'AIJ. Across wind acceleration',...
    'AIJ-GBV H-70 comfort criteria','AIJ-GBV H-90 comfort criteria',...
```

```
    'ISO 10137 comfort criteria',...
    'Recorded along wind response',...
    'Recorded across wind response','location','northwest')
xlabel('10 minute mean wind velocity [m/s]','fontsize',fs)
ylabel('Acceleration [cm/s^2]','fontsize',fs)
```

Appendix B

This appendix contains the design code procedures to evaluate wind induced response prediction of the Eurocode EN 1991-1-4, the ASCE and the AIJ design codes. The procedures are presented, practically identically as they are presented in the codes.

B1: Response prediction – EN 1991-1-4 Annex B

The method of evaluating the peak along wind acceleration response described in EN 1991-1-4 Annex B determines the standard deviation of along wind acceleration response with the expression:

$$\sigma_{a,x}(z) = \frac{c_f \cdot \rho \cdot b \cdot I_v(z_s) \cdot v_m^2 \cdot (z_s)}{m_{1,x}} \cdot R \cdot K_x \cdot \Phi_{1,x}(z)$$

where:

c_f is the force coefficient of wind action

ρ is the density of air, taken as 1,25 kg/m^3

b is the width of the structure

$I_v(z_s)$ is the turbulence intensity at the height z = z_s above ground

$v_m(z_s)$ is the mean wind velocity for z = z_s

z_s is the reference height, taken as 0,6H for vertical structures or 29.34 m for this case

R is the square root of resonant response

K_x is the non-dimensional coefficient

$m_{1,x}$ is the along wind fundamental equivalent mass

$\Phi_{1,x}$ is the fundamental along wind mode shape, obtained from the finite element model as noted above

The force coefficient c_f is determined by the expression:

$$c_f = c_{f,0} \cdot \psi_r \cdot \psi_\lambda$$

where:

$c_{f,0}$ is the force coefficient of rectangular sections with sharp corners, evaluated in accordance to section 7.6 in EN 1991-1-4 and taken as 2,1.

ψ_r is the reduction factor for square sections with rounded corners, taken as 1.

ψ_λ is the end-effect factor for elements with free-end flow, taken as 1.

The turbulence intensity is determined using the expression:

$$I_v(z) = \frac{\sigma_v}{v_m(z)} = \frac{k_I}{c_o(z) \cdot \ln(\frac{z}{z_0})}$$

where:

k_I is the turbulence factor, taken as 1.

c_o is the orography factor, taken as 1.

z_0 is the roughness length, taken as 0.05 with regards to the terrain category 2.

The mean wind velocity at the reference height is determined by:

$$v_m(z) = c_r(z) \cdot c_o \cdot v_b$$

where:

c_r is the roughness factor.

c_o is the orography factor, taken as 1.

v_b is the basic wind velocity, the 10 minute mean wind velocity at 10 height.

The roughness factor is determined with:

$$c_r = k_r \cdot \ln\left(\frac{z}{z_0}\right)$$

where:

k_r is a terrain factor

z_0 is the roughness length, taken as 0.05 with regards to the terrain category 2.

The terrain factor is depending on the roughness length and is determined using the expression:

$$k_r = 0{,}19 \cdot \left(\frac{z_0}{z_{0,II}}\right)^{0{,}07}$$

where:

z_0 is the roughness length, taken as 0.05 with regards to the terrain category.

$z_{0,II}$ is the roughness length 0,05 of terrain category 2.

As the terrain category of the case studied is terrain category 2 the k_r is simply 0,19.

The resonant response is determined using:

$$R^2 = \frac{\pi^2}{2 \cdot \delta} \cdot S_L(z_s, n_{1,x}) \cdot R_h(\eta_h) \cdot R_b(\eta_b)$$

where:

δ is the total logarithmic decrement of damping.

S_L is the non-dimensional power spectral density function.

R_b, R_h are the aerodynamic admittance functions.

The total logarithmic decrement of damping is estimated by the expression:

$$\delta = \delta_s + \delta_a + \delta_d$$

where:

δ_s is the logarithmic decrement of structural damping, taken as the critical damping ratio, 2% as noted above, multiplied with 2π.

δ_a is the logarithmic decrement of aerodynamic damping for the fundamental mode.

δ_d is the logarithmic decrement of damping due to special devices, taken as 1 as there are no special damping devices installed in the building.

The logarithmic decrement of aerodynamic damping is estimated by:

$$\delta_a = \frac{c_f \cdot \rho \cdot b \cdot v_m(z_s)}{2 \cdot n_1 \cdot m_e}$$

where:

c_f is the force coefficient of wind action.

ρ is the density of air, taken as 1,25 kg/m^3.

$v_m(z_s)$ is the mean wind velocity for $z = z_s$.

n_1 is the fundamental frequency of along wind vibration.

m_e is the equivalent mass per unit length, which for cantilevered structures with varying mass distribution may be approximated as the average value of mass over the upper third of the structure, or the top five floors of the building observed.

The non-dimensional power spectral density function is determined by the expression:

$$S_L(z,n) = \frac{\mathrm{n} \cdot S_v(z,n)}{\sigma_v^2} = \frac{6{,}8 \cdot f_L(z,n)}{\left(1 + 10{,}2 \cdot f_L(z,n)\right)^{5/3}}$$

where

f_L is a non-dimensional frequency determined by:

$$f_L(n,z) = \frac{n \cdot \mathrm{L(z)}}{v_m(z)}$$

where

n is the natural frequency

$v_m(z_s)$ is the mean wind velocity for z = z_s.

$L(z)$ is the turbulence length scale determined by the expression:

$$L(z) = L_t \cdot \left(\frac{z}{z_t}\right)^{\alpha}$$

where:

L_t is the reference length scale, generally taken as 300 m.

z_t is the reference height , generally taken as 200 m.

α is 0,67 + 0,05 ln(z_0), where the roughness length, z_0, is 0,05 m according to the terrain category.

The aerodynamic admittance functions for a fundamental mode shape are approximated by the expressions:

$R_h = \frac{1}{\eta_h} - \frac{1}{2 \cdot \eta_h^2}(1 - e^{-2 \cdot \eta_h})$ $\quad R_h = 1$ for $\eta_h = 0$

$R_b = \frac{1}{\eta_b} - \frac{1}{2 \cdot \eta_b^2}(1 - e^{-2 \cdot \eta_b})$ $\quad R_b = 1$ for $\eta_b = 0$

where: $\eta_h = \frac{4{,}6 \cdot h}{L(z_s)} \cdot f_L(z_s, n_{1,x})$ and $\eta_b = \frac{4{,}6 \cdot b}{L(z_s)} \cdot f_L(z_s, n_{1,x})$

where:

h is the height of the structure.

b is the width of the structure.

$L(z)$ is the turbulence length scale.

f_L is a non-dimensional frequency

z_s is the reference height

$n_{1,x}$ is the fundamental frequency of along wind vibration.

The non-dimensional coefficient is approximated by the expression

$$K_x = \frac{(2 \cdot \zeta + 1) \cdot \left\{(\zeta + 1) \cdot \left[\ln\left(\frac{z_s}{z_0}\right) + 0{,}5\right] - 1\right\}}{(\zeta + 1)^2 \cdot ln\left(\frac{z_s}{z_0}\right)}$$

where:

ζ is the exponent of the mode shape as noted above.

z_s is the reference height

z_0 is the roughness length

With the standard deviation of the characteristic along wind acceleration determined, the peak along wind acceleration response is evaluated by multiplying the standard deviation with a peak factor, k_p, that is by definition the ratio of the maximum fluctuation of the response of the structure to the standard deviation of the response. The peak factor is determined by the expression:

$$k_p = \sqrt{2 \cdot \ln(\nu \cdot T)} + \frac{0{,}6}{\sqrt{2 \cdot \ln(\nu \cdot T)}}$$

where:

ν is the up-crossing frequency, which may be taken as the natural frequency.

T is the averaging time for the mean wind velocity, taken as 600 s to represent a 10 minute interval.

B2: Response prediction – EN 1991-1-4 Annex C

The peak factor is the same as in Annex B as previously described. The standard deviation of the along wind acceleration response is determined by the expression:

$$\sigma_{a,x}(y,z) = c_f \cdot \rho \cdot I_v(z_s) \cdot v_m^2(z_s) \cdot R \cdot \frac{K_y \cdot K_z \cdot \Phi(y,z)}{\mu_{ref} \cdot \Phi_{max}}$$

where:

c_f is the force coefficient of wind action as previously described for the Annex B method.

ρ is the density of air, taken as 1,25 kg/m^3

$I_v(z_s)$ is the turbulence intensity at the height z = z_s above ground as previously described for the Annex B method.

$v_m(z_s)$ is the mean wind velocity for z = z_s as previously described for the Annex B method.

z_s is the reference height, taken as 0,6H for vertical structures as previously described for the Annex B method.

R is the square root of resonant response.

K_y is a constant depending on the horizontal mode shape, taken as 1.

K_z is a constant depending on the vertical mode shape, taken as 5/3 for a parabolic mode shape of along wind vibration in the EW direction and 3/2 for a linear mode shape of along wind vibration in the NS direction.

$\Phi(y,z)$ is the mode shape, obtained from the finite element model as previously noted.

Φ_{max} is the mode shape value at the point with maximum amplitude, taken as 1.

μ_{ref} is the reference mass per unit area, taken as the previously described equivalent mass per unit length divided by the floor area of the building.

The resonant response factor is determined by the expression:

$$R^2 = \frac{\pi^2}{2 \cdot \delta} \cdot S_L(z_s, n_{1,x}) \cdot K_s(n_{1,x})$$

where:

δ is the total logarithmic decrement of damping as previously described for the Annex B method.

S_L is the non-dimensional power spectral density function as previously described for the Annex B method.

$n_{1,x}$ is the fundamental frequency of along wind vibration.

z_s is the reference height.

K_s is the size reduction function.

The size reduction function is approximated with the expression:

$$K_s(n) = \frac{1}{1 + \sqrt{\left(G_y \cdot \varphi_y\right)^2 + (G_z \cdot \varphi_z)^2 + \left(\frac{2}{\pi} \cdot G_y \cdot \varphi_y \cdot G_z \cdot \varphi_z\right)^2}}$$

where:

$\varphi_y = \frac{c_y \cdot b \cdot n}{v_m(z_s)}$ and $\varphi_z = \frac{c_z \cdot b \cdot n}{v_m(z_s)}$

G_y is a constant depending on the horizontal mode shape, taken as 1/2.

G_z is a constant depending on the vertical mode shape, taken as 5/18 for a parabolic mode shape of along wind vibration in the EW direction and 3/8 for a linear mode shape of along wind vibration in the NS direction.

B3: Response prediction – ASCE

The rms along wind acceleration is determined by the expression:

$$\sigma_{\ddot{x}}(z) = \frac{0{,}85 \cdot \phi(z) \cdot \rho \cdot B \cdot h \cdot C_{fx} \cdot \bar{V}_{\bar{z}}^2}{m_1} \cdot I_{\bar{z}} \cdot K \cdot R$$

where:

$\phi(z)$ is the fundamental along wind mode shape, obtained from the finite element model as noted above

ρ is the density of air, taken as 1,25 kg/m^3

B is the width of the building normal to the wind direction

h is the building height, taken as 48,9 m

C_{fx} is the mean along wind force coefficient, taken as 1,35 in accordance to the height and width ratio

V_z is the mean hourly wind velocity at height z

m_1 is the modal mass

I_z is the turbulence intensity

R is the resonant response factor

K is a constant taken as $(1{,}65)^{\hat{\alpha}} / (\hat{\alpha} + \xi + 1)$

where

$\hat{\alpha}$ is a constant taken as 1/9,5 according to exposure class C

ξ is the mode shape exponent

The mean hourly wind velocity at height z is determined with the expression:

$$\bar{V}_{\bar{z}} = \bar{b} \cdot \left(\frac{\bar{z}}{10}\right)^{\bar{\alpha}} \cdot V$$

where:

$\bar{b}$ is a constant taken as 0,65 according to exposure class C

$\bar{\alpha}$ is a constant taken as 1/,65 according to exposure class C

V is the basic 3 second gust velocity at 10 m height above ground

As the response acceleration is intended to be compared to the 10 minute mean wind velocity, the basic 3 second gust velocity at 10 m height, V, is evaluated by multiplying the 10 minute mean wind velocity at 10 m height with a gust factor of 1,45 as suggested in chapter 3.4 as the average gust factor at the IMO.

The turbulence intensity is determined by:

$$I_{\bar{z}} = c \cdot \left(\frac{10}{\bar{z}}\right)^{1/6}$$

where:

c is a constant taken as 0,20 according to exposure class C

$\bar{z}$ is the equivalent height of the structure defined as 0,6h which is 29.34 m for this case

The resonant response factor is determined with the expression:

$$R = \sqrt{\frac{1}{\beta} \cdot R_n \cdot R_h \cdot R_B \cdot (0{,}53 + 0{,}47 \cdot R_L)}$$

where:

β is the critical damping ratio

The R-factors are determined with the expressions:

$$R_n = \frac{4{,}74 N_1}{(1 + 10.3 N_1)^{5/3}}$$

$$N_1 = \frac{n_1 L_{\bar{z}}}{\bar{V}_{\bar{z}}}$$

$$L_{\bar{z}} = \ell \left(\frac{\bar{z}}{10}\right)^{\bar{\epsilon}}$$

$$R_l = \frac{1}{\eta} - \frac{1}{2\eta^2}(1 - e^{-2\eta})$$

$$R_l = R_h \qquad for \qquad \eta = \frac{4.6 \cdot n_1 \cdot h}{\bar{V}_{\bar{z}}}$$

$$R_l = R_B \qquad for \qquad \eta = \frac{4.6 \cdot n_1 \cdot B}{\bar{V}_{\bar{z}}}$$

$$R_l = R_L \qquad for \qquad \eta = \frac{15.4 n_1 L}{\bar{V}_{\bar{z}}}$$

where:

n_1 is the natural frequency of the structure

L is the horizontal depth of the building in the wind direction

With the root mean square of the response acceleration determined, the peak along wind response acceleration is evaluated by multiplying the root mean square of the response acceleration with a peak factor. The peak factor is determined with the expression:

$$g_{\dot{x}} = \sqrt{2 \cdot ln(n_1 \cdot T)} + \frac{0{,}5772}{\sqrt{2 \cdot ln(n_1 \cdot T)}}$$

where:

T is the time over which the minimum acceleration is computed, taken as 600 to represent 10 minutes

B4: Response prediction – AIJ – Along wind response

The along wind acceleration response is determined by the expression:

$$a_{Dmax} = \frac{q_H \cdot g_{aD} \cdot B \cdot H \cdot C_H \cdot C'_g \cdot \lambda \cdot \sqrt{R_D}}{M_D}$$

where:

q_H is the velocity pressure

g_{aD} is a peak factor similar to the peak factors of the other two design codes considered

B is the projected width of the building

H is the reference height, taken as the mean roof height or for this case, the total height of the structure, 48,9 m

C_H is the wind force coefficient at reference height

C'_g is the root mean square overturning moment coefficient

λ is the mode correction factor of general wind force

R_D is the resonance factor

M_D is the generalized mass of the building for along wind vibration

The peak factor is determined by:

$$g_{aD} = \sqrt{2 \cdot \ln(600 \cdot f_D) + 1{,}2}$$

where:

f_D is the natural frequency of the structure

The velocity pressure is determined with the expression:

$$q_H = \frac{1}{2} \cdot \rho \cdot U_H^2$$

where:

ρ is the density of air, taken as 1,25 kg/m^3

U_H is the design wind velocity, determined from the following expression:

$$U_H = U_0 \cdot K_D \cdot E_H \cdot k_{rW}$$

where:

U_0 is the basic wind velocity, the 10 minute mean wind velocity at 10 m height

K_D is the wind directionality factor, taken as 1 to represent wind acting normal to the building face

E_H is the wind velocity profile factor at reference height H

r_{kW} is the return period conversion factor

The wind velocity profile factor is determined with the expression:

$$E_H = E_r \cdot E_g$$

where:

E_g is the topography factor, taken as 1

E_r is the exposure factor for flat terrain categories, determined by the expression:

$$E_r = 1{,}7 \cdot \left(\frac{Z}{Z_G}\right)^{\alpha} \quad for \quad Z_b < Z \leq Z_G$$

where:

Z is the height above ground

Z_b is a wind profile factor, taken as 5 in accordance to terrain category 2

Z_G is a wind profile factor, taken as 350 in accordance to terrain category 2

α is a wind profile factor, taken as 0,15 in accordance to terrain category 2

The return period conversion factor is determined by:

$$k_{rW} = 0{,}63 \cdot (\lambda_U - 1) \cdot \ln(r) - 2{,}9 \cdot \lambda_U + 3{,}9$$

where:

λ_U is the ratio of 500 year recurrence wind velocity and the basic wind velocity

r is the design return period, taken as 50 years

The wind force coefficient at reference height is taken as the difference of the external pressure coefficient on windward face and the leeward face. The external pressure coefficient on the windward face is determined as 0,8 k_z, where k_z is taken as $0{,}8^{2\alpha}$ for height greater than 0,8 H. The external pressure coefficient is taken as -0,5 if the width of the building face is greater than the depth, or 0,35 if the width of the building face is less than the depth.

The root mean square overturning moment coefficient is determined by the expression:

$$C'_g = 2 \cdot I_H \cdot \frac{0{,}49 - 0{,}14 \cdot \alpha}{\left\{1 + \frac{0{,}63 \cdot \left(\frac{\sqrt{B \cdot H}}{L_H}\right)^{0{,}56}}{\left(\frac{H}{B}\right)^{k}}\right\}}$$

where:

I_H is the turbulence intensity at reference height

L_H is the turbulence scale at reference height

k is a factor depending on the building geometry, taken as 0,07 if the height is greater than the width, or as 0,15 if the width is greater than the height

The turbulence intensity at height Z is determined with the expression:

$$I_Z = I_{rZ} \cdot E_{gI}$$

where:

I_{rZ} is the turbulence intensity on flat terrain categories, determined by the expression:

$$I_{rZ} = 0{,}1 \cdot \left(\frac{Z}{Z_G}\right)^{-\alpha-0{,}05} \quad for \quad Z_b < Z \leq Z_G$$

E_{gI} is the topography factor for turbulence intensity, taken as 1

The turbulence scale is determined by the expression:

$$L_Z = 100 \cdot \left(\frac{Z}{30}\right)^{0{,}5} \quad for \quad 30\,m < Z \leq Z_G$$

The mode correction factor of general wind force is determined by:

$$\lambda = 1 - 0{,}4 \cdot \ln(\beta)$$

where:

β is the mode shape exponent

The resonance factor is determined by the expressions:

$$R_D = \frac{\pi \cdot F_D}{4 \cdot \zeta_D}$$

$$F_D = \frac{I_H^2 \cdot F \cdot S_D \cdot \left(0{,}57 - 0{,}35 \cdot \alpha + 2 \cdot R \cdot \sqrt{0{,}053 - 0{,}042 \cdot \alpha}\right)}{C'_g}$$

$$F = \frac{4 \cdot \frac{f_D \cdot L_H}{U_H}}{\left\{1 + 71 \cdot \left(\frac{f_D \cdot L_H}{U_H}\right)^2\right\}^{5/6}}$$

$$S_D = \frac{0{,}9}{\left\{1 + 6 \cdot \left(\frac{f_D \cdot H}{U_H}\right)^2\right\}^{0{,}5} \cdot \left(1 + 3 \cdot \left(\frac{f_D \cdot B}{U_H}\right)\right)}$$

$$R = \frac{1}{1 + 20 \cdot \left(\frac{f_D \cdot B}{U_H}\right)}$$

where:

ζ_D is the critical damping ratio for the first mode in along wind direction

B5: Response prediction – AIJ – Across wind response

The peak response acceleration in the across wind direction is determined by the expression:

$$a_{Lmax} = \frac{q_H \cdot g_{aL} \cdot B \cdot H \cdot C'_L \cdot \lambda \cdot \sqrt{R_L}}{M_L}$$

where:

q_H is the velocity pressure, determined as for the along wind response

g_{aL} is a peak factor, determined as for the along wind response, but using the natural frequency of the first mode in the across wind direction

B is the projected width of the building

H is the reference height, taken as the mean roof height or for this case, the total height of the structure, 48,9 m

C'_L is the root mean square overturning moment coefficient

λ is the mode correction factor of general wind force, determined as for the along wind response

R_L is the resonance factor

M_L is the generalized mass of the building for across wind vibration

The root mean square overturning moment coefficient for across wind vibration is determined by:

$$C'_L = 0{,}0082 \cdot \left(\frac{D}{B}\right)^3 - 0{,}071 \cdot \left(\frac{D}{B}\right)^2 + 0{,}22 \cdot \left(\frac{D}{B}\right)$$

where:

D is the depth of the building

The resonance factor for across wind vibration is determined by the expressions:

$$R_L = \frac{\pi \cdot F_L}{4 \cdot \zeta_L}$$

$$F_L = \sum_{j=1}^{m} \frac{4 \cdot \kappa_j \cdot \left(1 + 0{,}6 \cdot \beta_j\right) \cdot \beta_j}{\pi} \cdot \frac{\left(\frac{f_L}{f_{sj}}\right)^2}{\left\{1 - \left(\frac{f_L}{f_{sj}}\right)^2\right\}^2 + 4 \cdot {\beta_j}^2 \cdot \left(\frac{f_L}{f_{sj}}\right)^2}$$

$$\kappa_1 = 0{,}85$$

$$\kappa_2 = 0{,}02$$

$$m = \begin{cases} 1 & for \quad \frac{D}{B} < 3 \\ 2 & for \quad \frac{D}{B} \geq 3 \end{cases}$$

$$f_{s1} = \frac{0{,}12}{\left\{1 + 0{,}38 \cdot \left(\frac{D}{B}\right)^2\right\}^{0{,}89}} \cdot \frac{U_H}{B}$$

$$f_{s2} = \frac{0{,}56}{\left(\frac{D}{B}\right)^{0{,}85}} \cdot \frac{U_H}{B}$$

$$\beta_1 = \frac{\left(\frac{D}{B}\right)^4 + 2{,}3 \cdot \left(\frac{D}{B}\right)^2}{\left\{2{,}4 \cdot \left(\frac{D}{B}\right)^4 - 9{,}2 \cdot \left(\frac{D}{B}\right)^3 + 18 \cdot \left(\frac{D}{B}\right)^2 + 9{,}5 \cdot \left(\frac{D}{B}\right) - 0{,}15\right\}} + \frac{0{,}12}{\left(\frac{D}{B}\right)}$$

$$\beta_2 = \frac{0{,}28}{\left(\frac{D}{B}\right)^{0{,}34}}$$

where:

f_L is the natural frequency for the first mode in the across wind direction

ζ_L is the critical damping ratio for the first mode in the across wind direction